Spring 2015

Optimization of Rare Earth Leaching from Ores and Concentrates

Grant Wallace
Montana Tech of the University of Montana

OPTIMIZATION OF RARE EARTH LEACHING FROM ORES AND CONCENTRATES

by

Grant Wallace

A thesis submitted in partial fulfillment of the
requirements for the degree of

Master of Science in Metallurgical/Mineral Processing Engineering

Montana Tech

2015

Abstract

The use of applied chemistry in the production and optimization of leach solutions from Rare Earth Element (REE) ores and concentrates was investigated. Ore and concentrate samples were characterized using scanning electron microscopy/mineral liberation analysis (SEM/MLA), X-ray Diffraction (XRD), and Inductively-coupled Plasma Atomic Emission Spectroscopy (ICP-AES). Multiple leach tests were performed to analyze the effects of temperature, residence time, and reagent concentration on the leaching of REEs. Analysis of leach solutions was carried out using ICP-AES. Modeling and statistical analysis of extraction behavior was carried out using DesignExpert 9. Modeling data for multiple REEs indicate that extraction is strongly influenced by temperature and reagent concentration, while leaching time plays a much less important role. Experimental design techniques were able to optimize REE recovery while minimizing the extraction of gangue elements, such as iron, and a series of series of parameters were determined that were optimal for REE extraction. Differences in extraction between some of the REEs indicate that a multistage, direct leaching, operation could be implemented to effectively extract REEs from both ores and concentrates.

Keywords: Rare Earths, Leaching, Statistical Optimization

Dedication

This work is dedicated to my parents, my brother, and all of the friends and family who have given their time, love, and support over the years. Thank you.

Acknowledgements

I would like to thank Dr. Bill Gleason and Dr. Larry Twidwell for all of their insight, help, and guidance as my advisor(s) on this project. I would also like to thank my committee members, Dr. Jerry Downey, Dr. Michael Webb, and Dr. Courtney Young for their additional support. In addition to my committee, I would also like to acknowledge Gary Wyss and Marcee Cameron who helped extensively with sample characterization and ICP work. Special thanks go out to Sean Dudley for all of his work on the ONR project, as well as the ONR undergraduate researchers, Maureen Chorney and Kennedy Southwick. Finally, I would like to thank Dr. David Shifler and the Office of Naval Research (ONR) for their financial support of this project, as well as Dr. Henry Kasaini and Jaye Pickarts with Rare Element Resources for supplying the ore and concentrate samples that made this project possible.

Table of Contents

List of Tables

List of Figures

List of Acronyms and Important Chemical Symbols

Ce: Cerium

D2EHPA: Di-(2-ethylhexyl) phosphoric acid

Dy: Dysprosium

Er: Erbium

Eu: Europium

Gd: Gadolinium

H_2SO_4: Sulfuric acid

HCl: Hydrochloric acid

HF: Hydrofluoric acid

HNO_3: Nitric acid

Ho: Holmium

HREE: Heavy Rare Earth Element(s)

ICP-AES: Inductively Coupled Plasma-Atomic Emission Spectroscopy

ICP-MS: Inductively Coupled Plasma-Mass Spectroscopy

La: Lanthanum

LiB_4: Lithium tetraborate

LREE: Light Rare Earth Element(s)

Lu: Lutetium

MLA: Mineral Liberation Analysis

NaOH: Sodium hydroxide

Nd: Neodymium

ONR: Office of Naval Research

Pm: Promethium

Pr: Praseodymium

REE: Rare Earth Element(s)

REO: Rare Earth Oxide(s)

RER: Rare Element Resources

SEM: Scanning Electron Microscope

Sm: Samarium

SO_2: Sulfur dioxide

Tb: Terbium

Th: Thorium

Tm: Thulium

U: Uranium

XRD: X-Ray Diffraction

Y: Yttrium

Yb: Ytterbium

1. Introduction

1.1. Background on Rare Earth Elements

The rare earth elements (REEs) are defined as the 15 elements found in the first row of the f-block series of elements on the Periodic Table, also known as the lanthanide series. Yttrium (Y) and scandium (Sc) are often included as REEs due to their similar chemical and physical properties. In their elemental form, REEs tend to be lustrous, silver-colored metal solids that are generally malleable, ductile, and reactive in nature (Gupta & Krishnamurthy, Extractive Metallugy of Rare Earths, 2005). The rare earths can be further categorized as either light or heavy rare earths (LREEs and HREEs). The LREE's are considered to consist of Lanthanum (La), Cerium (Ce), Praseodymium (Pr), Neodymium (Nd), Promethium (Pm), Samarium (Sm), and Europium (Eu) while the HREE's consist of the remaining lanthanides: gadolinium (Gd), terbium (Tb), dysprosium (Dy), holmium (Ho), erbium (Er), thulium (Tm), ytterbium (Yb), and lutetium (Lu).

The fact that REEs are given the title "rare" is somewhat misleading. REEs are relatively abundant within the earth's crust; however, they are not often found in concentrations that make them economical to mine and process. Table I presents some of the basic chemical and physical properties of the REE's (Sastri, Bunzli, Ramaxhandra Rao, Rayudu, & Perumareddi, 2003).

Table I: Chemical and Physical Properties of REE's

Element	Symbol	Atomic No.	Atomic Wt. (g/mol)	Terrestrial Abundance (ppm)	M.P. (^{o}C)	B.P. (^{o}C)	Density (g/cm^{3})	Crystal Structure***
Yttrium	Y	39	88.90	28	1522	3338	4.469	hcp
Lanthanum	La	57	139.91	18	918	3464	6.145	dhcp
Cerium	Ce	58	140.12	46	798	3433	6.770	fcc
Praseodymium	Pr	59	140.90	5.5	931	3520	6.773	dhcp
Neodymium	Nd	60	144.24	24	1021	3074	7.007	dhcp
Promethium*	Pm	61	147.00	-	1042	3000**	7.260	dhcp
Samarium	Sm	62	150.35	6.5	1074	1794	7.520	rhomb
Europium	Eu	63	151.96	1.0	822	1529	5.243	bcc
Gadolinium	Gd	64	157.25	6.4	1313	3273	7.900	hcp
Terbium	Tb	65	158.92	0.9	1356	3230	8.229	hcp
Dysprosium	Dy	66	162.50	4.5	1412	2567	8.550	hcp
Holmium	Ho	67	164.93	1.2	1474	2700	8.755	hcp
Erbium	Er	68	167.26	2.5	1529	2868	9.066	hcp
Thulium	Tm	69	168.93	0.2	1545	1950	9.321	hcp
Ytterbium	Yb	70	173.04	2.7	819	1196	6.965	fcc
Lutetium	Lu	71	174.97	0.8	1663	3402	9.840	hcp

*Product of Pu decay; **Estimated Value; ***hcp: hexagonal close packed, dhcp: double C hexagonal close packed, rhomb: rhombohedral, fcc: face centered cubic, bcc: body centered cubic

Similarities in the chemical and physical properties of REE's make identifying and separating REE's a difficult task. All of the REE's have very similar electronegativity values (~1.16-1.20) and atomic weights. The REE's are very electropositive and tend to form the +3 ion in aqueous solution. Some REE's, such as Ce, Eu, Tb, and Yb, are also capable of forming ions with a +2 or even +4 valence charge. However, these ions are always less stable than the +3 ion. The ability of an REE to form a stable +2/+3/+4 oxidation state is dependent on whether it is possible for the element to achieve an empty ($4f^{0}$), half-filled ($4f^{7}$), or completely-filled ($4f^{14}$) *f*-orbital electron configuration (Gupta & Krishnamurthy, Extractive Metallugy of Rare Earths, 2005). The REEs also react with other elements and compounds in nearly identical ways. For example, all of the REEs will dissolve in mineral acids in their metallic form with the exception of hydrofluoric acid (HF). Reactions between HF and metallic REEs results in a coating of rare

earth fluoride (REF_3) forming on the surface of the REE metal which prevents the reaction from continuing (Gupta & Krishnamurthy, Extractive Metallugy of Rare Earths, 2005).

Perhaps the most significant behavior associated with REEs is a phenomenon known as the "lanthanide contraction". While most elements experience an increase in atomic radius as one moves from left to right across the periodic table, REEs actually decrease in size as the elements increase in atomic weight, with the exception of Eu and Yb, in their elemental form. This trend is most noticeable amongst the +3 REE-cations. The cause of the lanthanide contraction is credited to incomplete shielding of 4*f* –electrons from the nucleus due to the directional shape of the 4*f* orbitals. A graph of the atomic radii of the REEs to demonstrate the lanthanide contraction is shown in Figure 1.

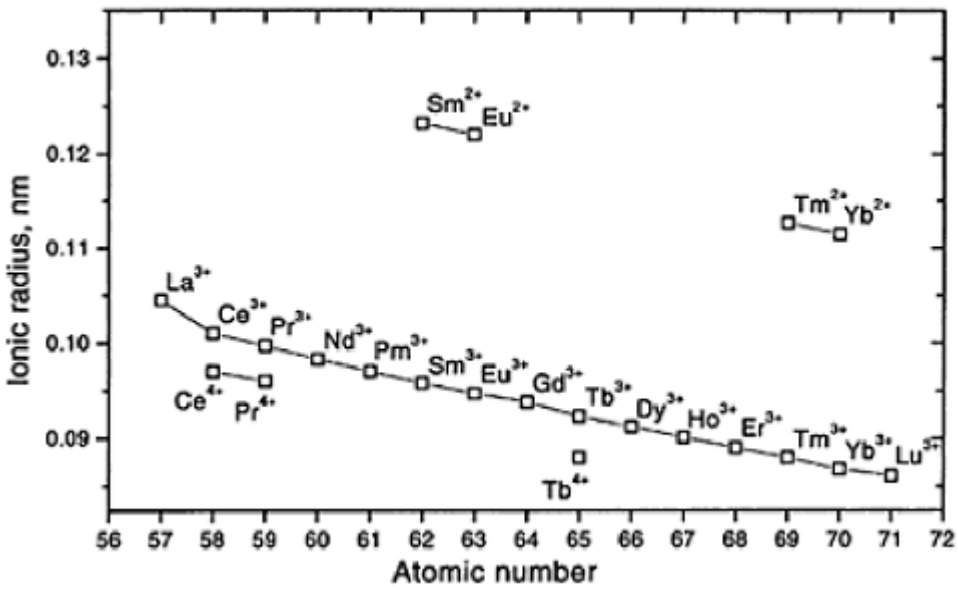

Figure 1: Lanthanide Contraction (Gupta & Krishnamurthy, Extractive Metallugy of Rare Earths, 2005)

The lanthanide contraction is responsible for a number of the chemical properties associated with REEs. Perhaps the most important of these properties is basicity. The basicity of a cation is a determining factor for a number of properties such as salt solubility and the stability

of complex ions. Basicity is driven primarily by ionic radii, with larger ions tending to be more basic than smaller ions. Because of this behavior, REEs are generally arranged in the following order from most to least basic:

$$La^{3+} > Ce^{3+} > Pr^{3+} > Nd^{3+} > Pm^{3+} > Sm^{3+} > Eu^{3+} > Gd^{3+} > Tb^{3+} > Dy^{3+} > Ho^{3+} > Y^{3+} > Er^{3+} > Tm^{3+} > Yb^{3+} > Lu^{3+} > Sc^{3+}$$

Although the differences in atomic radii are small, the differences in REE ionic radii play a critical role in traditional REE extraction and separation methods (Gupta & Krishnamurthy, Extractive Metallugy of Rare Earths, 2005). These separation methods will be elaborated upon in Section 1.4, Leaching and Separating REE's.

1.2. The Importance of REE's

REEs are key components in a number of modern products and industrial processes. REEs, particularly Sm and Nd, are used in the production of powerful, lightweight permanent magnets which are critical for the growing electronics and alternative fuel industries (Grasso, 2011). REEs are also used as cracking catalysts in the refining of petroleum products. Zeolites loaded with rare earth oxides are used to control the activity of the zeolite catalysts which, in turn, regulate coke and olefin selectivity (Wormsbecher, Wu-Cheng, & Wallenstein, 2010). High-end lasers, catalytic converters, fluorescent lighting, pigments, light-emitting diodes (LEDs), and certain steel alloys all utilize REEs in their construction (Gupta & Krishnamurthy, Extractive Metallugy of Rare Earths, 2005).

Demand for REEs has increased dramatically as the markets for alternative energy sources and electronics have expanded. Studies have predicted that the demand for REEs could increase by as much as 8.6% per year over the next 25 years (Alonso, et al., 2012). Predicted trends in REE demand by various industries are shown in Figure 2 (Alonso, et al., 2012).

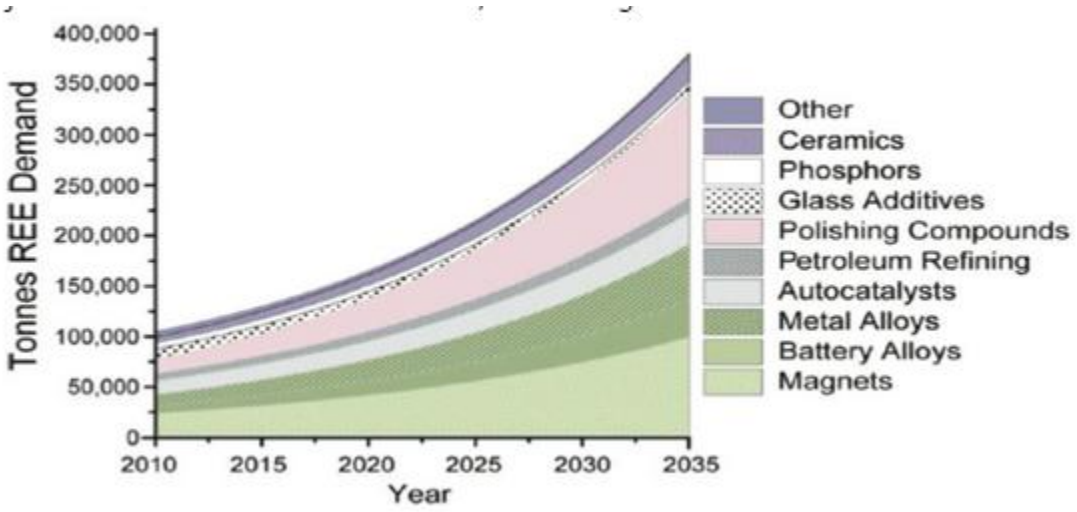

Figure 2: Predicted REE Demand

From the graph, it can be observed that the magnet and metal/battery alloys are predicted to experience dramatic increases in REE demand during the next 20 years. Again, this increase in demand is credited to a predicted increase in the demand for alternative energy (i.e. wind turbines, electric automobiles, fuel cells, etc.) and electronics which incorporate small, powerful magnetic components. Regardless of the source of the demand, increases to the global REE supply will have to occur in order to meet this expected growth in demand.

Currently, the global market for REEs is supplied almost exclusively by China. The United States was the leading producer of REEs until the 1980s. Since then, Chinese REE production has expanded to the point that Chinese rare earth oxides were responsible for 97% of global production in 2011 (Grasso, 2011). Currently, China's contribution to the global REE market has been reduced to 86%. However, China is still the major producer of REEs and rare earth products such as magnets and REE alloys. The increased competition caused the REE-production centers in the United States to shut down and, since the 1990's, the United States has relied on foreign imports to meet its demand for REE products.

The reduction in Chinese exports has brought the state of the REE market to the attention of many national governments, including the United States. The lack of developed domestic sources of REEs and the ability to manufacture REE products within the United States has become an issue of national security. REE products play a critical role in many defense technologies such as missile guidance systems, sonar/radar components, and laser technologies (Grasso, 2011). The United States government is currently engaged in promoting the development of domestic REE sources as well as research that will help make these sources economical and competitive on the global market (Humphries, Mark, 2013). Currently, there is only one U.S. REE mine in the production stage. The Mountain Pass operation, owned by MolyCorp, renewed operations in 2013 (Molycorp, 2013).

Other potential REE deposits are being investigated within the United States to reduce dependence on foreign suppliers. One such site is the Bear Lodge deposit which is being developed by Rare Element Resources Ltd. The Bear Lodge deposit is located in northeastern Wyoming and has been described as the largest disseminated REE deposit in North America. The potential mine site has a lengthy projected lifespan, but is currently still in the development stages (Rare Element Resources Ltd, 2013).

1.3. Leaching (General)

Leaching is a hydrometallurgical process that involves the extraction of metal ions from ores and mineral concentrates through the use of an aqueous reagent as a precursor to purification and the production of a pure metal product. Numerous reagents have been used in leaching operations, but mineral acids and bases are the most prevalent commercially. Selection of the leaching reagent is determined by the mineralogy of the ore/concentrate being processed,

the costs associated with using the reagent, and the ability of the reagent to be recycled (Gupta & Mukerjee, Hydrometallurgy in Extraction Processes, 1990). Successful leaching involves the leach solution penetrating the pore structure of the solid material. Diffusion is generally considered to be a major factor in leaching reactions. When considering solution reactions, three steps must be followed, of which, one or more may control the reaction rate. These three steps are: 1) the reactants must diffuse towards one another, 2) a reaction must occur between the two reactants, and 3) the products of the chemical reaction must diffuse away from one another (Wadsworth & Miller, 1979). Since typical agitation leaching involves finely-ground material, reaction behavior must be considered on an individual particle basis. General leaching reactions have been described using the shrinking core model to understand the basic kinetics. The shrinking core model involves transfer between an individual solid particle and the surrounding leaching reagent as the reagent diffuses into the particle, interacts with the particle surface, and the reaction products diffuse away from the reaction area. An illustration of the shrinking core model is presented in Figure 3.

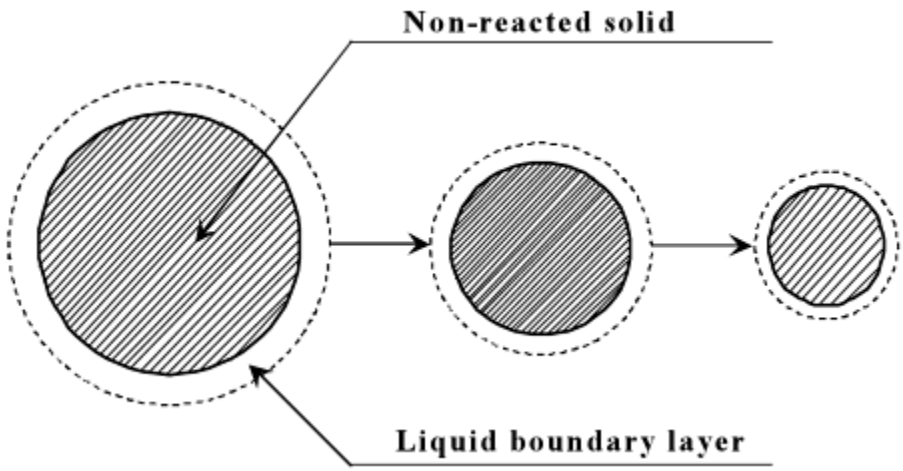

Figure 3: Shrinking Core Model of a Particle Reacting With a Liquid Solution (Havlik, 2014)

As the particle reacts with the leach solution, portions of the particle dissolve upon contact with the solution, and the particle reduces in size. This decrease in particle size changes the amount of surface area available to react with the leaching reagent which alters the overall reaction rate. As the amount of available surface area decreases, the rate of reaction will be reduced. Maximizing exposure to the leaching reagent is essential for successful extraction which is why agitation is often implemented to maintain particle suspension. Leaching chemistry can become quite complex due to the issues associated with the transfer of reactants and products. Leaching reactions will be slowed by the build-up of reaction products at the particle surface. Again, agitation is often implemented to disperse the reaction products and allow for reagent to interact with the particles. Temperature and initial reagent concentrations can also significantly affect the rate at which particles are leached (Twidwell, Huang, & Miller, 1980).

1.4. Leaching and Separating REE's

The kinetics of REE leaching were investigated to gain a better understanding of the leaching process at the individual particle level. According to Tian Jun, et al., the leaching of mid and heavy REEs from weathered clay deposits, located in Jianxi province, China, using ammonium sulfate followed the shrinking core model. Four different equations were produced by the authors to describe four different controlling operations: chemical reaction controls, outer diffusion controls, inner diffusion controls, and mixed controls. Inner diffusion of the reagent appeared to control leaching kinetics, making particle size an important factor when attempting to leach REEs. (Tian, Yin, Chi, Rao, Jiang, & Ouyang, 2010).

REE leaching was also found to follow the shrinking core model when HCl, HNO_3 and H_2SO_4 were used as lixiviants. In the work done by Kandil, et al., the kinetics of micro-scale column leaching of Egyptian REE phosphate deposits were investigated. Of the three acids used

in this study, HCl was found to have the lowest activation energy at 10.3 kJ/M. Activation energy is the minimum energy required to initiate a chemical reaction. The activation energies of HNO_3 and H_2SO_4 were also determined to be 13.85 and 16.7 kJ/M respectively. This information supports the use of HCl over other acids because the lower activation energy associated with HCl implies that less energy should be required to initiate REE leaching. Again, leaching was determined to be regulated by the diffusion of the lixiviant through a boundary layer on the surface of the solid phosphate particles (Kandil, Moussa, Aly, Kamel, Gouda, & Kouraim, 2010).

The most common REE-bearing minerals are bastnasite, a REE-fluorocarbonate ($(REE)CO_3F$), and monazite, a phosphate mineral ($(REE)PO_4$). Both bastnasite and monazite are primarily sources of light REEs and are the most commonly processed minerals. Heavy REEs are often associated with xenotime, an yttrium phosphate mineral. Traditionally, the processes involved with extracting REEs have been very costly and generally involved multiple pretreatment and purification steps before separation measures could be initiated. An understanding of the conventional bastnasite leaching process used in China was gained from the paper written by R. Chi, et al. In China, bastnasite ores are concentrated to approximately 66% REE via flotation. The concentrate is then roasted in the presence of sulfuric acid to convert the bastnasite to a REE-sulfate before it is leached with hydrochloric acid. Finally, the REEs are precipitated using oxalic acid. Oxalic acid is a large, organic molecule that chelates to the REE ions, forming REE-oxalates that become too large to remain in solution. However, this process is quite harmful to the environment due to the production of HF and SO_2 gases. The work being conducted by Chi, et al, involves an attempt to design an alternative strategy to the traditional leaching process through the use of an ammonium chloride roasting operation followed by leaching with hot water. The conversion of the REEs to chlorides instead of sulfates increases the

solubility of the REEs and allows for a less aggressive leaching environment to be used. The final precipitation of REEs would continue to be carried out using oxalic acid. The process proposed by Chi, et al suggests that chlorination of REEs, followed by conversion to rare earth oxide (REO) precipitates, could produce excellent recovery of REEs (>90%) (Chi, Zhang, Zhu, Zhou, Wu, & Wang, 2004).

A process for extracting REEs from bastnasite concentrates was developed by Molycorp in 1965. A finely-ground (65% -325 mesh) bastnasite concentrate consisting of 70% REE-oxides was subjected to leaching with HCl for four hours at near boiling temperatures. Residual REE-fluorides were converted to hydroxides through the addition of sodium hydroxide (NaOH) requiring another four hours of reaction time. Neutralization of excess HCl in the leach solution was done by the addition of the REE hydroxides until a pH of 3 was achieved in order to prevent the leaching of REEs, and other metals, into solution. Solution purification was then carried out by the addition of small amount of sodium hydroxide and sulfuric acid, which produced precipitates of iron hydroxide and lead sulfate. Thorium and any excess sulfate were removed through the addition of barium chloride (Gupta & Krishnamurthy, Extractive Metallugy of Rare Earths, 2005).

A number of processes have been developed for extracting REEs from monazite. In the U.S., monazite was most commonly processed using a tightly-controlled sulfuric acid leaching process which selectively extracted REEs, or Th, depending on the acid concentration (Gupta & Krishnamurthy, Extractive Metallugy of Rare Earths, 2005). Monazite leaching has also been successfully carried out under basic conditions. Another commonly-used process involved the leaching of a finely-ground monazite concentrate with a 60-70% NaOH solution which had been heated to approximately 150°C. REE-hydroxides, Th, and U precipitated and were further treated

to produce purified REE-chlorides through a series of neutralization and precipitation steps (The Minerals, Metals and Materials Society, 2014).

Following leaching, REEs are usually separated from one other through the processes of solvent extraction or ion exchange. The similarities between the REEs cause their separation to be a very complex and costly process. Solvent extraction involves the separation of the components of a homogenous liquid by distributing the desired components between two, immiscible, liquid phases (Othmer, 1983). The specific process used for REE separation by solvent extraction varies depending on the leach solution environment. For HCl leach solutions, organic phosphoric acids, most commonly di-(2-ethylhexyl) phosphoric acid (D2EHPA), are used to remove REE ions from the aqueous solution and into the organic phase. The separating reagent is often diluted with an organic solvent. From this point, the various REEs are isolated from one another through numerous separation stages that exploit the subtle differences in the atomic weight, basicity, and, in some cases, ionic charge (Thorsen, 1983). Although the number of separation stages required for successful solvent extraction of REEs can be numerous, the speed of the process, and the ability to continuously process large volumes of concentrated solution, make solvent extraction a viable process for commercial REE separation and purification. However, solvent extraction is not without its drawbacks. Less abundant REEs, such as Tb, Yb, and Lu, are difficult to effectively isolate using solvent extraction. In addition, solvent extraction is only a viable option when the purity of the REE products is not required to exceed 99.9%. For greater product purity, ion exchange is recommended (Gupta & Krishnamurthy, Extractive Metallugy of Rare Earths, 2005).

Ion exchange is often used in commercial REE separation processes where high-purity products of 99.99% or greater are desired. In a typical ion exchange process, an aqueous solution

containing the desired REEs in ionic form is exposed to a charged resin which is charged opposite to target REE. The desired ion is drawn out of solution by this charge difference and loosely binds to the substrate, replacing a preexisting ion (Rosenqvist, 1974). In REE ion exchange, the aqueous solution containing the REE ions passes through a column containing the collector resin. The loaded resin is then exposed to a solution of chelating agent, often ethylenediaminetetraacetate (EDTA), which forms REE-EDTA complexes and causes the REEs to be removed from the resin. REE ions are removed using EDTA according to the stability of the REE-EDTA complex with the most stable REE-EDTA complexes leaving the resin column first. Complex stability is determined by the size of the REE ionic radius which, due to the lanthanide contraction, means that the REEs are separated sequentially by decreasing atomic number (Lu-Ce) with Y eluting between Tb and Dy. To effectively separate the heavier, and less concentrated, REEs, elevated temperatures (90-95°C) are used. Higher temperatures also improve REE separation in the presence of non-REE impurities such as Fe (Gupta & Krishnamurthy, Extractive Metallugy of Rare Earths, 2005).

Impurities can be detrimental to an ion exchange process. Fouling of the resins can occur when ions bind permanently to the resin or impurity ions will out-compete the desired ions and prevent separation from occurring. Ion exchange processes are also more costly due to the expenses associated with the resins, and they are often slower than other separation methods, such as solvent extraction (Tavlarides, Bae, & Lee, 1987).

1.5. Thesis Statement

This study investigates the leaching of ore and concentrate samples originating from the Bear Lodge site. Three ore samples and three concentrate samples were provided. The concentrates have been labeled RE1, RE2, and RE3, while the ores have been labeled as RE4,

RE5, and RE6. The goal of this study is to optimize REE extraction from the Bear Lodge samples via leaching with hydrochloric acid (HCl) as a precursor to the development of a cost-effective extraction process and to demonstrate the use of statistical analysis software to the industry. Optimization of leaching parameters will be carried out using the statistical analysis software, DesignExpert 9 and a leaching "recipe" will be determined that will provide optimal conditions for REE extraction and recovery.

2. Experimental Procedures

2.1. Characterization

2.1.1. XRD

Samples of the six RER samples were analyzed using X-ray diffraction. A Rigaku Ultima IV X-ray Diffractometer using Cu-Kα radiation at 40 kV and 40 mA was used to analyze the samples. A small amount of each sample was finely ground (-100 micron) using a small mortar and pestle. After grinding, the sample was then loosely packed onto a microscope slide. Each sample was packed in such a way that the material was arranged in a random manner to avoid skewing XRD data. Analysis of the XRD spectra was carried out using Rigaku's PDXL software.

2.1.2. Scanning Electron Microscopy/Mineral Liberation Analysis (SEM/MLA)

To determine the mineralogy of the various REE samples, each sample was analyzed using a LEO 1430VP Scanning Electron Microscope (SEM) outfitted with two Ametek Apollo-40 EDS detectors. The Mineral Liberation Analysis (MLA) software utilized the X-ray Back-scattered Electron (XBSE) method. This method relies on using variations in the gray-scale of backscattered electrons to differentiate mineral phases. The X-rays gathered from these mineral phases are compared to a mineral X-ray database for identification.

The samples were mounted in an epoxy matrix according to the following procedure. Ultra-fine particles (-400 mesh) were removed by wet sieving a sample of each material through a 230 mesh screen. The -230/+400 mesh portion of each REE sample was then collected for mounting. For the ore samples (RE4-RE6), a 5 gram sample of each was required for analysis; while the concentrates (RE1-RE3) required 5-8 g of material. For this analysis, approximately 7 g of concentrate was used in each sample. The REE samples were then mixed with approximately 2 g of graphite to promote conductivity in the SEM, and each mixture was added to 9-10 g of epoxy. A dark, viscous material was formed and poured into a small cube-shaped mold.

Once the epoxy hardened, the cubes were cut in half to produce cross-section mounts of each sample. These cross-sections were housed inside resin mounts that were polished on a Beuhler Ecomet 3 Variable Speed Grinder/Polisher. Multiple polishing operations were required in order to achieve a satisfactory surface for analysis on the SEM. The samples were polished for seven minutes on a diamond wheel. Next, a series of polishing steps were carried out using 240, 320, and 400 grit grinding wheels. After these polishing steps, the samples were polished for 20 minutes on a polishing wheel coated with a diamond suspension. Finally, the samples were polished for another 20 minutes using a diamond finishing solution. Prior to MLA analysis, the polished samples were sputtered with graphite to enable electron conduction inside the SEM.

2.1.3. Lithium Tetraborate Fusions

Elemental analysis of the REE samples was also determined by Inductively Coupled Plasma-Atomic Emission Spectroscopy (ICP-AES) through the use of lithium tetraborate (LiB_4) fusions. Lithium tetraborate fusions provide a way to analyze the composition of solid samples by ICP-AES. The LiB_4 is blended with the sample of interest and heated in a furnace to produce

a glass bead that can be digested with acid into an aqueous state for analysis. For this method, 1.0 g of LiB_4 was blended with 0.1 g of sample. Three additional fusion samples were also made using 0.1 g of an REE standard for quality control. Another two fusion samples were spiked with 0.1 g of the REE standard as additional quality control. Half of the LiB_4 was added to a graphite crucible, followed by the REE sample. These were blended together before the remaining half of the LiB_4 was added. Samples were analyzed using an ICP Thermo-Scientific iCAP 6000. Table II contains the masses of sample used in each of the fusions. It should be noted that "LCS" represents the mixed REE standard used for quality control purposes.

Table II: LiB_4 Fusion Components

Sample I.D	Crucible No.	Sample Wt (g)	LCS Wt (g)
PB	1	-	1.018
LCS1-REE	2	-	0.1212
LCS2-CCU1D	3	-	0.0652
RE1	4	0.1024	-
D-RE1	5	0.1022	-
MS	6	0.1015	0.1006
D-MS	7	0.1050	0.1043
RE2	8	0.1064	-
RE3	9	0.1044	-
RE4	10	0.1087	-
RE5	11	0.1095	-
RE6	12	0.1066	-

The samples were placed in a furnace and fused at 1000°C for 15 minutes. Each LiB_4 bead was placed in 50 mL of ICP blank (10% HCl, 5% HNO_3) and allowed to digest for 24 hours while being stirred on a shaker table. A 50% dilution of each of these samples was taken and analyzed using ICP-AES.

2.2. Leaching Test Work

2.2.1. Preliminary Leach Tests (Proof of Concept)

The purpose of the early leaching experiments was to establish an acceptable leaching procedure and to determine the reagent that would be the focus of further experimentation.

Hydrochloric acid (HCl) and nitric acid (HNO_3) were compared in a series of 36 individual experiments to determine the leaching abilities of each acid. The first set consisted of six experiments involving each of the RER samples. A small amount (0.5-0.6 g) of each sample was leached at room temperature for 60 minutes using 100 mL of 1.0M HCl. The samples were agitated in solution using an orbital shaker. Table III contains the masses of each RER sample used in these leaching experiments.

Table III: Preliminary HCl Leach Tests (Ambient Temp.)

Sample ID	Mass (g)
RE1	0.589
RE2	0.655
RE3	0.602
RE4	0.582
RE5	0.665
RE6	0.498

A second series of six experiments was carried out using HNO_3 as the leaching agent. A stock solution of HNO_3 was prepared with a pH of 0.02 using 120 mL of 65% HNO_3 solution diluted with 600 mL of 18MΩ deionized H_2O. Small amounts of each RER sample were added to 100 mL of the HNO_3 stock solution and leached at room temperature for 60 minutes. Each sample was agitated using an orbital shaker. The masses of each sample used in the HNO_3 leach tests are shown in Table IV.

Table IV: Preliminary HNO_3 Leach Tests (Ambient Temp.)

Sample ID	Mass (g)
RE1	0.58
RE2	0.66
RE3	0.67
RE4	0.62
RE5	0.75
RE6	0.67

A third set of six experiments were carried out using 18 MΩ H_2O as a control group. 100 mL of H_2O was used to leach samples of each of the RER samples. These leach tests were also

carried out at room temperature for 60 minutes using an orbital shaker to provide agitation. The masses of each RER sample used in the leach tests are provided in Table V.

Table V: Preliminary H_2O Leach Tests (Ambient Temp.)

Sample ID	Mass (g)
RE1	0.50
RE2	0.64
RE3	0.49
RE4	0.68
RE5	0.49
RE6	0.59

Additional leaching experiments were carried out using the same reagents but at elevated temperature (60°C). Samples of each RER sample were leached using 100 mL of HCl, HNO_3, and 18 MΩ H_2O. Agitation and heat were supplied using a Cole-Parmer multi-stage hot/stir plate. Leaching was carried out for 60 minutes. The pH of each solution was measured before and after leaching using a pH probe. Table VI contains the masses of each RER sample used in the elevated-temperature leaching tests as well as the pH measurements before and after leaching.

Table VI: Preliminary Leach Tests at Elevated Temperature (60°C)

Sample ID	Sample Mass (g)	pH (Before Leaching)	pH (After Leaching)
1.0M HCl			
RE1	0.55	0.40	0.07
RE2	0.53	0.42	0.00
RE3	0.52	0.41	-0.10
RE4	0.57	0.41	-0.06
RE5	0.54	0.43	-0.01
RE6	0.50	0.44	0.06
HNO_3			
RE1	0.51	0.00	-0.08
RE2	0.50	0.00	-0.07
RE3	0.56	0.00	-0.01
RE4	0.55	0.00	-0.01
RE5	0.54	0.00	0.03
RE6	0.56	0.00	0.05
H_2O			
RE1	0.56	ND	ND
RE2	0.66	ND	ND
RE3	0.59	ND	ND
RE4	0.67	ND	ND
RE5	0.65	ND	ND

RE6	0.61	ND	ND

Following leaching, the leach solutions were collected via filtration using Whatman no. 2 (8 µm) filters and samples of each solution were analyzed using ICP-AES.

2.2.2. Scoping Tests

2.2.2.1. Establishment of Reagent Boundaries

The variables to be analyzed using the DesignExpert 9 statistical analysis were temperature (^{o}C), time (minutes), and HCl concentration in units of g_{HCl}/0.5 g_{sample}. For the design matrix, it was necessary to define upper and lower boundaries for each of the variables. Lower and upper boundaries for temperature were set at ambient temperature and 90°C in order to prevent boiling from occurring in the aqueous solution. Boundaries for time were set at 30 minutes and 120 minutes. These values were selected to resemble industrial leaching constraints. Using data produced by the MLA analysis of the Bear Lodge samples, reactions for each of the REE-bearing minerals were used to determine the stoichiometric requirement (lower bound) of HCl. The reactions for each of the REE minerals are as follows:

Ancylite

$$SrCe(CO_3)_2OH \cdot H_2O + 5HCl \leftrightarrow SrCl_2 + CeCl_3 + 4H_2O + 2CO_{2(g)} \quad (1)$$

Bastnasite

$$CeCO_3F_{(s)} + 3HCl_{(aq)} \leftrightarrow CeCl_{3(aq)} + H_2O_{(l)} + CO_{2(g)} + HF_{(aq)} \quad (2)$$

Cerianite

$$CeO_{2\,(s)} + 4HCl_{(aq)} \leftrightarrow CeCl_{4(aq)} + 2H_2O_{(l)} \quad (3)$$

Monazite

$$CePO_{4(s)} + 3HCl_{(aq)} \leftrightarrow CeCl_{3(aq)} + H_3PO_{4(aq)} \quad (4)$$

Parisite

$$Ca(Ce)_2(CO_3)_3F_2 + 8HCl \leftrightarrow CaCl_2 + 2CeCl_3 + 3H_2O + 2HF_{(aq)} + 3CO_{2(g)} \quad (5)$$

Xenotime

$$YPO_{4(s)} + 3HCl_{(aq)} \leftrightarrow YCl_{3(aq)} + H_3PO_{4(aq)} \quad (6)$$

The scoping trials consisted of ten individual tests. Of these tests, five were carried out on RE1 to measure the effect on REE concentrates, and another five tests were performed using RE4 to represent the ore samples. Because 0.5 g of solid sample/100 mL of solution was to be used in the scoping tests, it was determined from these equations that the lower bound for the design matrix would be set at 0.2 g of HCl. This value was determined using a series of stoichiometric calculations involving the previously-mentioned reactions and the mineral composition values for RE3 determined by MLA. The stoichiometric requirements of HCl for each reaction were summed to obtain the value for the lower boundary for the design matrix. A sample calculation for determining the HCl requirement for the reaction with bastnasite is shown in equation (7).

$$gHCl_{bastnasite} = \frac{0.50g_{RE3} \times \left(\frac{24.83\%}{100}\right)}{219.12\, {}^{g_{bastnasite}}/_{mol}} \times \frac{3mol_{HCl}}{1mol_{bastnasite}} \times \frac{36.46g_{HCl}}{mol_{HCl}} = 0.06gHCl \quad (7)$$

This lower boundary value was multiplied by 50 (10 g HCl) to establish the upper bound of the design matrix in order to provide a concentration range large enough to include the optimal value.

For each scoping test, 37.35% by weight HCl solution was used as the leaching agent. Appropriate amounts were weighed out on a balance before being diluted in order to provide

enough solution to suspend the solid samples. The table below provides an example of the scoping test matrices that were carried out using RE1 and RE4.

Table VII: Scoping Test Design Matrix

Sample Name	HCl Conc. ($g_{HCl}/0.5g_{solids}$)	Temp (^oC)	Time (min)
RE1	0.2	25	60
RE1	0.2	90	60
RE1	5.1	60	60
RE1	10.0	25	60
RE1	10.0	90	60
RE4	0.2	25	60
RE4	0.2	90	60
RE4	5.1	60	60
RE4	10.0	25	60
RE4	10.0	90	60

2.2.2.2. Scoping Tests under Ambient Conditions (25°C)

HCl solution was prepared by weighing 0.536 g of 37.35% HCl solution into a 40mL centrifuge vial for the tests involving 0.2 g HCl. Tests using 10.0 g of HCl required 26.779 g of HCl solution. In all cases, the final volumes in each vial were then diluted to 35 mL. Following dilution, 0.50 g of each sample (RE1 and RE4) were added to separate vials. The vials were then placed on a small shaker table and agitated for 60 minutes. Filtration was used to separate the solid residue from the leach solutions and both were collected in scintillation vials. The leach solutions were later analyzed using ICP-AES. Table VIII contains information on each test in regards to sample mass and the amounts of HCl used.

Table VIII: Ambient Temp. Scoping Test Parameters

Experiment ID	Sample Wt (g)	HCl Solution (g)	HCl (g)	Time (min)
$0.2g_{HCl}$/RE1	0.50	0.56	0.21	60
$10g_{HCl}$/RE1	0.51	26.61	9.92	60
$0.2g_{HCl}$/RE4	0.53	0.56	0.21	60
$10g_{HCl}$/RE4	0.52	26.55	9.92	60

2.2.2.3. Scoping Tests at 90°C

The scoping tests carried out at 90°C used the same HCl concentrations that were used in the 25°C leach tests. However, for the elevated temperature tests, the HCl was added to a 100 mL volumetric flask and the concentrated acid solution was then diluted. Once the leaching agents had been prepared, 0.5 g of solid REE sample was measured out in the manner previously described. The leaching agents were transferred into beakers and heated on a hot/stir plate until they reached a temperature of approximately 90°C. Once the solutions reached the desired temperature, the solids were added and allowed to leach for 60 minutes. Following leaching, the leach solutions were filtered and collected. Table IX contains information about each individual leach test at 90°C.

Table IX: 90°C Scoping Test Parameters

Experiment ID	Sample Wt (g)	HCl Solution (g)	HCl (g)	Time (min)
$0.2g_{HCl}$/RE1	0.53	0.55	0.21	60
$10g_{HCl}$/RE1	0.52	26.87	10.03	60
$0.2g_{HCl}$/RE4	0.53	0.56	0.21	60
$10g_{HCl}$/RE4	0.55	26.86	10.03	60

2.2.2.4. Scoping Tests at 60°C

In order to provide midpoints for the extraction data, two of the ten scoping tests were carried out at 60°C. The procedure for these two tests was identical to the tests performed at 90°C. Table X provides information on how each sample was prepared for testing.

Table X: 60°C Scoping Test Parameters

Experiment ID	Sample Wt (g)	HCl Solution (g)	HCl (g)	Time (min)
$5.1g_{HCl}$/RE1	0.51	13.70	5.11	60
$5.1g_{HCl}$/RE4	0.52	13.70	5.11	60

2.2.3. Design Matrix Tests

2.2.3.1. Matrix Parameters

A response surface experimental design matrix for RE1 was prepared using the StatEase software, DesignExpert 9. The matrix consisted of 20 individual experiments, six of which were set as midpoints. The three variables analyzed by the design matrix were reagent concentration (gHCl/0.5g sample), temperature (^{o}C), and leaching time (min). An example of the design matrix used to analyze the extraction of REEs from RE1 is provided below in Table XI. It should be noted that 25°C represents the experiments carried out under ambient conditions.

Table XI: Sample Design Matrix

Experiment No.	HCl Conc. ($g_{HCl}/0.5g_{solids}$)	Temp (^{o}C)	Time (min)	Ce extraction
1	0.2	25.0	30	-
2	10	25.0	30	-
3	0.2	90.0	30	-
4	10	90.0	30	-
5	0.2	25.0	120	-
6	10	25.0	120	-
7	0.2	90.0	120	-
8	10	90.0	120	-
9	0.2	57.5	75	-
10	10	57.5	75	-
11	5.1	25.0	75	-
12	5.1	90.0	75	-
13	5.1	57.5	30	-
14	5.1	57.5	120	-
15	5.1	57.5	75	-
16	5.1	57.5	75	-
17	5.1	57.5	75	-
18	5.1	57.5	75	-
19	5.1	57.5	75	-
20	5.1	57.5	75	-

In addition to Ce extraction, the matrices used to analyze the six samples also included La, Eu, Dy, Nd, Pr, Th, Gd, Fe, and Al extraction values as responses that can be individually analyzed and modeled.

2.2.3.2. Leach Testing

For sample RE1, each experiment was performed according to the specifications listed in the design matrix. For each experiment, approximately 0.5g of sample was leached using 100mL of solution. The 37.35% HCl solution was used to prepare the leach solutions in the same manner as the scoping tests. The masses of RE1 and HCl used in each experiment are provided in Appendix D: Raw Data from Design Matrices**.**

Experiments carried out at ambient temperature were agitated using a shaker table. Elevated temperature experiments were carried out on a hot plate and agitated using a magnetic stirrer. Experiments 5, 6, and 11-15 were performed simultaneously using a large multi-stage Cole-Parmer hot plate. Following leaching, each solution was separated from the remaining solid material via vacuum filtration and was analyzed using ICP-AES. It was decided another four tests were necessary to improve data modeling. Experiment #2, 3, 5, and 8 were carried out to finish the design matrix for RE1. The sixth midpoint experiment (#20) was not carried out for the RE1 design matrix.

The experimental process shown in Table XI was repeated for four RER samples: RE2, RE4, RE5, and RE6. Multiple experiments were performed simultaneously using a shaker table to agitate the experiments carried out at ambient temperature (25°C) and the Cole-Parmer multi-stage hot plate for the experiments at elevated temperatures. For each RER sample, experiments #1, 2, 5, 6, and 11 were run simultaneously on the shaker table. The experiments done at 60°C, experiments #9, 10, 13, and 14, were carried out together using the Cole-Parmer hot plate. The tests done at 90°C, experiments #3, 4, 7, 8, and 12, were also carried out simultaneously on the Cole-Parmer hot plate. The six midpoint experiments, experiments #15-20, were performed together as well. Because of the large number of tests run at 60°C, the six midpoint experiments were performed separately from the other tests done at 60°C to ensure that each midpoint was

subjected to the same set of conditions. Tables showing the masses of RER sample, and the amounts of HCl solution, used in each experiment are provided in Appendix D: Raw Data from Design Matrices. Leach solutions were collected by filtration and all solutions were analyzed using ICP-AES.

2.2.4. Data Modeling and Analysis

Statistical analyses of the data were conducted using the software DesignExpert 9. The extraction factor data from the leaching experiments were entered into the design matrices. The data was analyzed using a central composite response surface method, with face-centered cubic distribution. A transformation model was selected from seven possible options: none, natural log, base ten log, square root, inverse square root, inverse, power, and logit. After a transform model was selected, a model equation was chosen. For the five RER samples modeled in this study, the selected model equation was the quadratic form. The DesignExpert 9 software produced an Analysis of Variance (ANOVA) evaluation of each data set, and a p-test was carried out to evaluate whether the selected model, and the three parameters, were significant.

The ANOVA evaluation and p-test also determined how well a selected model/equation "fit" the experimental data. A model was considered to fit the data if the p-test value was less than 0.05. If the p-test value for a model was greater than 0.05, the model was considered by the program to be significant and the selection process was started over using a new transformation model. This evaluation continued until a model was selected that produced a p-test value less than 0.05. Once a model with a p-test value less than 0.05 was selected, the evaluation process was allowed to continue. The individual factors, temperature, time, and reagent concentration, were considered significant if the p-test values associated with each factor were less than 0.10.

Transform models that possessed a satisfactory ANOVA evaluation were further analyzed using a series of diagnostic evaluations. These diagnostics included plotting normal probability versus internal studentized residuals, predicted versus actual results, externally studentized residuals versus experiment run number, leverage evaluations, and Cook's Distance values.

A final evaluation of each selected model was performed by visually observing the fit of each experimental test result to the selected three-dimensional model surface.

3. Results and Discussion

3.1. Characterization

3.1.1. Mineral Liberation Analysis

From the SEM/MLA work, the mineralogical compositions of the six RER samples were obtained. The major mineral phases and the REE-bearing minerals relevant to this study are presented in Table XII**.** The modal mineralogy of each sample is presented in its entirety in Appendix A: Characterization Data.

Table XII: Abridged Mineralogy of RER Samples

Mineral Name	Mineral Formula	Wt%					
		RE1	RE2	RE3	RE4	RE5	RE6
Ancylite	$Sr(Ce,La)(CO_3)_2(OH)$ •H2O	0.58	0.45	2.28	0.11	0.02	16.68
Bastnasite	$(Ce,La)(CO_3)F$	5.31	5.79	24.83	2.09	0.14	0.05
Cerianite	$(Ce,Th)O_2$	5.88	5.31	0.01	2.19	0.48	0.02
Monazite	$(La,Ce)PO_4$	8.14	5.29	22.30	1.51	0.91	1.21
Parisite	$Ca(Ce,La)_2(CO_3)_3F_2$	8.53	9.37	31.06	3.01	0.66	0.34
Xenotime	YPO_4	0.0009	.0036	0.0000	.0056	0.000	0.000
Iron Oxides	FeO	17.37	1.27	0.11	34.67	13.16	20.44
Feldspar	$KAlSi_3O_8$	4.56	0.32	0.00	2.58	3.32	0.03
Manganese Oxide	MnO	10.41	1.42	19.04	8.25	2.67	1.42
Hollandite	$BaMn_8O_{16}$	6.95	0.05	0.00	3.40	0.86	0.32
Biotite	$K(Mg,Fe)_3(AlSi_3O_{10})(OH)_2$	12.34	1.89	0.00	3.42	9.46	5.84

From the MLA data, it was determined that the REEs exist in the six samples primarily as REE-carbonates and REE-phosphates. Xenotime, which commonly contains trace amounts of

heavy REEs, is present in very small amounts relative to the other mineralogical components. Based on the composition of RE3, it was determined that this sample, due to the high concentrations of REE-bearing minerals and the low levels of other gangue minerals, was most likely a hydrometallurgical precipitate and would not be subjected to leaching in a industrial setting. It was decided that RE3 would not be used in the design matrix experiments as leach solutions produced from RE3 would not be representative of a true leaching process.

3.1.2. X-ray Diffraction

Examples of the spectra produced via Powder XRD for the six RER samples are shown in Figure 4 and Figure 5. Additional XRD spectra are provided in Appendix A: Characterization Data.

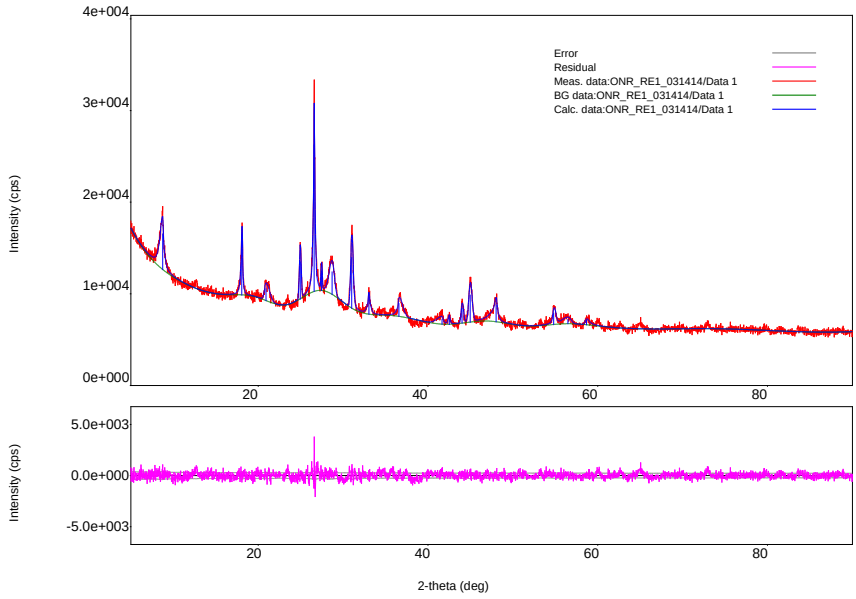

Figure 4: XRD Spectra of RE1 Concentrate

Figure 4 shows the XRD spectra for the concentrate sample, RE1. An example of the XRD spectra for an ore sample, RE4, is shown in Figure 5.

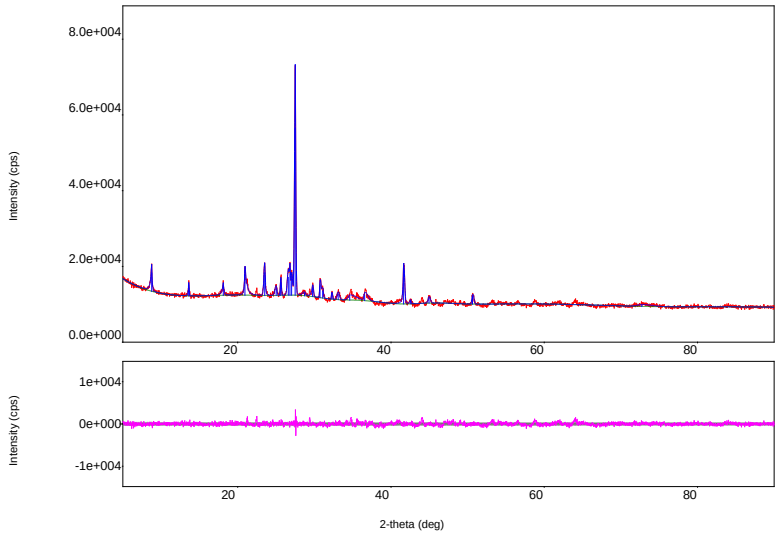

Figure 5: XRD Spectra of RE4 Ore

From the XRD spectra and the reports produced by the PDXL software, it was observed that the major mineral phases identified by MLA were also present. This validated the use of MLA to characterize the RER samples in this series of experiments.

3.1.3. ICP-AES/ICP-MS Fusions

Initial characterization analyses for the six RER samples were performed by Hazen Research Inc. for another graduate research project (Carter, 2013). These data are presented in Table XIII.

Table XIII: ICP Analysis (Hazen Research Inc.)

	Wt%										
Sample	**Ce**	**Dy**	**Er**	**Eu**	**Gd**	**La**	**Nd**	**Pr**	**Sm**	**Tb**	**Yb**
RE1	7.08	0.054	0.018	0.076	0.140	4.79	2.27	0.769	0.450	0.014	0.005
RE2	7.48	0.059	0.020	0.078	0.141	5.32	2.44	0.816	0.460	0.015	0.006
RE3	12.7	0.137	0.041	0.113	0.242	8.96	3.49	1.26	0.652	0.027	0.014
RE4	2.14	0.021	0.008	0.021	0.035	1.39	0.603	0.204	0.119	0.005	0.003
RE5	0.680	0.007	0.003	0.011	0.013	0.416	0.274	0.085	0.061	0.002	<0.001
RE6	3.15	0.014	0.005	0.026	0.035	2.10	0.929	0.321	0.161	0.004	0.001

The Hazen Research ICP data was used to determine extraction factors for the preliminary leach tests. Although the Hazen data provides REE elemental analysis, it does not

allow for the extraction of non-REEs, such as iron, to be analyzed. Non-REE extraction is important to this investigation as gangue elements could affect potential purification and separation of the REEs in solution. Because much of the data for this investigation would be done using the in-house ICP-AES, it was decided that primary elemental analysis of the RER samples should be done using that instrument to maintain consistency.

Primary analysis of the LiB_4 fusions of the six RER samples was done using ICP-AES. The elemental compositions of the six samples are shown in Table XIV**.** It should be noted that Table XIV only contains the elements that were later modeled using DesignExpert9. The full elemental analysis of the RER samples has been included Appendix A: Characterization Data.

Table XIV: Abridged ICP-AES Head Analyses for RER Samples

Sample	**Wt%**								
	Ce	**Dy**	**Eu**	**Gd**	**La**	**Nd**	**Pr**	**Fe**	**Th**
RE1	10.049	0.261	0.130	0.331	9.626	4.446	1.282	18.896	0.252
RE2	10.414	0.278	0.134	0.347	10.573	4.620	1.337	20.150	0.289
RE3	19.253	0.495	0.210	0.661	20.709	7.011	2.133	0.291	-0.033
RE4	2.666	0.084	0.036	0.105	2.806	1.100	0.341	31.187	0.079
RE5	0.930	0.031	0.018	0.047	0.820	0.468	0.139	15.306	0.028
RE6	4.019	0.088	0.041	0.112	4.207	1.598	0.486	20.432	0.055

In addition to the ICP-AES fusions, samples of RE1, RE2, RE4, RE5, and RE6 were sent to MSE Technology Application Inc. for a comparative elemental analysis using inductively coupled plasma-mass spectroscopy (ICP-MS). The ICP-MS analysis only accounted for the REEs and Th. The weight percent values for the elements modeled using DesignExpert 9 are presented in Table XV**.** The full ICP-MS analysis is available in the Appendix A: Characterization Data.

Table XV: Abridged ICP-MS Head Analyses for RER Samples (MSE Laboratory)

Sample	Wt %							
	Ce	**Dy**	**Eu**	**Gd**	**La**	**Nd**	**Pr**	**Th**
RE1	6.254	0.045	0.082	0.169	6.176	2.997	0.717	0.192
RE2	5.416	0.044	0.072	0.148	5.673	2.613	0.630	0.174
RE4	1.463	0.012	0.019	0.042	1.460	0.621	0.148	0.068
RE5	0.550	<MDL*	0.011	0.021	0.493	0.293	0.063	0.041
RE6	1.653	<MDL*	0.018	0.033	1.689	0.735	0.175	0.034

*<MDL indicates concentration was below the minimum detection limit (MDL).

The analysis by ICP-AES produced higher values for REE concentration than the ICP-MS. However, the values for the various REEs are following similar trends between the two characterization methods. These differences were observed to increase as the values decrease in amount. For example, the values for Dy vary much more dramatically between methods than the values for Nd. The amount of variance is most likely due to detection issues such as interferences from other elements in solution. Accurate characterization of REEs has been known to be notoriously difficult due to their similar physical and chemical properties (Kang, Ting, & Eyring, 1992). The initial solid elemental compositions used in all subsequent calculations for the amount of REE leached have been based on the ICP-AES data previously presented.

3.2. Preliminary Leach Tests (Proof of Concept)

Results for the preliminary leach tests using 1.0M HCl, HNO_3, and 18MΩ H_2O were obtained using ICP-AES. Due to the inherent interferences associated with characterizing REEs, extraction results are presented as “Extraction factors”. Extraction factors were defined as a ratio of solution concentration to the concentration in the LiB_4 fusion samples. REE characterization by ICP-AES can experience a number of elemental interferences depending on the purity of the sample. The numbers of different REEs in the ore and concentrate samples, combined with the number of non-REE gangue minerals, produce a scenario where analysis by ICP-AES could experience interferences from competing elements. These competing elements can alter the measurement of REE concentrations in solution, producing values that are erroneously low or

high. However, the data can still be used to produce, and identify, trends in the concentrations of REEs and other elements in solution. These extraction factors are semi-quantitative and are presented to define trends in REE extraction behavior. Results for the 25°C HCl leach tests are presented in Table XVI.

Table XVI: REE Extraction Factors for Preliminary HCl Leach Tests (25°C)

Sample ID	Ce	Dy	Er	Eu	Gd	La	Nd	Pr	Sm	Tb	Yb
RE1	0.104	0.842	0.540	0.288	0.370	0.337	0.352	0.260	0.231	0.248	0.221
RE2	0.099	0.703	0.456	0.252	0.333	0.287	0.300	0.224	0.206	0.168	0.190
RE3	0.733	1.904	0.787	1.143	1.323	1.323	1.003	1.114	0.863	337.086	1.002
RE4	0.157	0.887	1.796	0.378	0.580	0.365	0.437	0.435	0.323	120.034	0.215
RE5	0.216	1.609	10.672	0.454	0.959	0.519	0.611	0.605	0.413	143.158	0.302
RE6	0.621	3.006	6.153	0.935	1.371	1.137	0.872	0.992	0.732	472.088	0.984

Table XVII contains the extraction factors for the leach tests carried out at 25°C using HNO_3 as the leaching reagent.

Table XVII: REE Extraction for Preliminary HNO_3 Leach Tests (25°C)

Sample ID	Ce	Dy	Er	Eu	Gd	La	Nd	Pr	Sm	Tb	Yb
RE1	0.101	0.867	0.374	0.275	0.372	0.218	0.310	0.296	0.231	96.145	0.214
RE2	0.119	0.789	0.349	0.277	0.372	0.233	0.282	0.284	0.225	94.636	0.212
RE3	0.667	1.731	0.602	1.043	1.186	1.217	0.913	1.020	0.790	303.925	0.894
RE4	0.186	0.852	1.325	0.409	0.597	0.383	0.422	0.428	0.338	109.710	0.229
RE5	0.257	1.698	11.836	0.526	1.064	0.559	0.654	0.644	0.474	138.533	0.305
RE6	0.532	2.541	4.155	0.800	1.145	0.982	0.736	0.846	0.629	392.910	0.822

The control group experiments used 18MΩ H_2O as the leaching agent. The results all tests using H_2O are presented in Appendix B: Proof-of-Concept H_2O Leach Test Results.

From the room temperature tests, it can be seen that the HCl and HNO_3 leach tests were much more successful at leaching REEs from the RER samples than the H_2O leach tests. This behavior was expected as most REE leaching operations are carried out under acidic conditions. Both the HCl and HNO_3 leach tests contain very high extraction factors for many of the REEs, especially Tb and Er. Extraction factors of this magnitude are not realistically feasible and are due to interferences as well as Tb, Dy, and Er being present in the RER samples in quantities

near the detection limit of the instrument. At ambient temperature (25°C), there is little difference between the amounts of REEs extracted using HCl or HNO_3. Without additional input from increased temperatures, both monoprotic acids will behave in a relatively similar manner.

Table XVIII shows the extraction factors for the 60°C HCl leach tests.

Table XVIII: REE Extraction for Preliminary HCl Leach Tests (60°C)

Sample ID	Ce	Dy	Er	Eu	Gd	La	Nd	Pr	Sm	Tb	Yb
RE1	0.56	2.00	4.79	0.74	0.56	0.94	1.04	0.72	0.69	299.35	0.56
RE2	0.47	1.86	2.93	0.70	0.57	0.86	0.93	0.66	0.63	284.03	0.49
RE3	0.73	1.73	0.79	0.92	0.63	1.08	1.28	0.82	0.89	336.25	0.80
RE4	0.45	1.53	6.21	0.72	0.71	0.92	1.01	0.71	0.67	237.02	0.41
RE5	0.54	2.24	78.33	0.81	1.21	1.14	1.12	0.83	0.72	218.52	0.47
RE6	0.64	2.86	14.63	0.76	0.42	0.97	1.14	0.77	0.80	473.80	0.82

Extraction factors from the 60°C HNO_3 leach tests are presented in Table XIX.

Table XIX: REE Extraction Factors for Preliminary HNO_3 Leach Tests (60°C)

Sample ID	Ce	Dy	Er	Eu	Gd	La	Nd	Pr	Sm	Tb	Yb
RE1	0.63	2.15	4.18	0.81	0.58	0.97	1.13	0.77	0.75	307.42	0.61
RE2	0.57	1.95	3.23	0.75	0.55	0.89	1.02	0.71	0.70	292.00	0.53
RE3	0.66	1.60	0.59	.84	0.56	0.97	1.18	0.74	0.80	300.33	0.75
RE4	0.44	1.34	5.18	0.64	0.60	0.81	0.92	0.63	0.60	206.29	0.40
RE5	0.66	1.98	81.23	0.73	0.93	0.99	1.04	0.75	0.72	191.85	0.47
RE6	0.58	2.67	13.75	0.70	0.37	0.86	1.03	0.71	0.75	423.21	0.74

As expected, the H_2O leach tests extracted little to no REEs from the RER samples. Both the HCl and HNO_3 leach tests produced significantly higher extraction factors when compared to both the 60°C H_2O leach tests as well as the HCl/HNO_3 leach tests carried out at 25°C. These extraction factors indicated that temperature has an effect on the extraction of REEs and could be implemented to improve REE extraction. Like the 25°C leach tests, there was little difference between the extraction factors associated with HCl and HNO_3. After analyzing the data, it was decided that HCl would be the focus of further experimentation as it performed as well as HNO_3 while being a better choice for producing “realistic” leach solutions. HCl is already used in many REE leaching operations and it is industrially preferred over HNO_3 due to the cost of the reagent and its highly corrosive nature.

3.3. Scoping Tests

Using the data obtained from the scoping tests and the LiB_4 fusions, it was possible to produce an "extraction factor" for the various elements. This extraction value is a ratio of the REE weight percent found in the leach solutions divided by the REE weight percent found in the solid sample fusions. Weight percent values were calculated from ICP-AES data using the following equation:

$$(A \times V/(M/(1000\ g/kg)) \times D)/10{,}000 = Wt\ \%\ REE \tag{8}$$

Where A represents the ICP-AES measurement of REE concentration in mg/L, V represents the volume of solution produced in L, M represents the mass of the solid sample leached in grams, and D represents the factor of dilution.

For the LiB_4 fusions, V was set at 50 mL (0.05 L) and the dilution factor (D) was set at 2. The leach test weight percent values were calculated using 100 mL (0.1 L) for V and a dilution factor of 5. Extraction factors were calculated by taking a ratio of the REE weight percent in the leach solution to the REE weight percent in the unleached solid samples found using the LiB_4 fusion data. This relationship is equivalent to a measurement of recovery and is expressed by the equation:

$$Ext\ Factor = \frac{Wt\%_{Leach}}{Wt\%_{solid}} \tag{9}$$

The extraction factors from the scoping tests are presented in following bar graphs for each element.

3.3.1. Cerium (Ce)

Bar graphs of Ce extraction factors for each of the scoping tests using RE1 and RE4 are shown in Figure 6 and Figure 7 respectively.

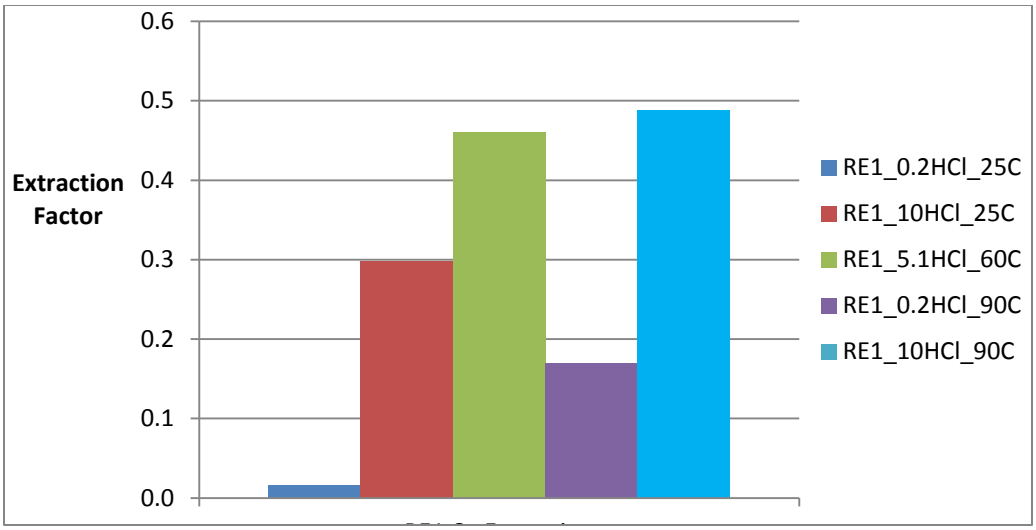

Figure 6: RE1-Ce Extraction

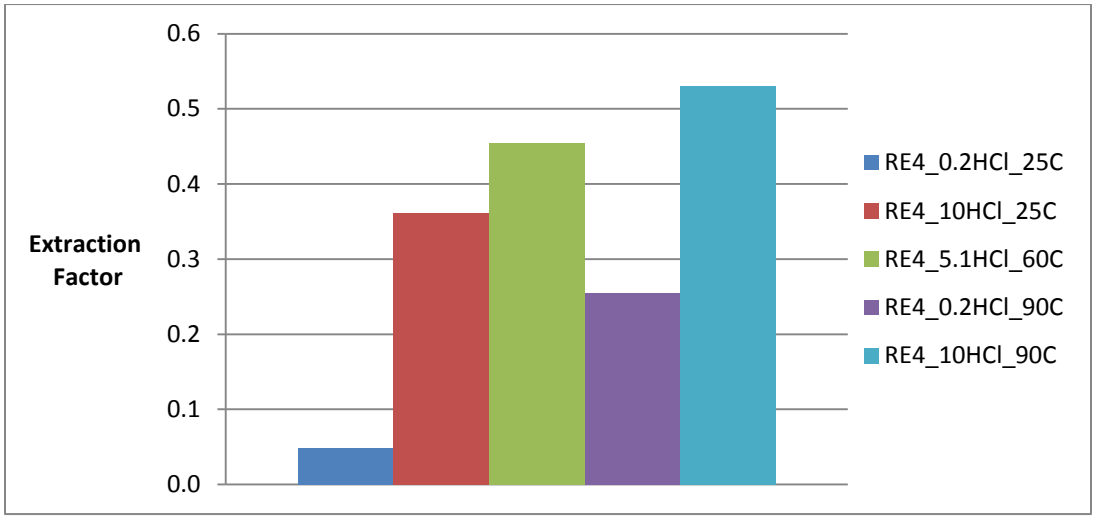

Figure 7: RE4-Ce Extraction

The extraction data for cerium indicates that chloride concentration is an important factor. The higher HCl concentrations produced a significantly higher extraction of Ce than the solutions of 0.2 g_{HCl}/0.5g solids. Temperature also increases Ce dissolution. This behavior can be observed in both the ore (RE4) and the concentrate (RE1). Solutions produced by leaching at elevated temperatures resulted in significantly greater Ce extraction than solutions with identical

concentrations of HCl that were part of ambient temperature leaching experiments. There is relatively little variation in extraction between the ore and the concentrate.

3.3.2. Dysprosium (Dy)

The results of the scoping tests for the extraction of Dy from RE1 are shown in Figure 8.

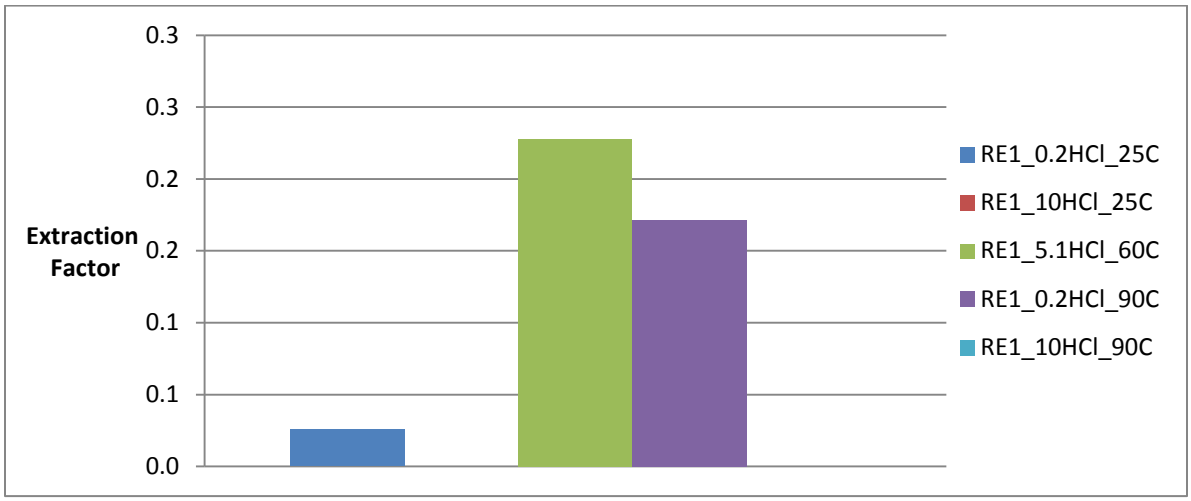

Figure 8: RE1- Dy Extraction

Graphs of the results from the scoping tests using RE4 are shown in Figure 9.

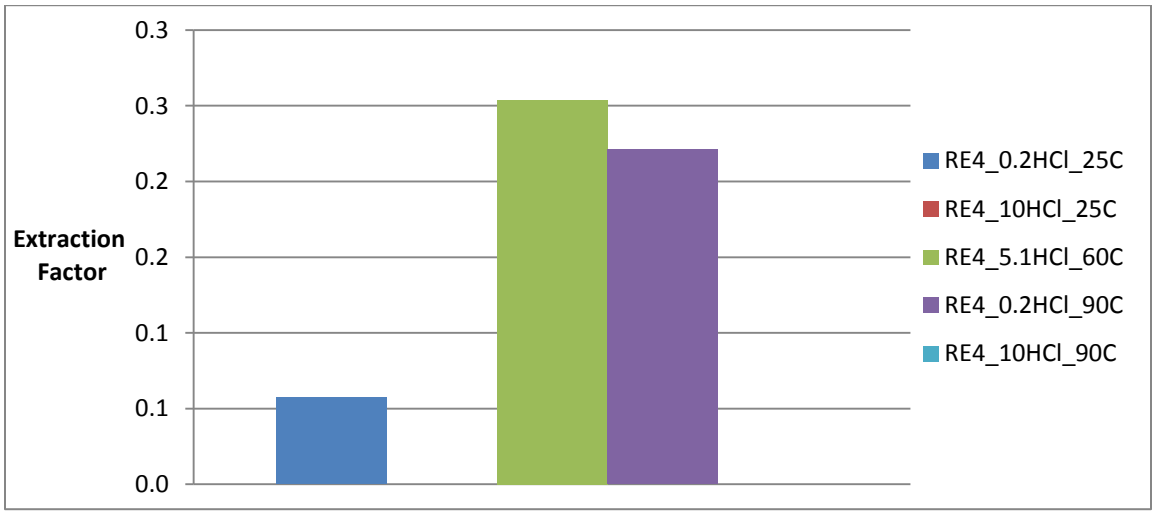

Figure 9: RE4- Dy Extraction

Like Ce, there is little variation in extraction of Dy when comparing the ore to the concentrate. The ore even appears to have slightly higher extraction values than the concentrate. However, the behavior of Dy is radically different from the other elements being analyzed as extraction drops to zero at high HCl concentrations. Temperature appears to improve concentration as extraction using 0.2g HCl increased at 90°C. Oversaturation of the solution with HCl may be creating a system where competition between ions is too great, causing the sudden decrease in Dy dissolution.

3.3.3. Europium (Eu)

Eu extraction factors for each of the scoping tests involving RE1 leaching are shown in Figure 10 and Figure 11 respectively.

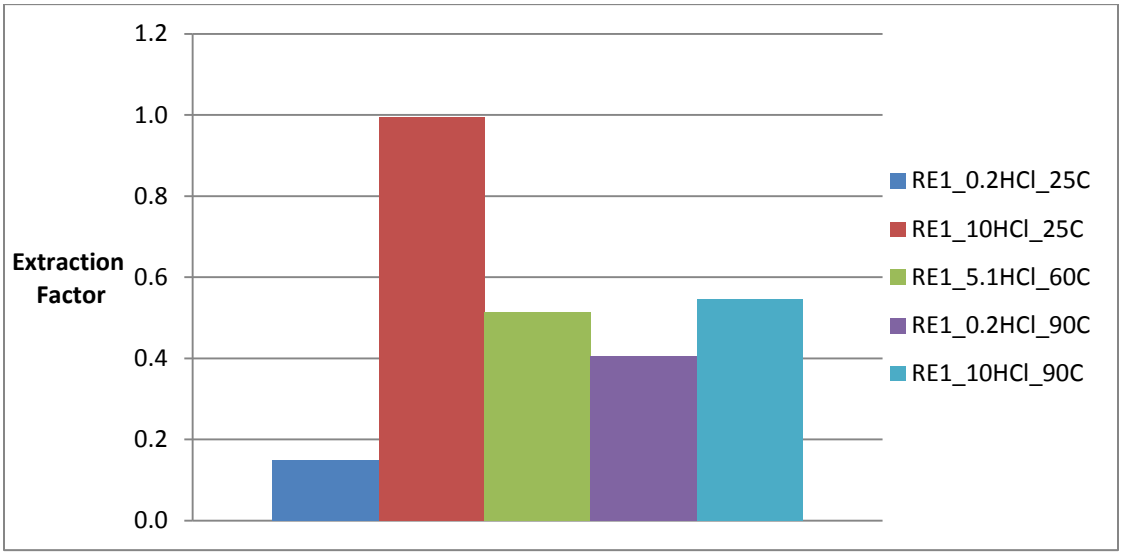

Figure 10: RE1-Eu Extraction

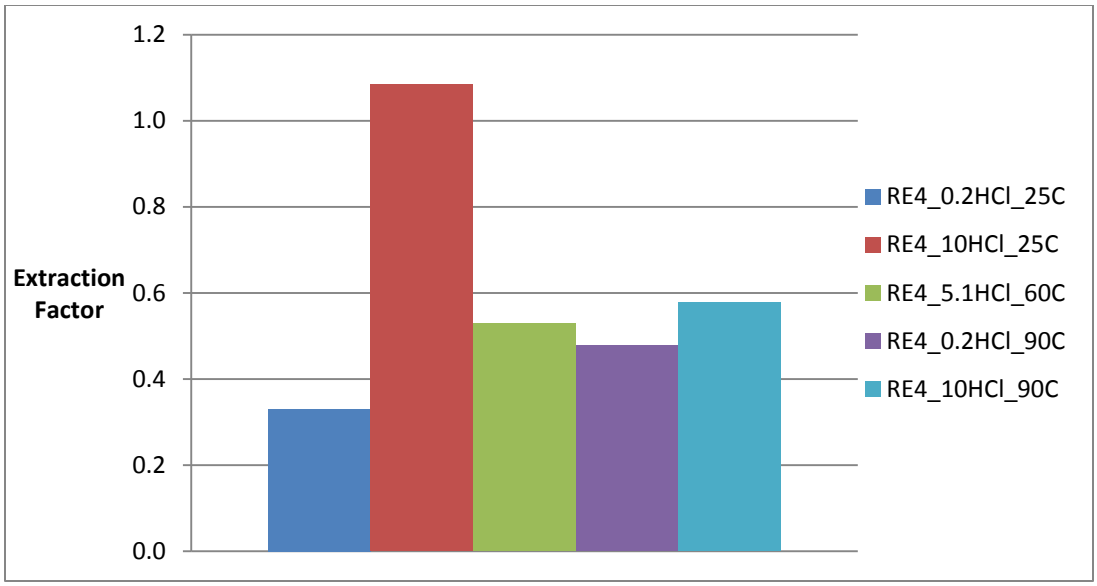

Figure 11: RE4-Eu Extraction

Europium is another element that appears to experience better extraction from the ore compared to the concentrate used in the scoping tests. In both the ore and the concentrate data, the greatest amount of extraction seemed to occur at room temperature with 10 g_{HCl}/0.5g of solids.

3.3.4. Gadolinium (Gd)

The results for Gd extraction from the RE1 scoping tests are shown in Figure 12.

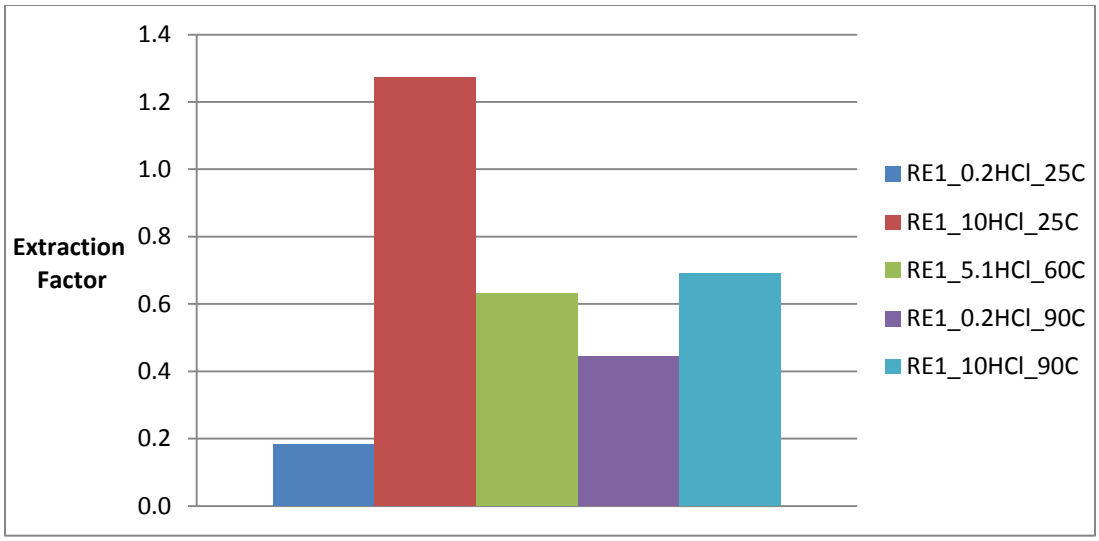

Figure 12: RE1-Gd Extraction

Gd extraction results from the RE4 scoping tests are shown in the graphs in Figure 13.

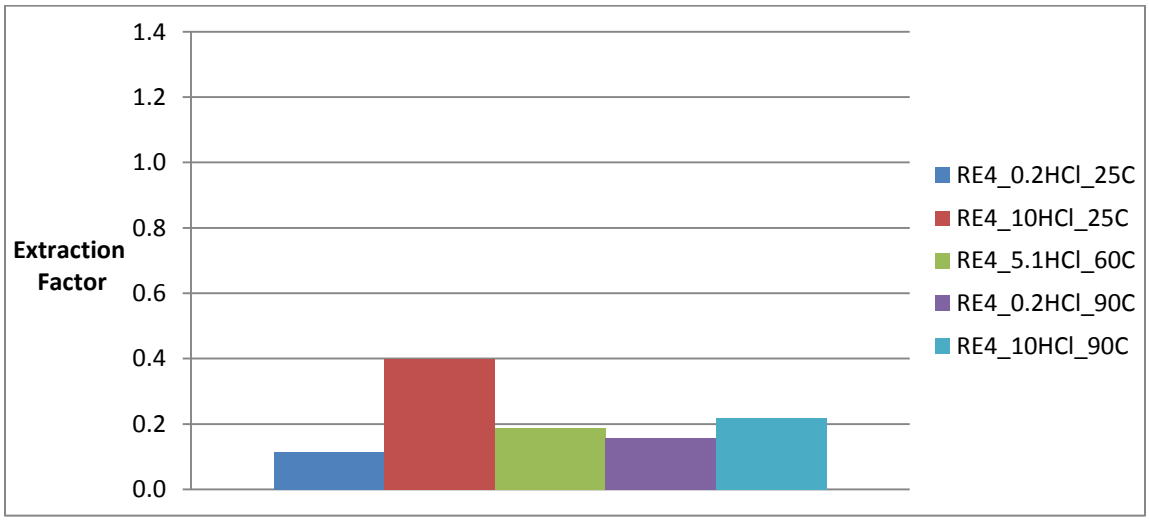

Figure 13: RE4-Gd Extraction

Unlike europium, gadolinium experiences a dramatic increase in extraction from the concentrate sample compared to the ore sample. In both samples, extraction increases rapidly when the concentration of HCl is increased from 0.2 g to 10 g at 25°C. However, the tests carried out at 90°C produced less extraction than the 10 g HCl test done at room temperature. The results

of these experiments are an indication that HCl concentration may play a greater role in Gd extraction than temperature.

3.3.5. Lanthanum (La)

The results for La extraction from the RE1 scoping tests are shown in Figure 14.

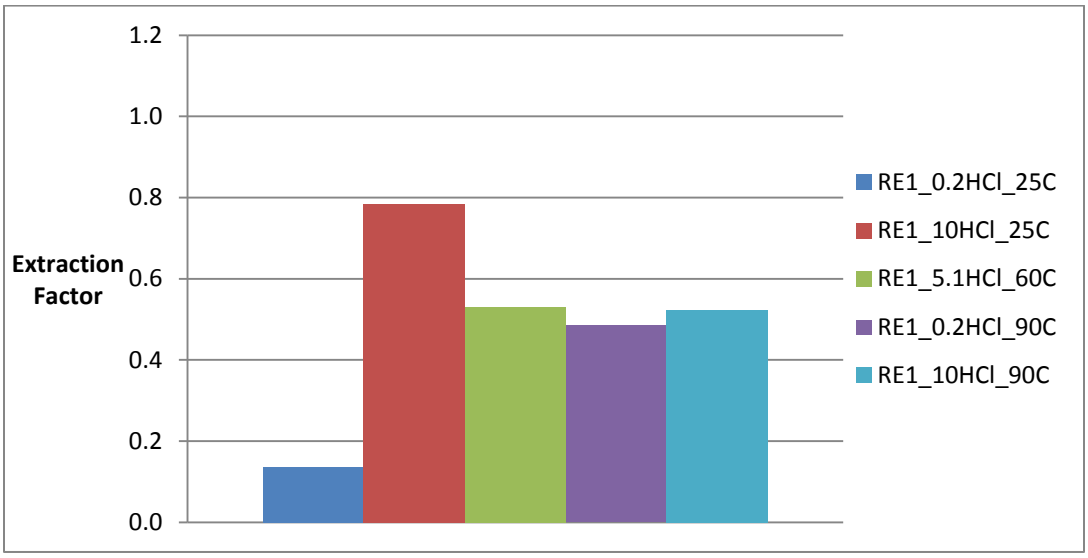

Figure 14: RE1-La Extraction

La extraction results from the RE4 scoping tests are shown in the graphs in Figure 15.

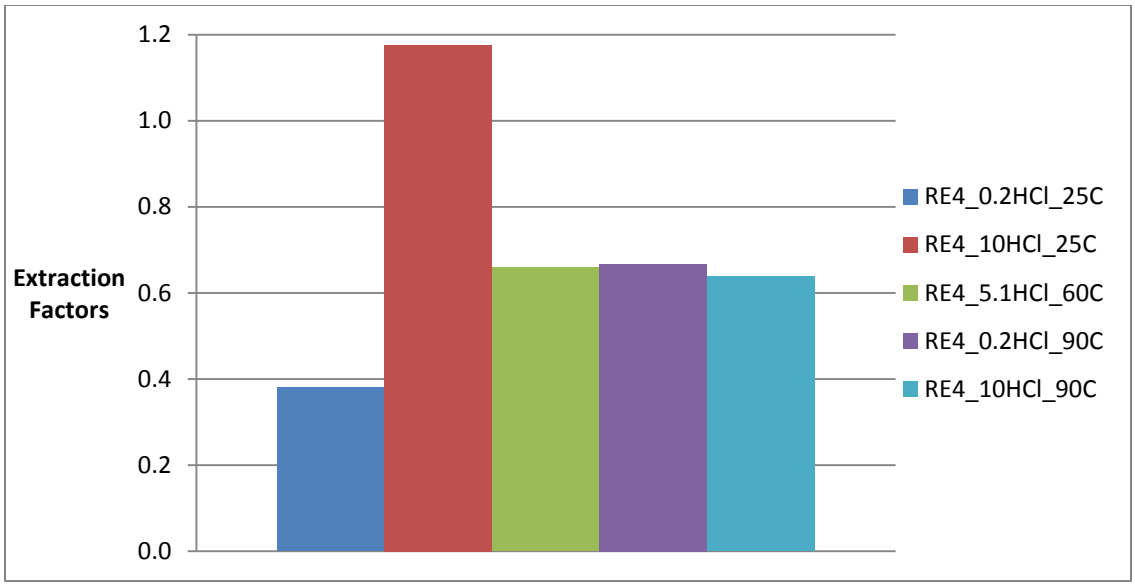

Figure 15: RE4- La Extraction

The extraction data for lanthanum shows that, although both sample types produced similar trends for lanthanum extraction, the ore sample produced higher extraction values than the concentrate sample. Like many of the other analyzed elements, Gd, Eu, Lu the experiment that produced the highest extraction value involved the solution containing 10 g_{HCl}/0.5g of solids at 25°C. Experiments involving similar concentrations and higher operating temperatures only produced extraction values of roughly half that of the largest extraction factor.

3.3.6. Lutetium (Lu)

The results of the scoping tests for the extraction of Lu from RE1 are shown in Figure 16.

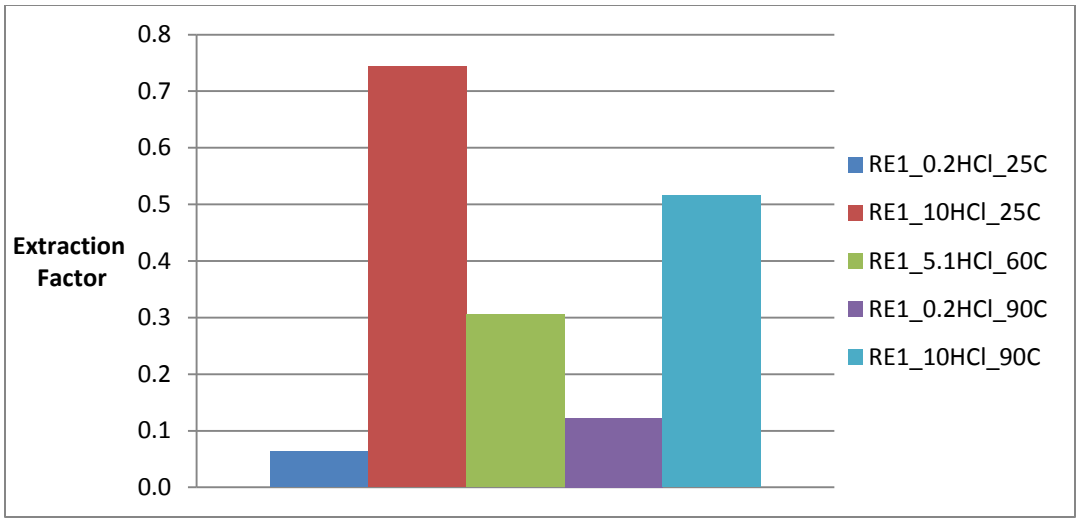

Figure 16: RE1-Lu Extraction

Figure 17 shows the graphs of Lu extraction from the RE4 scoping tests.

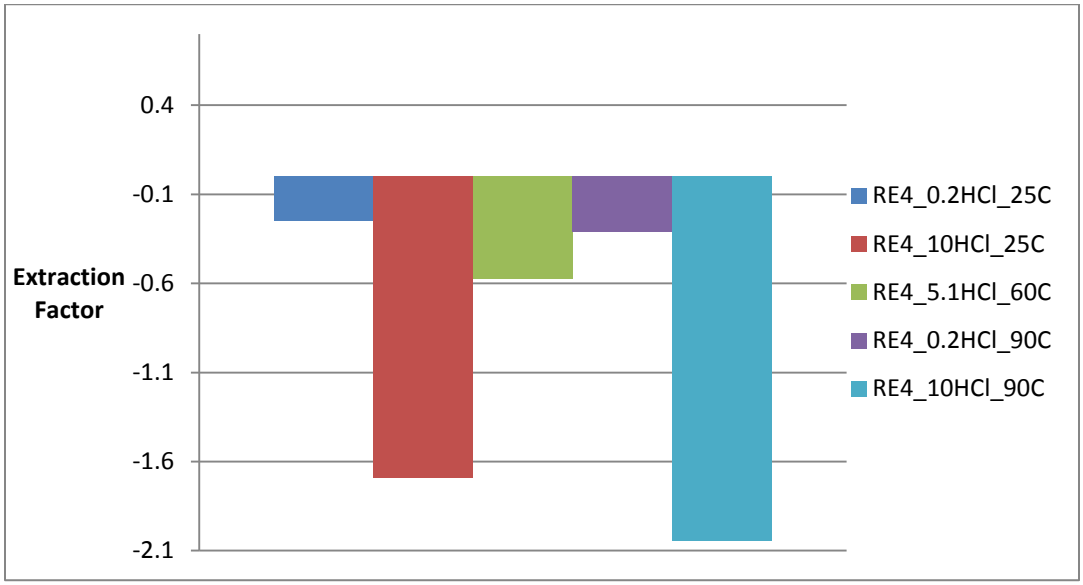

Figure 17: RE4-Lu Extraction

The results for Lutetium from the two series of scoping tests are interesting as the extraction factors for the ore sample are negative. These results are most likely due to the fact that the values for Lu found during the LiB_4 fusions were below the detection limit for the

instrument. This is not the case, however, with the values for Lu found in the concentrate sample, indicating that producing a REE concentrate does improve the recovery of certain REEs, especially those present in very small amounts. In reference to the concentrate data, the best value for extraction was produced by 10 g of HCl and an operating temperature of 25°C.

3.3.7. Composite Graphs

Bar charts containing graphs of the extraction of each element were produced for each of the scoping tests in order to analyze the overall effects of each group of parameters. Each series of bar graphs is organized according to reagent concentration, and temperature. Only the graphs for the RE4 scoping tests are shown in this section. A set of similar figures were prepared for the RE1 scoping tests results and are presented in Appendix C: RE1 Scoping Tests - Composite Graphs. Extraction factors are presented in Figure 18 for RE4 at ambient temperature using 0.2 $g_{HCl}/0.5g_{solids}$.

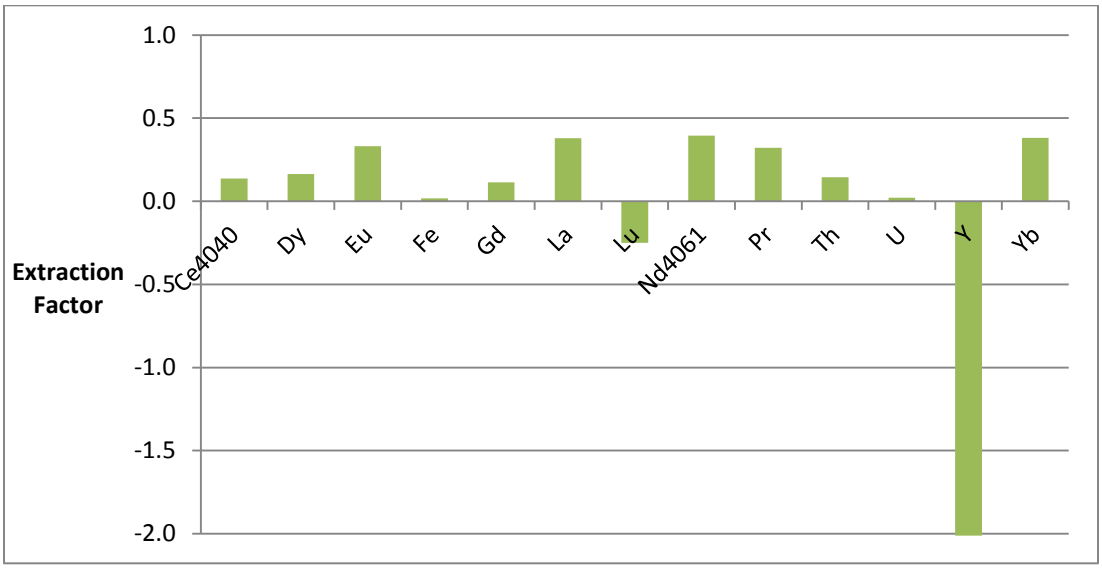

Figure 18: RE4-REE Extraction (0.2 g HCl, 25°C)

Figure 19 shows a similar series of graphs for the extraction factors for the RE4 scoping tests at ambient temperature using 10 $g_{HCl}/0.5g_{solids}$.

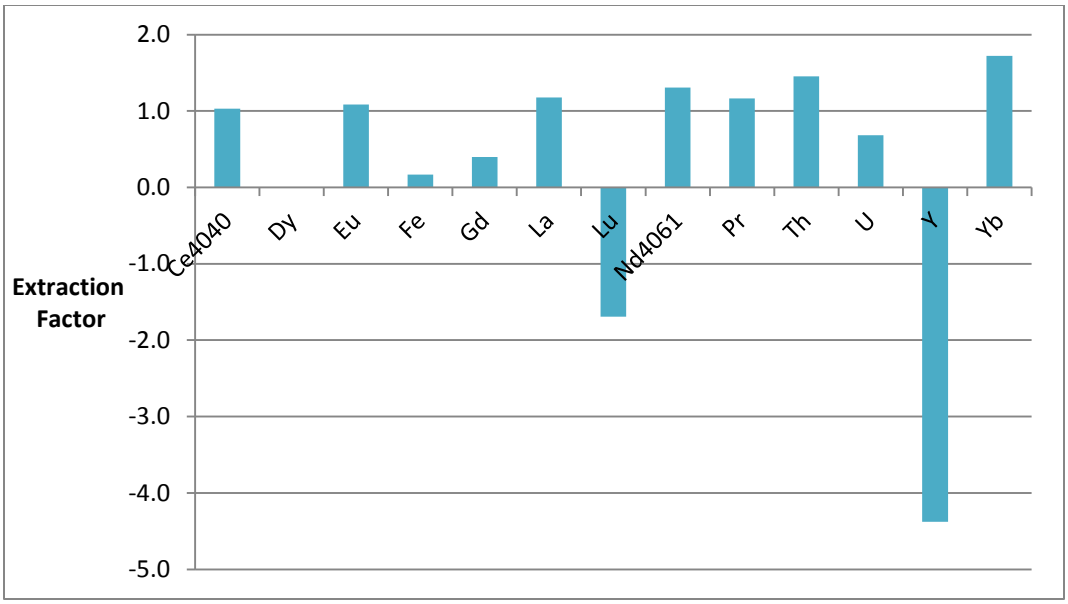

Figure 19: RE4-REE Extraction (10g HCl, 25°C)

The extraction results for the scoping test carried out at 60°C using 5.1 $g_{HCl}/0.5g_{solids}$ are presented in Figure 20.

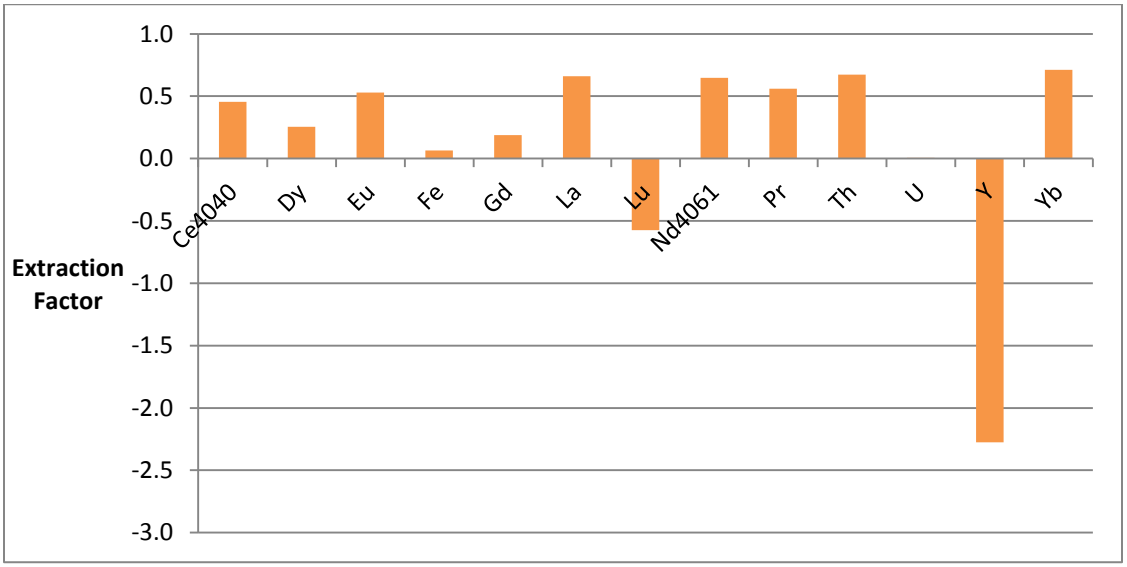

Figure 20: RE4- REE Extraction (5.1g HCl, 60°C)

A graph of the extraction factors for the RE4 scoping test done at 90°C using 0.2 $g_{HCl}/0.5g_{solids}$ is shown in Figure 21.

Figure 21: RE4- REE Extraction (0.2g HCl, 90°C)

Figure 22 shows the series of graphs of the results for the RE4 scoping test done at 90°C using 10 $g_{HCl}/0.5g_{solids}$.

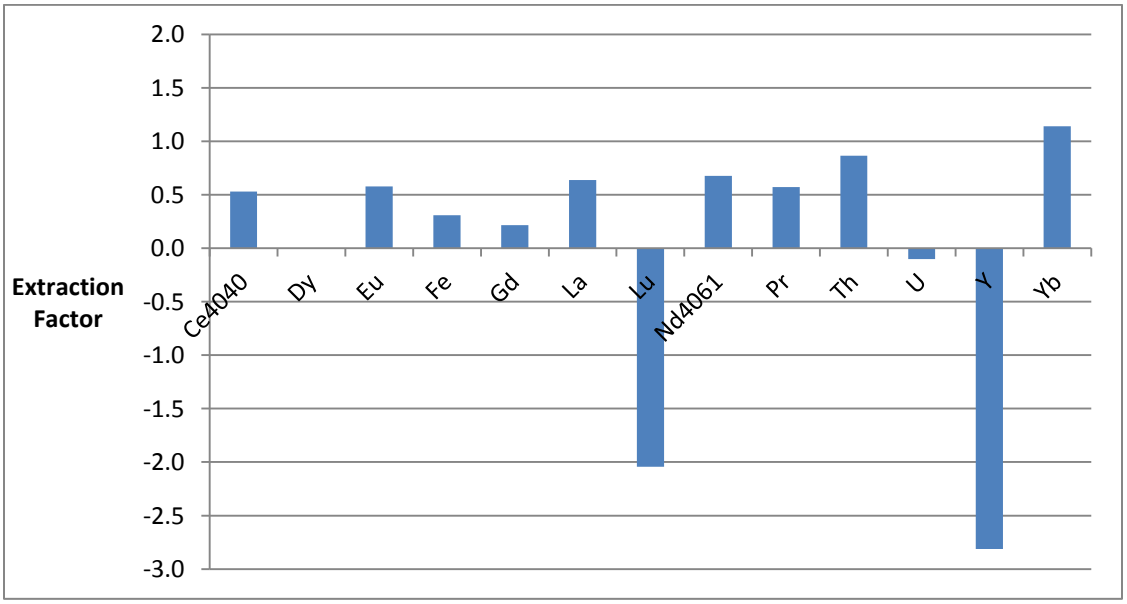

Figure 22: RE4-REE Extraction (10g HCl, 90°C)

From these graphs, it is possible to observe that the various elements respond differently to the variety of conditions. Enough variation is present between the different scoping tests that it is possible to conclude that 0.2 g and 10 g HCl would serve as suitable high and low boundaries for a statistical design matrix.

These graphs also show the amount of variation present in extraction factors under high and low temperatures and reagent concentrations. The amount of variation indicates that it is possible to affect REE extraction by changing the given parameters. Had there been no variation in the extraction factors for the various REEs, the chosen values for the upper and lower boundaries would have to have been reconsidered. A statistical design matrix was used to optimize extraction.

3.4. Design Matrix Leach Testing

The leach solutions from the design matrix experiments were analyzed using ICP-AES. Extraction factors for Al, Fe, Ce, La, Nd, Dy, Gd, Eu, Pr, and Th were produced for each of the five RER samples. Tables of the data from the individual design matrix experiments are presented in full in Appendix D: Raw Data from Design Matrices.

3.5. Extraction Modeling/Optimization

Due to the data compiled from the design matrices, it was decided that optimization of REE extraction should be presented on a single REE rather than attempting to incorporate all of the REEs present in the Bear Lodge samples. Europium was selected as the primary REE for optimization using DesignExpert 9 due to its value on the world market, its potential for military application, and the quality of the extraction data produced by ICP-AES. Statistical models for Al, Fe, Ce, La, Nd, Dy, Gd, Pr, and Th were also generated. The models and diagnostic graphs for the other analyzed elements are presented in Appendices E-I.

The following sections contain the modeling results for Eu extraction from each of the ore and concentrate samples, a statistical evaluation of each model, and a range of conditions at which Eu extraction was optimized. The extraction of the remaining REEs, iron, and, to a lesser extent, thorium, were all considered when selecting conditions for maximum Eu extraction. The ability to extract other REEs is critical for any REE leaching operation. Although this series of experiments was optimized for Eu extraction, the effect that Eu-optimization would have on the extraction of other REEs was important to consider. In addition to the extraction of REEs, another concern was the amount of gangue elements (such as Fe and Th) being leached into solution with the REEs. The presence of gangue elements in the leach solution can be problematic to separation stages that take place after leaching has been carried out. Iron, for example, is a very reactive metal and will interfere with solvent extraction and ion exchange operations by reacting with the organic extractant in place of the REEs or by binding to the resin substrate and fouling the ion exchange resin.

3.5.1. RE1- Eu Extraction

The extraction of Eu from RE1 was modeled using a power transform ($\lambda = 0.16$) combined with a modified quadratic relationship. An equation for Eu extraction was produced by DesignExpert 9 which describes extraction as a function of the experimental variables:

$$(Eu\ ext)^{0.16} = 0.475 + 0.081C + 4.122 \times 10^{-3}T - 3.075 \times 10^{-4}CT - 4.410 \times 10^{-3}C^2 \quad (10)$$

where C represents reagent concentration in grams of HCl per half-gram of solid sample ($g_{HCl}/0.5g_{solids}$) and T represents temperature in degrees Celsius (^{o}C).

From the equation, it is possible to observe that time does not have an effect on the leaching of Eu from RE1 within the established parameters. Eu extraction is a function of temperature and acid concentration.

The response surface graph of Eu extraction from concentrate RE1 is shown in Figure 23. Temperature and reagent concentration are plotted on the x and y axes and the extraction factor for Eu is plotted on the z-axis. Time is held constant at 75 minutes. Temperature is expressed in units of degrees Celsius (^{o}C) and reagent concentration is expressed in units of grams of HCl per half-gram of sample ($g_{HCl}/0.5g_{solids}$). The red dots on the graph represent the individual design matrix experiments that were used to produce the response surface.

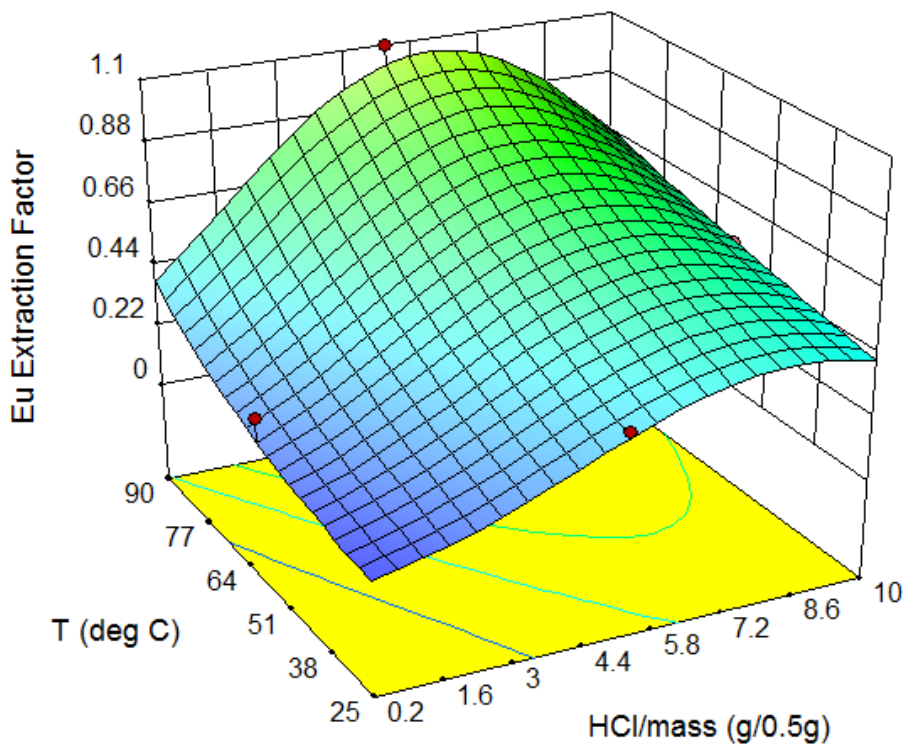

Figure 23: RE1- Eu Extraction Response (75min)

The nonlinear shape of the response surface curve indicates that optimization of Eu extraction should be possible using this set of variables. The response curve contains a region of

increased extraction beginning at an HCl concentration of approximately 4 $g_{HCl}/0.5g_{solids}$ and a temperature of 75°C. However, Eu extraction begins to decline after a reagent concentration of approximately $7.5g_{HCl}/0.5g_{solids}$ is reached. Higher temperatures, coupled with increasing reagent concentration, also decreased the amount of Eu extracted.

For this series of experiments, “good” extraction was determined to have been achieved with extraction factors of 0.5 or greater. For the extraction of Eu from RE1, the region where good extraction is feasible is narrow, however the amount of Eu extracted was the highest value observed for all of the ore and concentrate samples.

Figure 24 shows a contour plot of Eu extraction. Like the response surface curve, the effect of temperature and reagent concentration on Eu extraction is shown on the plot. The blue regions of the contour plot represent regions of poor extraction (<0.5). Improved extraction is represented by a transition to the green colored regions. The decrease in extraction at high reagent concentration can be seen on the far right edge of the contour plot.

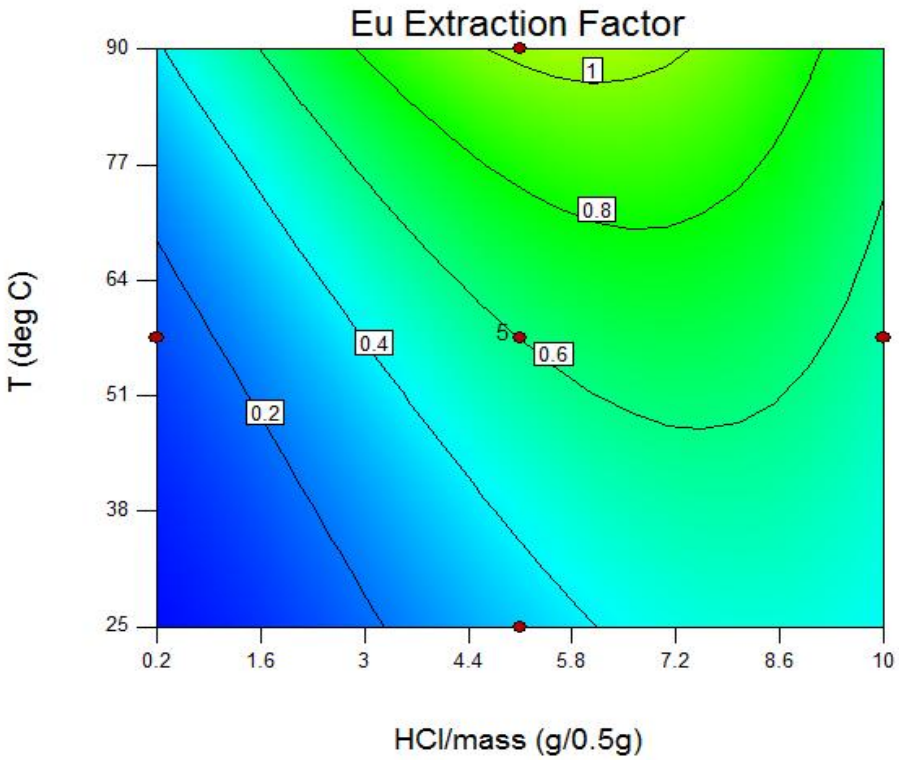

Figure 24: RE1- Eu Extraction Contour Plot (75min)

An evaluation of how well each model fit the experimental data was carried out using a series of diagnostics automatically performed by the software. Figure 25 shows a graph of the values predicted by the model compared to the experimental data. Ideally, the experiments would produce data that is identical to values predicted by the model. The solid line represents the theoretical predicted values, while the individual data points are the extraction values for Eu obtained using ICP-AES.

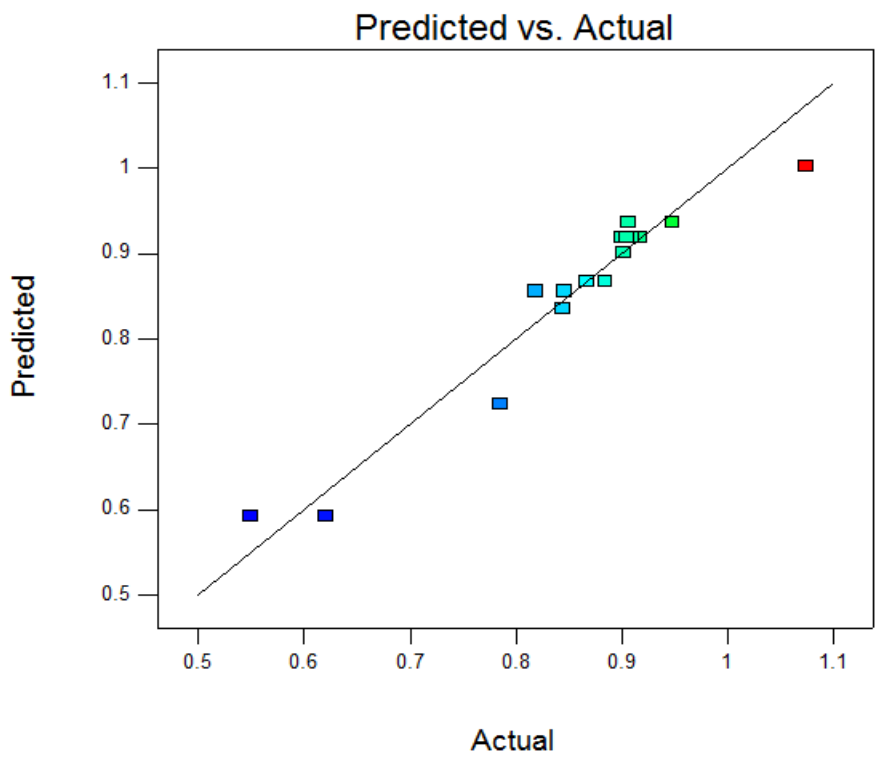

Figure 25: RE1- Predicted vs. Actual Diagnostic of Eu Extraction Model

The experimental results are in relative agreement with the predicted values from the modeling equation. Some deviation does occur, but the overall trend of the data shows a reasonable fit.

A graph of the Cook's Distance analysis is presented in Figure 26. The Cook's Distance analysis is a measurement of a data point's influence on the overall regression analysis. A data point with a large Cook's Distance value would indicate that the data point has a very large influence on how the model fits the data and said data point could be an outlier if the amount of influence is excessive. Excessive influence from one data point will result in an improper model being used to fit the data. Cook's distance values less than "1" are considered acceptable for the DesignExpert 9 analysis. Run numbers for each individual experiment are plotted on the x-axis

and the Cook's Distance values for each experiment's Eu extraction factor are plotted on the y-axis.

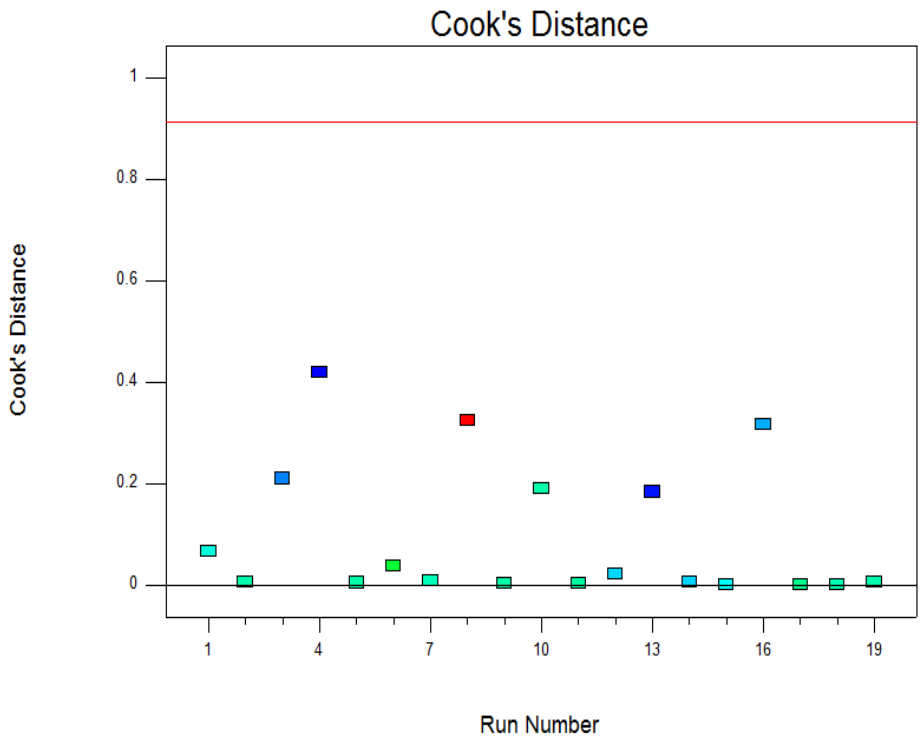

Figure 26: RE1- Cook's Distance Diagnostic of Eu Extraction Model

The Cook's Distance analysis further supports the use of Equation (10) for modeling Eu extraction. The Cook's Distance values for all of the extraction factors are small and are within the acceptable range (i.e. all data points fall below the red line shown near the top of the graph). This diagnostic indicates that none of the extraction factors should be considered outliers and that no single data point has provided excessive influence on the overall fit of the model.

A normal probability plot for Eu extraction is presented in Figure 27. The normal probability plot diagnostic determines how well the experimental data fits a normal distribution. The more that a data trend resembles a normal distribution, the better fit of the model used to predict extraction.

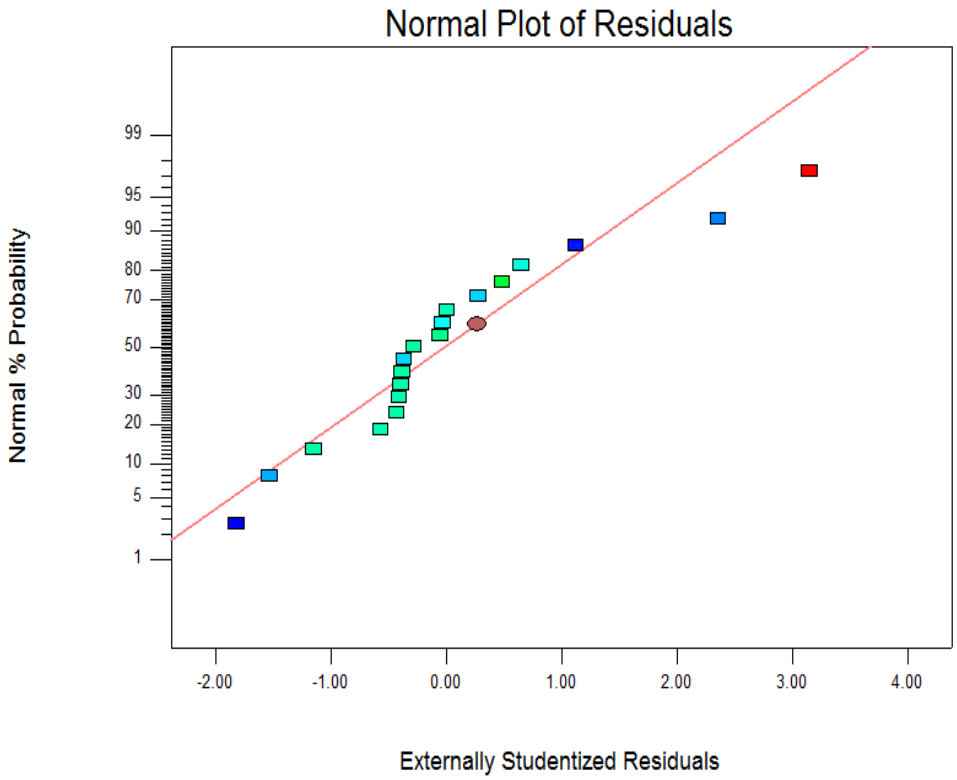

Figure 27: RE1- Normal Plot Diagnostic of Eu Extraction Model

The diagonal line represents the ideal normal distribution for the Eu extraction data. Although deviation from this line does occur, the overall trend of the data still follows that of a normal distribution. This diagnostic indicates an acceptable fit of the model.

With the verification of the extraction model, optimization of REE extraction from the RE1 concentrate could be carried out. Using Eu extraction as the primary REE response for optimization, an optimization graph based on Eu extraction was produced. This plot, presented in Figure 28 shows the region in which a value for Eu extraction greater than 0.5 could be achieved, while, at the same time, the extraction of Fe could be minimized. It should be noted that an extraction factor equates to 50% of the Eu being leached into solution.

HCl concentration is plotted on the x-axis while temperature is plotted on the y-axis. The yellow region indicates the range of conditions that will achieve Eu extractions greater than 0.5. Time is held constant at 30 minutes.

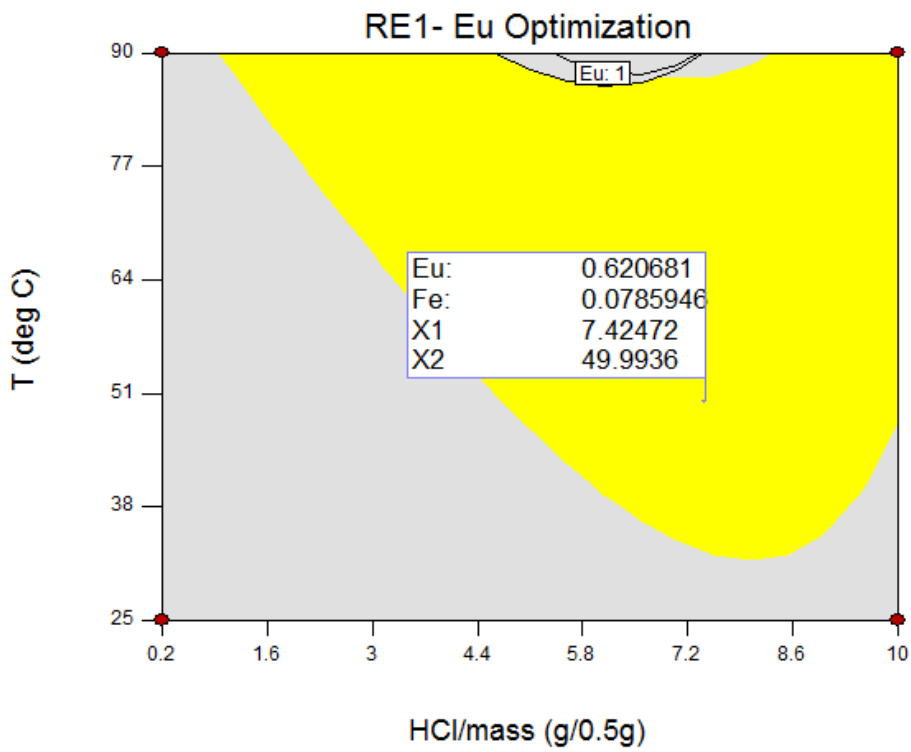

Figure 28: RE1- Optimization Region of Eu Extraction (30min)

From the graph, it is possible to observe that the range of conditions capable of achieving Eu extraction factors greater than 0.5 is relatively large. The flag present in the optimized range shows the approximate values for a set of conditions that would provide sufficient Eu extraction while minimizing Fe extraction and the amount of reagent and heat required. The values for reagent concentration and temperature are also shown on the flag as X1 and X2 respectively.

Based on an evaluation of various conditions using the Point Prediction Analysis program in DesignExpert 9, leaching conditions were set at 30 minutes, 50°C, and 7.5 $g_{HCl}/0.5g_{solids}$ with

the intent of maximizing Eu extraction while minimizing operation costs and Fe extraction. The predicted effects of these conditions on the leaching of REEs are shown in Table XX.

Table XX: RE1-Eu-optimized Extraction Factors ($7.5g_{HCl}/0.5g_{solids}$, 50°C, 30 minutes)

Species	Predicted Mean Ext Factor	Predicted Median Ext Factor	Std Deviation
Eu	0.618	0.605	0.138
Ce	0.508	0.488	0.142
Dy	0.164	0.162	0.030
Gd	0.359	0.351	0.077
La	0.644	0.634	0.130
Nd	0.551	0.541	0.120
Pr	0.594	0.583	0.133
Fe	0.073	0.071	0.016
Th	0.849	0.826	0.207

When the leaching of concentrate RE1 is optimized in regards to Eu extraction, The remaining REEs, with the exception of Dy and Gd, have extraction factors greater than 0.5. Although Dy and Gd do not have the same level of extraction, the values predicted under the set of experimental conditions approach the highest extraction factors observed for Dy and Gd in the design matrix experiments. The lower values for Dy and Gd could be due to competition from other elements in solution.

3.5.2. RE2-Eu Extraction

Eu extraction from RE2 was modeled using a transform of "None", a power series with lambda equal to one, and a modified quadratic model. The equation formed by the analysis of the data is provided in Equation (11),

$$Eu\ Ext = -0.21234 + 0.10468C + 9.10803 \times 10^{-3}T + 5.27895 \times 10^{-4}t \qquad (11)$$
$$-2.55169 \times 10^{-4}CT - 5.82391 \times 10^{-3}C^2$$

where *C* represents the concentration of HCl in grams of HCl per half-gram of solid sample ($g_{HCl}/0.5g_{solids}$), *T* represents temperature in degrees Celsius (°C) and *t* represents reaction time in minutes.

Figure 29 shows the response surface diagram for Eu extraction from RE2. Reagent concentration is plotted along the x-axis and temperature in degrees Celsius is plotted on the y-axis. Eu extraction is shown along the z-axis.

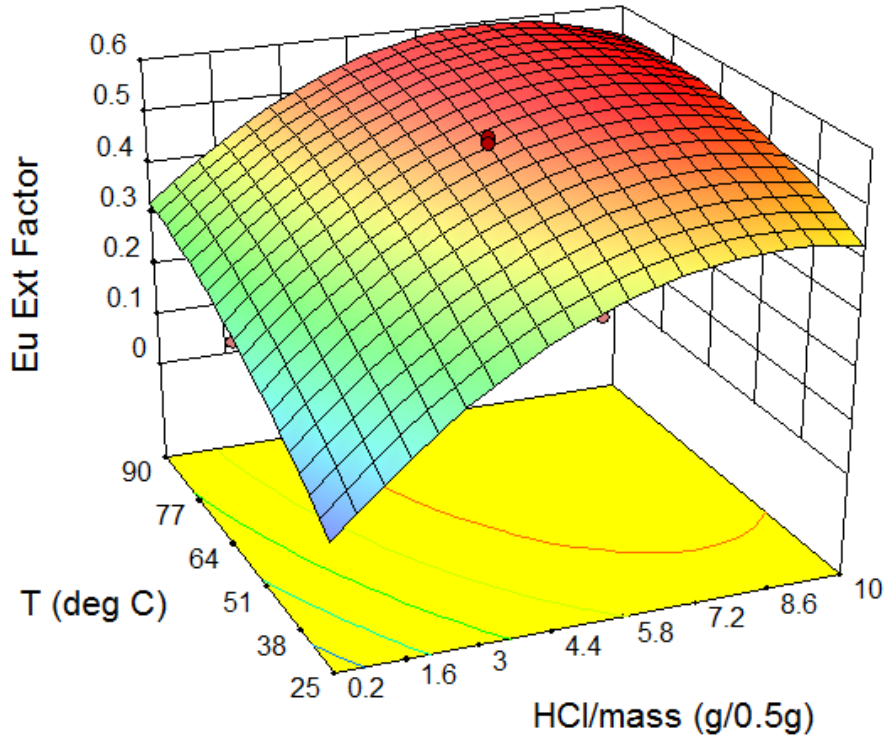

Figure 29: RE2-Eu Extraction Response (75min)

Optimization is possible due to the variation observed in the response surface. The variation in the shape of the response surface indicates that certain experimental conditions cause noticeably higher extraction factors. Had the response surface been represented by a linear, unvarying, shape, this would indicate that optimization would not have been possible under the conditions as altering any of the variables would not have produced a change in extraction.

Maximum extraction of Eu reaches approximately 0.6 under mid levels of reagent concentration and high temperatures. Extraction appears to decrease, however, at reagent concentrations beyond 6-7 $g_{HCl}/0.5g_{solids}$.

The contour plot in Figure 30 supports the information provided by the response surface plot. The red region in the graph indicates the region of highest Eu extraction. This region exists at mid to high reagent concentration and temperature.

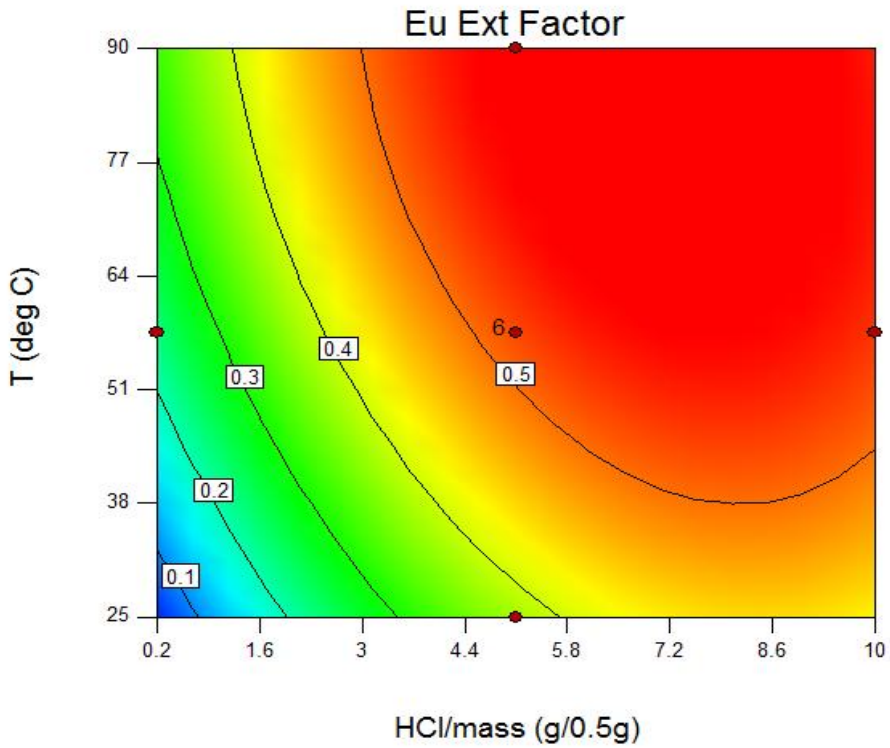

Figure 30: RE2-Eu Extraction Contour Plot (75min)

Diagnostic evaluations were conducted as described previously for the RE1 study to ensure that the selected model for RE2 is statistically valid. Figure 31 presents the predicted vs. actual plot of the Eu experimental data.

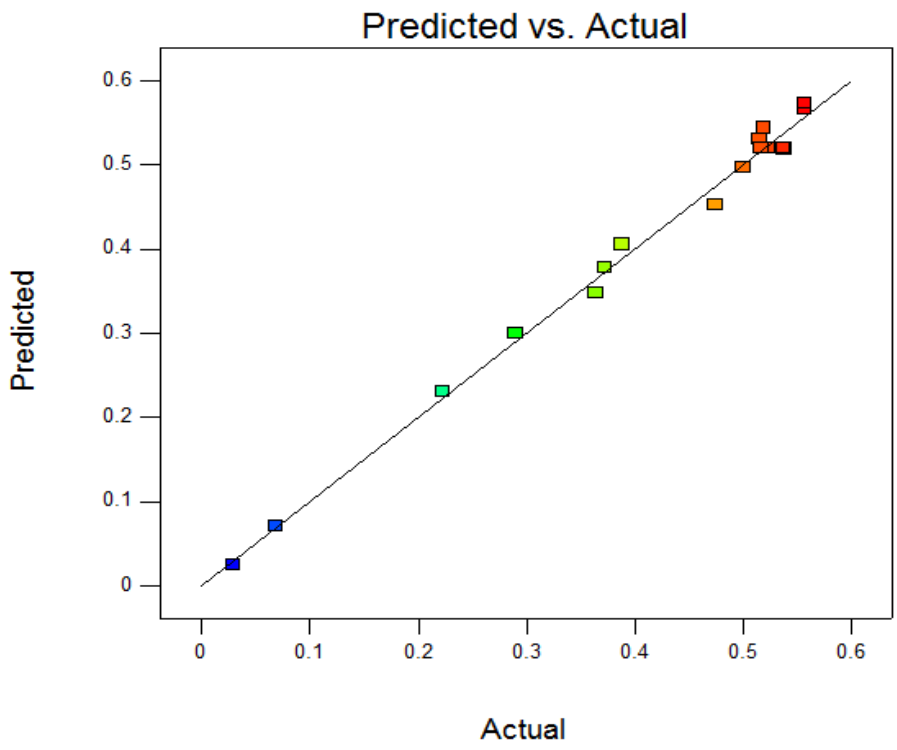

Figure 31: RE2- Predicted vs. Actual Diagnostic of Eu Extraction Model

The Predicted vs. Actual plot for the Eu extraction model indicates that the model fit the experimental data well. The experimental data points fall very close to the ideal linear trendline.

The Cook's distance diagnostic plot for the RE2 model is presented in Figure 32.

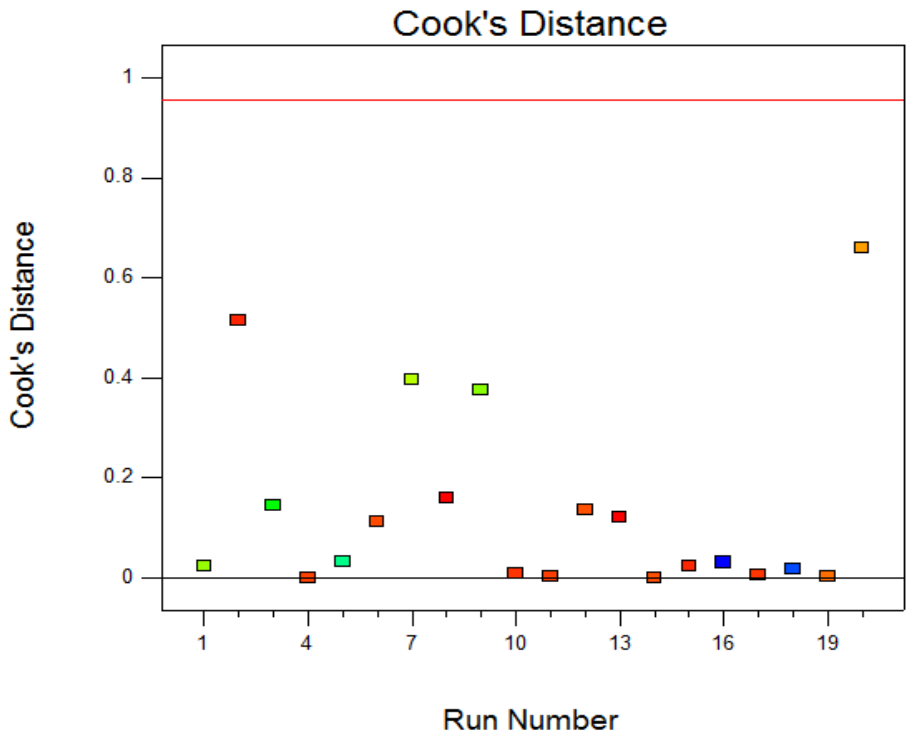

Figure 32: RE2- Cook's Distance Diagnostic of Eu Extraction Model

To pass the Cook's Distance diagnostic, all of the data points must be below the red cutoff line present at the top of the plot. The Eu extraction data passes this diagnostic, further supporting the use of the selected model.

A Normal Distribution plot of the residuals for each Eu extraction value from the RE2 leach tests is shown in Figure 33. The residuals for each data point are plotted on the x-axis and percent normal probability is plotted on the y-axis. The diagonal red line represents the ideal normal distribution.

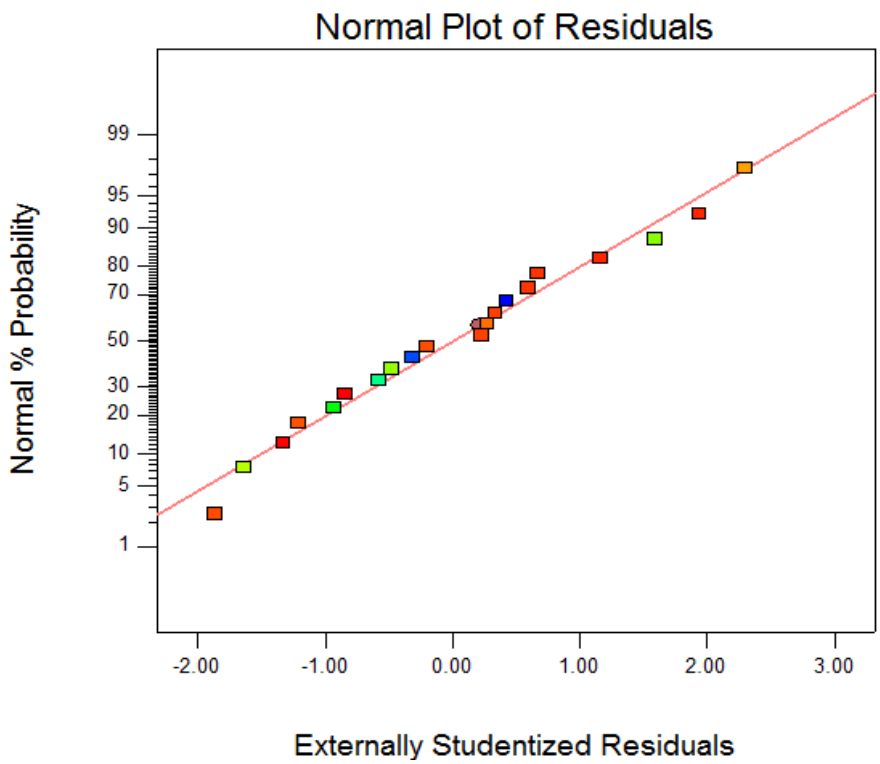

Figure 33: RE2-Normal Plot Diagnostic of Eu Extraction Model

The proximity of the data points to the trendline show that the data is normally distributed and that the model supports the data.

Optimization of Eu extraction from RE2 was carried out using DesignExpert 9. A graph showing the range of parameters that should produce Eu extractions greater than 0.5 is shown in Figure 34. Reagent concentration is plotted on the x-axis and temperature on the y-axis. Time is held constant at 60 minutes.

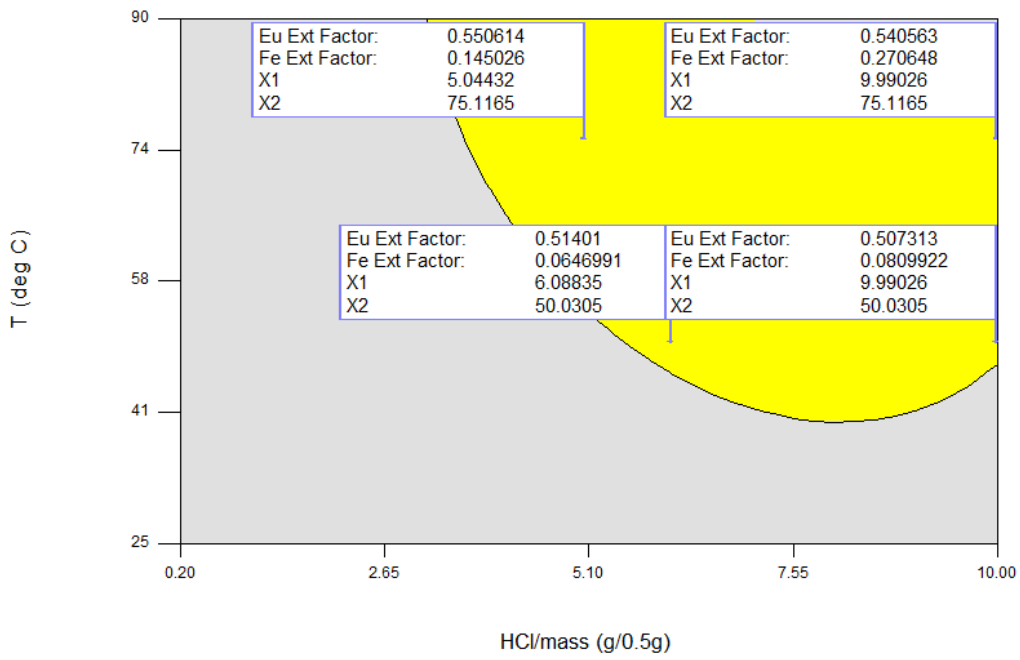

Figure 34: RE2- Optimization Region For Eu Extraction

These are possible conditions at which to optimize for Eu extraction while minimizing Fe extraction. By comparing the two tables of extraction values, it is possible to see that Fe experienced a greater response to the decreases in time, temperature, and reagent concentration than Eu. Fe extraction was more than halved by the drop in temperature from 75°C to 50°C and Fe extraction essentially doubled when temperature is held constant at 75°C and the HCl concentration is doubled. Eu extraction was less affected by these changes by experiencing relatively small changes in extraction factor under the same conditions. Reagent concentration and temperature have a much greater impact on Eu extraction than time, but the changes in Eu extraction due to changes in reagent concentration and temperature were considerably less dramatic than what was observed with Fe.

Using the Point Prediction analysis program in DesignExpert 9, leaching conditions were established at which Eu extraction would exceed 0.5 while keeping Fe extraction and operating

costs at a minimum. Conditions for a Eu-optimized leach were set at 4.50 $g_{HCl}/0.5g_{solids}$, 75°C, and 60 minutes. The predicted extraction values for Eu, Fe, Th, and the remaining REEs are shown in Table XXI.

Table XXI: RE2-Eu-optimized Extraction Factors ($4.5g_{HCl}/0.5g_{solids}$, 75°C, 60 minutes)

Species	Predicted Mean Extraction Factor	Predicted Median Extraction Factor	Std Dev.
Eu	0.534	0.534	0.016
Ce	0.400	0.400	0.021
Dy	0.152	0.152	0.007
Gd	0.376	0.376	0.010
La	0.572	0.572	0.020
Nd	0.473	0.473	0.016
Pr	0.529	0.529	0.018
Fe	0.114	0.113	1.066
Th	0.480	0.480	0.028

When optimized for Eu, Pr and La also experienced extraction factors greater than 0.5. Cerium and Nd were extracted at values below 0.5, but greater than 0.4. Dy and Gd both experienced significantly lower extraction factors than the other REEs, but, as observed in RE1, the values of extraction under the set conditions approached the highest values for Dy and Gd extraction observed in the design matrix experiments. Thorium extraction levels were considerably lower than the extraction values predicted using RE1 while Fe extraction increased.

3.5.3. RE4- Eu Extraction

Europium extraction from the ore sample, RE4, was modeled using the "None" transform and a modified quadratic relationship. Eu extraction is modeled using the following equation:

$$Eu\ ext = -0.19368 + 0.080045C + 0.010004T + 5.60868 \times 10^{-4}t - 2.29673 \times 10^{-4}CT - 4.11311 \times 10^{-3}C^2 \quad (12)$$

A response surface diagram of the Eu extraction model is shown in Figure 35. Reagent concentration is plotted on the x-axis in units of $g_{HCl}/0.5g_{solids}$ and temperature is plotted on the

y-axis in Celsius. The predicted response for Eu extraction is plotted on the z-axis. Time is held constant at 75 minutes.

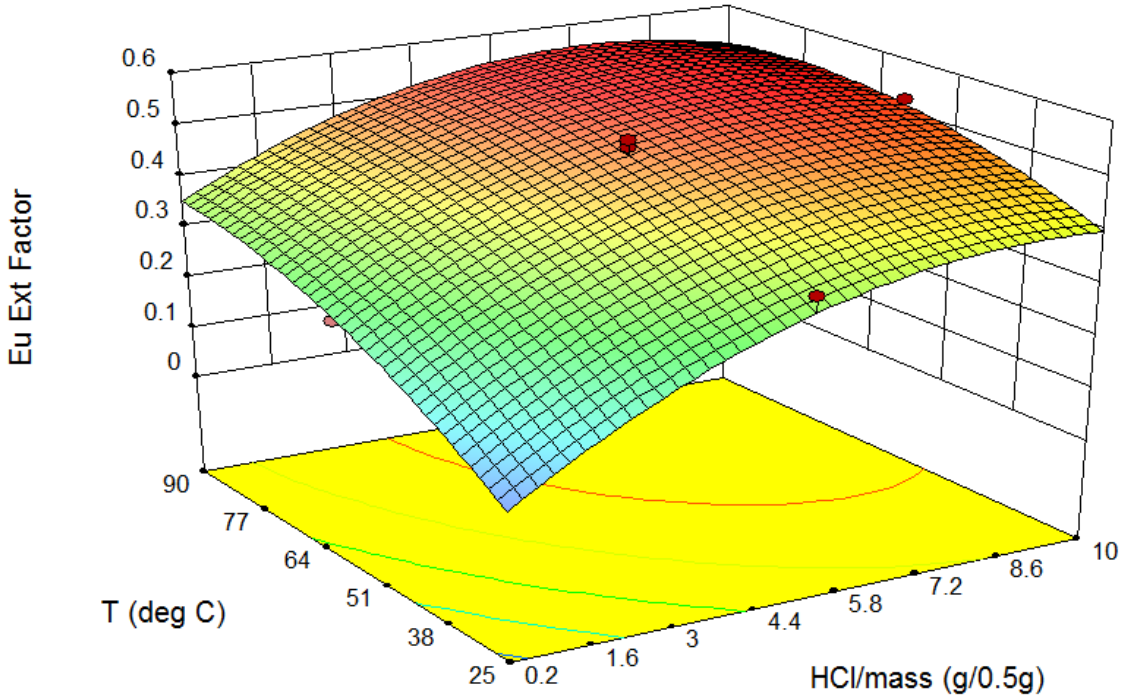

Figure 35: RE4-Eu Extraction Response (75min)

The model for Eu extraction from RE4 indicates that optimization is possible due to the variance observed in the response surface diagram. Extraction from RE4 reaches a maximum of approximately 0.55 at high temperatures and medium reagent concentration (~$6g_{HCl}/0.5g_{solids}$). The amount of extraction from RE4 is comparable with values from the two concentrate samples, RE1 and RE2.

The contour plot shown in Figure 36 further illustrates the optimization potential of Eu extraction under the established conditions. Reagent concentration is plotted on the x-axis in units of g of HCl per half-gram of solid ($g_{HCl}/0.5g_{solids}$). Temperature is plotted on the y-axis in degrees Celsius. Time is held constant at 75 minutes.

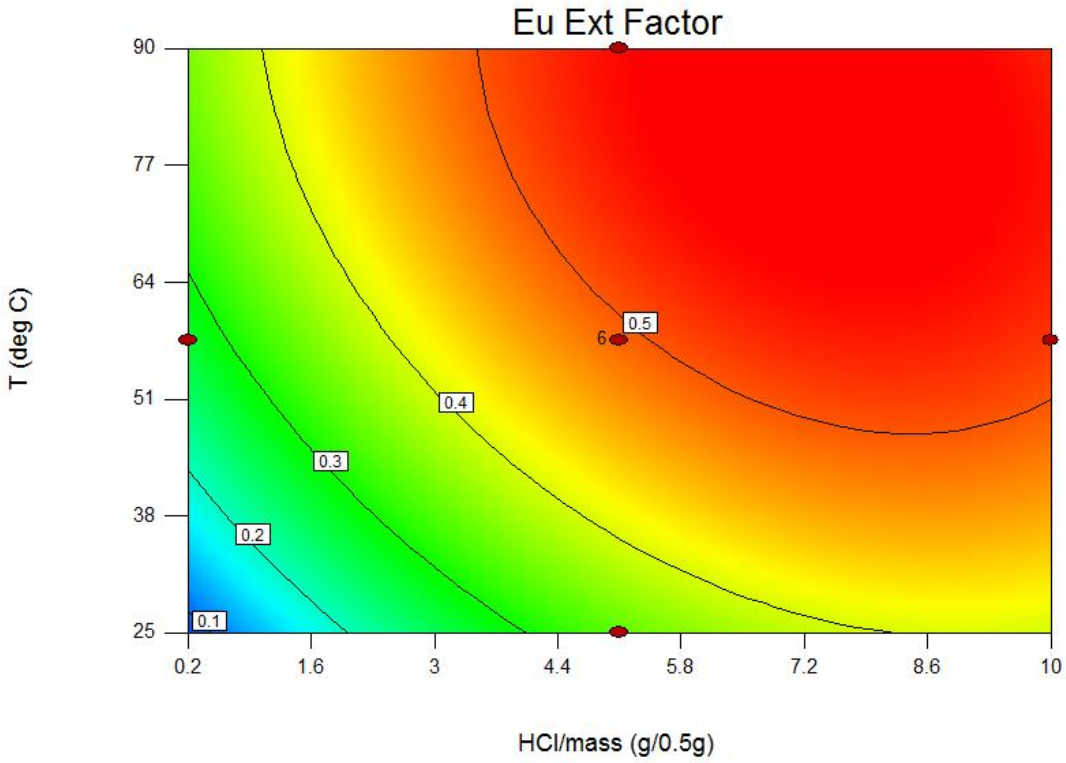

Figure 36: RE4-Eu Extraction Contour Plot (75min)

From the contour plot, it is possible to observe that Eu extraction from RE4 increases with increasing temperature and reagent concentration.

Modeling diagnostics for the Eu extraction model are also provided. Figure 37 shows the Predicted vs. Actual plot of the experimental Eu extraction data compared to a linear trend predicted by the model.

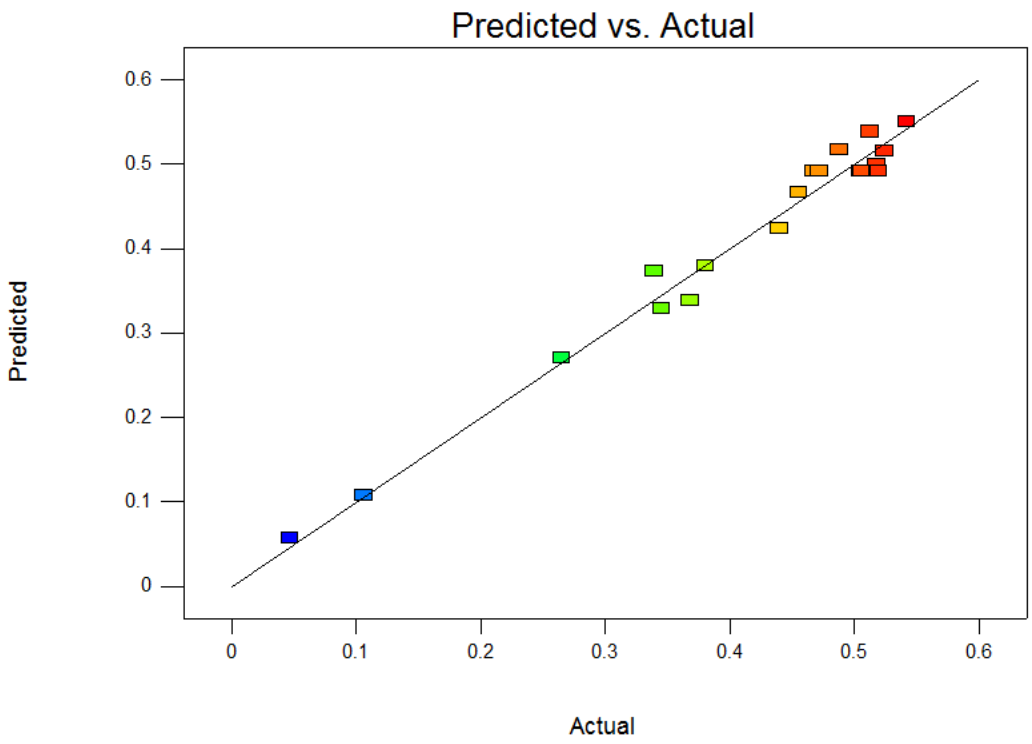

Figure 37: RE4- Predicted vs. Actual Diagnostic of Eu Extraction Model

The experimental data follows the predicted trend relatively well. This diagnostic indicates that the model used to predict Eu extraction fits the experimental data well.

The Cook's Distance diagnostic is shown in Figure 38. The x-axis plots the experimental data by run number, and the Cook's Distance values for the Eu extraction data from each run is plotted on the y-axis.

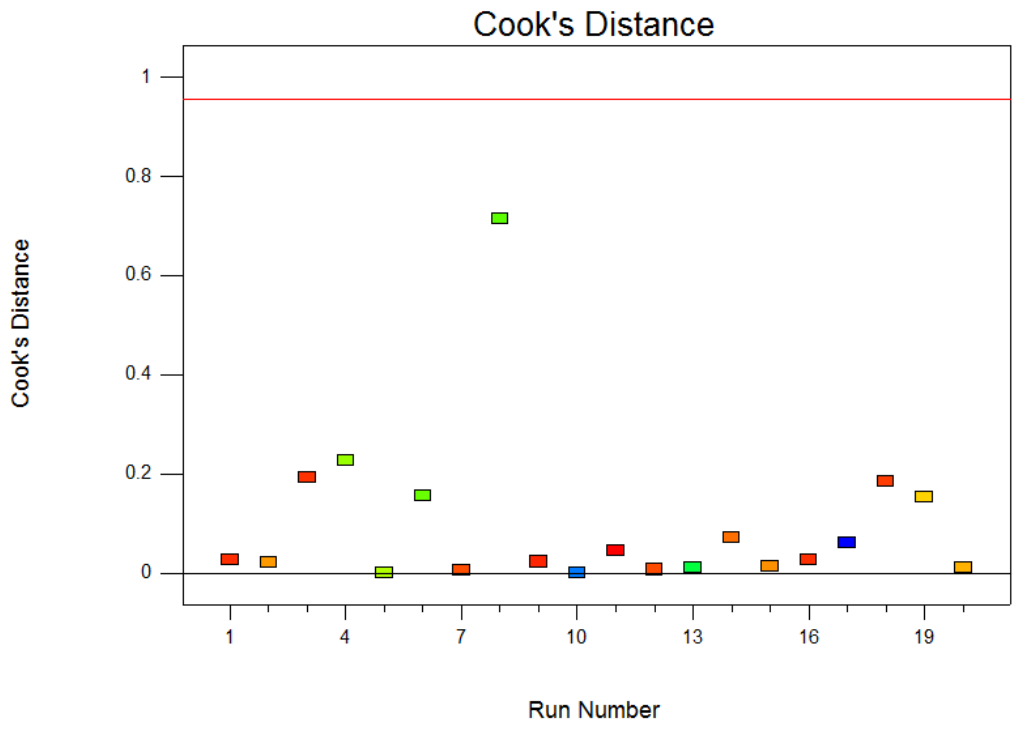

Figure 38: RE4- Cook's Distance Diagnostic of Eu Extraction Model

All of the data points produced Cook's Distance values within the acceptable range and indicate that excessive influence on the model from one single data point is not occurring and that it is not likely that any of the data points are outliers. The fit of the model is distributed across the entire data set and represents the data set as a whole. The Cook's Distance values support the use of the model selected to predict Eu extraction from RE4.

A Normal Distribution plot of the residuals for each Eu extraction value from the RE4 leach tests is shown in Figure 39. The residuals for each data point are plotted on the x-axis and percent normal probability is plotted on the y-axis. The diagonal red line represents the ideal normal distribution.

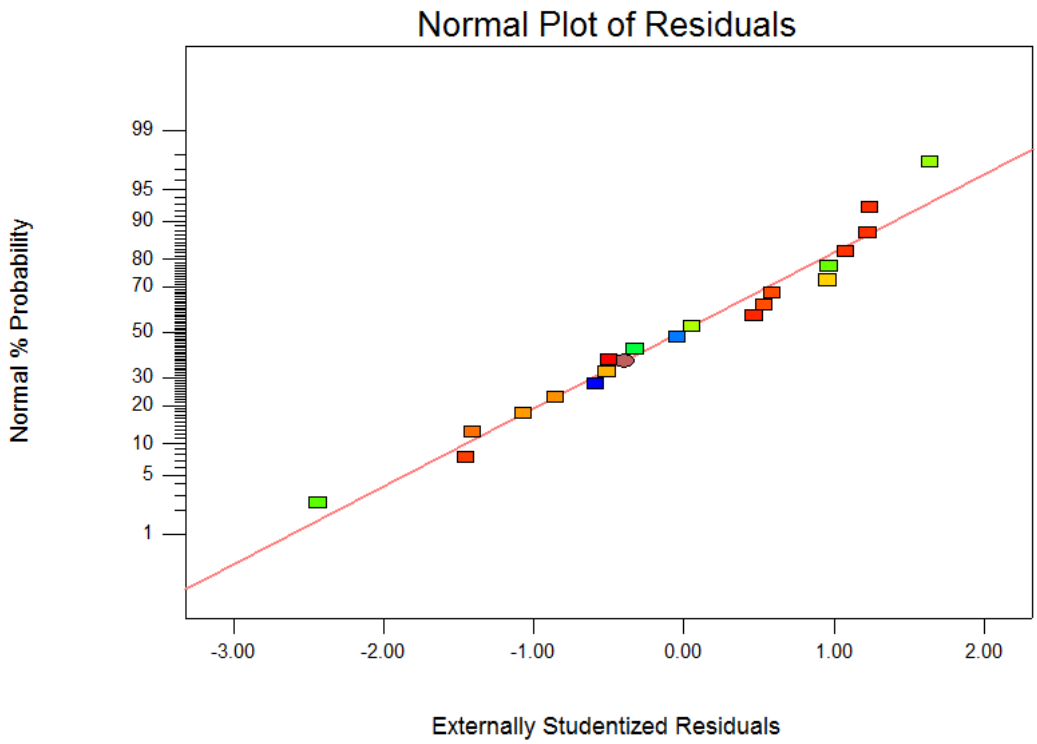

Figure 39: RE4- Normal Plot Diagnostic of Eu Extraction Model

From the graph, it can be observed that the residuals are relatively normally distributed. The distribution of the residuals indicates that there is little deviation between the experimental values and the predicted mean values produced by the model. The model is further supported by the normal plot diagnostic.

Optimization of Eu extraction from RE4 was carried out using DesignExpert 9. A graph showing the range of parameters that should produce Eu extractions greater than 0.5 is shown in Figure 40. Reagent concentration is plotted on the x-axis and temperature on the y-axis. Time is held constant at 60 minutes.

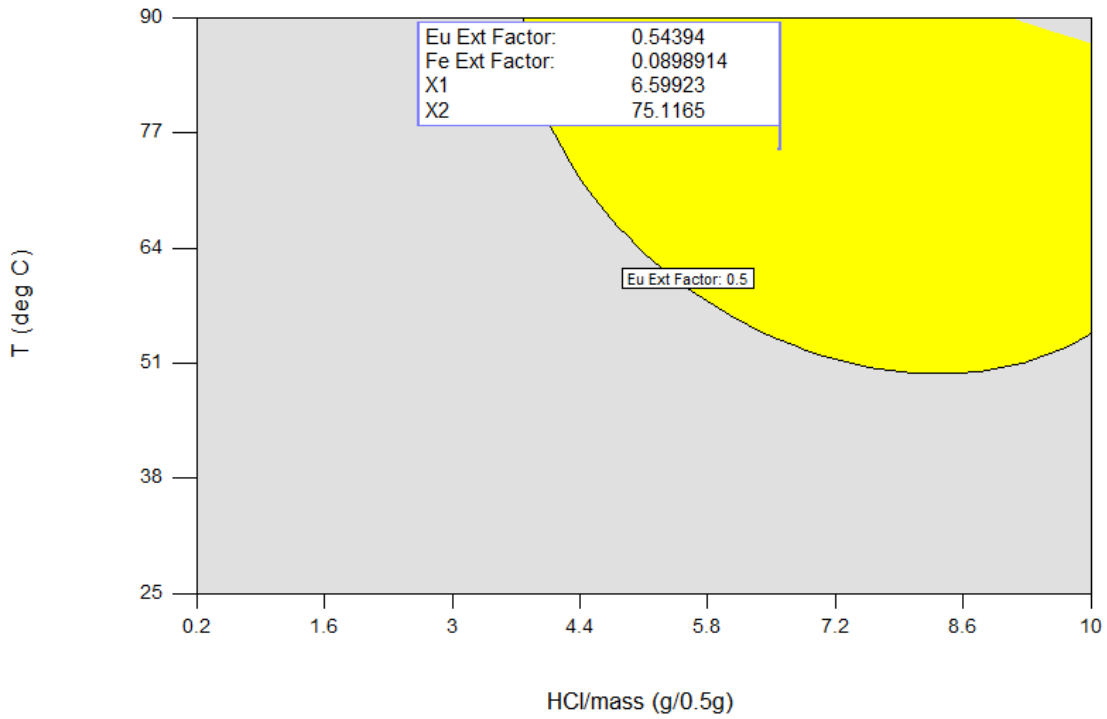

Figure 40: RE4- Optimization Region For Eu Extraction (60min)

The yellow region represents the set of parameters that will produce Eu extraction factors greater than 0.5. Using the Point Prediction function in DesignExpert 9, a set of conditions was established that maximized Eu extraction while also minimizing the amount of Fe extracted. These settings are shown on the flag inside the yellow region of the graph, where X1 represents reagent concentration (~6.6 $g_{HCl}/0.5g_{solids}$) and X2 represents temperature (~75°C). The effect of optimizing Eu extraction on the extraction of the remaining REEs is shown in Table XXII.

Table XXII: RE4-Eu-optimized Extraction Factors (6.6 gHCl/0.5gsolids, 75°C, 60 minutes)

Species	Predicted Mean Extraction Factor	Predicted Median Extraction Factor	Std Dev.
Eu	0.544	0.544	0.024
Ce	0.431	0.431	0.025
Dy	0.182	0.181	0.027
Gd	0.356	0.356	0.023
La	0.601	0.601	0.033
Nd	0.511	0.511	0.025
Pr	0.525	0.525	0.029
Fe	0.089	0.088	0.017
Th	0.655	0.655	0.026

By optimizing the extraction of Eu from RE4, other REEs, such as La, Nd, and Pr, were also extracted at values greater than 0.5. Ce and Gd experienced extraction factors lower than 0.5

3.5.4. RE5- Eu Extraction

Europium extraction from the ore sample, RE5, was modeled using the "None" transform and a modified quadratic relationship. Eu extraction is modeled using the following equation:

$$Eu\ ext = -0.044442 + 0.11910C + 3.18945 \times 10^{-3}T + 4.45502 \times 10^{-4}t - 7.73306 \times 10^{-3}C^2 - 1.15859 \times 10^{-5}T^2 \quad (13)$$

A response surface diagram of Eu extraction is shown in Figure 41. Reagent concentration is plotted on the x-axis in units of $g_{HCl}/0.5g_{solids}$ and temperature is plotted on the y-axis in Celsius. The predicted response for Eu extraction is plotted on the z-axis. Time is held constant at 75 minutes.

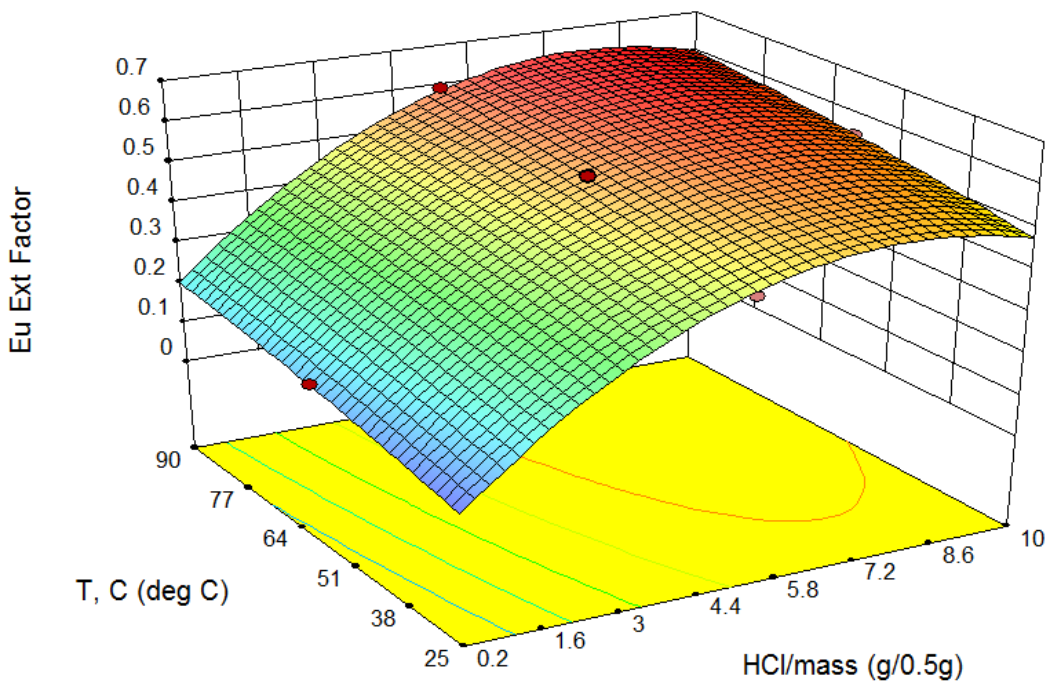

Figure 41: RE5- Eu Extraction Response (75min)

The amount of variance present in the 3-D response surface diagram indicates that optimization of Eu is possible under the assigned parameters. A maximum Eu extraction factor of approximately 0.6 occurs at reagent concentrations of 6.5-8.5 $g_{HCl}/0.5g_{solids}$ and temperatures in the range of 80-90°C.

The contour plot shown in Figure 42 provides additional information on the optimization potential of Eu extraction. Reagent concentration is plotted on the x-axis in units of g of HCl per half-gram of solid ($g_{HCl}/0.5g_{solids}$). Temperature is plotted on the y-axis in degrees Celsius. Time is held constant at 75 minutes.

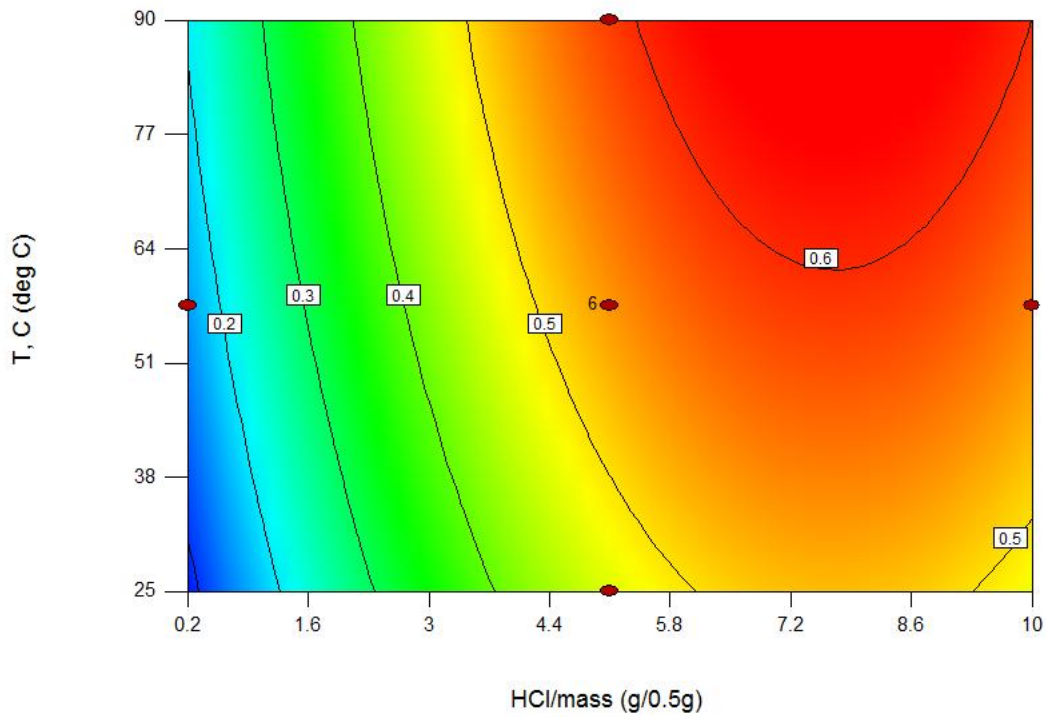

Figure 42: RE5- Eu Extraction Contour Plot (75min)

From the contour plot, the region at which Eu extraction is maximized can be observed in greater detail. Maximum Eu extraction is associated with reagent concentrations ranging from

5.8 to 10 $g_{HCl}/0.5g_{solids}$, and temperatures at which maximum Eu extraction occurs range from 65-90°C.

Modeling diagnostics for the RE5 Eu extraction model are provided. Figure 43 shows the Predicted vs. Actual plot of Eu extraction from RE5.

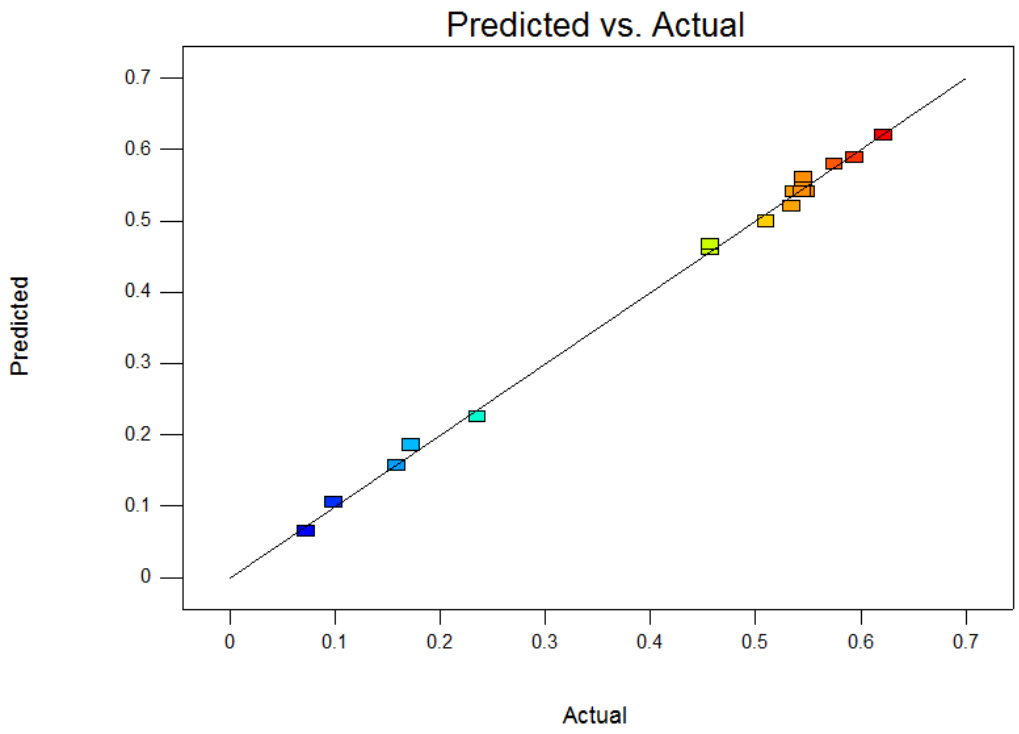

Figure 43: RE5- Predicted vs. Actual Diagnostic of Eu Extraction Model

Figure 43 shows that the Eu extraction values predicted by the model and the experimental Eu extraction values are nearly identical. The similarities between the predicted and experimental values indicate that the model fits the experimental data well.

A graph of the Cook's Distance diagnostic for the RE5 experiments is shown in Figure 44. The x-axis plots the experimental data by run number, and the Cook's Distance values for the Eu extraction data from each run is plotted on the y-axis.

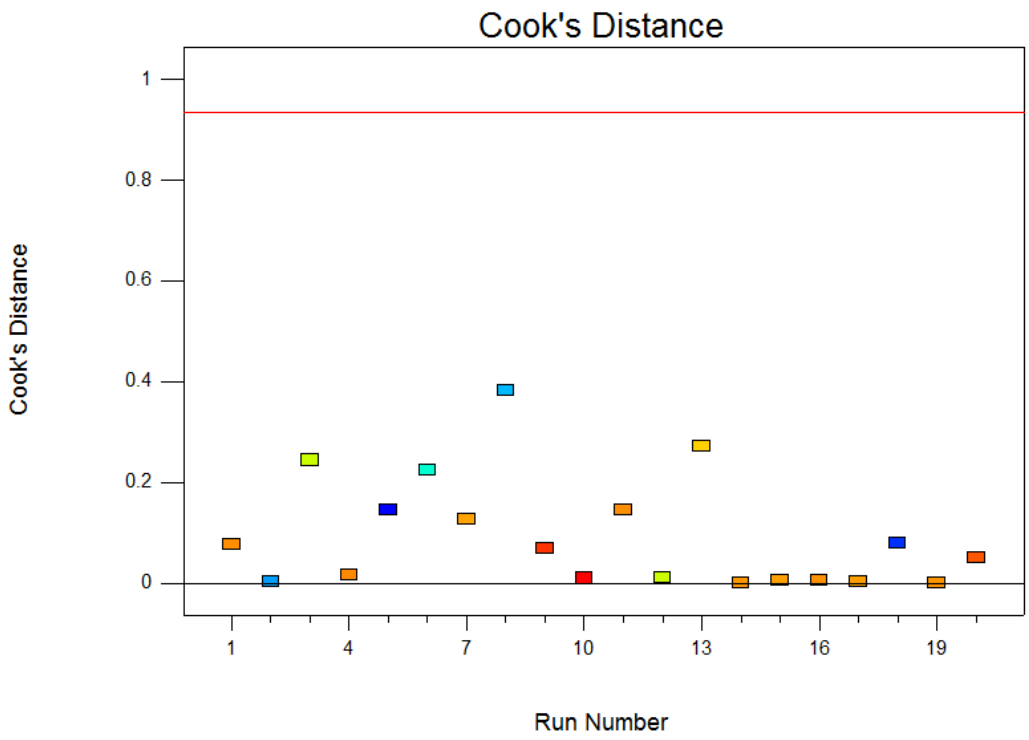

Figure 44: RE5- Cook's Distance Diagnostic of Eu Extraction Model

The experimental data points produced Cook's Distance values within the acceptable range. Excessive influence on the model from one single data point is not occurring and it is unlikely that any of the data points are outliers. The fit of the model is distributed across the entire data set and represents the data set as a whole. The Cook's Distance values support the use of the model selected to predict Eu extraction from RE5.

A Normal Distribution plot of the residuals for Eu extraction from RE5 is shown in Figure 45. The residuals for each data point are plotted on the x-axis and percent normal probability is plotted on the y-axis. The diagonal red line represents the ideal normal distribution

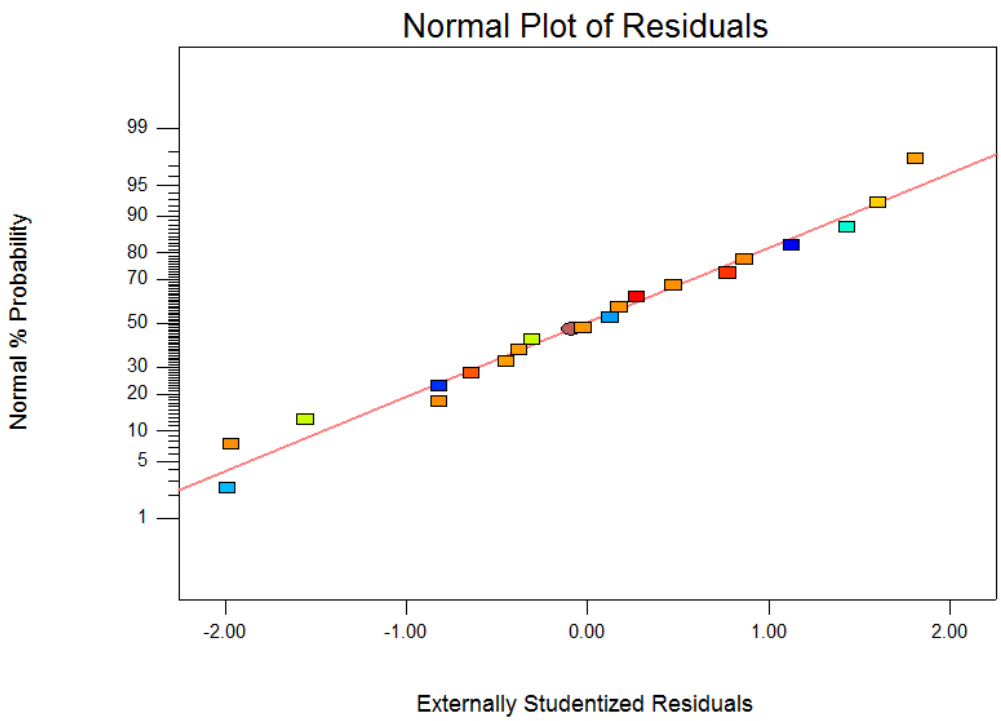

Figure 45: RE5- Normal Plot Diagnostic of Eu Extraction Model

From the graph, it can be observed that the residuals are relatively normally distributed. The distribution of the residuals indicates that there is little deviation between the experimental values and the predicted mean values produced by the model. The normal plot diagnostic further supports the use of the selected model to predict Eu extraction values.

Optimization of Eu extraction from RE5 was carried out using DesignExpert 9. A graph showing the conditions that should produce Eu extraction values greater than 0.5 is shown in Figure 46. Reagent concentration is plotted on the x-axis and temperature on the y-axis. Time is held constant at 60 minutes.

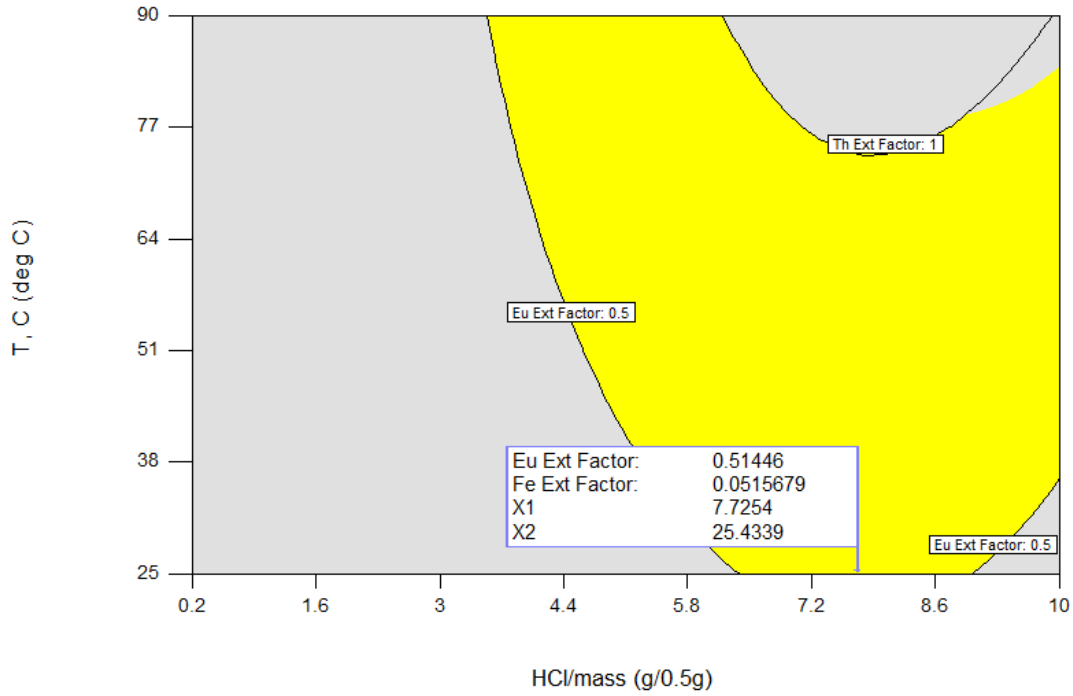

Figure 46: RE5- Optimization Region of Eu Extraction (60min)

The set of parameters able to induce Eu extraction factors greater than 0.5 is represented by the yellow region on the graph. Using the Point Prediction function in DesignExpert 9, a set of conditions was established that maximized Eu extraction while taking the minimization of Fe extracted into account. These conditions are shown on the flag inside the yellow region of the graph, where X1 represents reagent concentration (~7.7 $g_{HCl}/0.5g_{solids}$) and X2 represents temperature (~25°C). The effect of optimizing Eu extraction on the extraction of the remaining REEs is shown in Table XXIII.

Table XXIII: RE5-Eu-optimized Extraction Factors (7.7gHCl/0.5gsolids, 25°C, 60 minutes)

Species	Predicted Mean Extraction Factor	Predicted Median Extraction Factor	Std Dev.
Eu	0.513	0.513	0.009
Ce	0.310	0.309	0.014
Dy	0.136	0.136	0.013
Gd	0.402	0.402	0.014
La	0.644	0.644	0.011
Nd	0.508	0.508	0.010
Pr	0.523	0.523	0.010
Fe	0.051	0.051	0.765
Th	0.720	0.719	0.046

By observing the different REE extraction factors, it can be seen that multiple REEs (La, Nd, and Pr) all experience extraction factors greater than 0.5. Gd and Ce experienced slightly lower extraction factors and Dy is shown to have a much lower extraction value of 0.136. However, the behavior exhibited by Dy is present in all of the previously discussed samples. Fe extraction was also able to be held at 0.051 which is significantly lower than any of the REEs present in solution. Decent extraction values for REEs from RE5 were able to be obtained at relatively low temperatures without using high amounts of reagent.

3.5.5. RE6- Eu Extraction

From the leach test data using RE6, europium extraction was modeled using a power series transform ($\lambda = 0.896$) and a modified quadratic relationship. Eu extraction is modeled using the following equation:

$$(Eu\ ext)^{0.86} = 0.31550 + 0.034445C + 3.30736 \times 10^{-3}T + 5.85933 \times 10^{-4}t - 3.60247 \times 10^{-5}CT - 2.01274 \times 10^{-3}C^2 - 1.71530^{-5}T^2 \quad (14)$$

A response surface diagram of Eu extraction is shown in Figure 47. Reagent concentration is plotted on the x-axis in units of $g_{HCl}/0.5g_{solids}$ and temperature is plotted on the y-axis in Celsius. The predicted response for Eu extraction is plotted on the z-axis. Time is held constant at 75 minutes.

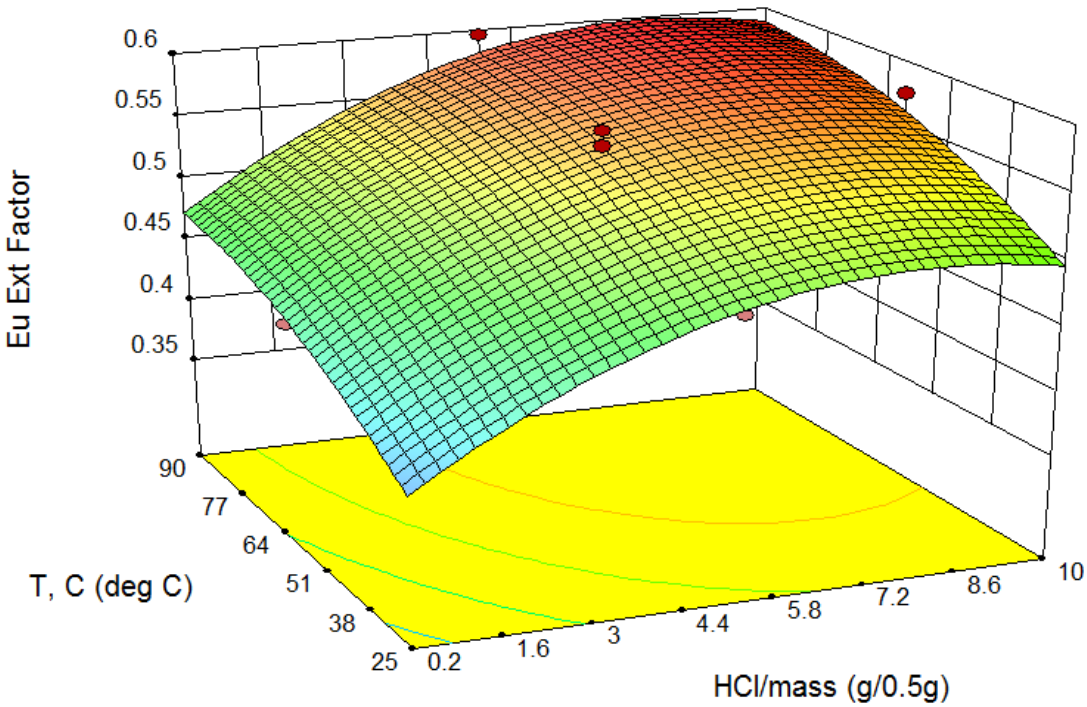

Figure 47: RE6- Eu Extraction Response (75min)

The amount of variance present in the 3-D response surface diagram indicates that optimization of Eu is possible under the assigned parameters. Eu extraction reaches a maximum value of approximately 0.6 at reagent concentrations of 5.8-8.0 $g_{HCl}/0.5g_{solids}$ and temperatures in the range of 70-90°C.

The contour plot shown in Figure 48 provides additional information on the optimization potential of Eu extraction. Reagent concentration is plotted on the x-axis in units of g of HCl per half-gram of solid ($g_{HCl}/0.5g_{solids}$). Temperature is plotted on the y-axis in degrees Celsius. Time is held constant at 75 minutes.

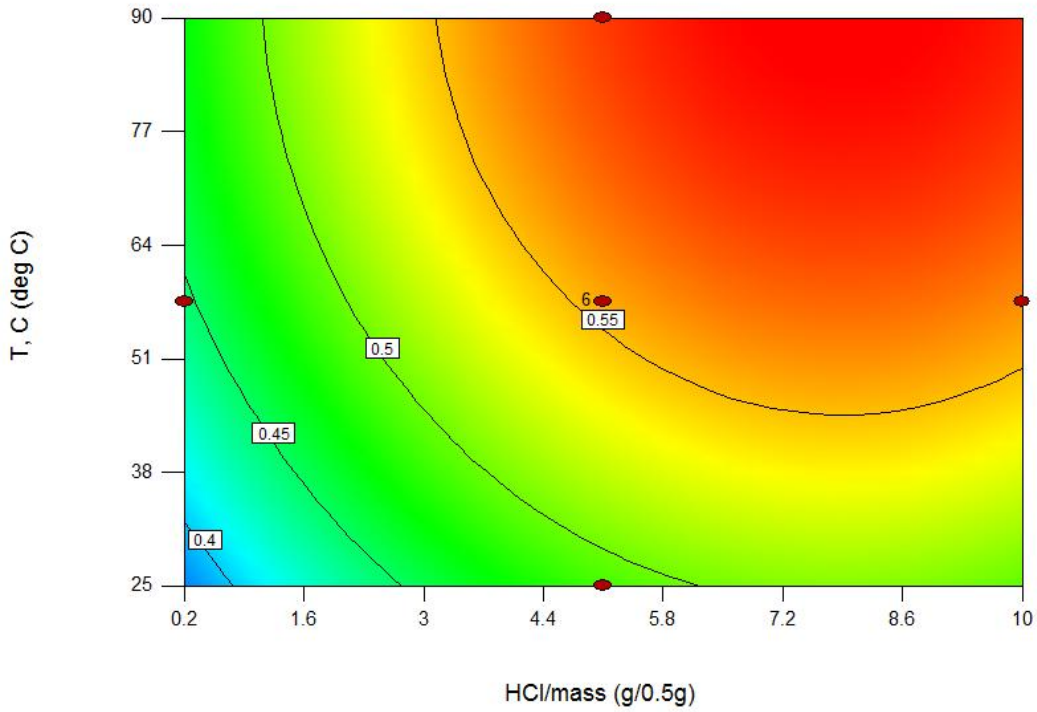

Figure 48: RE6- Eu Extraction Contour Plot (75min)

From the contour plot, the region at which Eu extraction is maximized can be observed. Maximum Eu extraction is associated with reagent concentrations ranging from 4.5 to 10 $g_{HCl}/0.5g_{solids}$, and temperatures at which maximum Eu extraction occurs range from 60-90°C.

Modeling diagnostics for the RE6 Eu extraction model are provided. Figure 49 shows the Predicted vs. Actual plot of Eu extraction from RE6.

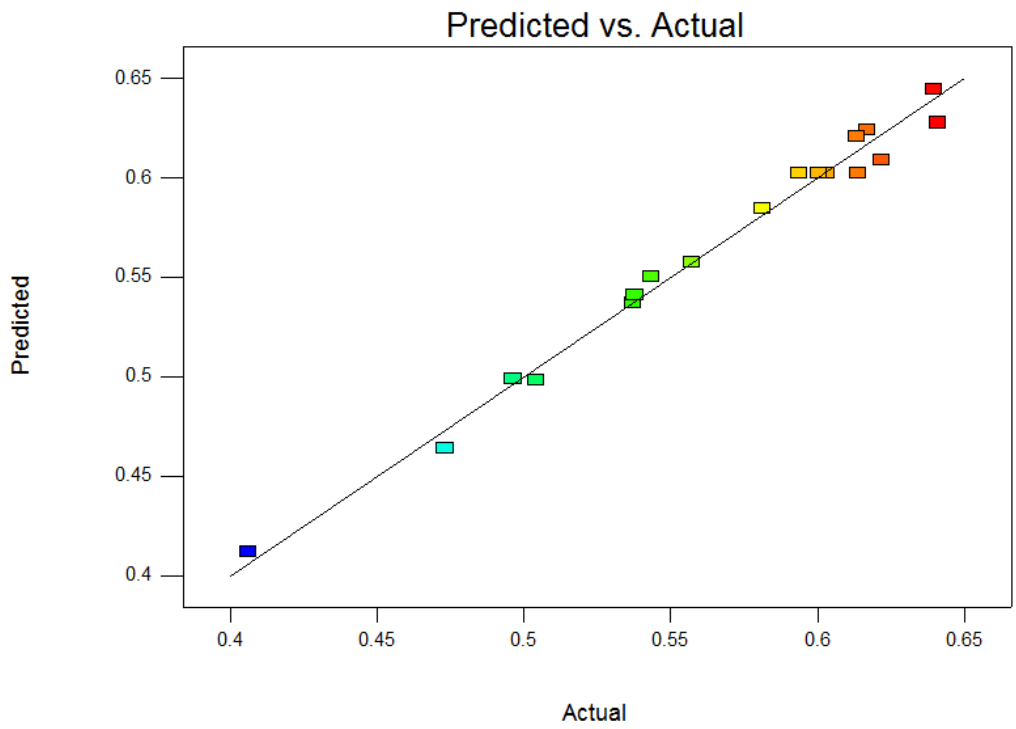

Figure 49: RE6- Predicted vs. Actual Diagnostic of Eu Extraction Model

Figure 49 shows that the Eu extraction values predicted by the model and the experimental Eu extraction values produce a trend that is similar in nature to the values predicted by the model. The similarities between the predicted and experimental values indicate that the model fits the experimental data well.

A graph of the Cook's Distance diagnostic for the RE6 experiments is shown in Figure 50. The x-axis plots the experimental data by run number, and the Cook's Distance values for the Eu extraction data from each run are plotted on the y-axis.

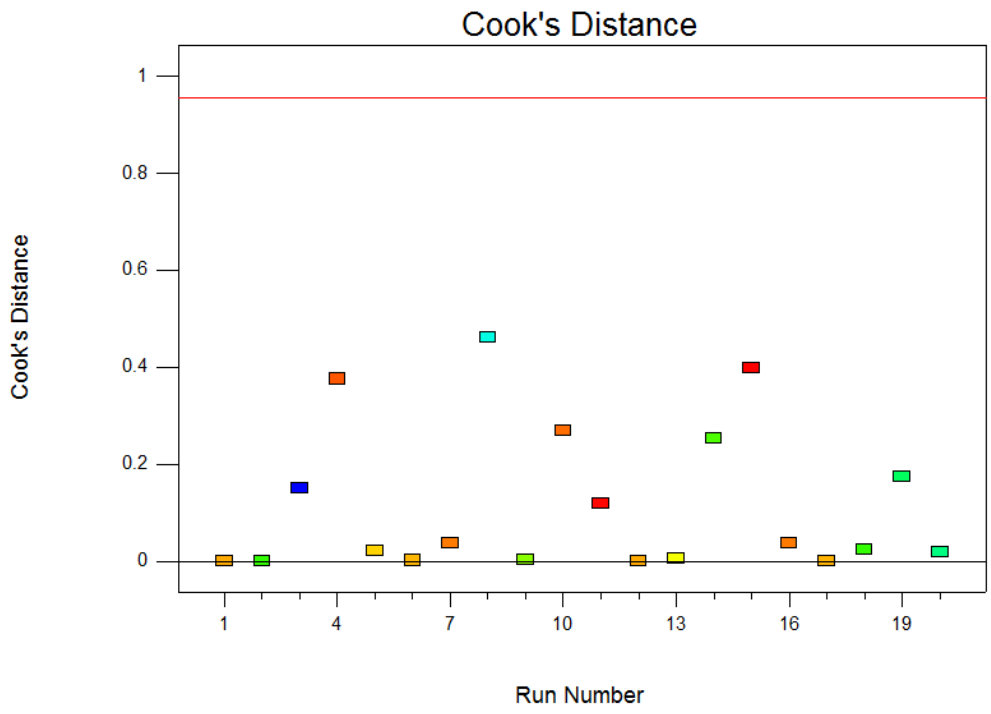

Figure 50: RE6- Cook's Distance Diagnostic of Eu Extraction Model

The experimental data points produced Cook's Distance values within the acceptable range. Excessive influence on the model from one single data point is not occurring and it is unlikely that any of the data points are outliers. The fit of the model is distributed across the entire data set and represents the data set as a whole. The Cook's Distance values support the use of the model selected to predict Eu extraction from RE6.

A Normal Distribution plot of the residuals for Eu extraction from RE6 is shown in Figure 51. The residuals for each data point are plotted on the x-axis and percent normal probability is plotted on the y-axis. The diagonal red line represents the ideal normal distribution

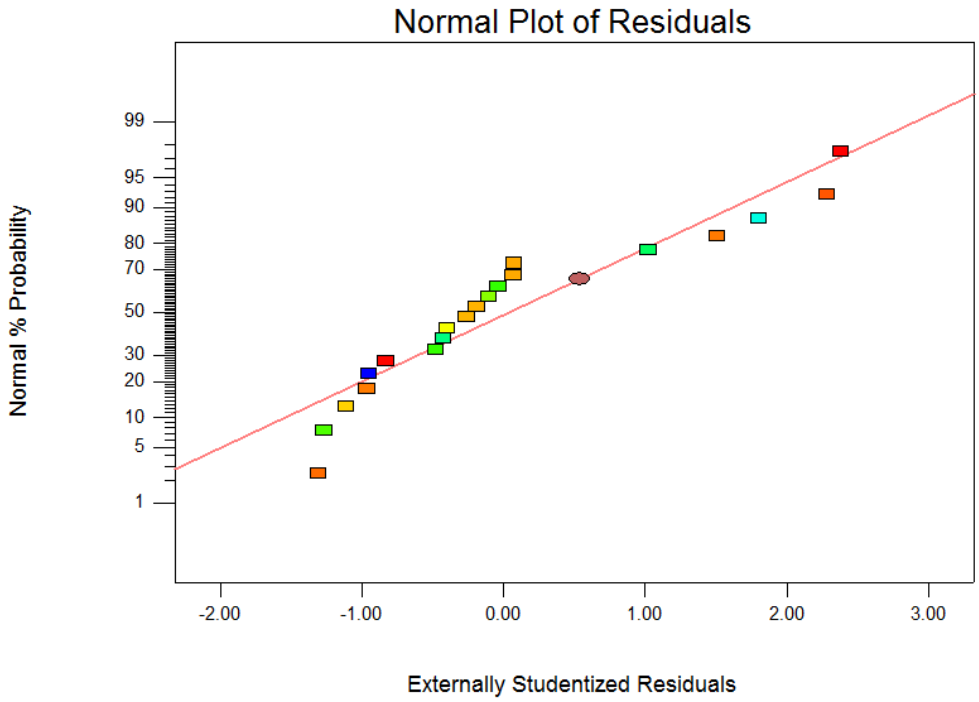

Figure 51: RE6- Normal Plot Diagnostic of Eu Extraction Model

Although some deviation from the ideal trendline is present, the data residuals still take on a trend that resembles a normal distribution. The normal distribution of the data residuals supports the use of the equation used to model the extraction of Eu from RE6.

Optimization of Eu extraction from RE6 was carried out using DesignExpert 9. A graph showing the conditions that should produce Eu extraction values greater than 0.5 is shown in Figure 52. Reagent concentration is plotted on the x-axis and temperature on the y-axis. Time is held constant at 60 minutes.

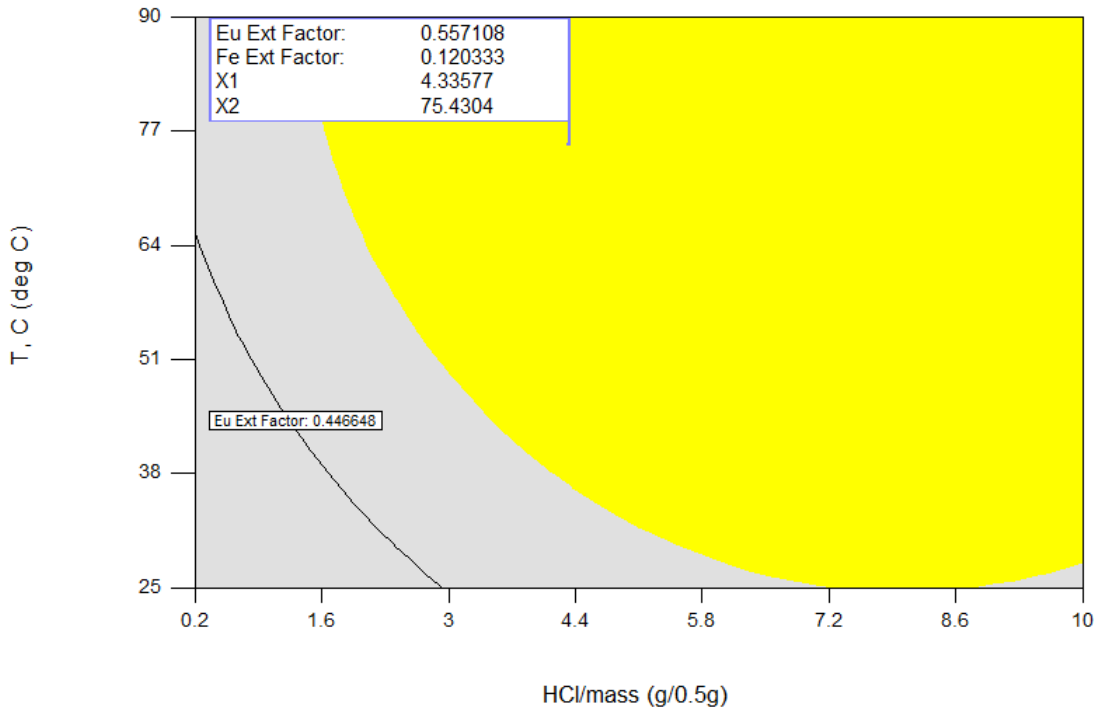

Figure 52: RE6- Optimization Region of Eu Extraction (60min)

The yellow region on the graph represents the set of parameters that produce Eu extraction factors greater than 0.5. Using the Point Prediction function in DesignExpert 9, a set of conditions was established that maximized Eu extraction while minimizing the extraction of Fe. These conditions are shown on the flag inside the yellow region of the graph, where X1 represents reagent concentration (~4.3 $g_{HCl}/0.5g_{solids}$) and X2 represents temperature (~75°C). The effect of optimizing Eu extraction on the extraction of the remaining REEs is shown in Table XXIV.

Table XXIV: RE6-Eu-optimized Extraction Factors (4.3gHCl/0.5gsolids, 75°C, 60 minutes)

Species	Predicted Mean Extraction Factor	Predicted Median Extraction Factor	Std Dev.
Eu	0.556	0.556	0.009
Ce	0.458	0.458	0.008
Dy	0.014	0.014	0.005
Gd	0.274	0.274	0.008
La	0.554	0.554	0.008
Nd	0.607	0.607	0.012
Pr	0.524	0.524	0.007
Fe	0.118	0.116	0.029
Th	0.606	0.606	0.039

From the table, it can be observed that Eu can be extracted from RE6 with an extraction factor greater than 0.5 while also limiting the extraction factor of Fe to approximately 0.1. Pr, La, and Nd can also be extracted with extraction factors greater than 0.5 when conditions are optimized for Eu. Gd and Dy experienced significantly less leaching than the other samples with extraction factors of 0.274 and 0.014, respectively.

3.6. Comparison of Optimization Data and Models

Using the Point Prediction function in DesignExpert 9, the Eu optimization data was manipulated in order to compare Eu extractions from the five RER samples. The optimization conditions for each RER sample were compared to determine which sample(s) produced the highest Eu extraction factors.

A graph of the initial Eu concentration and Eu extraction factor for each of the five samples is presented in Figure 53. Each sample is presented in sequential order along the x-axis while initial weight percent and extraction are plotted on the two y-axes.

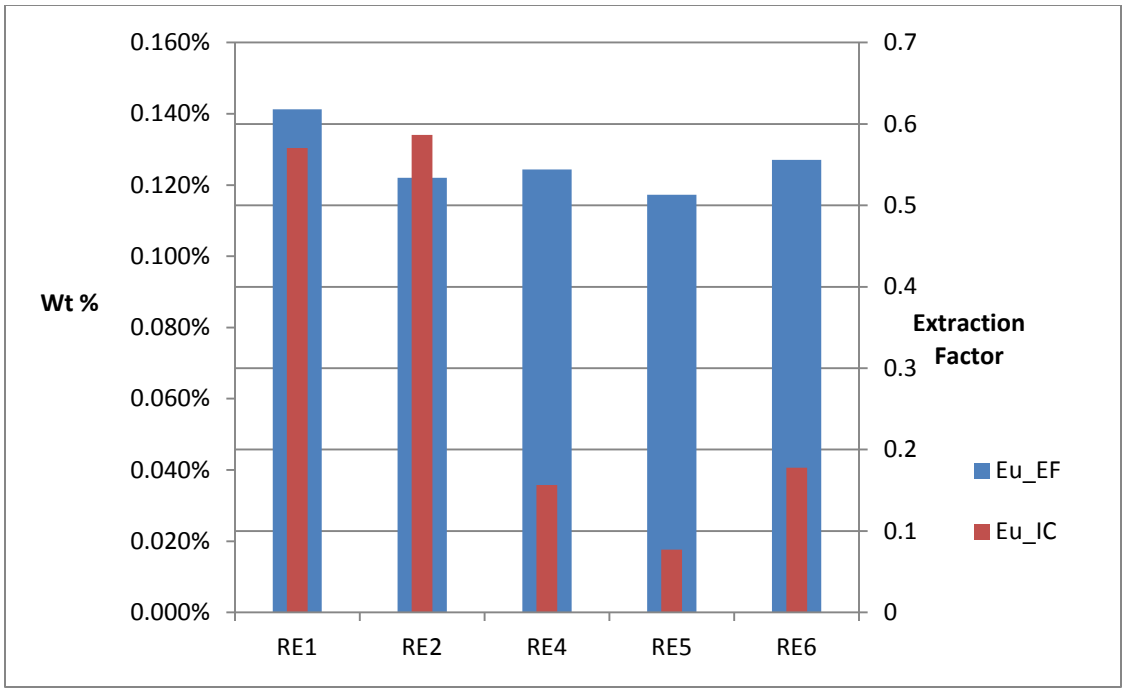

Figure 53: Eu Extraction Factor (EF) vs. Eu Initial Concentration (IC) (Individually Optimized)

RE1 produced the highest Eu extraction factor, despite having the second-highest initial concentration. There appears to be no correlation between initial concentration and extraction factor for Eu.

Because RE1 produced the highest overall Eu extraction under the selected optimal conditions, the Point Prediction program was used to investigate the behavior of the remaining four RER samples under the same set conditions. A graph of the predicted Eu extraction factors for the five samples under the RE1-optimized conditions is provided in Figure 54.

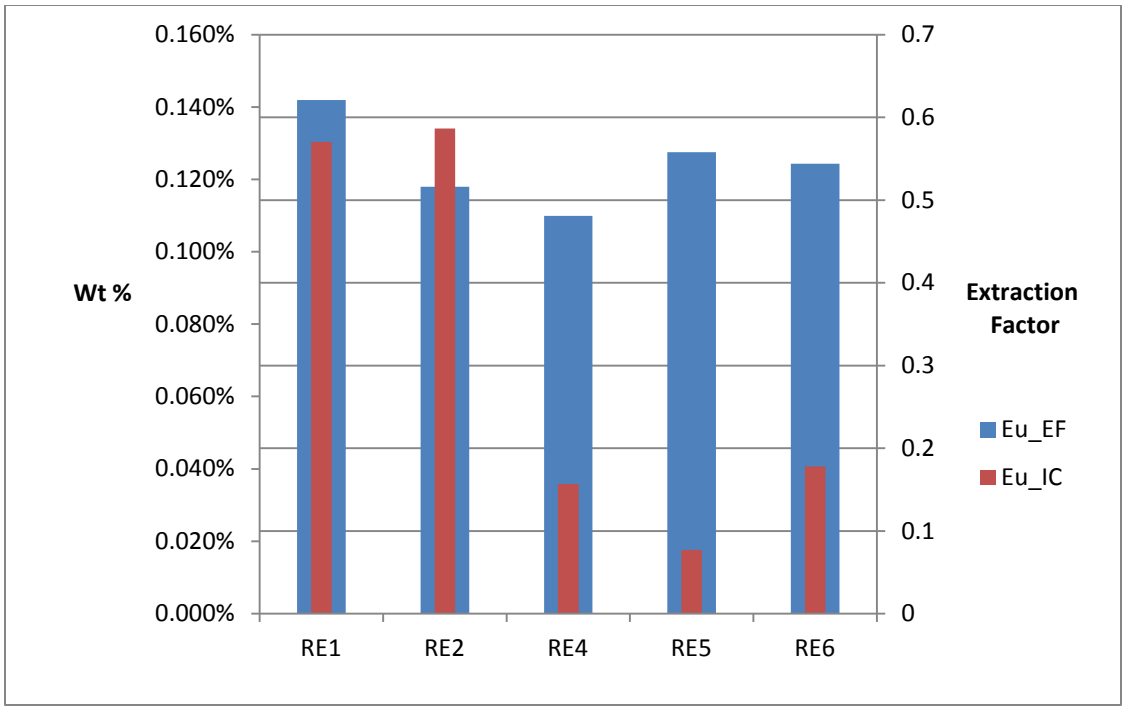

Figure 54: Eu Extraction Factor (EF) vs. Eu Initial Concentration (IC) (7.5g_{HCl}, 50°C, 30 min)

Again, there appears to be no correlation between initial Eu concentration and the value of the extraction factor under the RE1-optimized conditions. All of the RER samples, apart from RE1, experience decreases in Eu extraction. However, the observed decreases were relatively small and, with the exception of RE4, Eu extraction factors remained above 0.5. The effect of the RE1-optimized conditions on the other REEs was also investigated. The predicted values for RE2 under the RE1-optimized conditions are presented in Table XXV.

Table XXV: RE2 Point Prediction Values (RE1-Optimized Conditions)

Species	Predicted Mean Extraction Factor	Predicted Median Extraction Factor	Std Dev.
Eu	0.516	0.516	0.016
Ce	0.404	0.404	0.021
Dy	0.148	0.148	0.007
Gd	0.357	0.357	0.010
La	0.539	0.539	0.020
Nd	0.453	0.453	0.016
Pr	0.505	0.505	0.018
Fe	0.061	0.061	1.856
Th	0.589	0.589	0.031

The predicted extraction factors are similar to the initial predicted extraction factors for RE2. One exception is the Fe extraction factor which is significantly smaller than the initial predicted value. All of the REE extraction factors experienced slight decreases under the RE1-optimized conditions.

The predicted extraction factors under the RE1-optimized conditions for RE4, RE5, and RE6 are presented in Table XXVI.

Table XXVI: Point Prediction Values for RE4, RE5, and RE6 (RE1-Optimized Conditions)

Species	Predicted Mean Extraction Factor	Predicted Median Extraction Factor	Std Dev.
RE4			
Eu	0.481	0.481	0.024
Ce	0.332	0.332	0.022
Dy	0.175	0.174	0.026
Gd	0.321	0.321	0.023
La	0.532	0.532	0.033
Nd	0.455	0.455	0.025
Pr	0.480	0.480	0.029
Fe	0.019	0.018	0.003
Th	0.482	0.482	0.022
RE5			
Eu	0.558	0.558	0.009
Ce	0.431	0.431	0.018
Dy	0.120	0.120	0.012
Gd	0.415	0.415	0.014
La	0.664	0.664	0.011
Nd	0.529	0.529	0.009
Pr	0.536	0.536	0.001
Fe	0.113	0.113	0.472
Th	0.828	0.827	0.050
RE6			
Eu	0.544	0.544	0.009
Ce	0.453	0.453	0.008
Dy	0.013	0.013	0.005
Gd	0.277	0.277	0.009
La	0.541	0.541	0.008
Nd	0.588	0.588	0.012
Pr	0.518	0.518	0.007
Fe	0.118	0.116	0.029
Th	0.690	0.690	0.037

The three ore samples behaved similarly to RE2 under the RE1-optimized conditions. All REE extraction factors were comparable to the values produced under each sample's optimal conditions for Eu extraction despite slight decreases in the value of each REE extraction factor.

Again, Fe extraction was affected much more by the changes in leaching conditions than the REEs. Predicted Fe extraction factors for RE5 were much higher under the RE1-optimized conditions while Fe extraction for RE4 experienced a large decrease and the Fe extraction factor for RE6 remained constant.

A summary of the modeling and validation data is presented in Table XXVII.

Table XXVII: Comparison of Eu Extraction Models and Equations

Element	**Eu_RE1**	**Eu_RE2**	**Eu_RE4**	**Eu_RE5**	**Eu_RE6**
Transform	Power ($\lambda = 0.016$)	None	None	None	Power ($\lambda = 0.86$)
Model	Modified Quad	Modified Quad	Modified Quad	Modified Quad	Modified Quad
Model Fit Comment*	Very Good	Excellent	Excellent	Excellent	Very Good
Model Factors					
C	**x**	**x**	**x**	**x**	**x**
T	**x**	**x**	**x**	**x**	**x**
t		**x**	**x**	**x**	**x**
CT	**x**	**x**	**x**	**x**	
Ct					**x**
Tt					
C^2	**x**	**x**	**x**	**x**	**x**
T^2		**x**	**x**	**x**	**x**
t^2					
C^2T					
Model Diagnostics					
Predicted/ Actual	Very Good	Excellent	Very Good	Excellent	Very Good
Lack of Fit	<0.05	<0.05	Not Significant (0.4386)	<0.05	Not Significant (0.2207)
R^2	Excellent	Excellent	Excellent	Excellent	Excellent
Adequate Precision	>4 (23.896) Excellent	>4 (57.477) Excellent	>4 (34.302) Excellent	>4 (109.040) Excellent	>4 (47.284) Excellent
Cook's Distance	Excellent	Excellent	Excellent	Excellent	Excellent
Leverage	Excellent	Excellent	Excellent	Excellent	Excellent
*Comment on all data fit to 3D visualization surface					

From the table, it can be observed that Eu extraction behavior is similar for RE2, RE4, RE5, and RE6. The behavior of RE1 is somewhat different in the fact that time does not appear to be a significant factor for Eu extraction. The absence of time as a significant factor was also observed in other REEs extracted from RE1 as well as Dy extraction from RE2, RE4, and RE5 and Gd extraction from RE5. The R^2 values, Cook's Distance, and Leverage diagnostics were excellent for all of the models used to describe the extraction of Eu. An area of concern was observed in the significant lack of fit values for RE1, RE2, and RE5. However, the quality of the diagnostic plots, and a visual observation of how well each data point fit the models provided sufficient support to continue using the selected models. The models used to describe the extraction behavior of the remaining REEs and gangue elements were analyzed in a similar manner to Eu and were found to be satisfactory.

The Point Prediction values show that a process optimized for Eu recovery can also recover other REEs (Ce, La, Nd, and Pr) with similar extraction factors, while Dy and Gd were consistently extracted to a lesser degree. This behavior supports the use of a multi-stage leaching process on these samples. Initial leaching stages would be implemented to remove Eu, Ce, La, Nd, and Pr. Further leaching operations could be conducted to recover Dy, Gd, and other HREE's. The optimal conditions for these subsequent leaching steps would need to be studied in greater detail in order to establish specific operating parameters.

The Point Prediction values for each sample also showed that it is possible to select operating conditions that selectively leach REEs over gangue elements, such as Fe. The ability to leach desirable metals out of a material, while leaving gangue elements behind has significant potential for industrial applications. Being able to minimize gangue element extraction can

generate considerable savings for any mining operation as it could reduce, or even eliminate, the need for gangue removal operations following leaching.

Applying the optimized conditions for RE1 to the other RER samples produced minimal losses in the predicted REE extractions (Table XXVI). This indicates that the leaching process for one material is able to effectively extract REEs from the other materials as well. This allows for a flexible process that is capable of utilizing multiple feed types. The flexibility of the leaching process is further supported by the fact that many of the optimization regions for the RER samples overlap one another. Figure 55 shows the Eu optimization region for RE1 with the optimization parameters for RE1, RE2, RE4, and RE5 plotted for comparison. RE6 was not plotted because of how close its optimized conditions were to those of RE2 and RE4.

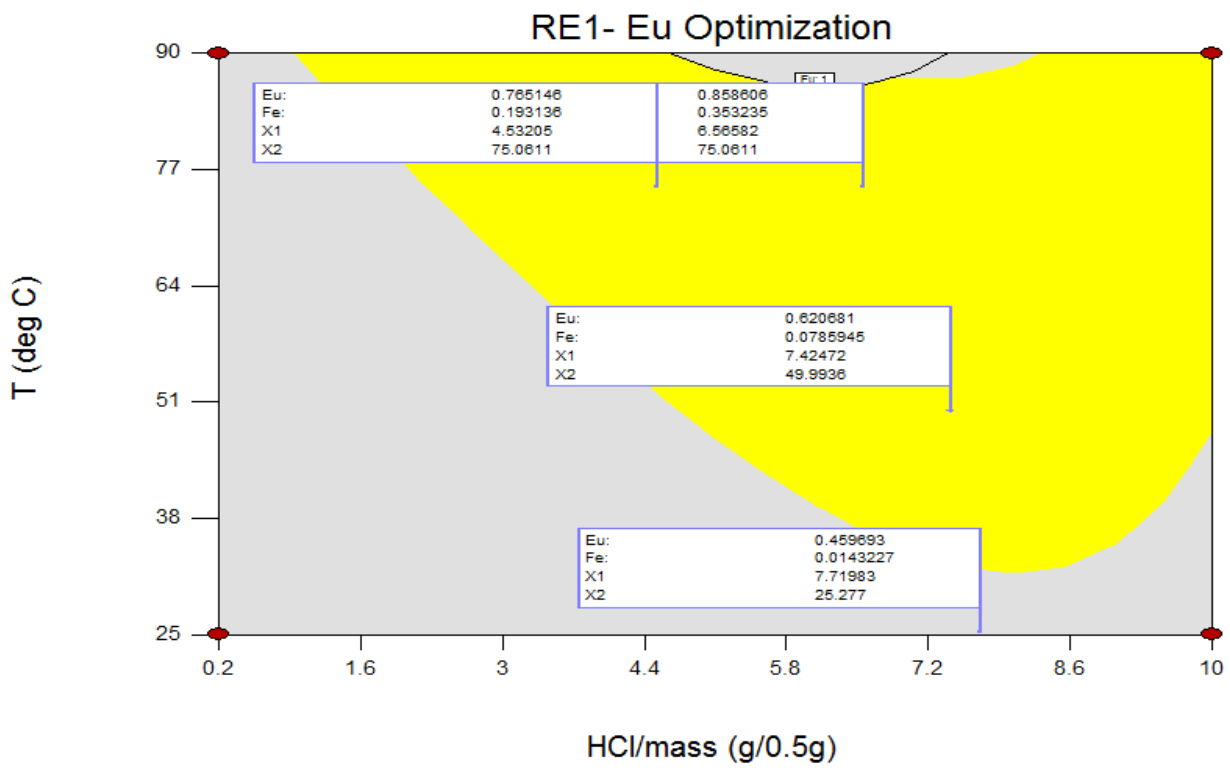

Figure 55: Comparison of Optimized conditions for RE1, RE2, RE4 and RE5

From the graph, it can be seen that all of the optimized parameters, with the exception of RE5, exist within the Eu-optimized region for RE1.

The results from this study also show promise for industrial application. Using statistical modeling, it is possible to model an industrial operation in advance, allowing for the optimal conditions to be identified and predictions to be made in the event of future disturbances, or changes, to the process. Control over process variables can be tightened, or loosened, depending on the nature of the material being introduced to the leaching process.

4. Conclusions and Future Work

4.1. Conclusions

The conducted study met the goals established in the thesis statement. From the collected data and analyses, it is possible to make the following conclusions:

- Optimization of REE extraction from the RER samples using statistical modeling is possible.
- Optimization of Eu can be done while still achieving effective extraction of other REEs (Ce, La, Nd, and Pr).
- The optimal Eu extraction conditions for one sample can be applied to other samples with minimal loss in Eu extraction
- Substantial Eu extraction can be carried out while minimizing the extraction of gangue elements, such as Fe.
- The differences in Eu extraction and the extraction of Gd, and Dy indicate a multi-stage leaching operation could be possible. Eu, Nd, Pr, and La could be extracted first, followed by Gd and Dy as the amount of REE's competing for interaction with the lixiviant would be decreased in the additional leaching stages.

- The experimental procedure used in this study for statistical modeling and optimization of REE extraction is suitable for industry.

4.2. Future Work

The development of improved REE-leaching methods can be further investigated. Potential areas for further work include the development of the suggested multi-stage leaching operation, especially in regards to implementation, potential leaching reagents, scale-up experiments, etc. Minimizing the extraction of other gangue elements (Ca, Na, Sr, etc.) and continuing the implementation of statistical modeling and analysis towards optimization of REE extraction are other areas of potential research that could be further investigated. The absence of time as a significant factor for REE extraction, especially from RE1, should also be further investigated. In addition to continued leaching research, optimized REE leach solutions should be prepared for use in REE separation studies associated with this project (Dudley, 2015).

5. Bibliography

Alonso, E., Sherman, A. M., Wallington, T. J., Everson, M. P., Field, F. R., Roth, R., et al. (2012). Evaluating Rare Earth Element Availability: A Case with Revolutionary Demand from Clean Technologies. *Environmental Science and Technology* , 3406-3414.

Carter, A. (2013). *Chlorination and Vapor Phase Extraction of Rare Earth Element Concentrate from the Bear Lodge Property, Wyoming.* Butte, MT: ProQuest LLC.

Chi, R., Tian, J., Zhu, G., Wu, Y., Li, S., & Wang, C. (2006). Kinetics of rare earth leaching from a manganese-removed weathered rare earth mud in hydrochloric acid solutions. *Separation Science and Technologies* , 1099-1113.

Chi, R., Zhang, X., Zhu, G., Zhou, Z., Wu, Y., & Wang, C. (2004). Recovery of rare earth from bastnasite by ammonium chloride roasting with fluorine deactivation. *Minerals Engineering* , 1037-1043.

de Vasconcellos, M., da Rocha, S., Pedreira, W., Queiroz, C., & Abrao, A. (200-203). Enrichment of yttrium from rare earth concentrate by ammonium carbonate leaching and peroxide precipitation. *Journal of Alloys and Compounds* , 2006.

Dudley, S. P. (2015). Rare Earth Element Recovery and Resulting Modification of Resin Structure. *2014 TMS Annual Meeting & Exhibition.* Orlando, FL: TMS.

Feng, X., Long, Z., Cui, D., Wang, L., Huang, X., & Zhang, G. (2013). Kinetics of rare earth leaching from roasted ore of bastnaesite with sulfuric acid. *Transactions of Nonferrous Metals Society of China* , 849-854.

Grasso, V. B. (2011). *Rare Earth Elements in National Defense: Background, Oversight Issues, and Options for Congress.* Washington, D.C.: Congressional Research Service.

Gupta, C. K., & Krishnamurthy, N. (2005). *Extractive Metallugy of Rare Earths.* Boca Raton, FL: CRC Press.

Gupta, C. K., & Mukerjee, T. K. (1990). *Hydrometallurgy in Extraction Processes.* Boca Raton, FL: CRC Press.

Havlik, T. (2014). *Hydrometallurgy: Principles and Applications.* Elsevier.

Humphries, Mark. (2013). *Rare Earth Elements: The Global Supply Chain.* Washington, D.C.: Congressional Research Service.

Kandil, A., Moussa, A., Aly, M., Kamel, A., Gouda, M., & Kouraim, M. (2010). Column leaching of lanthanides from abu tartur phosphate ore with kinetic study. *Journal of Rare Earths* , 576.

Kang, Z., Ting, Z., & Eyring, L. (1992). The preparation and characterization of hydroxybarbonate colloidal particles of individual and mixed rare earth elements. *Journal of Alloys and Compounds* , 477-482.

Kim, W., Bae, I., Chae, S., & Shin, H. (2009). Mechanochemical decomposition of monazite to assist the extraction of rare earth elements. *Journal of Alloys and Compounds* , 610-614.

Li, M., Zhang, X., Liu, Z., Hu, Y., Wang, M., & Liu, J. (2013). Kinetics of leaching fluoride from mixed rare earth concentrate with hydrochloric acid and aluminum chloride. *Hydrometallurgy* , 71-76.

Merriman, David; Roskil Consulting Group Ltd. (2013). *Review of the Global Supply of Rare Earths.* Royal Society of Chemistry: Environmental Chemistry Group 2013. Roskil Consulting Group Ltd.

Molycorp. (2013). *Molycorp's History*. Retrieved February 20, 2015, from Molycorp: http://www.molycorp.com/about-us/our-history/

Othmer, D. F. (1983). Random Reminiscences of Problems in Solvent Extraction. In T. C. Lo, M. H. Baird, & C. Hanson (Eds.), *Handbook of Solvent Extraction* (pp. xi-xvii). New York: Jon Wiley and Sons Inc.

Parhi, P. K., Park, K. H., Nam, C. W., Park, J. T., & Barik, S. P. (2013). Extraction of rare earth metals from deep sea nodule using H2SO4 solution. *International Journal of Mineral Processing* , 89-92.

Rare Element Resources Ltd. (2013). *Company Overview*. Retrieved February 20, 2015, from Rare Element Resources: www.rareelementresources.com

Ritcey, G. M., & Ashbrook, A. W. (1970). *Solvent Extraction: Principles and Applications to Process Metallurgy* (Vol. 2). New York: Elsevier Scientific Publishing Company.

Rosenqvist, T. (1974). Ion Exchange. In T. Rosenqvist, *Principles of Extractive Metallurgy* (pp. 456-457). McGraw-Hill Inc.

Sastri, V. S., Bunzli, J.-C., Ramaxhandra Rao, V., Rayudu, G. V., & Perumareddi, J. R. (2003). *Modern Aspects of Rare Earths and Their Complexes.* Amsterdam: Elsevier.

Tavlarides, L. L., Bae, J. H., & Lee, C. K. (1987). Solvent Extraction, Membranes, and Ion Exchange in Hydrometallurgical Dilute Metals Separation. *Separation Science and Technology* , 581-617.

The Minerals, Metals and Materials Society. (2014). Monazite. In N. R. Neelameggham, S. Alam, H. Oosterhof, A. Jha, & S. Wang (Eds.), *Rare Metal Technology 2014* (pp. 82-85). Hoboken, New Jersey: John Wiley & Sons Inc.

Thorsen, G. (1983). Commercial Processes for Rare Earths and Thorium. In T. C. Lo, M. H. Baird, & C. Hanson (Eds.), *Handbook of Solvent Extraction* (pp. 717-723). New York, NY: John Wiley and Sons Inc.

Tian, J., Yin, J., Chi, R., Rao, G., Jiang, M., & Ouyang, K. (2010). Kinetics on leaching rare earth from the weathered crust elution-deposited ores with ammonium sulfate solution. *Hydrometallurgy* , 166-170.

Twidwell, L. G., Huang, H. H., & Miller, J. D. (1980). *Unit Processes In Extractive Metallurgy: Hydrometallurgy.*

Wadsworth, M. E., & Miller, J. D. (1979). Hydrometallurgical Processes. In M. E. Wadsworth, & J. D. Miller, *Rate Processes of Extractive Metallurgy* (pp. 133-244). Springer U.S.

Wormsbecher, R., Wu-Cheng, C., & Wallenstein, D. (2010). *Role of the Rare Earth Elements in Fluid Catalytic Cracking*. Retrieved February 16, 2015, from Grace Davison: https://grace.com/catalysts-and-fuels/en-us/Documents/108-The%20Role%20of%20the%20Rare%20Earth%20Elements%20in%20Fluid%20Catalytic%20Cracking.pdf

Appendix A: Characterization Data

This appendix contains additional characterization data not presented in the main body of this thesis.

Table XXVIII: Modal Mineralogy of RER Samples (SEM/MLA)

Mineral	Formula	REE 1 Wt%	REE 2 Wt%	REE 3 Wt%	REE 4 Wt%	REE 5 Wt%	REE 6 Wt%
Aegirine	NaFeSi2O6	0.16	0.20	0.00	0.36	2.44	0.01
Alunite	KAl3(SO4)2(OH)6	0.01	0.01	0.01	0.01	0.00	0.00
Ancylite	Sr(Ce,La)(CO3)2(OH) . H2O	0.58	0.45	2.28	0.11	0.02	16.68
Apatite	Ca5(PO4)3F	0.74	0.75	0.00	0.28	0.60	0.65
Barite	BaSO4	2.69	2.45	0.01	0.61	0.02	1.22
Bastnasite	(Ce,La)(CO3)F	5.31	5.79	24.83	2.09	0.14	0.05
Biotite	K(Mg,Fe)3(AlSi3O10)(OH)2	12.34	11.89	0.00	3.42	9.46	5.84
Calcite	CaCO3	0.00	0.00	0.04	0.73	0.02	39.06
Cerianite	(Ce,Th)O2	5.88	5.31	0.01	2.19	0.48	0.02
Chalcopyrite	CuFeS2	0.01	0.00	0.03	0.00	0.05	0.00
Coronadite	PbMn8O16	0.62	0.80	0.00	0.55	0.11	0.23
FeO	Fe2.5O3.5	17.37	21.27	0.11	34.67	13.16	20.44
Fluorite	CaF2	0.00	0.00	0.00	0.00	0.01	0.00
Goyazite	SrAl3(PO4)(PO3OH)(OH)6	0.07	0.08	0.00	0.07	0.01	0.00
Grossular	Ca3Al2Si3O12	0.02	0.01	0.00	0.00	0.00	0.00
Hollandite	BaMn8O16	6.95	6.05	0.00	3.40	0.86	0.32
Hornblende	(Ca2,Na)(Mg2FeAl)Si6O22(OH)2	0.02	0.02	0.00	0.00	0.01	0.17
Ilmenite	FeTiO3	0.61	0.69	0.00	1.05	1.53	0.51
Jarosite	KFe3(SO4)2(OH)6	0.04	0.01	0.00	0.01	0.00	0.04
K_Feldspar	KAlSi3O8	7.54	8.96	0.01	31.09	61.87	8.78
Mica	KAl2(AlSi3O10)(OH)2	4.56	3.32	0.00	2.58	3.32	0.03
MnO	(MnO(OH))(MnCO3)Ba0.1	10.41	11.42	19.04	8.25	2.67	1.42
Monazite	(La,Ce)PO4	8.14	5.29	22.30	1.51	0.91	1.21
Parisite	Ca(Ce,La)2(CO3)3F2	8.53	9.37	31.06	3.01	0.66	0.34
Plagioclase	(Na,Ca)(Al,Si)4O8	0.22	0.16	0.00	0.04	0.02	0.00
Pyrite	FeS2	0.00	0.00	0.00	0.01	0.00	0.25
Quartz	SiO2	4.37	3.81	0.20	3.07	0.68	0.26
Rhodonite_Ba	(Mn,Fe,Mg,Ca)SiO3Ba0.05	2.47	1.47	0.05	0.46	0.88	0.17
Rutile	TiO2	0.31	0.40	0.01	0.41	0.03	0.06
Strontianite	SrCO3	0.00	0.00	0.00	0.00	0.00	2.23
Titanite	CaTiSiO5	0.00	0.00	0.00	0.00	0.02	0.00
Xenotime	YPO4	0.00	0.00	0.00	0.01	0.00	0.00
Zircon	ZrSiO4	0.00	0.00	0.00	0.00	0.01	0.00
Total		100.00	100.00	100.00	100.00	100.00	100.00

Table XXIX: SEM/MLA Elemental Analysis of RER Samples

Element	REE 1 - Wt%	REE 2 - Wt%	REE 3 - Wt%	REE 4 - Wt%	REE 5 - Wt%	REE 6 - Wt%
Al	2.50	2.35	0.00	3.78	7.28	1.24
Ba	3.52	3.24	1.22	1.47	0.37	0.87
C	1.48	1.61	4.65	0.87	0.20	6.02
Ca	1.15	1.13	2.34	0.67	0.37	15.96
Ce	8.36	7.67	23.15	2.63	0.65	3.53
Cu	0.00	0.00	0.01	0.00	0.02	0.00
F	1.09	1.20	4.36	0.41	0.09	0.05
Fe	14.58	17.22	0.10	25.73	11.91	15.70
H	0.14	0.13	0.11	0.07	0.07	0.17
K	2.65	2.68	0.00	4.94	9.89	1.78
La	6.41	5.91	22.94	1.91	0.49	3.50
Mg	0.83	0.75	0.00	0.22	0.58	0.35
Mn	9.52	9.53	9.66	6.30	1.96	1.02
Na	0.03	0.03	0.00	0.04	0.24	0.01
O	33.96	33.80	27.86	36.44	42.39	39.78
P	1.22	0.85	2.95	0.26	0.23	0.28
Pb	0.14	0.18	0.00	0.13	0.02	0.05
S	0.38	0.34	0.01	0.09	0.02	0.31
Si	8.38	7.97	0.11	12.27	22.43	4.03
Sr	0.15	0.12	0.52	0.04	0.01	5.15
Th	3.13	2.82	0.01	1.17	0.26	0.01
Ti	0.38	0.46	0.00	0.58	0.51	0.20
Y	0.00	0.00	0.00	0.00	0.00	0.00
Zr	0.00	0.00	0.00	0.00	0.00	0.00
Total	100.00	100.00	100.00	100.00	100.00	100.00

Table XXX: ICP-AES LiB_4 Fusion Results

Element	RE1	RE2	RE3	RE4	RE5	RE6
Al3944	8.566%	8.029%	4.584%	10.138%	13.863%	3.411%
Ca4226	3.647%	3.793%	5.348%	1.833%	1.637%	29.756%
Ce4040	10.049%	10.414%	19.253%	2.666%	0.930%	4.019%
Dy4000	0.261%	0.278%	0.495%	0.084%	0.031%	0.088%
Er3264	-0.014%	-0.015%	-0.017%	0.018%	0.008%	-0.006%
Eu3819	0.130%	0.134%	0.210%	0.036%	0.018%	0.041%
Fe2382	18.896%	20.150%	0.291%	31.187%	15.306%	20.432%
Gd3422	0.331%	0.347%	0.661%	0.105%	0.047%	0.112%
Ho3456	-0.011%	-0.011%	0.025%	-0.020%	-0.032%	-0.011%
K_7664	6.692%	6.979%	0.383%	16.771%	23.169%	5.325%
La3337	9.626%	10.573%	20.709%	2.806%	0.820%	4.207%
Lu2615	0.001%	0.001%	0.003%	0.000%	0.000%	0.00%
Mg2790	1.189%	1.228%	0.660%	0.480%	1.374%	0.989%
Na5895	0.421%	0.372%	19.521%	0.387%	1.102%	0.150%
Nd4061	4.446%	4.620%	7.011%	1.100%	0.468%	1.598%
Pr4143	1.282%	1.337%	2.133%	0.341%	0.139%	0.486%
S_1820	0.535%	0.513%	0.133%	0.214%	0.119%	0.492%
Sc2273	0.002%	0.003%	0.002%	-0.003%	-0.004%	-0.001%
Sm3609	0.339%	0.347%	0.408%	0.092%	0.048%	0.103%
Tb3380	9.030%	9.878%	19.176%	2.539%	0.749%	3.779%
Th2837	0.252%	0.289%	-0.033%	0.079%	0.028%	0.055%
Tm3131	-0.037%	-0.038%	-0.063%	-0.018%	-0.007%	-0.015%
U_2635	0.285%	0.382%	-0.061%	0.339%	0.089%	0.247%
Y_3242	0.113%	0.158%	0.811%	-0.027%	-0.164%	-0.024%
Yb2116	0.007%	0.009%	0.025%	0.004%	0.000%	0.001%

Table XXXI: ICP-MS LiB_4 Fusion Results

Client ID Lab ID	RE1 1406113-001A	RE2 1406113-002A	RE4 1406113-003A	RE5 1406113-004A	RE6 1406113-005A
Ce4040	6.254%	5.416%	1.463%	0.550%	1.653%
Dy3531	0.045%	0.044%	0.012%	<MDL	<MDL
Er3499	0.011%	0.013%	<MDL	<MDL	<MDL
Eu3819	0.082%	0.072%	0.019%	0.011%	0.018%
Gd3350	0.169%	0.148%	0.042%	0.021%	0.033%
Ho3398	0.022%	0.019%	<MDL	<MDL	<MDL
La3337	6.176%	5.673%	1.460%	0.493%	1.689%
Lu2195	<MDL	<MDL	<MDL	<MDL	<MDL
Nd4156	2.997%	2.613%	0.621%	0.293%	0.735%
Pr4225	0.717%	0.630%	0.148%	0.063%	0.175%
Sc3613	0.003%	0.002%	0.001%	0.001%	0.001%
Sm3609	0.283%	0.250%	0.062%	0.037%	0.060%
Tb3509	<MDL	<MDL	<MDL	<MDL	<MDL
Th2832	0.192%	0.174%	0.068%	0.041%	0.034%
Tm3425	0.007%	<MDL	<MDL	<MDL	<MDL
Y_3710	0.102%	0.104%	0.062%	0.011%	0.007%
Yb3289	0.006%	0.006%	0.003%	0.001%	0.001%

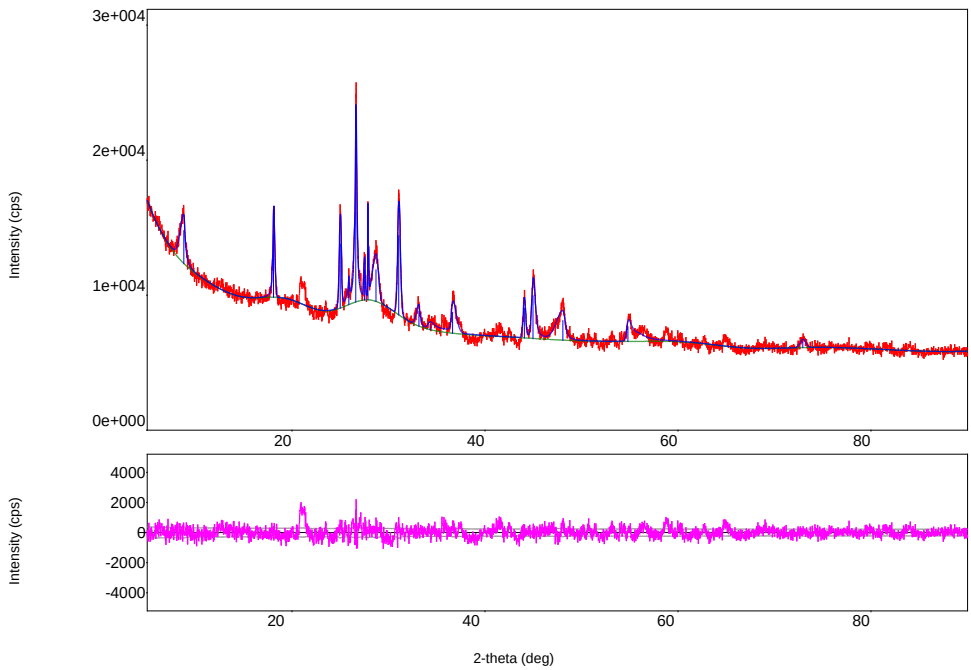

Figure 56: XRD Spectra of RE2 Concentrate

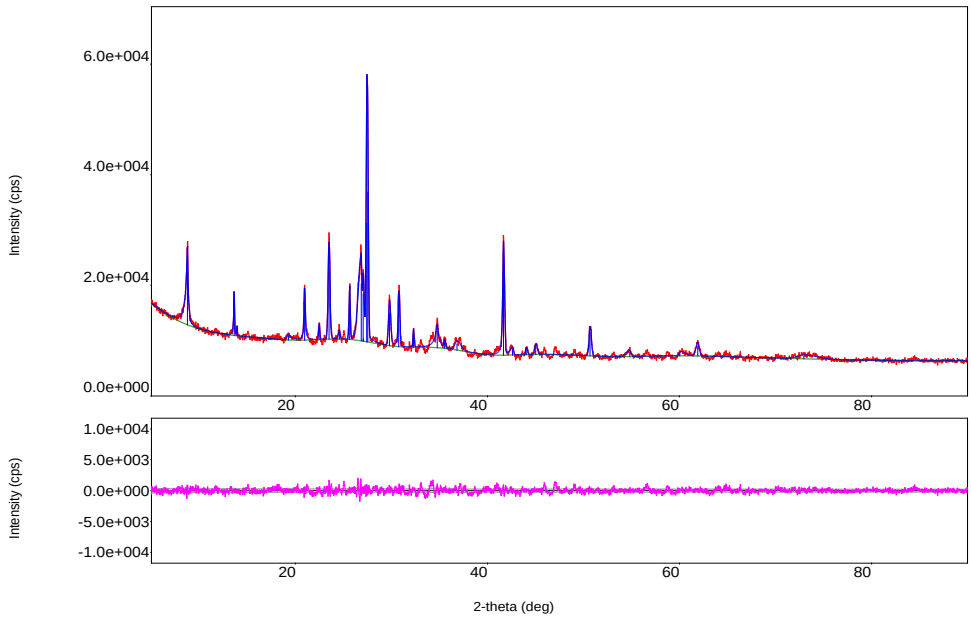

Figure 57: XRD Spectra of RE5 Ore

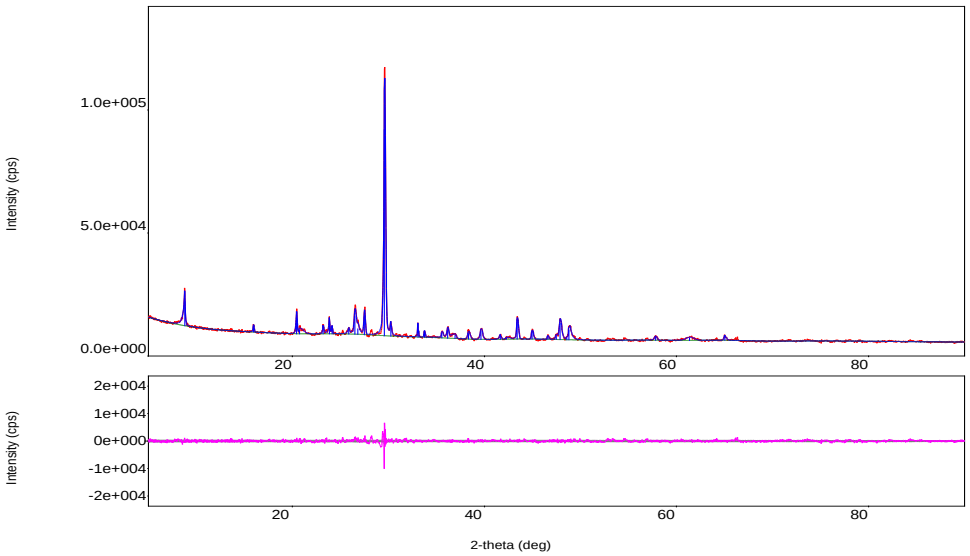

Figure 58: XRD Spectra of RE6 Ore

Appendix B: Proof-of-Concept H_2O Leach Test Results

This appendix contains the ICP-AES results for the H_2O leach tests conducted as part of the proof-of-concept study.

Table XXXII: REE Extraction for Preliminary H_2O Leach Tests (25°C)

Sample ID	Ce	Dy	Er	Eu	Gd	La	Nd	Pr	Sm	Tb	Yb
RE1	0.000	0.001	0.004	0.000	0.000	0.001	0.000	0.000	0.001	0.084	0.000
RE2	0.000	0.003	0.007	0.000	0.001	0.000	0.000	0.000	0.000	0.057	0.000
RE3	0.000	0.000	-0.001	0.000	0.000	0.000	0.000	0.000	0.000	-0.002	-0.001
RE4	0.000	0.008	-0.003	-0.001	0.001	0.001	0.001	-0.001	0.000	-0.005	-0.001
RE5	0.002	0.017	0.013	0.000	0.007	0.006	0.002	-0.003	0.000	0.149	-0.012
RE6	0.000	0.008	-0.013	-0.002	0.001	0.001	0.000	0.000	-0.001	0.000	-0.010

Table XXXIII: REE Extraction Factors for Preliminary H_2O Leach Tests (60°C)

Sample ID	Ce	Dy	Er	Eu	Gd	La	Nd	Pr	Sm	Tb	Yb
RE1	0.001	0.000	0.020	0.001	0.003	0.001	0.001	0.001	-0.000	0.214	0.000
RE2	0.000	0.007	0.008	0.000	0.001	0.000	0.000	0.001	-0.000	0.072	-0.001
RE3	0.000	0.001	0.001	0.000	0.001	0.000	0.000	0.000	-0.000	0.006	-0.000
RE4	0.000	0.012	0.006	-0.001	0.007	0.000	-0.000	0.001	-0.003	0.025	-0.002
RE5	0.001	0.030	0.062	0.001	0.000	0.003	0.002	0.004	-0.001	0.419	-0.002
RE6	0.000	0.005	0.006	0.000	0.000	0.000	-0.000	0.001	-0.001	0.057	0.005

Appendix C: RE1 Scoping Tests - Composite Graphs

This appendix contains the remaining composite graphs for the scoping tests that were not presented in the main body of the document.

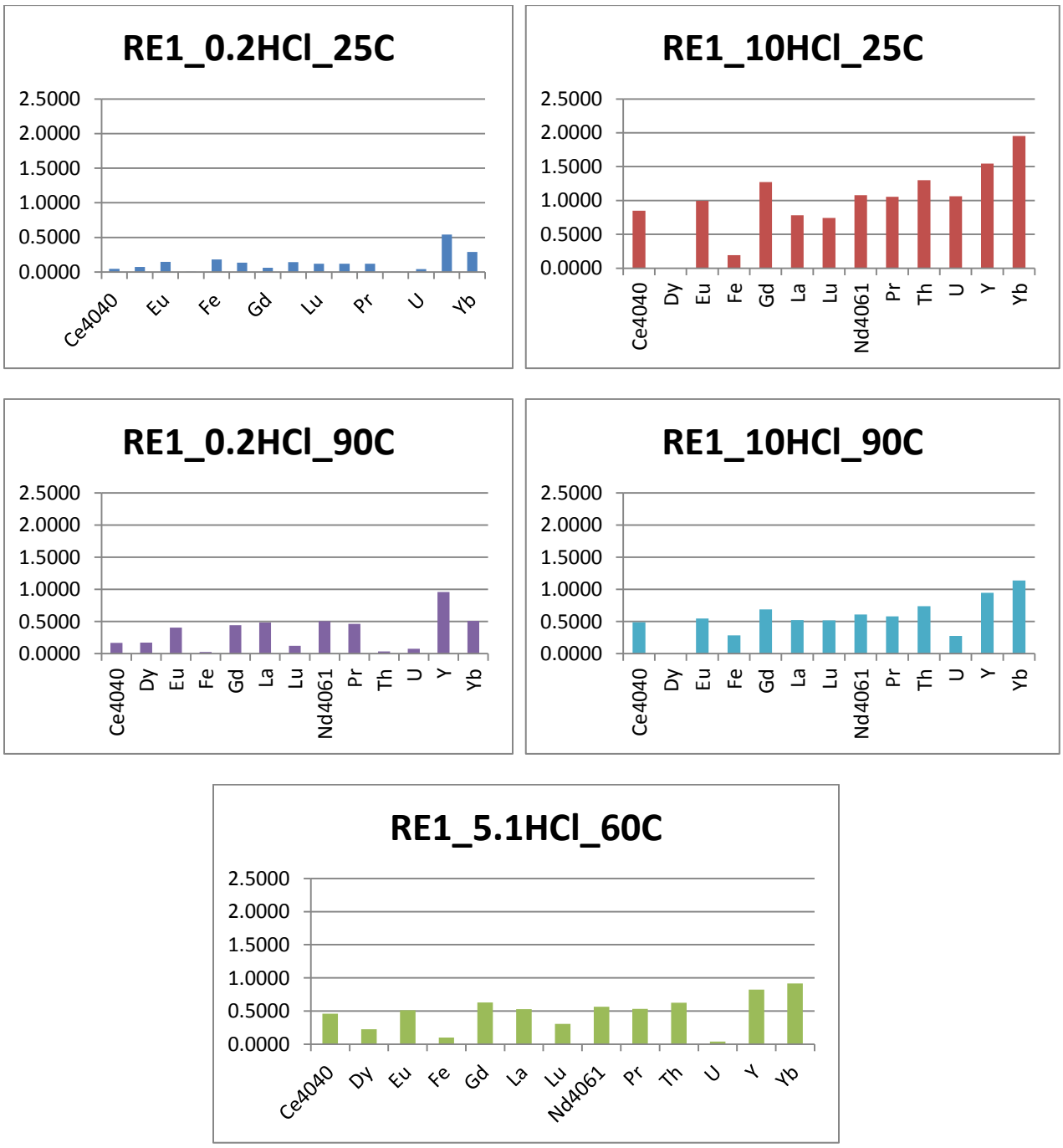

Figure 59: RE1 Scoping Tests - Composite Graphs

Appendix D: Raw Data from Design Matrices

This appendix contains the raw data from the five experimental design matrices used to analyze REE extraction from the five RER samples tested in this study. Reagent concentrations, sample masses, and ICP-AES data are presented in the following tables.

Table XXXIV: RE1 Design Matrix Sample and Reagent Masses

Experiment No.	HCl Conc. ($g_{HCl}/0.5g_{solids}$)	Mass 37.35% HCl Soln. (g)	RE1 Sample Mass (g)
1	0.2	0.5722	0.52
2	10	26.8185	0.52
3	0.2	0.5553	0.51
4	10	26.8164	0.51
5	0.2	0.5740	0.51
6	10	26.8021	0.53
7	0.2	0.5667	0.52
8	10	26.7974	0.52
9	0.2	0.6044	0.51
10	10	26.7954	0.51
11	5.1	13.8304	0.52
12	5.1	13.6717	0.53
13	5.1	13.6965	0.52
14	5.1	13.6681	0.52
15	5.1	13.9737	0.51
16	5.1	13.6848	0.52
17	5.1	13.6837	0.50
18	5.1	13.6930	0.51
19	5.1	13.7915	0.51
20	5.1	-	-

Table XXXV: RE2 Design Matrix Sample and Reagent Masses

Experiment No.	HCl Conc. ($g_{HCl}/0.5g_{solids}$)	Mass 37.35% HCl Soln. (g)	RE2 Sample Mass (g)
1	0.2	0.5515	0.5072
2	10	26.7843	0.5055
3	0.2	0.5539	0.5045
4	10	26.8947	0.5070
5	0.2	0.5803	0.5042
6	10	26.8634	0.5073
7	0.2	0.5879	0.5039
8	10	26.8450	0.5030
9	0.2	0.5461	0.5018
10	10	26.7868	0.5057
11	5.1	13.6737	0.5020
12	5.1	13.6891	0.5056
13	5.1	13.7080	0.5080
14	5.1	13.7600	0.5033
15	5.1	13.6942	0.5088
16	5.1	13.6723	0.5031
17	5.1	13.7461	0.5009
18	5.1	13.7196	0.5038
19	5.1	13.7201	0.5067
20	5.1	13.7700	0.5066

Table XXXVI: RE4 Design Matrix Sample and Reagent Masses

Experiment No.	HCl Conc. ($g_{HCl}/0.5g_{solids}$)	Mass 37.35% HCl Soln. (g)	RE4 Sample Mass (g)
1	0.2	0.5605	0.5114
2	10	26.8356	0.5091
3	0.2	0.5593	0.5050
4	10	26.8220	0.5089
5	0.2	0.5639	0.5095
6	10	26.8772	0.5068
7	0.2	0.5755	0.5073
8	10	26.9025	0.5099
9	0.2	0.5567	0.5083
10	10	26.9158	0.5147
11	5.1	13.8730	0.5146
12	5.1	13.7356	0.5088
13	5.1	13.6790	0.5049
14	5.1	13.9310	0.5079
15	5.1	13.7267	0.5117
16	5.1	13.6576	0.5047
17	5.1	13.7355	0.5052
18	5.1	13.9499	0.5143
19	5.1	13.7498	0.5117
20	5.1	13.7929	0.5154

Table XXXVII: RE5 Design Matrix Sample and Reagent Masses

Experiment No.	HCl Conc. ($g_{HCl}/0.5g_{solids}$)	Mass 37.35% HCl Soln. (g)	RE5 Sample Mass (g)
1	0.2	0.6009	0.5060
2	10	26.8088	0.5048
3	0.2	0.5767	0.5008
4	10	26.8260	0.5016
5	0.2	0.5793	0.5065
6	10	26.8061	0.5078
7	0.2	0.5956	0.5021
8	10	26.8441	0.5028
9	0.2	0.5506	0.5011
10	10	26.8157	0.5052
11	5.1	13.7688	0.5021
12	5.1	13.6580	0.5028
13	5.1	13.6832	0.5072
14	5.1	13.6789	0.5033
15	5.1	13.6844	0.5068
16	5.1	13.6734	0.5078
17	5.1	13.6955	0.5063
18	5.1	13.6706	0.5046
19	5.1	13.6943	0.5016
20	5.1	13.6701	0.5072

Table XXXVIII: RE6 Design Matrix Sample and Reagent Masses

Experiment No.	HCl Conc. ($g_{HCl}/0.5g_{solids}$)	Mass 37.35% HCl Soln. (g)	RE6 Sample Mass (g)
1	0.2	0.5427	0.5027
2	10	26.8334	0.5046
3	0.2	0.5404	0.5042
4	10	26.8097	0.5020
5	0.2	0.5479	0.5044
6	10	26.8192	0.5031
7	0.2	0.6137	0.5020
8	10	26.8884	0.5024
9	0.2	0.5432	0.5018
10	10	26.8135	0.5051
11	5.1	13.6675	0.5027
12	5.1	13.6647	0.5034
13	5.1	13.7176	0.5031
14	5.1	13.6844	0.5043
15	5.1	13.6966	0.5027
16	5.1	13.6847	0.5042
17	5.1	13.7532	0.5014
18	5.1	13.7026	0.5023
19	5.1	13.7461	0.5018
20	5.1	13.6709	0.5013

Table XXXIX: RE1 Design Matrix Extraction Factors

Experiment ID	Al	Ce	Dy	Eu	Gd	La	Nd	Pr	Th	U	Y	Fe
1	0.015	0.006	0.009	0.024	0.026	0.015	0.016	0.015	0.002	0.006	0.088	0.001
2	0.039	0.275	0.125	0.410	0.304	0.430	0.379	0.386	0.437	0.046	0.833	0.014
3	0.075	0.104	0.082	0.287	0.257	0.356	0.280	0.294	0.018	0.061	0.670	0.008
4	0.184	0.571	0.152	0.719	0.478	0.760	0.659	0.682	0.857	0.448	1.479	0.499
5	0.024	0.014	0.019	0.051	0.052	0.043	0.036	0.038	0.001	0.017	0.231	0.001
6	0.051	0.380	0.144	0.465	0.314	0.488	0.420	0.437	0.535	0.057	0.912	0.021
7	0.111	0.136	0.100	0.353	0.310	0.447	0.349	0.372	0.025	0.072	0.815	0.017
8	0.182	0.435	0.120	0.544	0.359	0.581	0.495	0.515	0.653	0.283	1.191	0.424
9	0.054	0.077	0.064	0.221	0.200	0.260	0.202	0.218	0.016	0.038	0.541	0.007
10	0.149	0.413	0.115	0.525	0.365	0.564	0.475	0.507	0.592	0.550	1.020	0.197
11	0.042	0.174	0.102	0.348	0.281	0.382	0.314	0.338	0.314	0.034	0.740	0.011
12	0.211	1.203	0.328	1.571	1.077	1.504	1.375	1.511	1.829	0.832	3.104	0.798
13	0.098	0.390	0.149	0.519	0.364	0.562	0.467	0.504	0.524	0.093	0.996	0.054
14	0.154	0.456	0.151	0.583	0.394	0.625	0.518	0.566	0.627	0.285	1.110	0.146
15	0.130	0.410	0.153	0.536	0.376	0.575	0.477	0.523	0.554	0.083	1.015	0.078
16	0.147	0.418	0.141	0.541	0.378	0.582	0.487	0.528	0.575	0.290	1.029	0.110
17	0.148	0.426	0.156	0.554	0.387	0.592	0.494	0.540	0.568	0.088	1.044	0.096
18	0.137	0.415	0.149	0.540	0.377	0.577	0.481	0.524	0.552	0.142	1.017	0.085
19	0.143	0.417	0.153	0.538	0.375	0.579	0.482	0.524	0.561	0.092	1.025	0.088

Table XL: RE2 Design Matrix Extraction Factors

Experiment ID	Al	Ce	Dy	Eu	Gd	La	Nd	Pr	Th	U	Y	Fe
1	0.014	0.007	0.010	0.029	0.030	0.020	0.019	0.020	0.001	0.004	0.078	0.001
2	0.037	0.253	0.116	0.389	0.290	0.405	0.341	0.377	0.385	0.026	0.642	0.011
3	0.081	0.105	0.082	0.290	0.253	0.347	0.267	0.302	0.017	0.039	0.541	0.008
4	0.189	0.414	0.126	0.538	0.372	0.563	0.473	0.521	0.580	0.229	0.903	0.345
5	0.023	0.020	0.023	0.068	0.066	0.062	0.051	0.057	0.002	0.012	0.171	0.001
6	0.059	0.380	0.147	0.475	0.325	0.495	0.414	0.461	0.505	0.041	0.766	0.021
7	0.125	0.139	0.104	0.365	0.313	0.442	0.340	0.386	0.029	0.039	0.678	0.017
8	0.214	0.430	0.134	0.557	0.379	0.578	0.485	0.533	0.613	0.172	1.036	0.421
9	0.058	0.079	0.065	0.223	0.197	0.254	0.199	0.224	0.010	0.028	0.439	0.005
10	0.160	0.396	0.129	0.515	0.359	0.542	0.451	0.504	0.533	0.310	0.822	0.149
11	0.044	0.212	0.110	0.372	0.289	0.400	0.329	0.367	0.342	0.022	0.634	0.011
12	0.205	0.428	0.152	0.557	0.388	0.588	0.487	0.542	0.578	-0.022	0.909	0.289
13	0.116	0.376	0.151	0.501	0.351	0.531	0.441	0.494	0.490	0.016	0.806	0.050
14	0.167	0.401	0.156	0.519	0.362	0.549	0.457	0.511	0.522	-0.009	0.830	0.092
15	0.150	0.407	0.155	0.531	0.369	0.559	0.467	0.522	0.525	0.053	0.838	0.077
16	0.155	0.401	0.157	0.526	0.366	0.555	0.463	0.517	0.519	0.003	0.836	0.075
17	0.152	0.407	0.160	0.529	0.369	0.559	0.468	0.522	0.527	0.005	0.847	0.073
18	0.155	0.409	0.152	0.538	0.375	0.564	0.471	0.529	0.534	0.127	0.856	0.085
19	0.150	0.397	0.154	0.517	0.361	0.546	0.455	0.509	0.514	0.006	0.823	0.073
20	0.157	0.400	0.152	0.524	0.366	0.552	0.462	0.515	0.524	0.079	0.845	0.082

Table XLI: RE4 Design Matrix Extraction Factors

Experiment ID	Al	Ce	Dy	Eu	Gd	La	Nd	Pr	Th	U	Y	Fe
1	0.011	0.015	0.016	0.047	0.041	0.039	0.037	0.037	0.015	0.004	-0.271	0.002
2	0.015	0.173	0.108	0.339	0.249	0.374	0.320	0.340	0.314	0.007	-1.448	0.006
3	0.038	0.149	0.111	0.345	0.310	0.436	0.340	0.372	0.120	0.010	-1.622	0.008
4	0.092	0.419	0.120	0.518	0.338	0.562	0.478	0.468	0.658	-0.179	-2.491	0.266
5	0.010	0.037	0.037	0.106	0.089	0.106	0.091	0.096	0.040	0.002	-0.596	0.003
6	0.023	0.302	0.150	0.440	0.294	0.495	0.420	0.442	0.449	0.004	-1.877	0.009
7	0.049	0.174	0.122	0.381	0.292	0.480	0.378	0.409	0.117	0.015	-1.750	0.013
8	0.115	0.448	0.123	0.542	0.316	0.569	0.489	0.457	0.732	-0.311	-3.121	0.358
9	0.022	0.110	0.087	0.265	0.210	0.322	0.254	0.277	0.116	0.005	-1.307	0.007
10	0.063	0.416	0.154	0.524	0.340	0.582	0.491	0.508	0.615	0.117	-2.532	0.070
11	0.019	0.184	0.120	0.368	0.274	0.418	0.347	0.373	0.341	0.002	-1.623	0.006
12	0.095	0.407	0.160	0.512	0.337	0.569	0.477	0.482	0.613	-0.250	-2.389	0.197
13	0.038	0.281	0.251	0.455	0.316	0.516	0.435	0.465	0.419	0.000	-1.911	0.015
14	0.060	0.373	0.153	0.488	0.325	0.531	0.457	0.478	0.507	0.047	-2.118	0.035
15	0.050	0.336	0.154	0.467	0.297	0.524	0.447	0.472	0.468	-0.002	-1.944	0.025
16	0.051	0.330	0.154	0.472	0.280	0.515	0.446	0.463	0.488	-0.003	-1.977	0.035
17	0.054	0.382	0.166	0.520	0.349	0.578	0.490	0.521	0.530	0.033	-2.172	0.027
18	0.056	0.369	0.169	0.504	0.341	0.559	0.478	0.501	0.511	0.013	-2.181	0.029
19	0.057	0.369	0.166	0.506	0.337	0.561	0.479	0.503	0.524	-0.002	-2.108	0.032
20	0.054	0.379	0.170	0.519	0.351	0.570	0.494	0.516	0.521	0.019	-2.168	0.028

Table XLII: RE5 Design Matrix Extraction Factors

Experiment ID	Al	Ce	Dy	Eu	Gd	La	Nd	Pr	Th	U	Y	Fe
1	0.018	0.020	0.034	0.073	0.080	0.046	0.043	0.040	0.026	0.020	-0.032	0.011
2	0.042	0.241	0.121	0.457	0.371	0.584	0.456	0.475	0.536	-0.017	-0.081	0.039
3	0.047	0.069	0.047	0.173	0.159	0.203	0.151	0.157	0.020	0.055	-0.050	0.031
4	0.122	0.491	0.067	0.575	0.301	0.658	0.529	0.494	0.936	-0.767	-0.097	0.389
5	0.025	0.030	0.040	0.099	0.104	0.076	0.066	0.064	0.023	0.041	-0.039	0.016
6	0.053	0.334	0.120	0.510	0.392	0.618	0.494	0.510	0.638	0.040	-0.082	0.057
7	0.062	0.105	0.058	0.236	0.203	0.324	0.230	0.242	0.044	0.071	-0.060	0.044
8	0.134	0.532	0.078	0.622	0.284	0.681	0.558	0.509	1.013	-0.895	-0.106	0.444
9	0.042	0.060	0.047	0.159	0.150	0.169	0.131	0.134	0.035	0.052	-0.050	0.029
10	0.104	0.463	0.070	0.546	0.375	0.636	0.512	0.507	0.795	0.057	-0.087	0.194
11	0.045	0.238	0.119	0.457	0.371	0.593	0.456	0.476	0.517	-0.007	-0.081	0.041
12	0.128	0.506	0.078	0.594	0.315	0.694	0.554	0.526	0.932	-0.541	-0.098	0.348
13	0.081	0.360	0.124	0.534	0.405	0.643	0.509	0.520	0.675	-0.121	-0.086	0.106
14	0.103	0.438	0.115	0.546	0.394	0.646	0.513	0.517	0.755	-0.200	-0.086	0.160
15	0.096	0.417	0.121	0.548	0.402	0.650	0.518	0.524	0.753	-0.169	-0.087	0.141
16	0.096	0.414	0.119	0.536	0.391	0.636	0.508	0.515	0.725	-0.149	-0.085	0.140
17	0.096	0.415	0.116	0.540	0.397	0.642	0.512	0.518	0.734	-0.140	-0.086	0.139
18	0.099	0.421	0.116	0.542	0.394	0.640	0.510	0.514	0.750	-0.177	-0.086	0.149
19	0.100	0.427	0.118	0.545	0.397	0.646	0.513	0.520	0.751	-0.183	-0.086	0.150
20	0.098	0.416	0.119	0.537	0.395	0.641	0.509	0.516	0.734	-0.192	-0.085	0.140

Table XLIII: RE6 Design Matrix Extraction Factors

Experiment ID	Al	Ce	Dy	Eu	Gd	La	Nd	Pr	Th	U	Y	Fe
1	0.008	0.298	0.001	0.351	0.170	0.388	0.401	0.372	0.282	0.046	-	0.009
2	0.058	0.416	0.014	0.485	0.241	0.510	0.536	0.488	0.559	0.038	-	0.038
3	0.017	0.380	0.015	0.451	0.217	0.506	0.522	0.477	0.003	0.063	-	0.001
4	0.190	0.459	-0.001	0.570	0.280	0.547	0.600	0.516	0.746	-0.275	-	0.339
5	0.009	0.362	0.011	0.419	0.197	0.477	0.486	0.447	0.276	0.052	-	0.008
6	0.083	0.431	0.008	0.506	0.245	0.521	0.566	0.490	0.570	0.027	-	0.053
7	0.054	0.418	0.008	0.492	0.231	0.548	0.578	0.508	0.028	0.069	-	0.007
8	0.209	0.482	0.001	0.595	0.235	0.569	0.644	0.523	0.762	-0.331	-	0.401
9	0.015	0.381	0.014	0.443	0.200	0.500	0.529	0.465	0.111	0.047	-	0.004
10	0.172	0.477	0.003	0.576	0.280	0.564	0.636	0.531	0.680	-0.088	-	0.195
11	0.071	0.420	0.024	0.486	0.231	0.509	0.553	0.477	0.528	0.031	-	0.035
12	0.204	0.482	0.001	0.596	0.278	0.571	0.641	0.533	0.736	-0.228	-	0.313
13	0.119	0.449	0.020	0.532	0.259	0.541	0.592	0.511	0.599	0.006	-	0.076
14	0.180	0.468	0.013	0.566	0.280	0.559	0.617	0.530	0.675	-0.057	-	0.147
15	0.167	0.471	0.016	0.567	0.278	0.565	0.620	0.534	0.663	-0.030	-	0.118
16	0.162	0.459	0.015	0.555	0.279	0.552	0.600	0.528	0.660	-0.024	-	0.114
17	0.165	0.456	0.015	0.553	0.276	0.547	0.599	0.524	0.644	-0.030	-	0.114
18	0.166	0.451	0.016	0.545	0.273	0.539	0.593	0.515	0.640	-0.034	-	0.117
19	0.164	0.463	0.016	0.555	0.275	0.554	0.606	0.529	0.650	-0.033	-	0.114
20	0.164	0.456	0.016	0.552	0.277	0.548	0.597	0.524	0.649	-0.031	-	0.113

Appendix E: Modeling Data for RE1

Appendices E through I contain additional modeling data for the other REE extraction factors from the five RER samples. Response surface graphs, modeling equations, and contour plots of extraction are presented, as well as diagnostic graphs and ANOVA data.

Aluminum (Al)

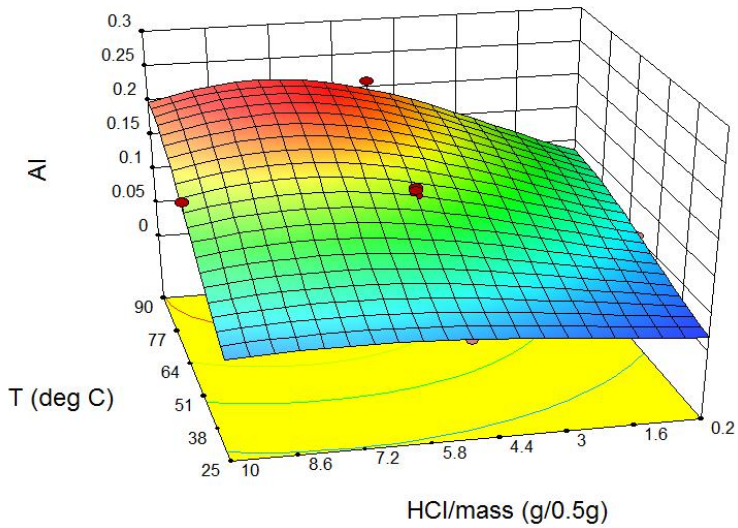

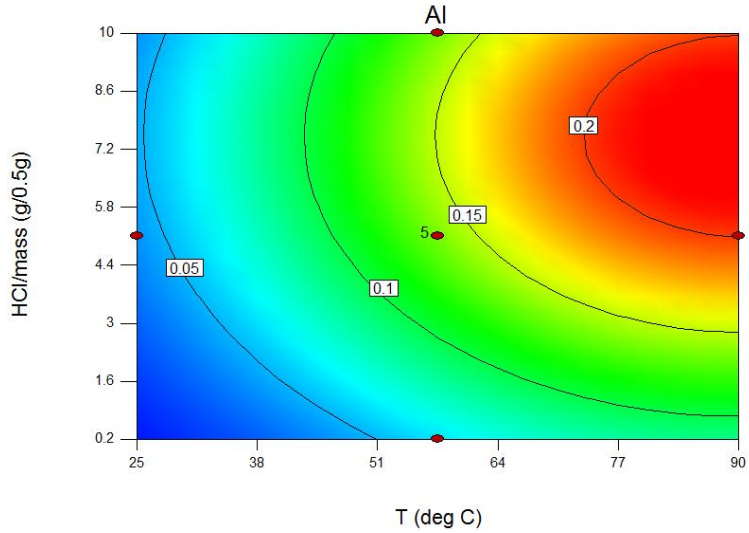

Equation: $Log_{10}(Al) = -2.52319 + 0.12539C + 0.028048T + 2.30538 \times 10^{-3}t - 1.53491 \times 10^{-4}Ct - 7.57166 \times 10^{-3}C^2 - 1.55331 \times 10^{-4}T^2$

Figure 60: Contour Plot, Model Equation, and Response Surface of Al Extraction from RE1 (Time: 75 min)

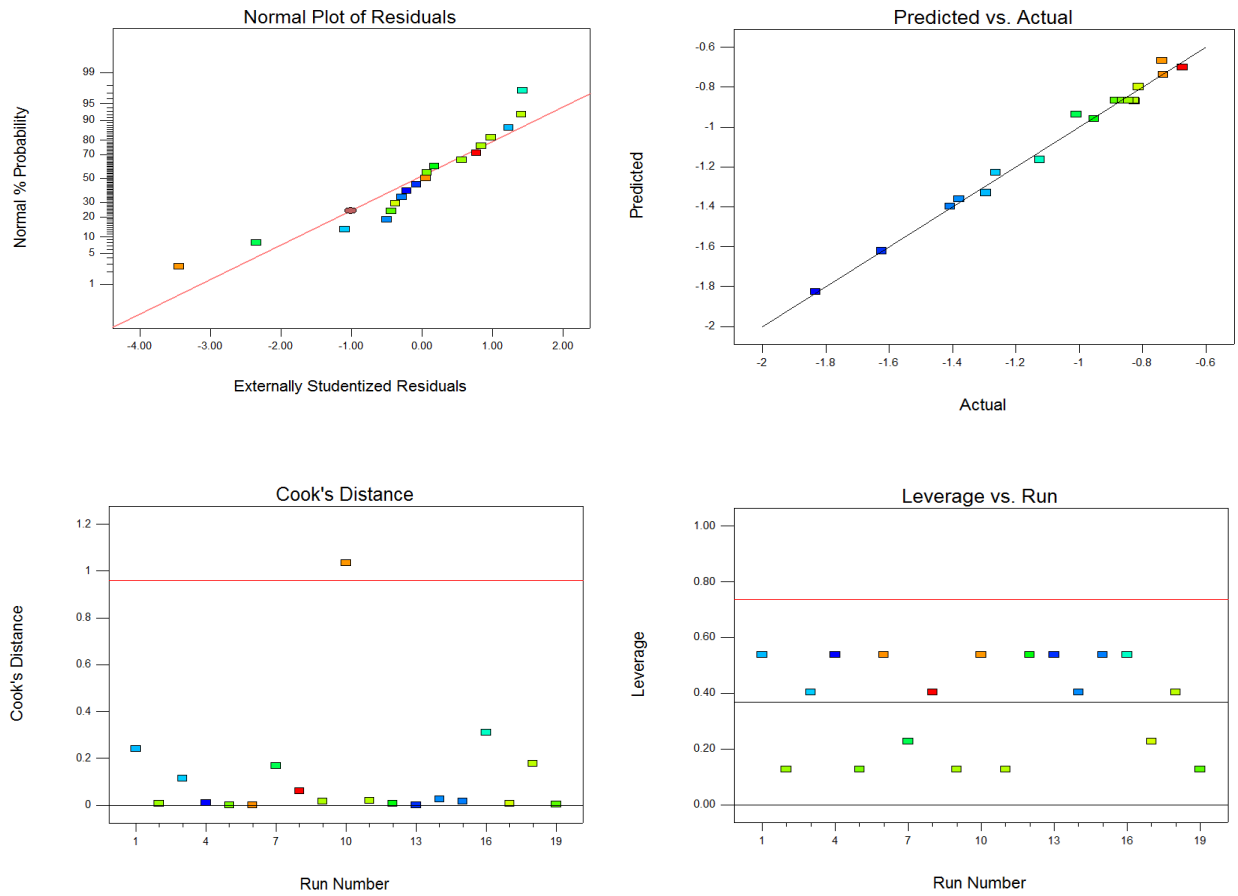

Figure 61: Diagnostics for Al Extraction Model (RE1)

Table XLIV: ANOVA Data for Al Extraction From RE1

Source	Sum of Squares	df	Mean Square	F-Value	p-value	Notes
Model	1.92	6	0.32	181.32	< 0.0001	significant
C-HCl/mass	0.32	1	0.32	182.59	< 0.0001	
T-Temp	1.10	1	1.10	620.29	< 0.0001	
t-Time	0.047	1	0.047	26.58	0.0002	
Ct	9.164E-003	1	9.164E-003	5.19	0.0419	
C^2	0.10	1	0.10	59.04	< 0.0001	
T^2	0.085	1	0.085	48.09	< 0.0001	
Residual	0.021	12	1.766E-003			
Lack of Fit	0.019	8	2.379E-003	4.40	0.0843	not significant
Pure Error	2.161E-003	4	5.403E-004			
Cor Total	1.94	18				
Additional ANOVA Data						
Std. Dev.	0.042					
R^2	0.9891					
Adj. R^2	0.9836					
Pred. R^2	0.9677					
Adequate Precision	45.403					

Cerium (Ce)

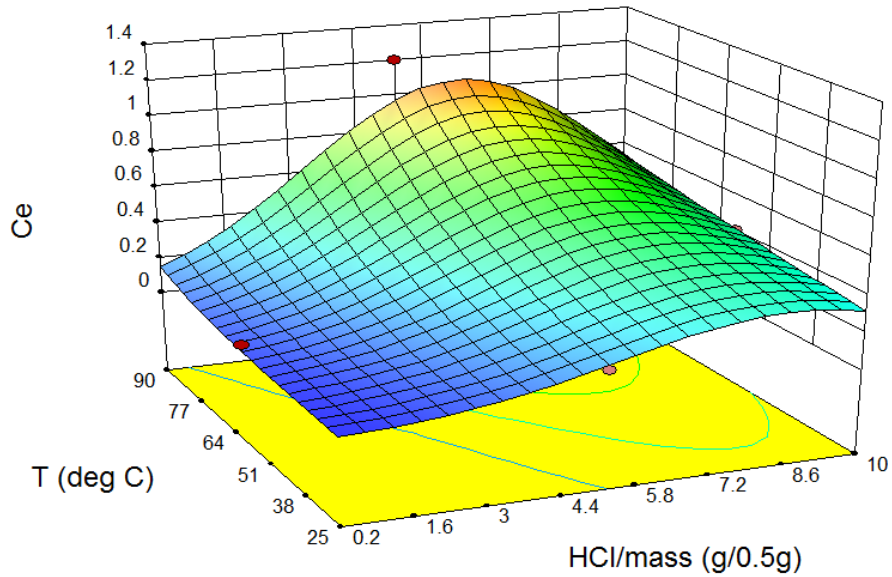

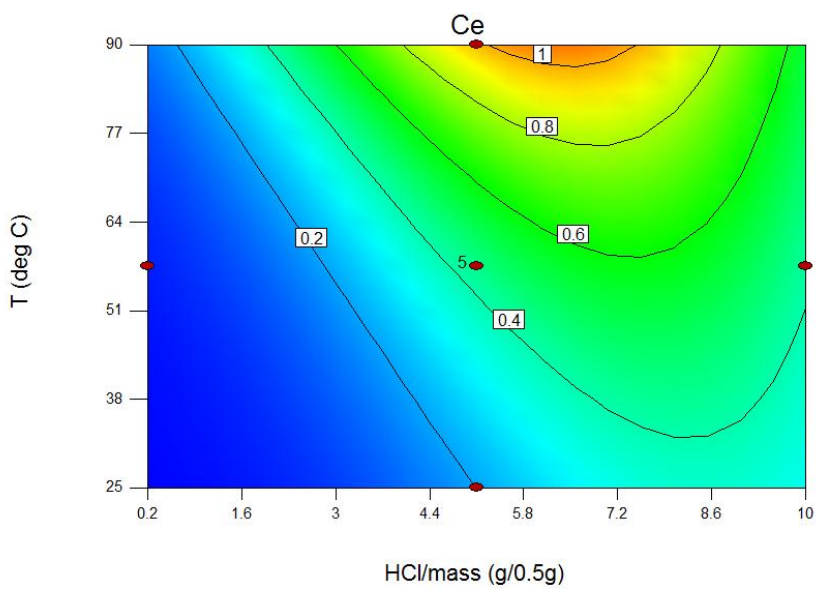

Equation: $Log_{10}(Ce) = -2.50607 + 0.41223C + 0.017989T - 1.45072 \times 10^{-3}CT - 0.022105C^2$

Figure 62: Contour Plot, Model Equation, and Response Surface of Ce Extraction from RE1 (Time: 75 min)

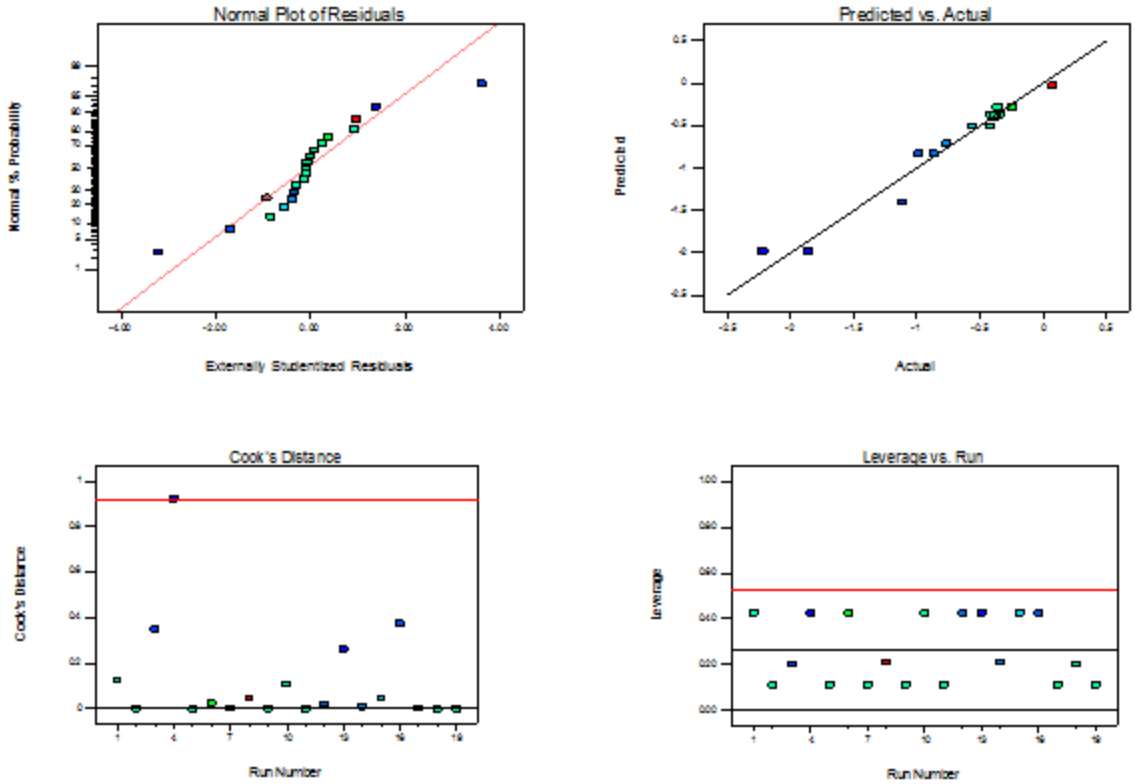

Figure 63: Diagnostics for Ce Extraction Model (RE1)

Table XLV: ANOVA Data for Ce Extraction From RE1

Source	Sum of Squares	df	Mean Square	F-Value	p-value	Notes
Model	5.51	4	1.38	89.18	< 0.0001	significant
C-HCl/mass	2.56	1	2.56	166.00	< 0.0001	
T-Temp	1.18	1	1.18	76.70	< 0.0001	
CT	0.43	1	0.43	27.64	0.0001	
C^2	1.33	1	1.33	86.39	< 0.0001	
Residual	0.22	14	0.015			
Lack of Fit	0.22	10	0.022	596.16	< 0.0001	significant
Pure Error	1.450E-004	4	3.625E-005			
Cor Total	5.73	18				
Additional ANOVA Data						
Std. Dev.	0.12					
R^2	0.9622					
Adj. R^2	0.9512					
Pred. R^2	0.9122					
Adequate Precision	30.688					

Dysprosium (Dy)

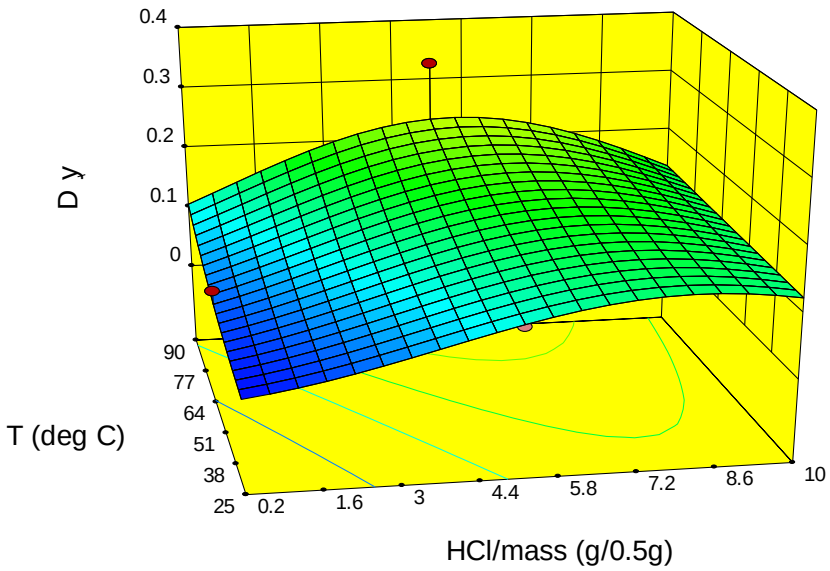

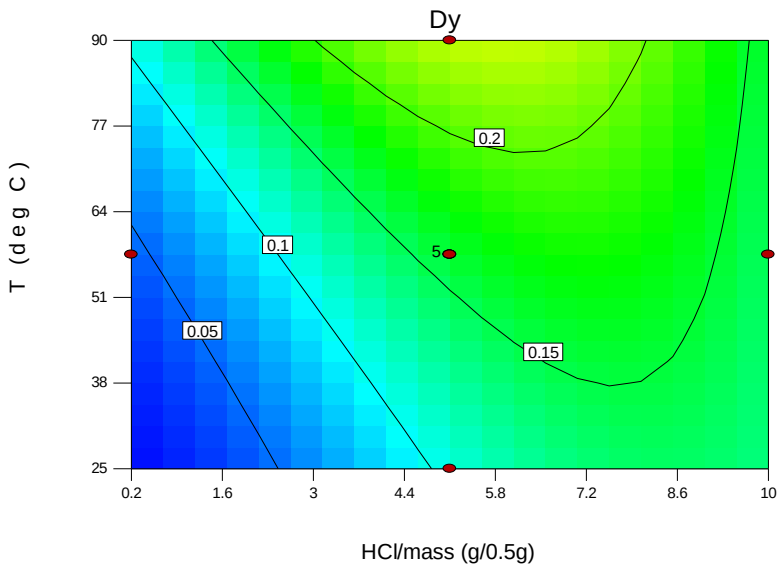

Equation: $Dy^{0.21} = 0.31185 + 0.0.072306C + 3.35979 \times 10^{-3}T - 3.13083 \times 10^{-4}CT - 3.96010 \times 10^{-3}C^2$

Figure 64: Contour Plot, Model Equation, and Response Surface of Dy Extraction from RE1 (Time: 75 min)

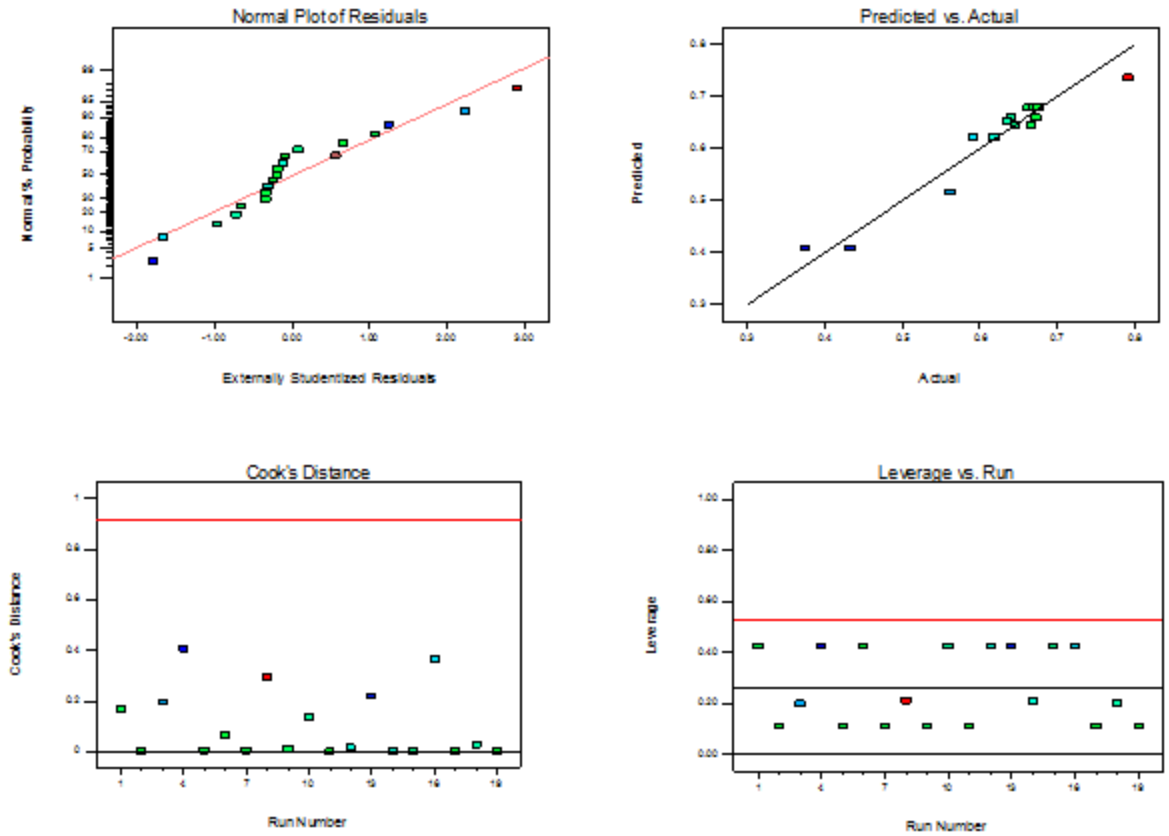

Figure 65: Diagnostics for Dy Extraction Model (RE1)

Table XLVI: ANOVA Data for Dy Extraction From RE1

Source	Sum of Squares	df	Mean Square	F-Value	p-value	Notes
Model	0.14	4	0.036	51.08	< 0.0001	significant
C-HCl/mass	0.046	1	0.046	66.85	< 0.0001	
T-Temp	0.033	1	0.033	47.24	< 0.0001	
CT	0.020	1	0.020	28.61	0.0001	
C^2	0.043	1	0.043	61.61	< 0.0001	
Residual	9.731E-003	14	6.951E-004			
Lack of Fit	9.607E-003	10	9.607E-004	31.10	0.0023	significant
Pure Error	1.235E-004	4	3.089E-005			
Cor Total	0.15	18				
Additional ANOVA Data						
Std. Dev.	0.026					
R^2	0.9359					
Adj. R^2	0.9175					
Pred. R^2	0.8640					
Adequate Precision	24.230					

Gadolinium (Gd)

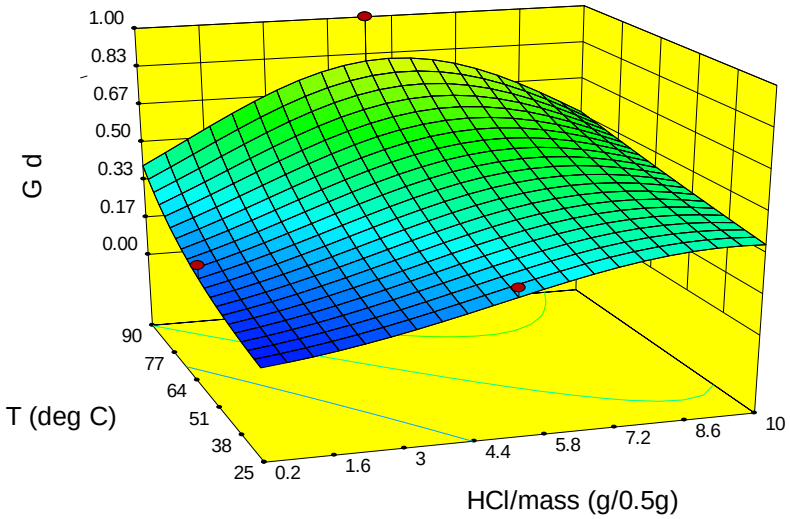

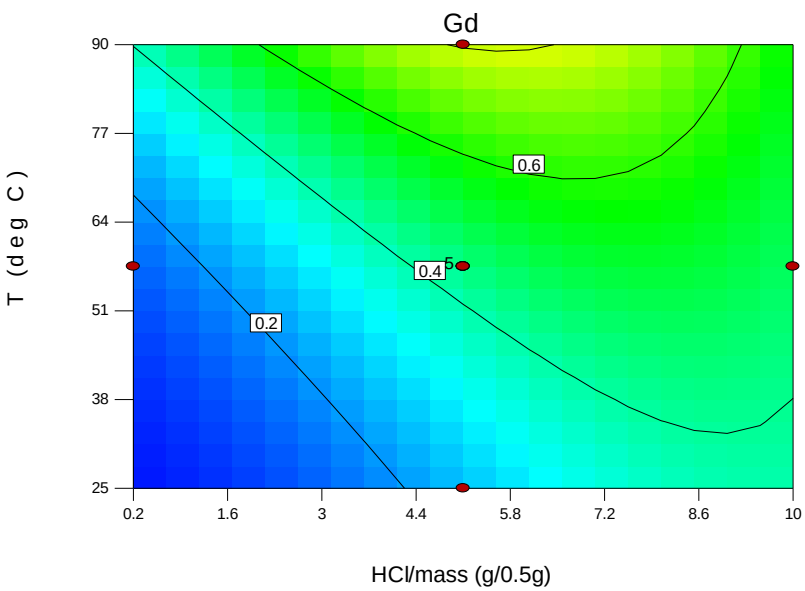

Equation: $Log_{10}(Gd) = -2.12678 + 0.24368C + 0.014070T + 9.4368 \times 10^{-3}t - 1.1868 \times 10^{-3}CT - 2.80087 \times 10^{-4}Ct - 0.010252C^2 - 4.88418 \times 10^{-5}t^2$

Figure 66: Contour Plot, Model Equation, and Response Surface of Gd Extraction from RE1 (Time: 75 min)

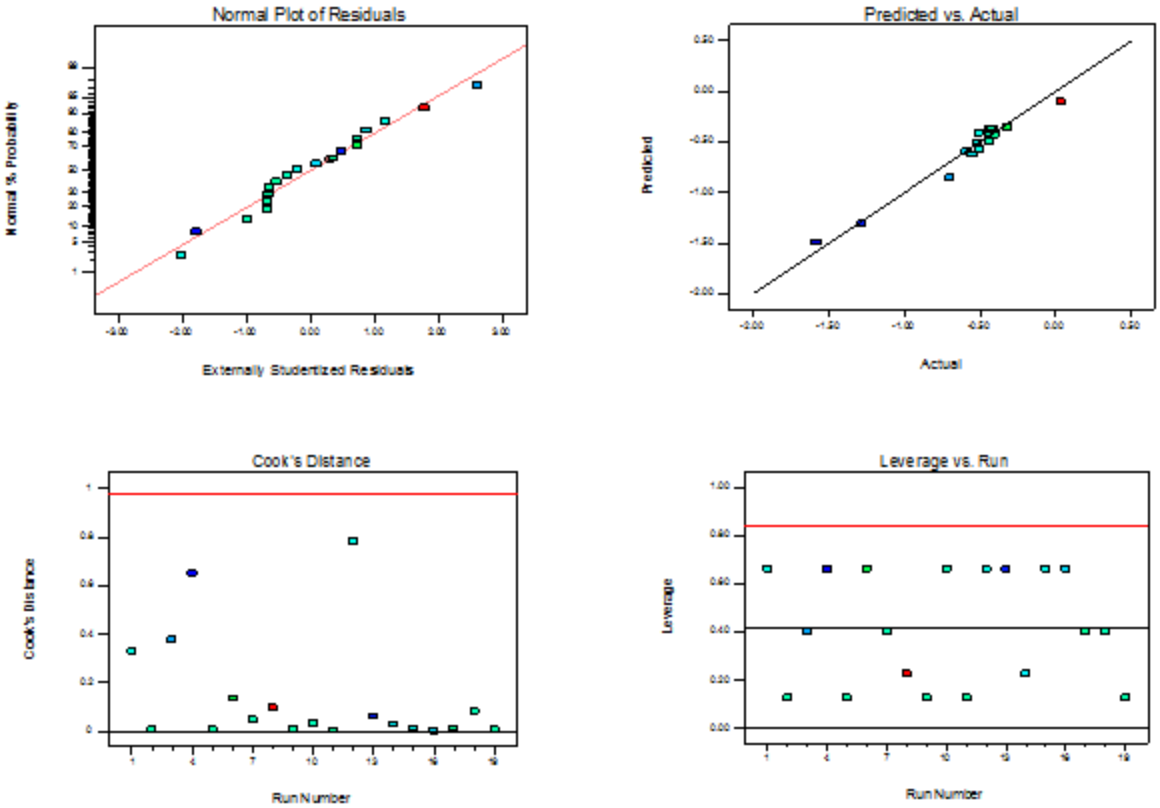

Figure 67: Diagnostics for Gd Extraction Model (RE1)

Table XLVII: ANOVA Data for Gd Extraction From RE1

Source	Sum of Squares	df	Mean Square	F-Value	p-value	Notes
Model	2.07	7	0.30	33.03	< 0.0001	significant
C-HCl/mass	0.60	1	0.60	66.73	< 0.0001	
T-Temp	0.68	1	0.68	75.89	< 0.0001	
t-Time	9.423E-003	1	9.423E-003	1.05	0.3268	
CT	0.29	1	0.29	31.94	0.0001	
Ct	0.031	1	0.031	3.41	0.0918	
C^2	0.19	1	0.19	21.37	0.0007	
t^2	0.031	1	0.031	3.45	0.0902	
Residual	0.098	11	8.946E-003			
Lack of Fit	0.098	7	0.014	472.38	< 0.0001	significant
Pure Error	1.189E-004	4	2.972E-005			
Cor Total	2.17	18				
Additional ANOVA Data						
Std. Dev.	0.095					
R^2	0.9546					
Adj. R^2	0.9257					
Pred. R^2	0.8285					
Adequate Precision	22.680					

Lanthanum (La)

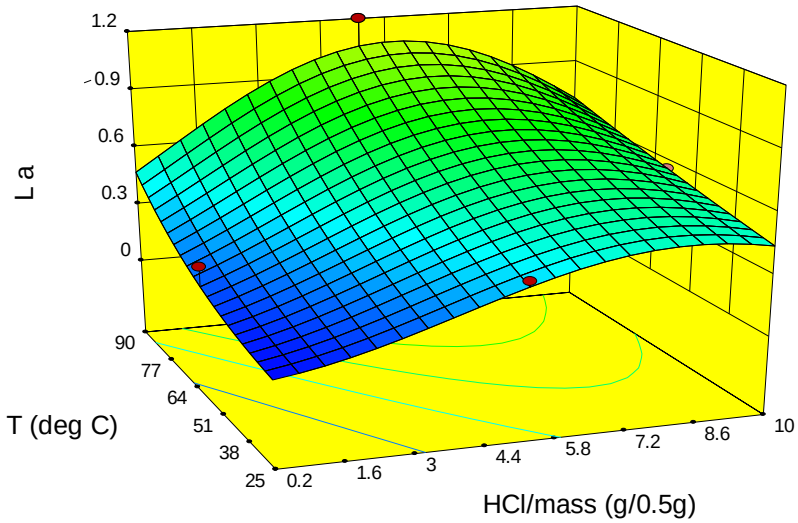

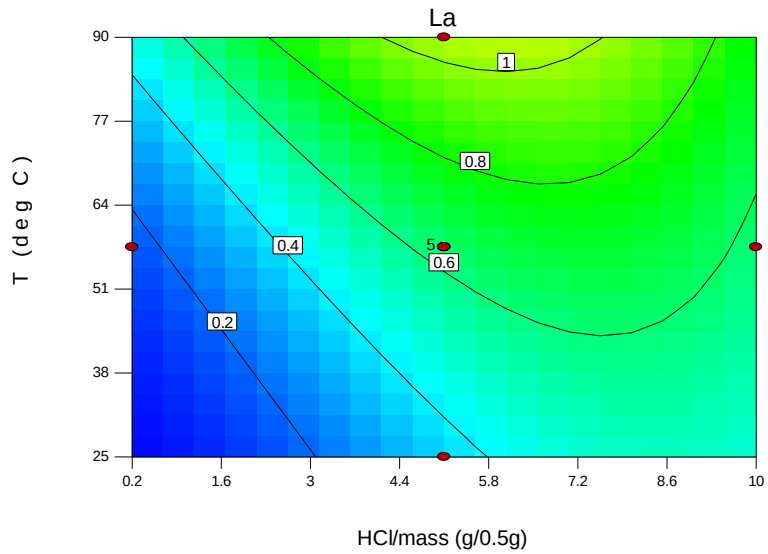

Equation: $\mathrm{La}^{0.29} = 0.16893 + 0.12475C + 6.85753 \times 10^{-3}T - 5.09793 \times 10^{-4}CT - 6.73597 \times 10^{-3}C^2$

Figure 68: Contour Plot, Model Equation, and Response Surface of La Extraction from RE1 (Time: 75 min):

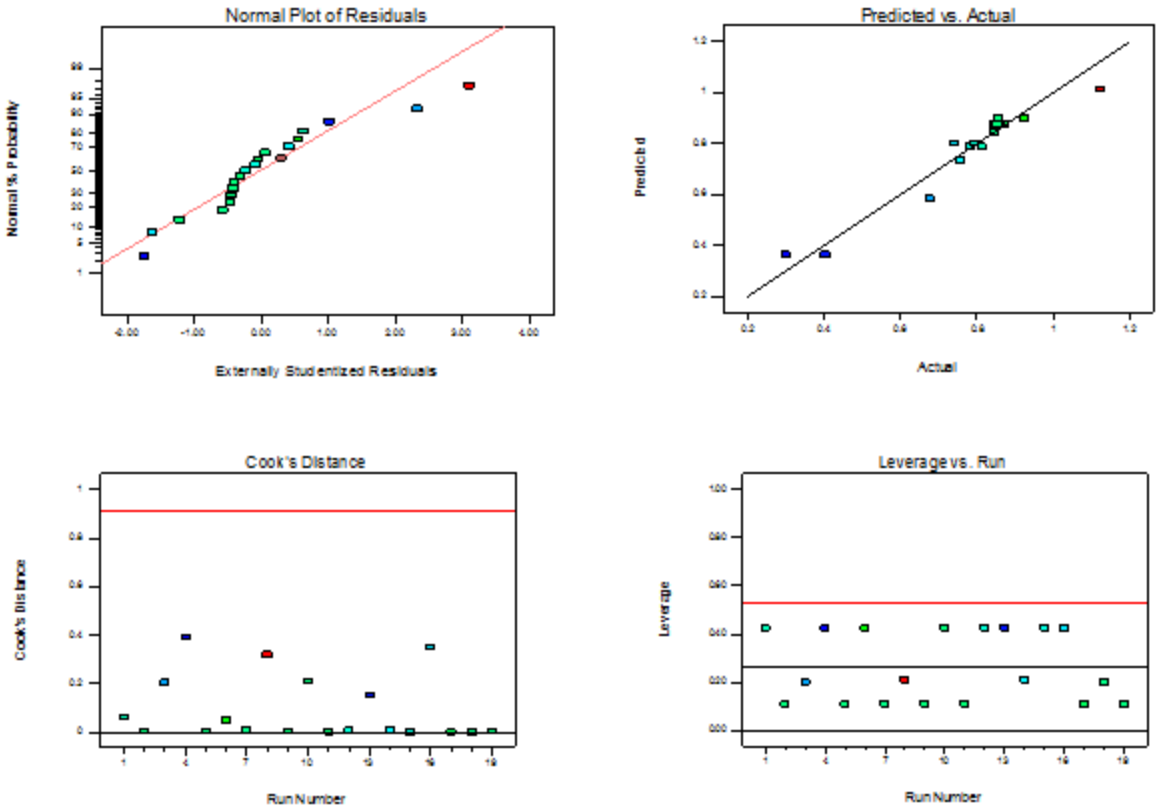

Figure 69: Diagnostics for La Extraction Model (RE1)

Table XLVIII: ANOVA Data for La Extraction From RE1

Source	Sum of Squares	df	Mean Square	F-Value	p-value	Notes
Model	0.54	4	0.13	50.08	< 0.0001	significant
C-HCl/mass	0.17	1	0.17	63.67	< 0.0001	
T-Temp	0.19	1	0.19	71.08	< 0.0001	
CT	0.053	1	0.053	19.58	0.0006	
C^2	0.12	1	0.12	46.00	< 0.0001	
Residual	0.038	14	2.694E-003			
Lack of Fit	0.038	10	3.768E-003	480.95	< 0.0001	significant
Pure Error	3.134E-005	4	7.834E-006			
Cor Total	0.58	18				
Additional ANOVA Data						
Std. Dev.	0.052					
R^2	0.9347					
Adj. R^2	0.9160					
Pred. R^2	0.8660					
Adequate Precision	24.437					

Neodymium (Nd)

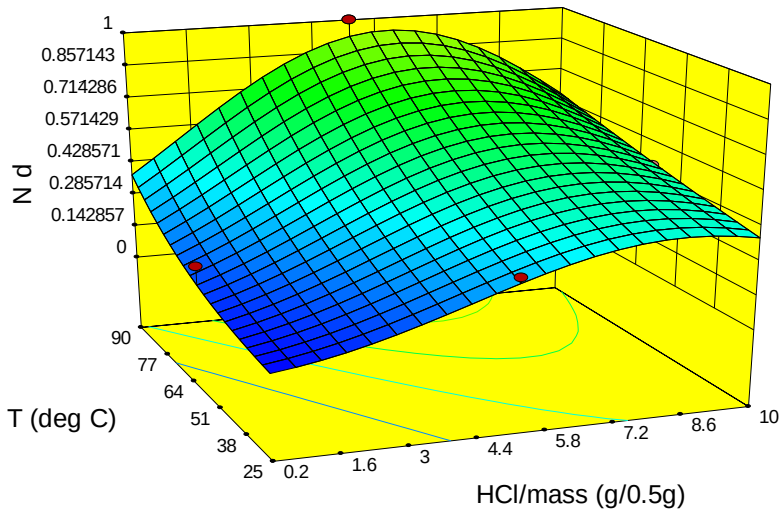

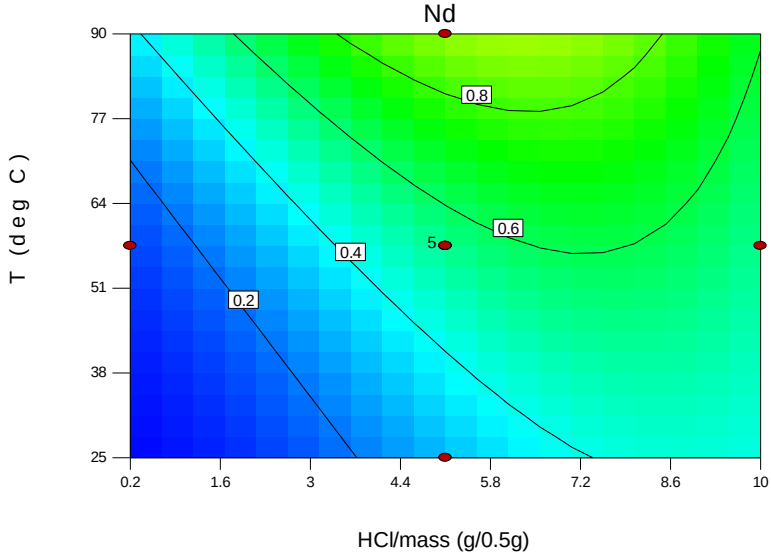

Equation: $\mathrm{La}^{0.29} = 0.31538 + 0.099476C + 5.37376 \times 10^{-3}T - 4.09995 \times 10^{-4}CT - 5.26707 \times 10^{-3}C^2$

Figure 70: Contour Plot, Model Equation, and Response Surface of La Extraction from RE1 (Time: 75 min)

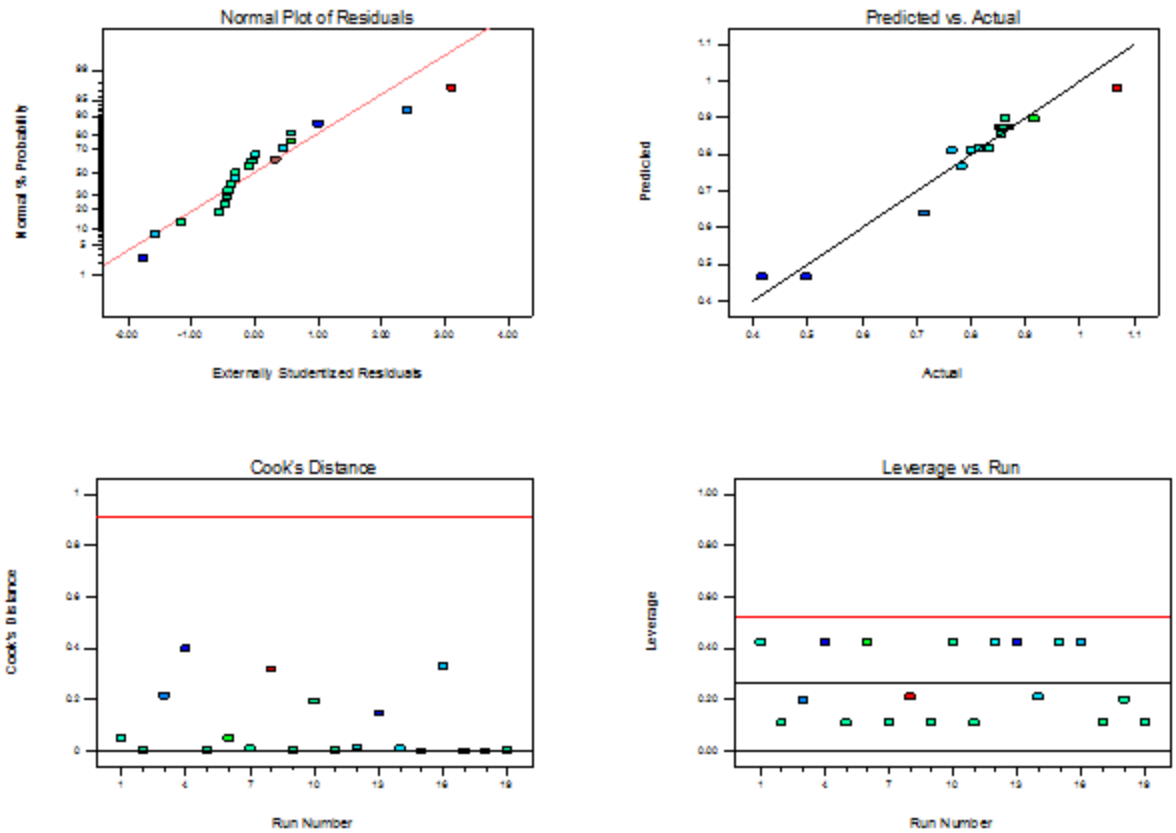

Figure 71: Diagnostics for Nd Extraction Model (RE1)

Table XLIX: ANOVA Data for Nd Extraction From RE1

Source	Sum of Squares	df	Mean Square	F-Value	p-value	Notes
Model	0.34	4	0.085	51.88	< 0.0001	significant
C-HCl/mass	0.12	1	0.12	71.70	< 0.0001	
T-Temp	0.11	1	0.11	69.12	< 0.0001	
CT	0.034	1	0.034	20.71	0.0005	
C^2	0.076	1	0.076	46.00	< 0.0001	
Residual	0.023	14	1.647E-003			
Lack of Fit	0.023	10	2.303E-003	382.38	< 0.0001	significant
Pure Error	2.409E-005	4	6.023E-006			
Cor Total	0.36	18				
Additional ANOVA Data						
Std. Dev.	0.041					
R^2	0.9368					
Adj. R^2	0.9187					
Pred. R^2	0.8713					
Adequate Precision	24.681					

Praseodymium (Pr)

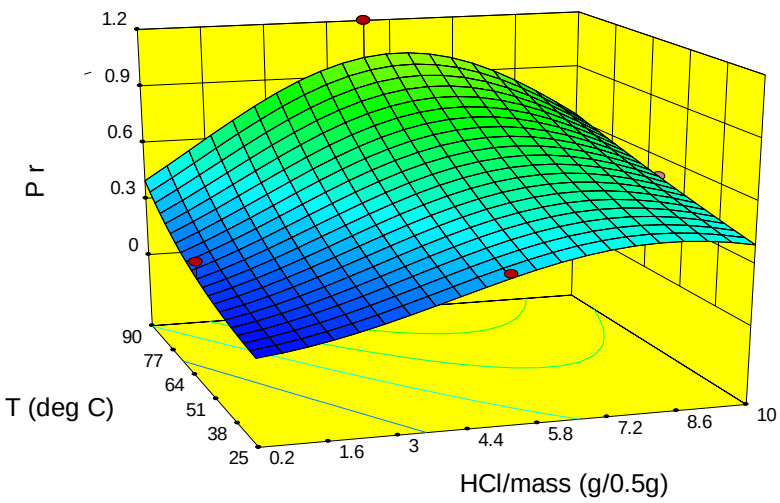

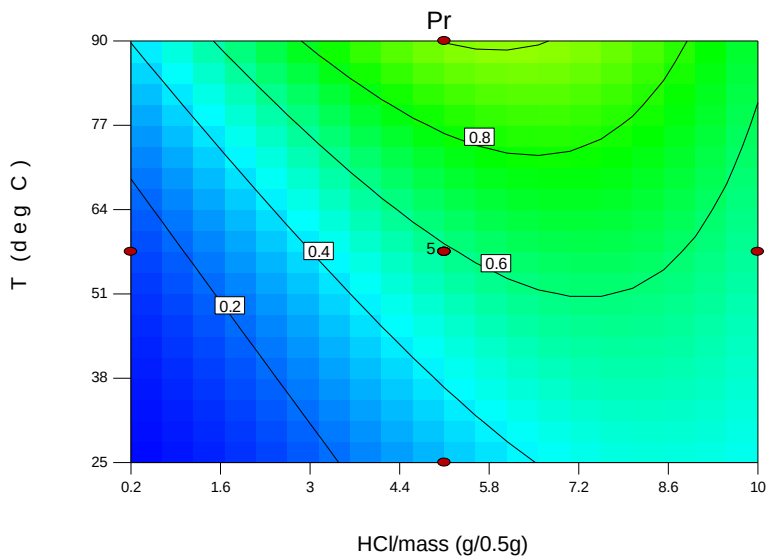

Equation: $\mathrm{Pr}^{0.23} = 0.26962 + 0.11004C + 5.81931 \times 10^{-3}T - 4.37283 \times 10^{-4}CT - 6.01276 \times 10^{-3}C^2$

Figure 72: Contour Plot, Model Equation, and Response Surface of Pr Extraction from RE1 (Time: 75 min)

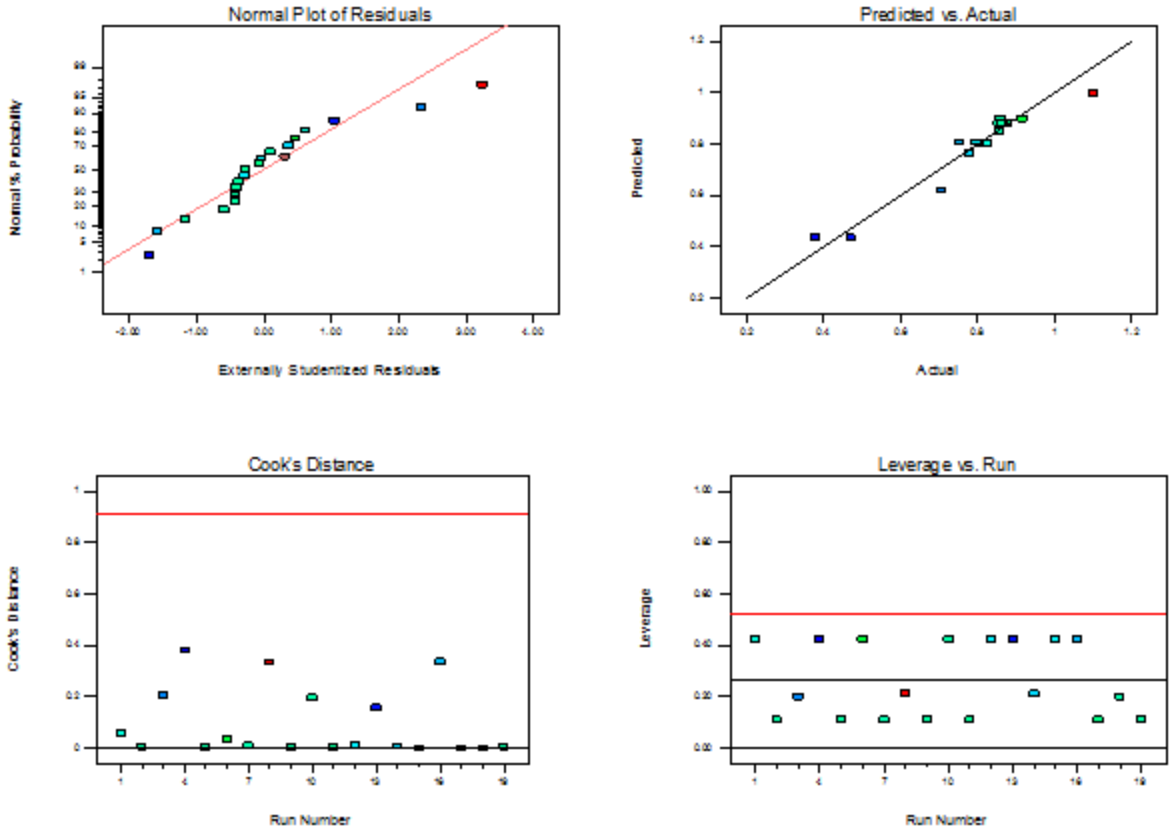

Figure 73: Diagnostics for Pr Extraction Model (RE1)

Table L: ANOVA Data for Pr Extraction From RE1

Source	Sum of Squares	df	Mean Square	F-Value	p-value	Notes
Model	0.41	4	0.10	48.09	< 0.0001	significant
C-HCl/mass	0.13	1	0.13	63.04	< 0.0001	
T-Temp	0.14	1	0.14	64.32	< 0.0001	
CT	0.039	1	0.039	18.34	0.0008	
C^2	0.099	1	0.099	46.67	< 0.0001	
Residual	0.030	14	2.115E-003			
Lack of Fit	0.030	10	2.959E-003	412.48	< 0.0001	significant
Pure Error	2.869E-005	4	7.173E-006			
Cor Total	0.44	18				
Additional ANOVA Data						
Std. Dev.	0.046					
R^2	0.9322					
Adj. R^2	0.9128					
Pred. R^2	0.8619					
Adequate Precision	23.852					

Thorium (Th)

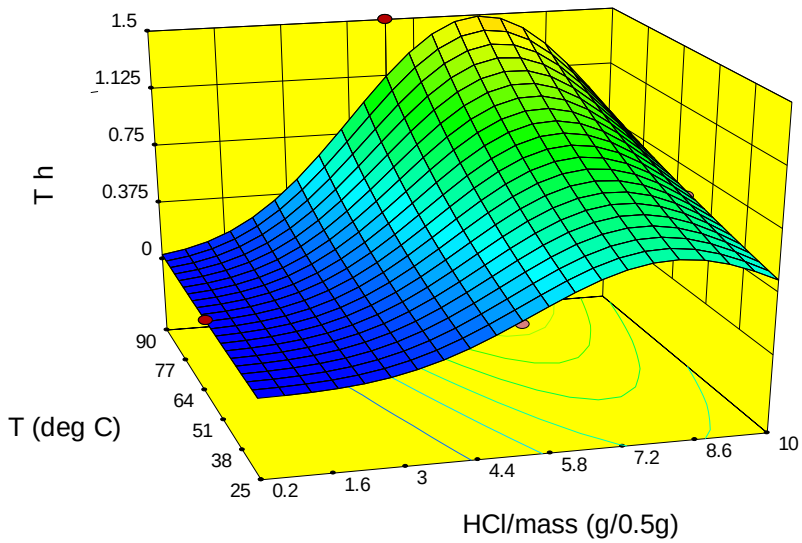

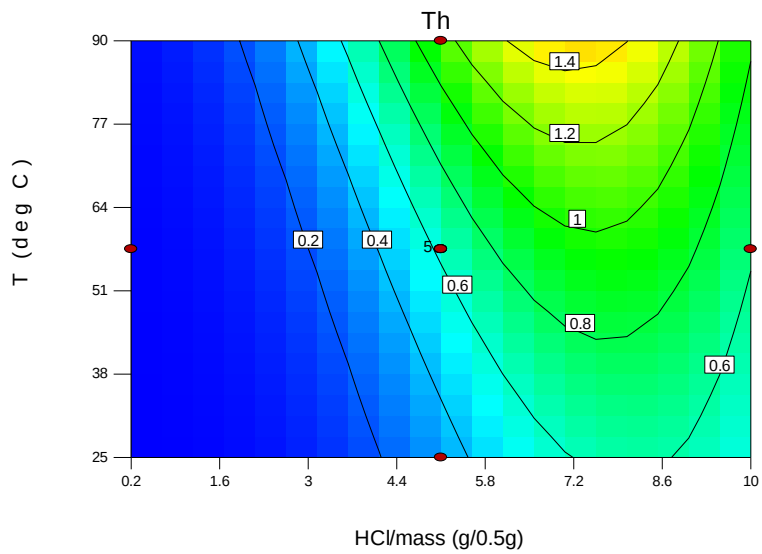

Equation: $\mathrm{Th}^{0.1} = 0.42924 + 0.11860C + 2.77749 \times 10^{-3}T - 1.92771 \times 10^{-4}CT - 7.13706 \times 10^{-3}C^2$

Figure 74: Contour Plot, Model Equation, and Response Surface of Th Extraction from RE1 (Time: 75 min)

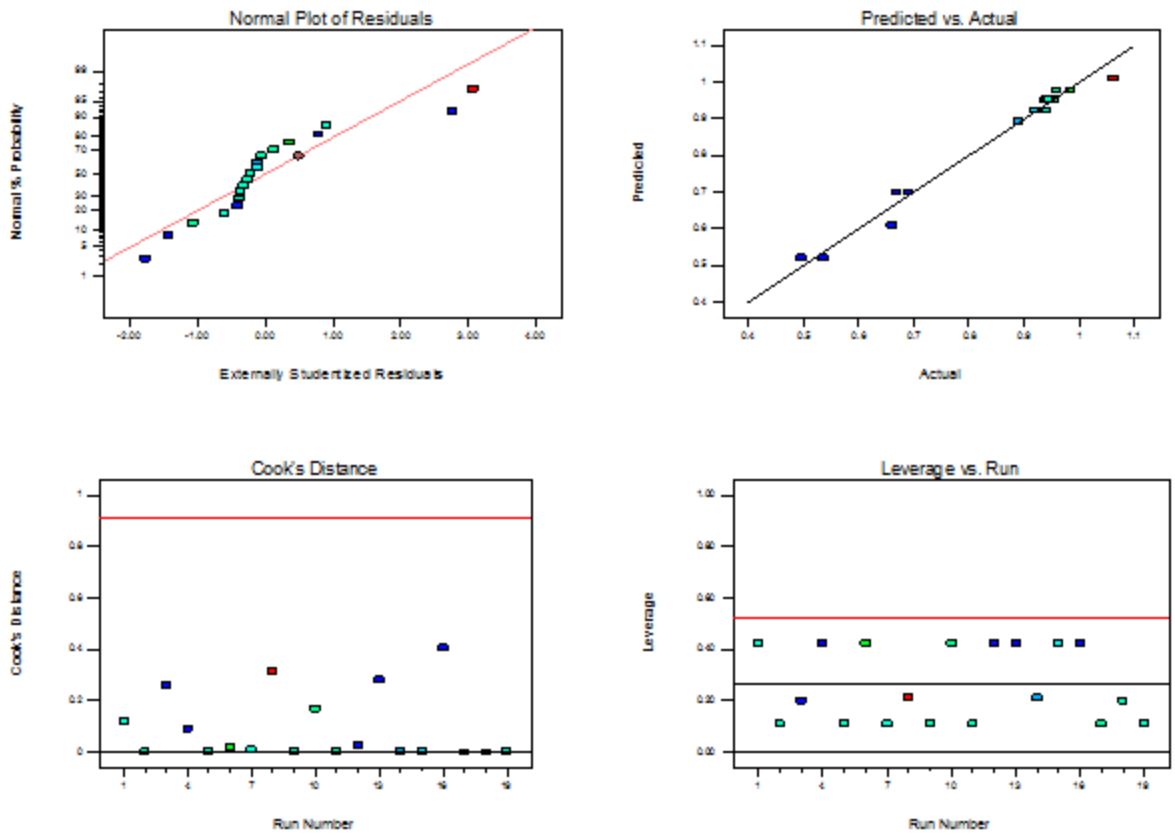

Figure 75: Diagnostics for Th Extraction Model (RE1)

Table LI: ANOVA Data for Th Extraction From RE1

Source	Sum of Squares	df	Mean Square	F-Value	p-value	Notes
Model	0.47	4	0.12	198.96	< 0.0001	significant
C-HCl/mass	0.29	1	0.29	489.93	< 0.0001	
T-Temp	0.034	1	0.034	57.59	< 0.0001	
CT	7.539E-003	1	7.539E-003	12.77	0.0031	
C^2	0.14	1	0.14	235.55	< 0.0001	
Residual	8.267E-003	14	5.905E-004			
Lack of Fit	8.257E-003	10	8.257E-004	318.52	< 0.0001	significant
Pure Error	1.037E-005	4	2.592E-006			
Cor Total	0.48	18				
Additional ANOVA Data						
Std. Dev.	0.024					
R^2	0.9827					
Adj. R^2	0.9778					
Pred. R^2	0.9652					
Adequate Precision	39.210					

Iron (Fe)

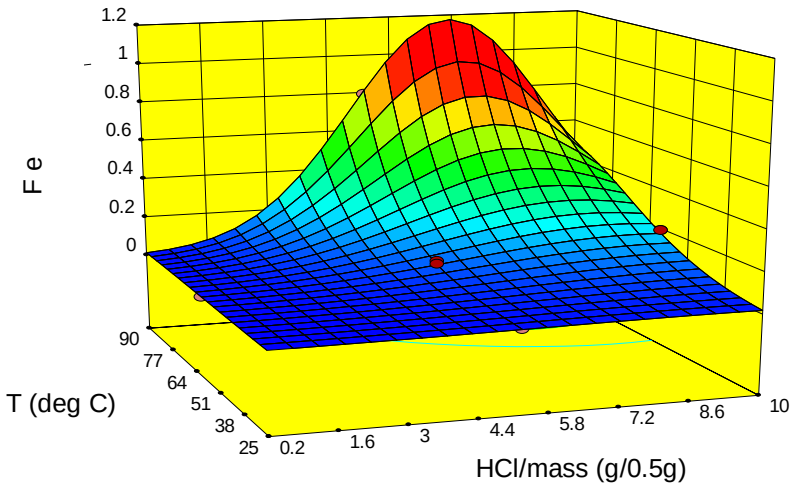

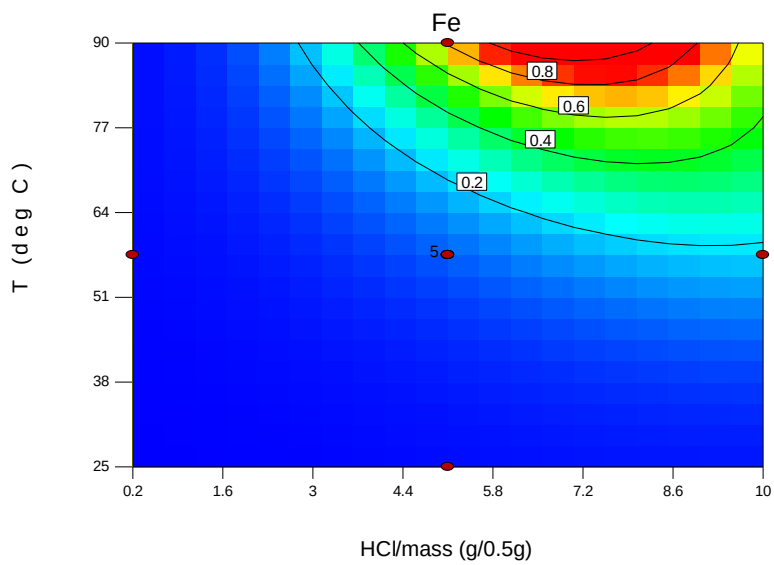

Equation: $Log_{10}(Fe) = -3.51231 + 0.080550C + 0.019778T + 2.07101 \times 10^{-3}t + 5.20949 \times 10^{-3}CT - 3.54627 \times 10^{-3}C^2 - 5.25462 \times 10^{-5}T^2 - 1.90617 \times 10^{-4}C^2T - 2.15566 \times 10^{-6}C^2T^2$

Figure 76: Contour Plot, Model Equation, and Response Surface of Fe Extraction from RE1 (Time: 75 min)

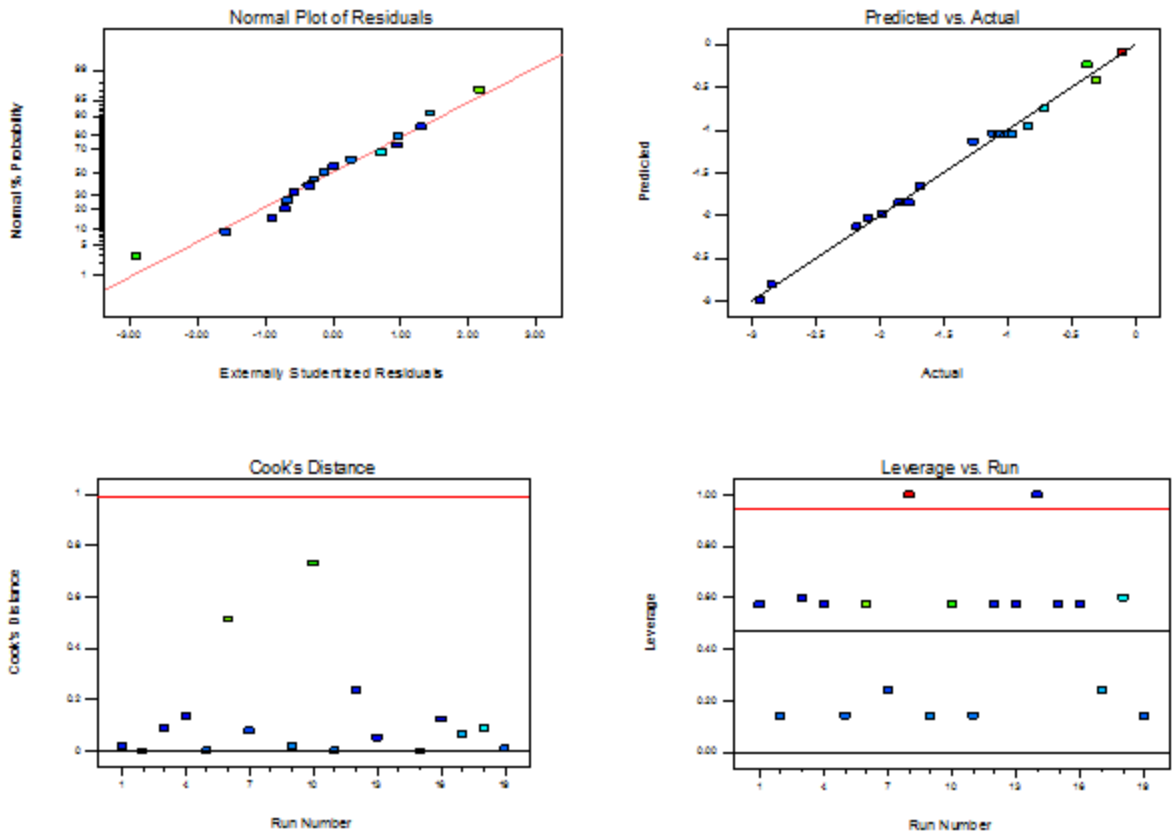

Figure 77: Diagnostics for Fe Extraction Model (RE1)

Table LII: ANOVA Data for Fe Extraction From RE1

Source	Sum of Squares	df	Mean Square	F-Value	p-value	Notes
Model	11.59	8	1.45	152.53	< 0.0001	significant
C-HCl/mass	4.76	1	4.76	501.70	< 0.0001	
T-Temp	1.76	1	1.76	185.80	< 0.0001	
t-Time	0.087	1	0.087	9.15	0.0128	
CT	0.11	1	0.11	11.59	0.0067	
C^2	0.24	1	0.24	25.79	0.0005	
T^2	9.800E-005	1	9.800E-005	0.010	0.9211	
C^2T	0.19	1	0.19	19.73	0.0013	
C^2T^2	0.069	1	0.069	7.31	0.0222	
Residual	0.095	10	9.494E-003			
Lack of Fit	0.082	6	0.014	4.24	0.0918	not significant
Pure Error	0.013	4	3.227E-003			
Cor Total	11.68	18				
Additional ANOVA Data						
Std. Dev.	0.097					
R^2	0.9919					
Adj. R^2	0.9854					
Pred. R^2	N/A					
Adequate Precision	43.177					

Appendix F: Modeling Data for RE2

Aluminum (Al)

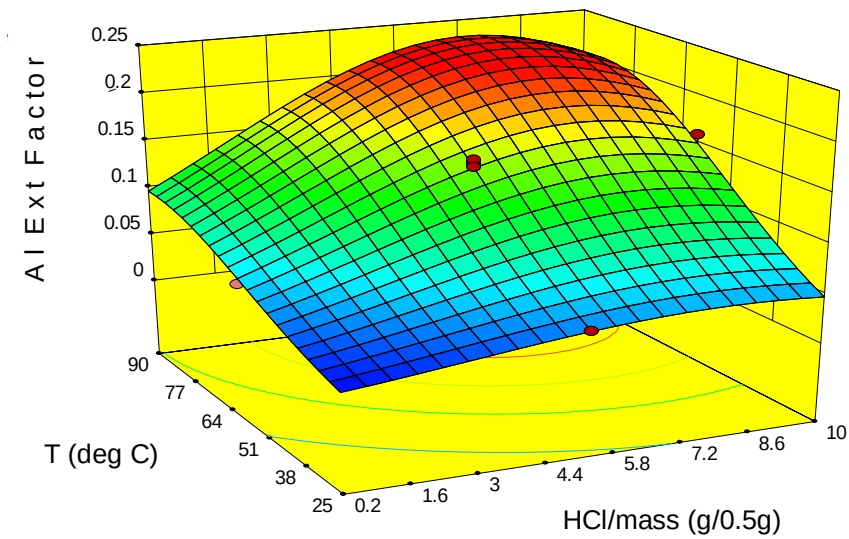

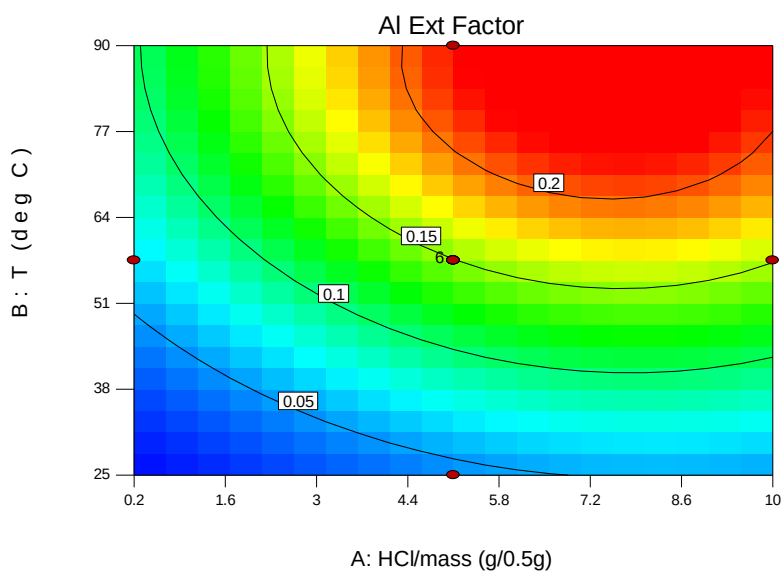

Equation: $Log_{10}(Al) = -2.66150 + 0.12642C + 0.032811T + 2.65101 \times 10^{-3}t - 1.80692 \times 10^{-4}CT - 1.45374 \times 10^{-5}Tt - 7.61505 \times 10^{-3}C^2 - 1.76007 \times 10^{-4}T^2$

Figure 78: Contour Plot, Model Equation, and Response Surface of Al Extraction from RE2 (Time: 75 min)

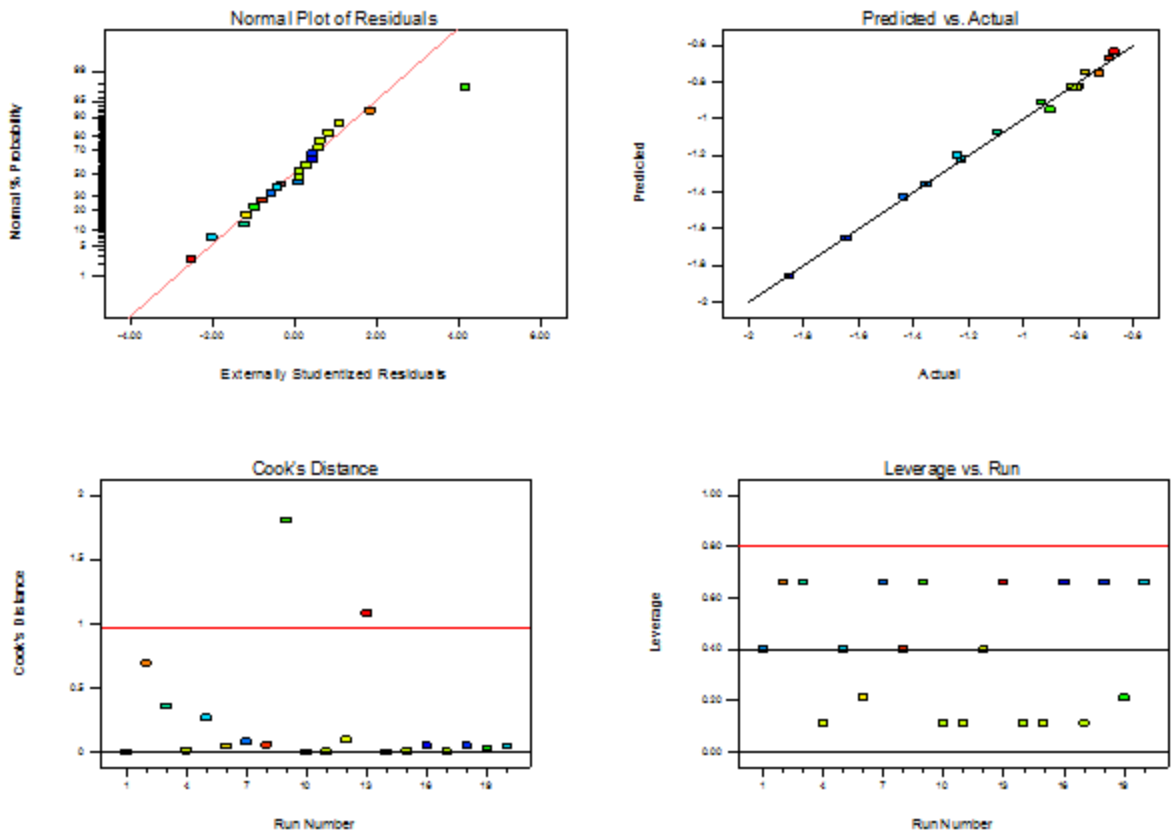

Figure 79: Diagnostics for Al Extraction Model (RE2)

Table LIII: ANOVA Data for Al Extraction from RE2

Source	Sum of Squares	df	Mean Square	F-Value	p-value	Notes
Model	2.15	7	0.31	331.33	< 0.0001	significant
C-HCl/mass	0.35	1	0.35	380.76	< 0.0001	
T-Temp	1.18	1	1.18	1269.34	< 0.0001	
t-Time	0.067	1	0.067	71.91	< 0.0001	
CT	6.624E-003	1	6.624E-003	7.14	0.0203	
Tt	3.616E-003	1	3.616E-003	3.90	0.0718	
C^2	0.11	1	0.11	115.31	< 0.0001	
T^2	0.11	1	0.11	119.21	< 0.0001	
Residual	0.011	12	9.277E-004			
Lack of Fit	0.011	7	1.537E-003	20.43	0.0021	significant
Pure Error	3.761E-004	5	7.522E-005			
Cor Total	2.16	19				
Additional ANOVA Data						
Std. Dev.	0.030					
R^2	0.9949					
Adj. R^2	0.9919					
Pred. R^2	0.9727					
Adequate Precision	63.621					

Cerium (Ce)

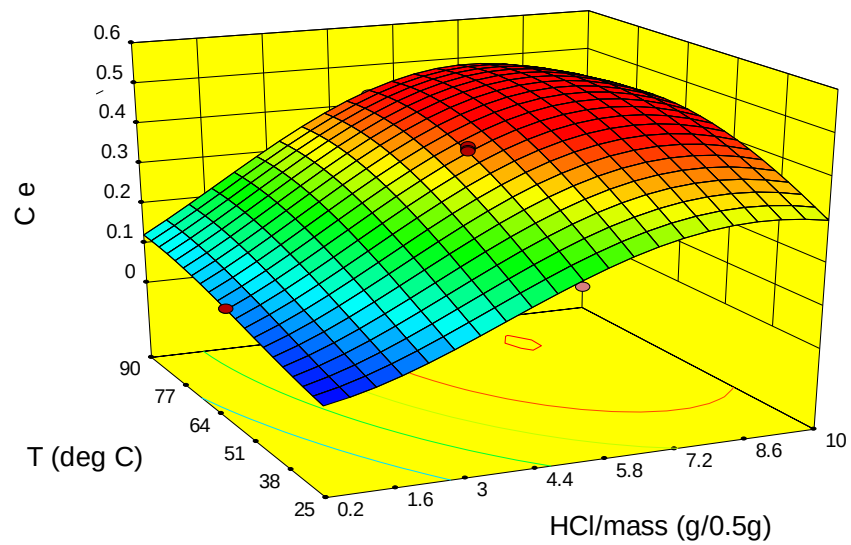

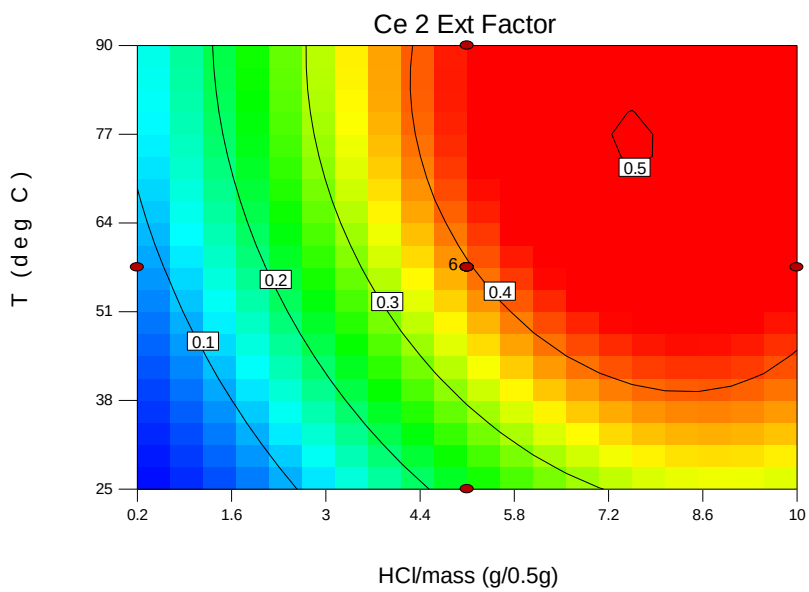

Equation: $Ce^{0.41} = -0.15251 + 0.11760C + 0.010657T + 1.09467 \times 10^{-3}t - 2.70942 \times 10^{-4}CT - 9.48305 \times 10^{-6}Tt - 6.40492 \times 10^{-3}C^2 - 5.18296 \times 10^{-5}T^2$

Figure 80: Contour Plot, Model Equation, and Response Surface of Ce Extraction from RE2 (Time: 75 min)

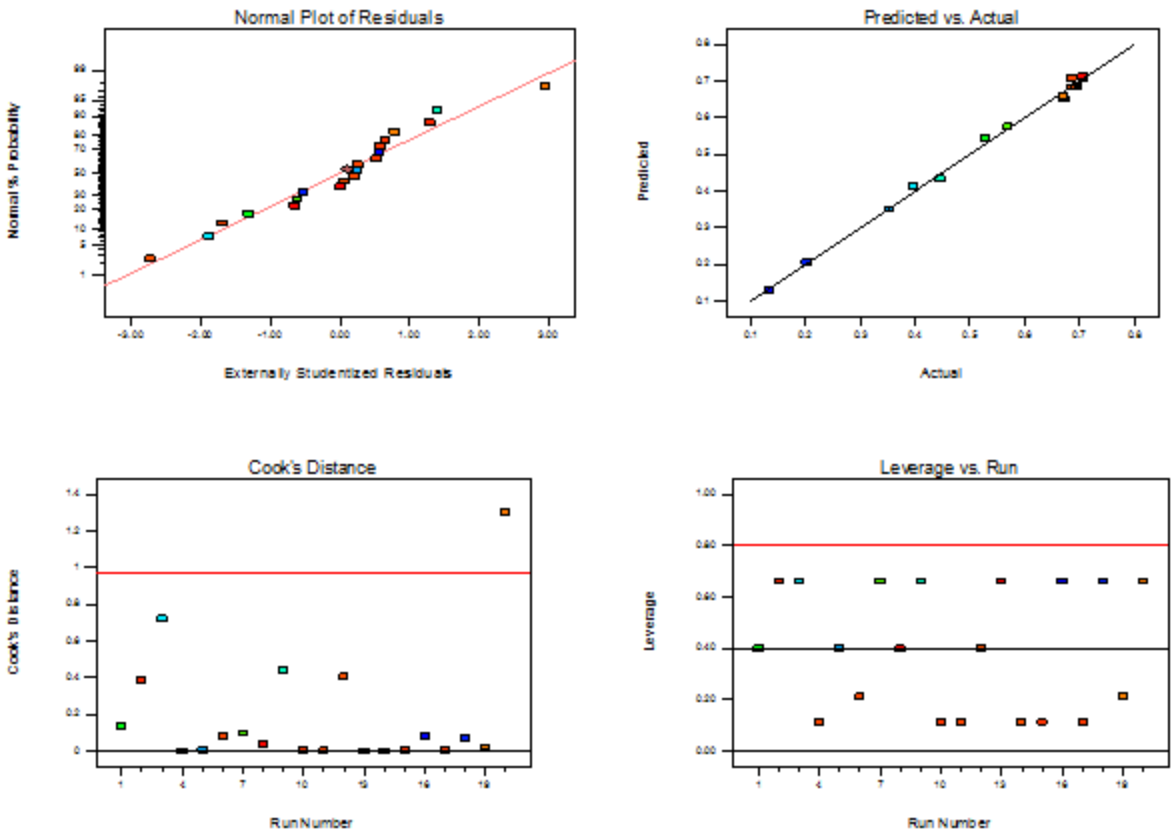

Figure 81: Diagnostics for Ce Extraction Model (RE2)

Table LIV: ANOVA Data for Ce Extraction from RE2

Source	Sum of Squares	df	Mean Square	F-Value	p-value	Notes
Model	0.60	7	0.086	382.08	< 0.0001	significant
C-HCl/mass	0.32	1	0.32	1438.14	< 0.0001	
T-Temp	0.072	1	0.072	318.51	< 0.0001	
t-Time	6.112E-003	1	6.112E-003	27.20	0.0002	
CT	0.015	1	0.015	66.27	< 0.0001	
Tt	1.539E-003	1	1.539E-003	6.85	0.0225	
C^2	0.076	1	0.076	336.73	< 0.0001	
T^2	9.590E-003	1	9.590E-003	42.67	< 0.0001	
Residual	2.697E-003	12	2.247E-004			
Lack of Fit	2.640E-003	7	3.771E-004	33.15	0.0007	significant
Pure Error	5.689E-005	5	1.138E-005			
Cor Total	0.60	19				
Additional ANOVA Data						
Std. Dev.	0.015					
R^2	0.9955					
Adj. R^2	0.9929					
Pred. R^2	0.9797					
Adequate Precision	61.649					

Dysprosium (Dy)

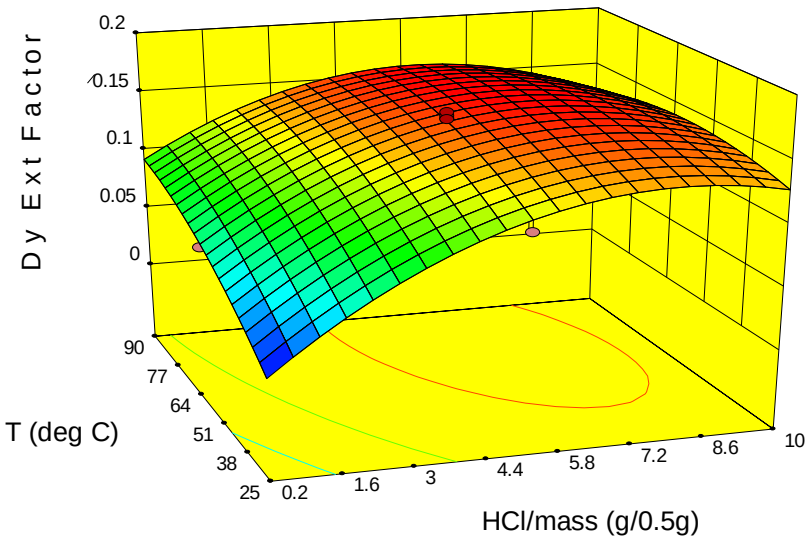

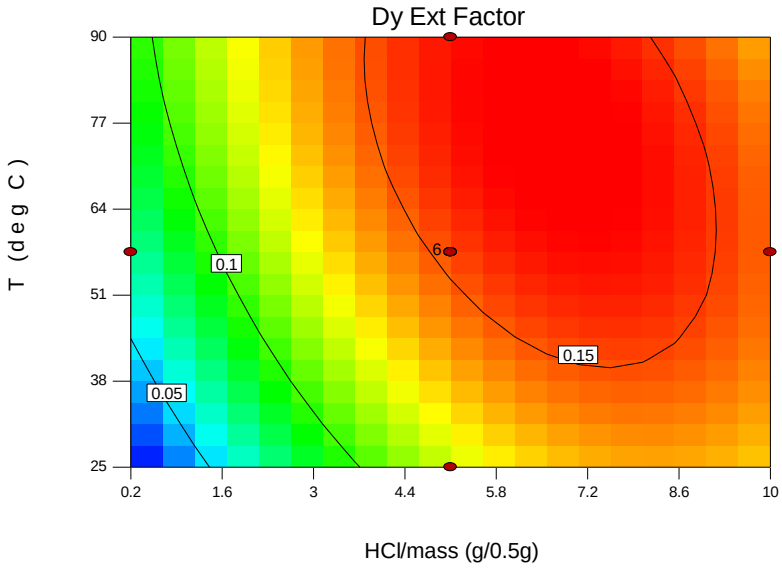

Equation: $Dy = -0.063099 + 0.035007C + 2.69885 \times 10^{-3}T + 1.71634 \times 10^{-4}t - 1.22540 \times 10^{-4}CT - 2.00605 \times 10^{-3}C^2 - 1.29106 \times 10^{-5}T^2$

Figure 82: Contour Plot, Model Equation, and Response Surface of Dy Extraction from RE2 (Time: 75 min)

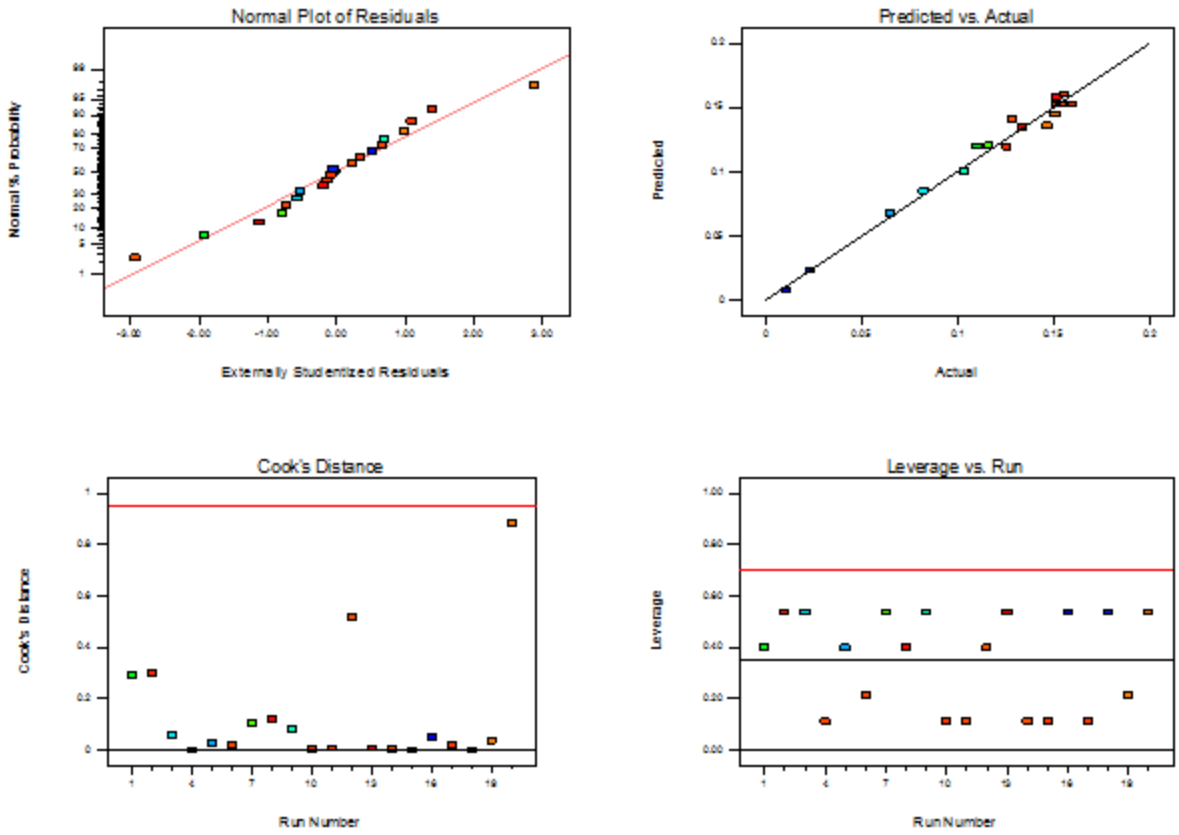

Figure 83: Diagnostics for Dy Extraction Model (RE2)

Table LV: ANOVA Data for Dy Extraction from RE2

Source	Sum of Squares	df	Mean Square	F-Value	p-value	Notes
Model	0.037	6	6.213E-003	125.07	< 0.0001	significant
C-HCl/mass	0.014	1	0.014	271.88	< 0.0001	
T-Temp	3.654E-003	1	3.654E-003	73.56	< 0.0001	
t-Time	5.965E-004	1	5.965E-004	12.01	0.0042	
CT	3.047E-003	1	3.047E-003	61.33	< 0.0001	
C^2	7.424E-003	1	7.424E-003	149.46	< 0.0001	
T^2	5.959E-004	1	5.959E-004	12.00	0.0042	
Residual	6.457E-004	13	4.967E-005			
Lack of Fit	5.977E-004	8	7.471E-005	7.77	0.0185	significant
Pure Error	4.807E-005	5	9.613E-006			
Cor Total	0.038	19				
Additional ANOVA Data						
Std. Dev.	7.048E-003					
R^2	0.9830					
Adj. R^2	0.9751					
Pred. R^2	0.9475					
Adequate Precision	36.608					

Gadolinium (Gd)

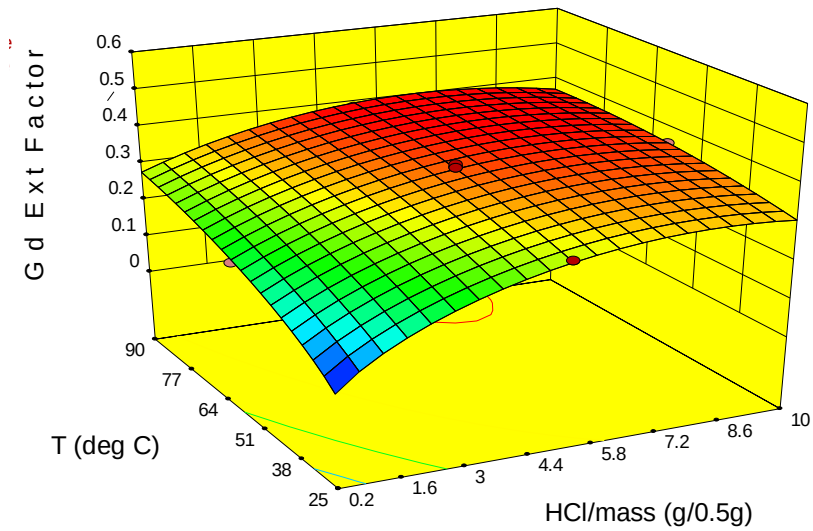

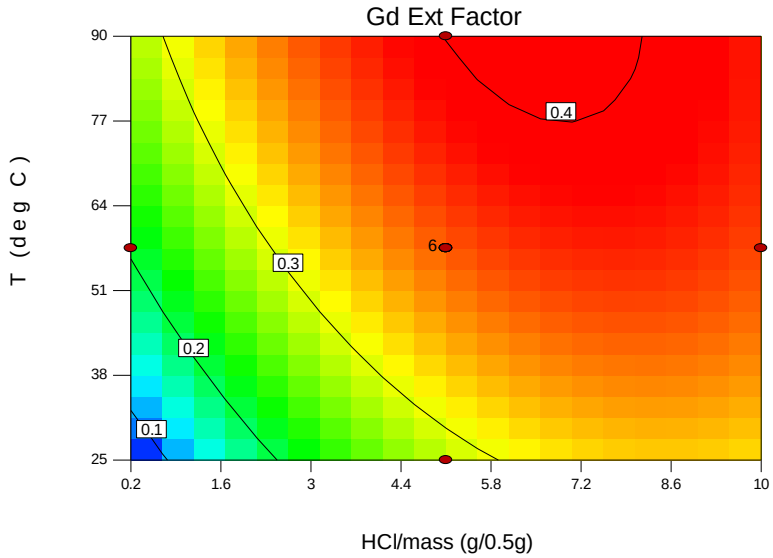

Equation: $Gd^{1.41} = -0.10923 + 0.050463C + 4.23974 \times 10^{-3}T + 2.49384 \times 10^{-4}t - 1.46760 \times 10^{-4}CT - 2.81976 \times 10^{-3}C^2 - 1.63571 \times 10^{-5}T^2$

Figure 84: Contour Plot, Model Equation, and Response Surface of Gd Extraction from RE2 (Time: 75 min)

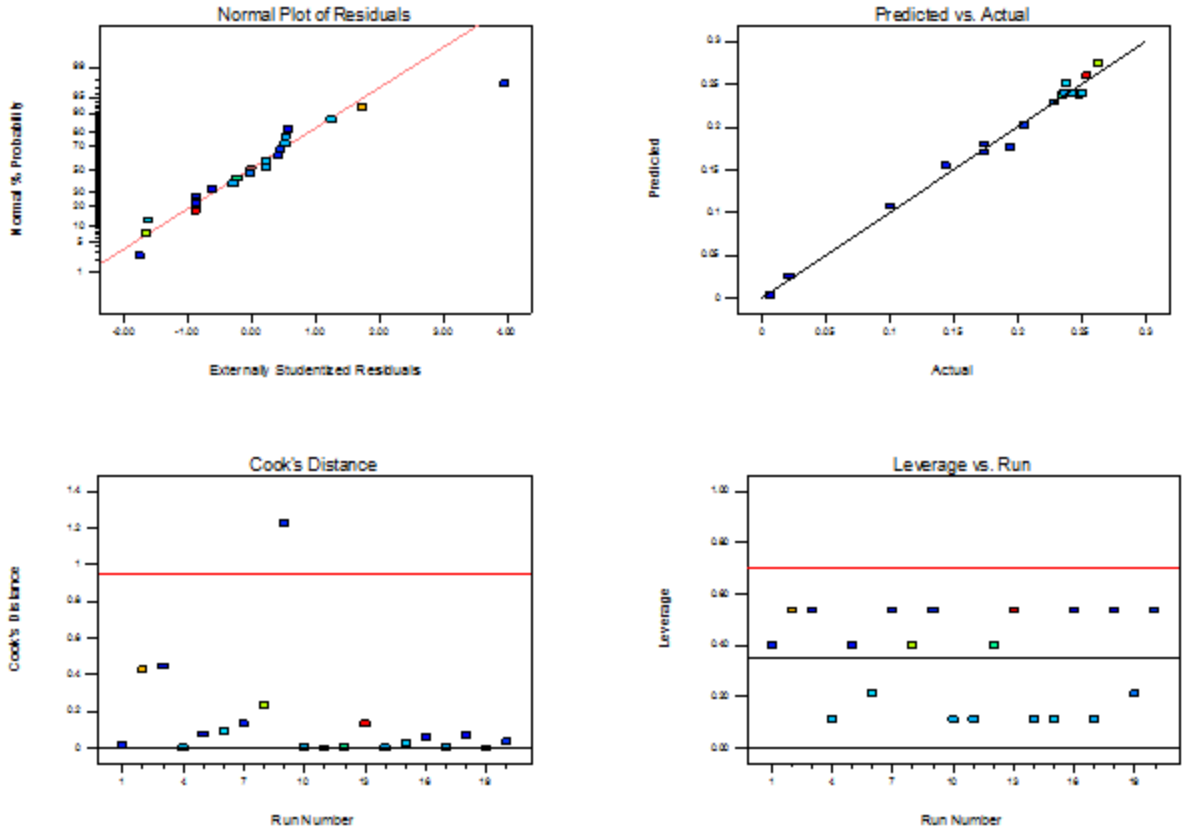

Figure 85: Diagnostics for Gd Extraction Model (RE2)

Table LVI: ANOVA Data for Gd Extraction from RE2

Source	Sum of Squares	df	Mean Square	F-Value	p-value	Notes
Model	0.11	6	0.018	195.08	< 0.0001	significant
C-HCl/mass	0.042	1	0.042	463.40	< 0.0001	
T-Temp	0.027	1	0.027	300.47	< 0.0001	
t-Time	1.259E-003	1	1.259E-003	13.82	0.0026	
CT	4.370E-003	1	4.370E-003	47.95	< 0.0001	
C^2	0.015	1	0.015	160.93	< 0.0001	
T^2	9.552E-004	1	9.552E-004	10.48	0.0065	
Residual	1.185E-003	13	9.114E-005			
Lack of Fit	1.082E-003	8	1.353E-004	6.59	0.0264	significant
Pure Error	1.027E-004	5	2.053E-005			
Cor Total	0.11	19				
Additional ANOVA Data						
Std. Dev.	9.547E-003					
R^2	0.9890					
Adj. R^2	0.9839					
Pred. R^2	0.9626					
Adequate Precision	48.149					

Lanthanum (La)

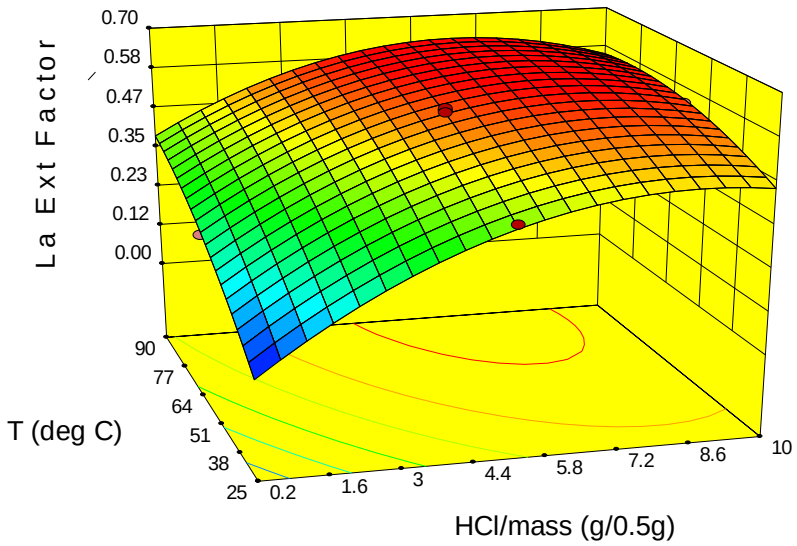

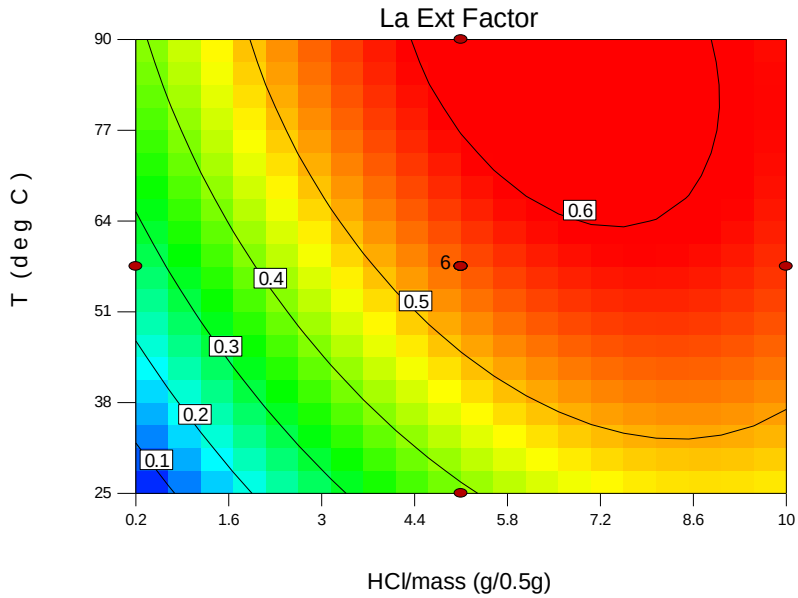

Equation: $La = -2.5119 + 0.11123C + 0.010334T + 5.81566 \times 10^{-4}t - 3.66004 \times 10^{-4}CT - 5.92438 \times 10^{-3}C^2 - 4.32747 \times 10^{-5}T^2$

Figure 86: Contour Plot, Model Equation, and Response Surface of La Extraction from RE2 (Time: 75 min)

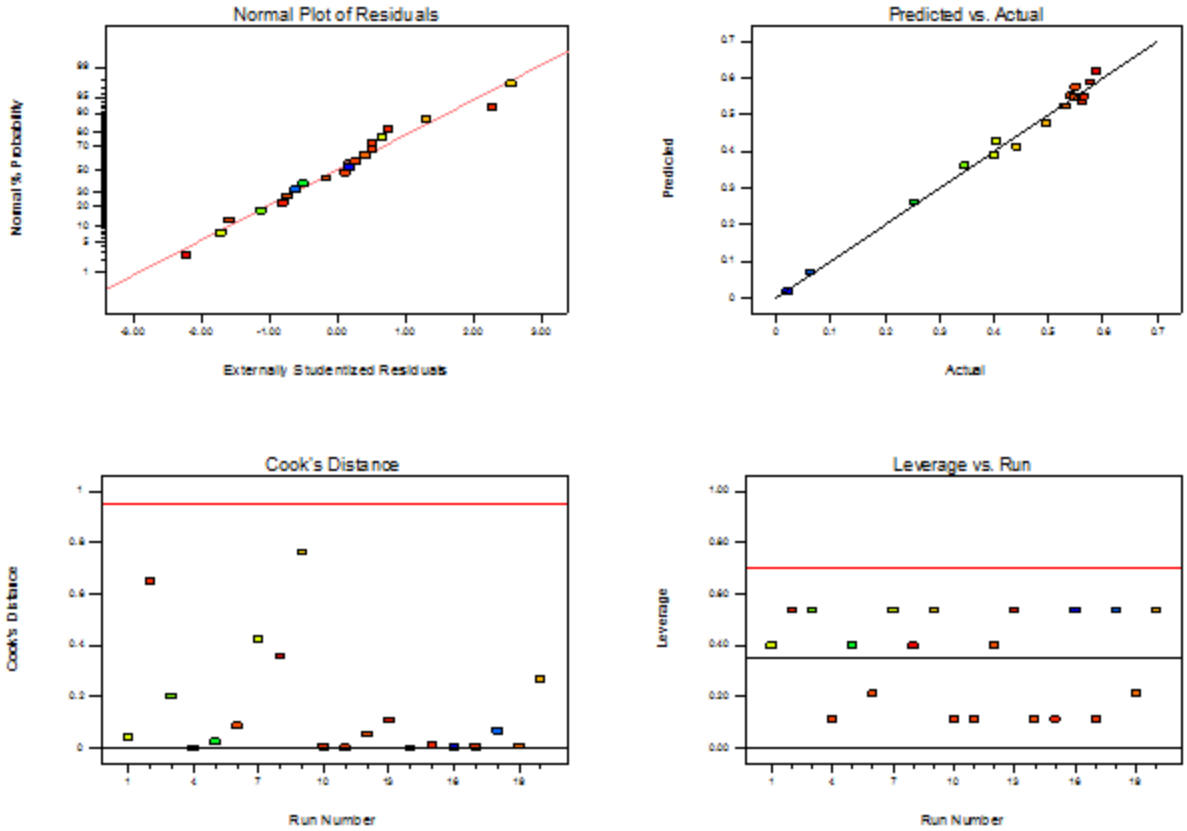

Figure 87: Diagnostics for La Extraction Model (RE2)

Table LVII: ANOVA Data for La Extraction from RE2

Source	Sum of Squares	df	Mean Square	F-Value	p-value	Notes
Model	0.53	6	0.088	228.60	< 0.0001	significant
C-HCl/mass	0.21	1	0.21	554.36	< 0.0001	
T-Temp	0.13	1	0.13	335.68	< 0.0001	
t-Time	6.849E-003	1	6.849E-003	17.86	0.0010	
CT	0.027	1	0.027	70.87	< 0.0001	
C^2	0.065	1	0.065	168.84	< 0.0001	
T^2	6.686E-003	1	6.686E-003	17.43	0.0011	
Residual	4.985E-003	13	3.835E-004			
Lack of Fit	4.795E-003	8	5.994E-004	15.76	0.0038	significant
Pure Error	1.901E-004	5	3.802E-005			
Cor Total	0.53	19				
Additional ANOVA Data						
Std. Dev.	0.020					
R^2	0.9906					
Adj. R^2	0.9863					
Pred. R^2	0.9673					
Adequate Precision	51.740					

Neodymium (Nd)

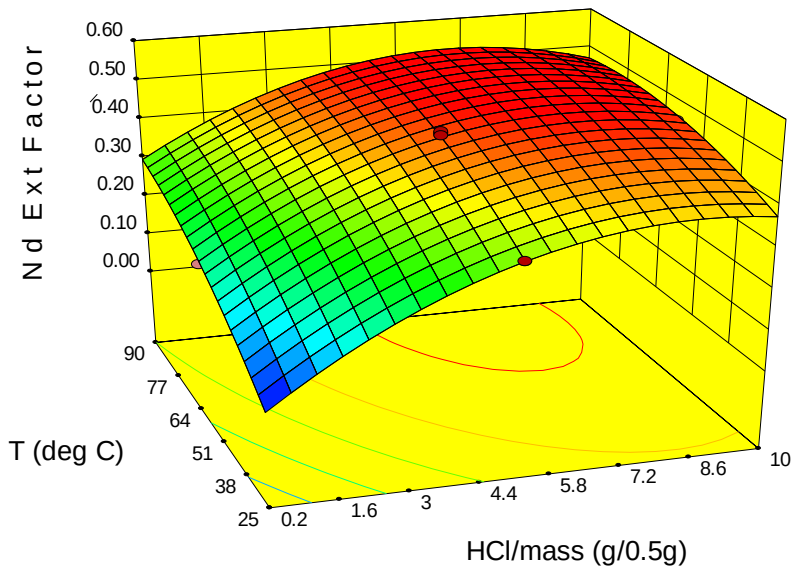

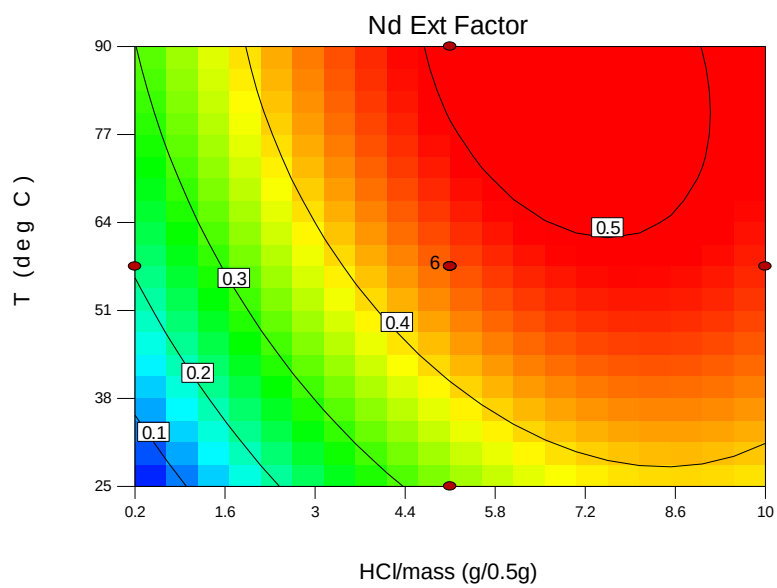

Equation: $Nd = -0.20271 + 0.0.093263C + 8.41548 \times 10^{-3}T + 4.59369 \times 10^{-4}t - 2.61813 \times 10^{-4}CT - 5.09265 \times 10^{-3}C^2 - 3.75272 \times 10^{-5}T^2$

Figure 88: Contour Plot, Model Equation, and Response Surface of Nd Extraction from RE2 (Time: 75 min)

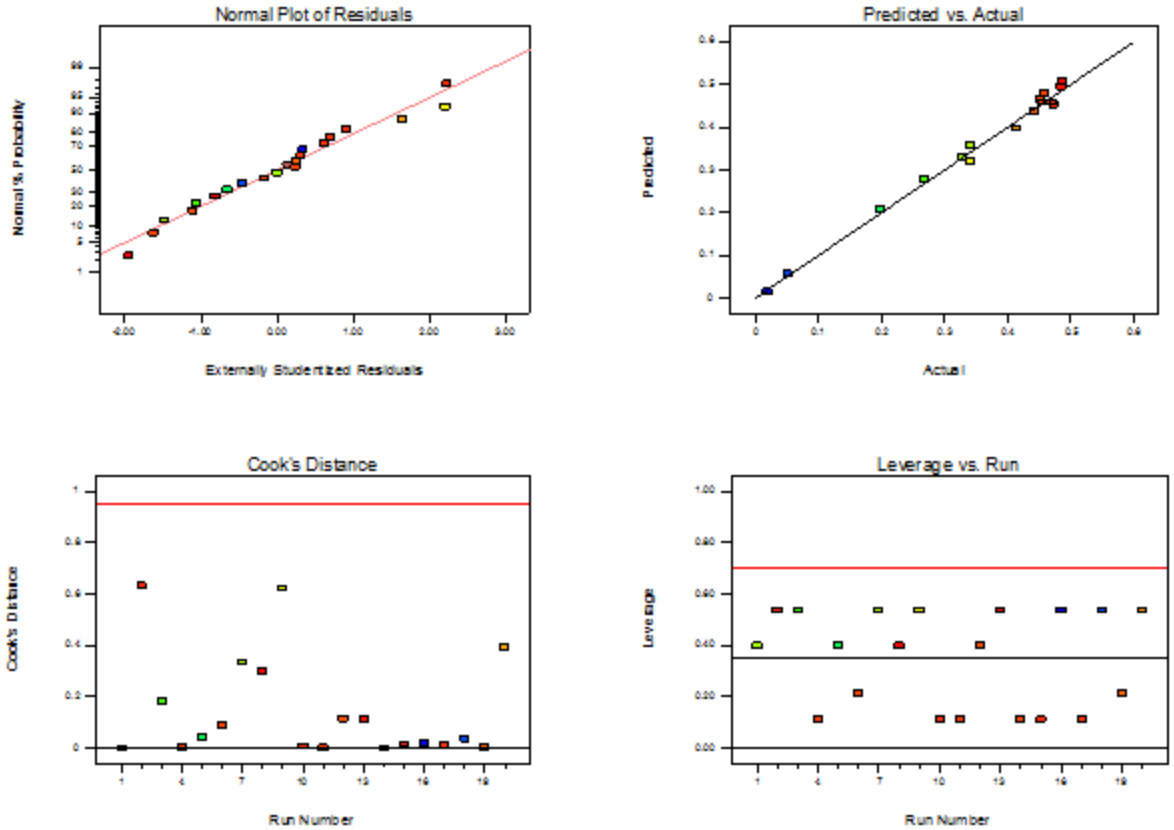

Figure 89: Diagnostics for Nd Extraction Model (RE2)

Table LVIII: ANOVA Data for Nd Extraction from RE2

Source	Sum of Squares	df	Mean Square	F-Value	p-value	Notes
Model	0.38	6	0.063	256.08	< 0.0001	significant
C-HCl/mass	0.17	1	0.17	676.39	< 0.0001	
T-Temp	0.081	1	0.081	329.70	< 0.0001	
t-Time	4.273E-003	1	4.273E-003	17.45	0.0011	
CT	0.014	1	0.014	56.80	< 0.0001	
C^2	0.048	1	0.048	195.39	< 0.0001	
T^2	5.028E-003	1	5.028E-003	20.53	0.0006	
Residual	3.183E-003	13	2.449E-004			
Lack of Fit	3.016E-003	8	3.770E-004	11.27	0.0082	significant
Pure Error	1.673E-004	5	3.345E-005			
Cor Total	0.38	19				
Additional ANOVA Data						
Std. Dev.	0.016					
R^2	0.9916					
Adj. R^2	0.9877					
Pred. R^2	0.9718					
Adequate Precision	53.258					

Praseodymium (Pr)

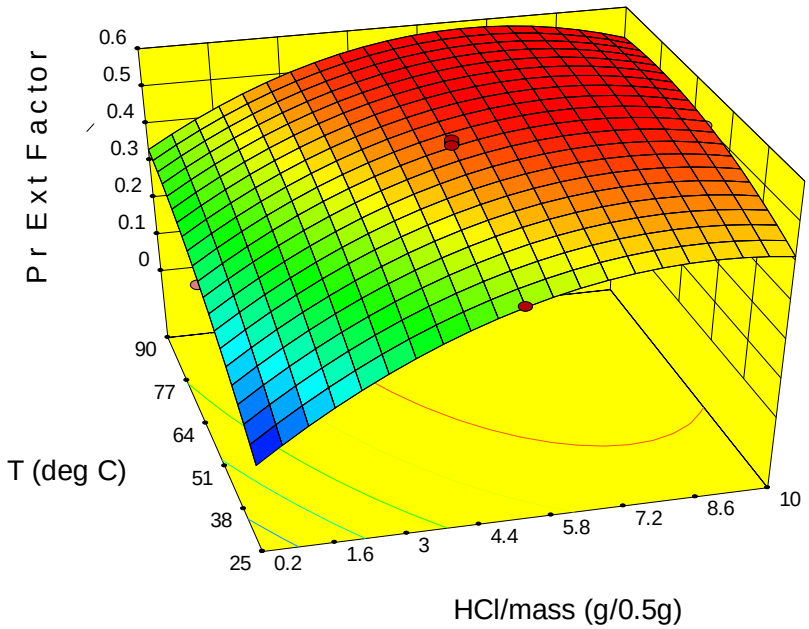

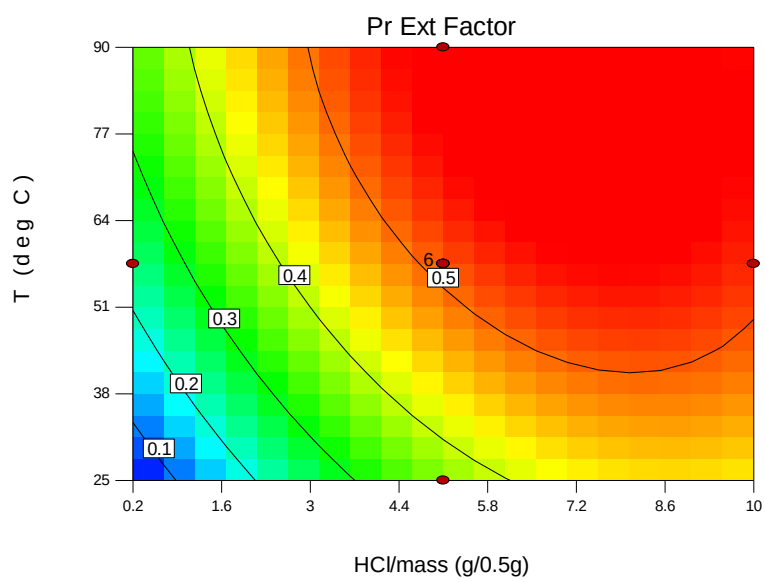

Equation: $Pr = -0.23437 + 0.10459C + 9.68067 \times 10^{-3}T + 5.21832 \times 10^{-4}t - 3.10871 \times 10^{-4}CT - 5.68484 \times 10^{-3}C^2 - 4.35415 \times 10^{-5}T^2$

Figure 90: Contour Plot, Model Equation, and Response Surface of Pr Extraction from RE2 (Time: 75 min)

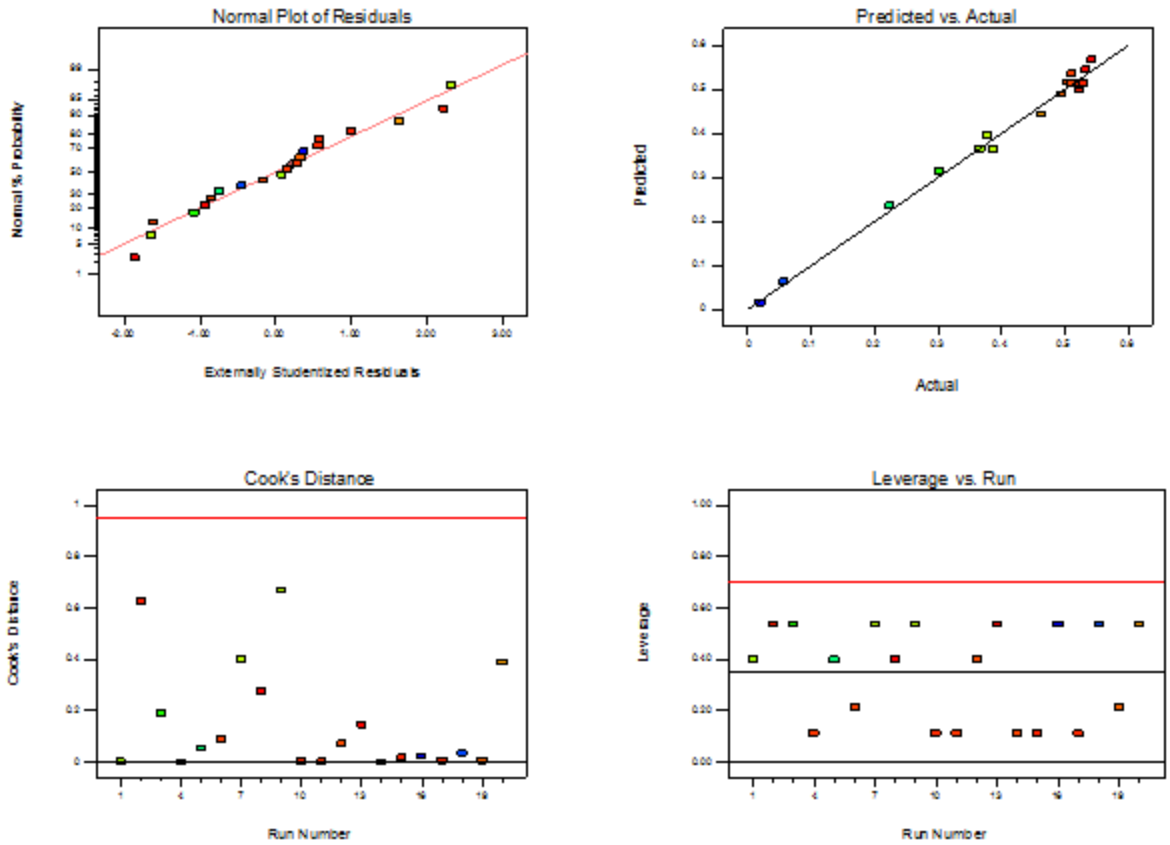

Figure 91: Diagnostics for Pr Extraction Model (RE2)

Table LIX: ANOVA Data for Pr Extraction from RE2

Source	Sum of Squares	df	Mean Square	F-Value	p-value	Notes
Model	0.47	6	0.078	239.59	< 0.0001	significant
C-HCl/mass	0.20	1	0.20	612.07	< 0.0001	
T-Temp	0.10	1	0.10	311.12	< 0.0001	
t-Time	5.514E-003	1	5.514E-003	17.03	0.0012	
CT	0.020	1	0.020	60.57	< 0.0001	
C^2	0.060	1	0.060	184.16	< 0.0001	
T^2	6.768E-003	1	6.768E-003	20.91	0.0005	
Residual	4.208E-003	13	3.237E-004			
Lack of Fit	3.975E-003	8	4.968E-004	10.62	0.0093	significant
Pure Error	2.338E-004	5	4.676E-005			
Cor Total	0.47	19				
Additional ANOVA Data						
Std. Dev.	0.018					
R^2	0.9910					
Adj. R^2	0.9869					
Pred. R^2	0.9693					
Adequate Precision	51.760					

Thorium (Th)

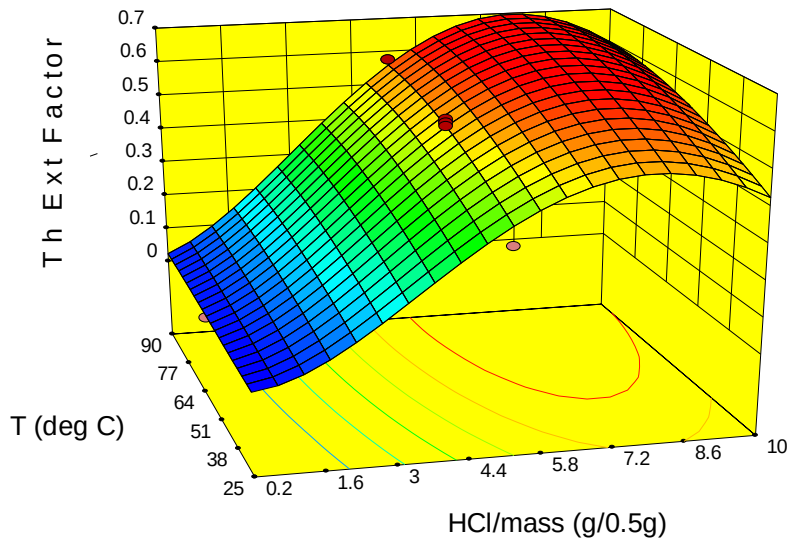

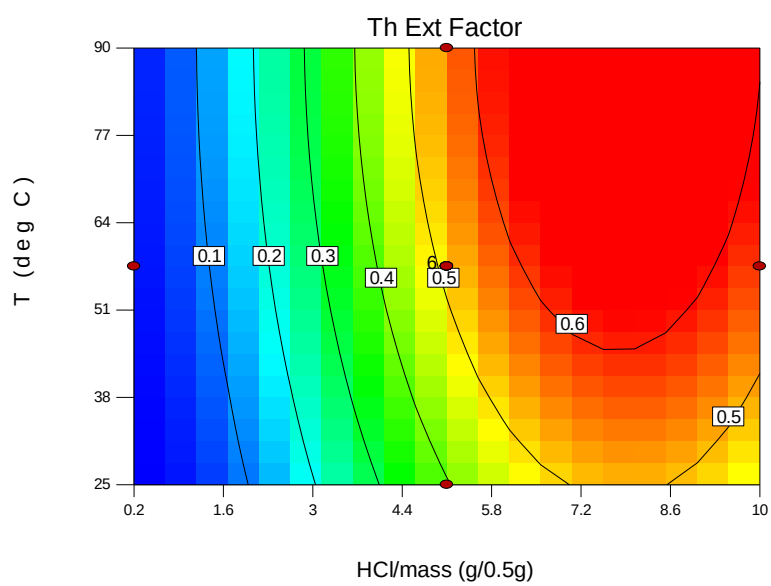

Equation:

$$\sqrt{Th} = -0.14250 + 0.18537C + 4.86586 \times 10^{-3}T + 4.03302 \times 10^{-4}t - 0.011917C^2 - 2.61515 \times 10^{-5}T^2$$

Figure 92: Contour Plot, Model Equation, and Response Surface of Th Extraction from RE2 (Time: 75 min)

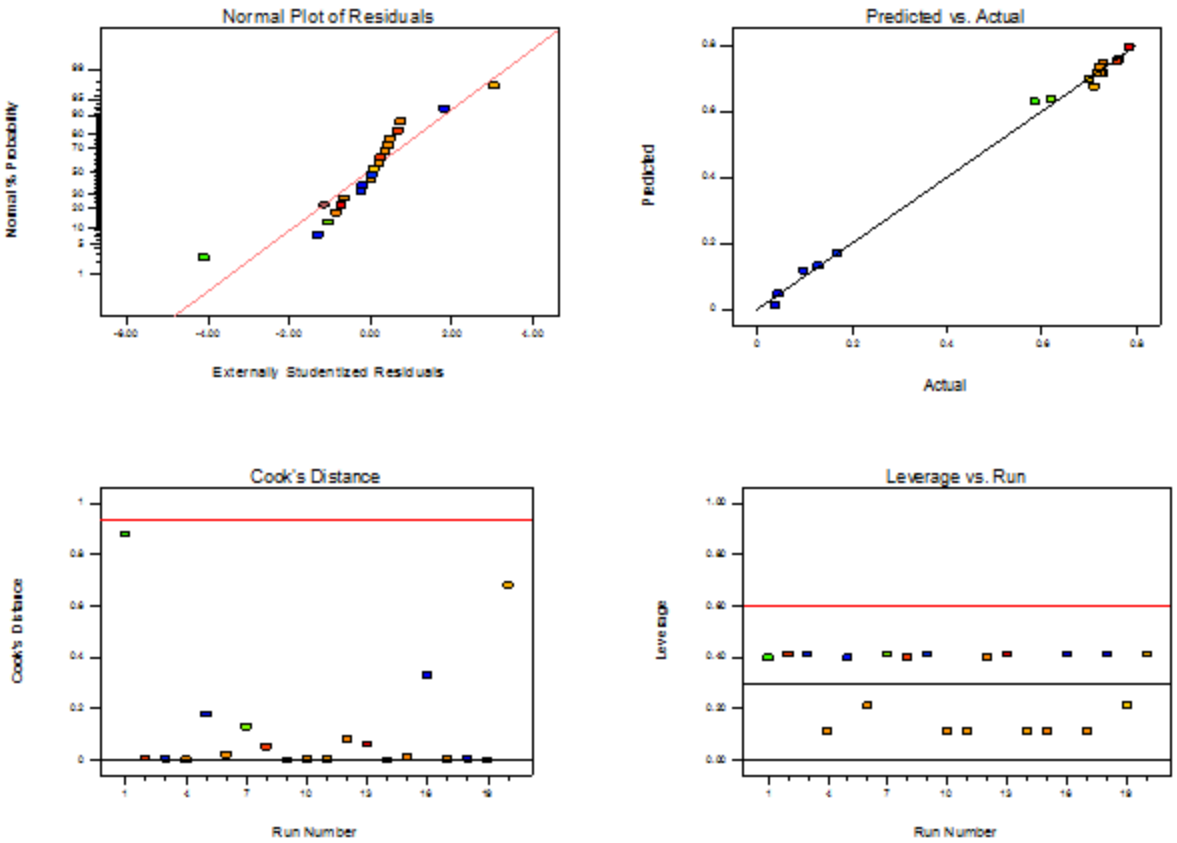

Figure 93: Diagnostics for Th Extraction Model (RE2)

Table LX: ANOVA Data for Th Extraction from RE2

Source	Sum of Squares	df	Mean Square	F-Value	p-value	Notes
Model	1.48	5	0.30	735.22	< 0.0001	significant
C-HCl/mass	0.98	1	0.98	2431.72	< 0.0001	
T-Temp	0.036	1	0.036	90.72	< 0.0001	
t-Time	3.294E-003	1	3.294E-003	8.19	0.0125	
C^2	0.26	1	0.26	651.54	< 0.0001	
T^2	2.442E-003	1	2.442E-003	6.07	0.0273	
Residual	5.630E-003	14	4.021E-004			
Lack of Fit	5.521E-003	9	6.135E-004	28.32	0.0009	significant
Pure Error	1.083E-004	5	2.167E-005			
Cor Total	1.48	19				
Additional ANOVA Data						
Std. Dev.	0.020					
R^2	0.9962					
Adj. R^2	0.9949					
Pred. R^2	0.9898					
Adequate Precision	71.244					

Iron (Fe)

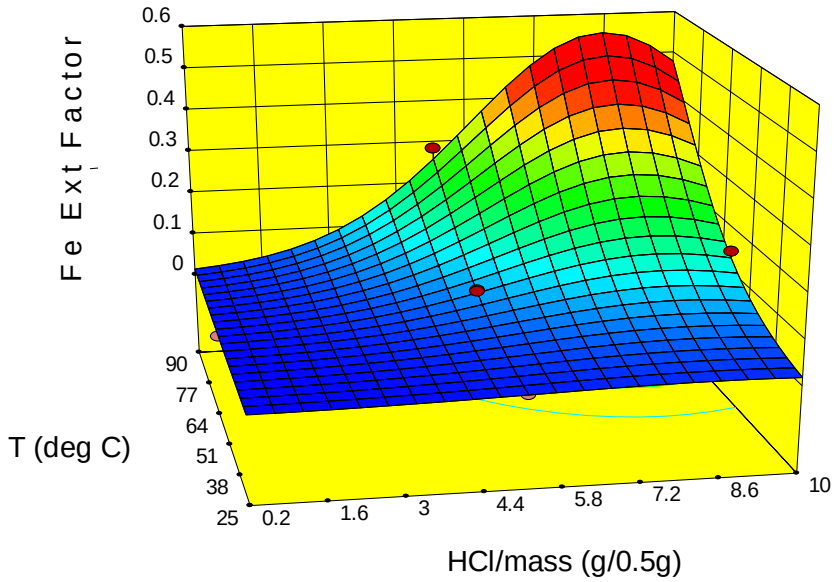

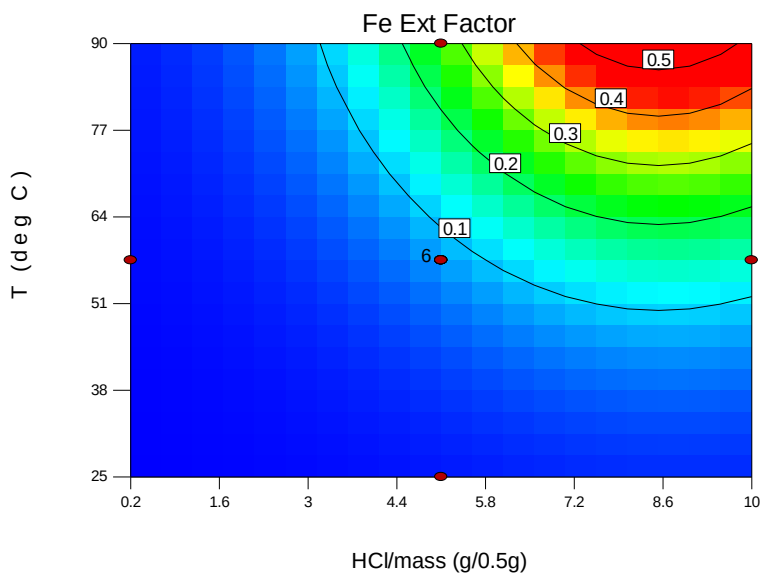

Equation: $Fe^{-0.11} = -2.59220 - 0.13654C - 0.014852T - 3.02975 \times 10^{-3}t + 5.39727 \times 10^{-5}CT + 7.76591 \times 10^{-3}C^2 + 6.65505 \times 10^{-5}T^2 + 1.17276 \times 10^{-5}t^2$

Figure 94: Contour Plot, Model Equation, and Response Surface of Fe Extraction from RE2 (Time: 75 min)

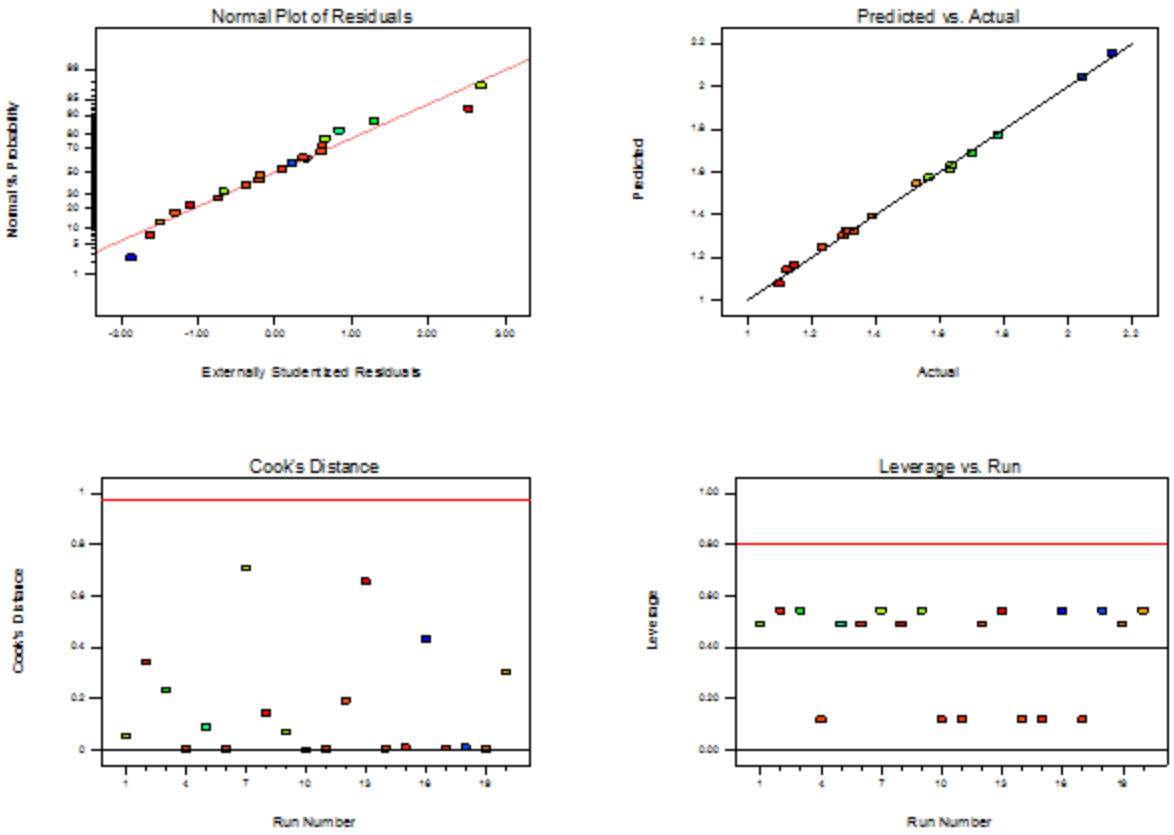

Figure 95: Diagnostics for Fe Extraction Model (RE2)

Table LXI: ANOVA Data for Fe Extraction from RE2

Source	Sum of Squares	df	Mean Square	F-Value	p-value	Notes
Model	1.57	7	0.22	783.49	< 0.0001	significant
C-HCl/mass	0.68	1	0.68	2386.11	< 0.0001	
T-Temp	0.55	1	0.55	1915.86	< 0.0001	
t-Time	0.020	1	0.020	70.22	< 0.0001	
Ct	1.133E-003	1	1.133E-003	3.97	0.0697	
C^2	0.096	1	0.096	334.69	< 0.0001	
T^2	0.014	1	0.014	47.57	< 0.0001	
t^2	1.551E-003	1	1.551E-003	5.43	0.0381	
Residual	3.428E-003	12	2.857E-004			
Lack of Fit	3.024E-003	7	4.320E-004	5.34	0.0417	significant
Pure Error	4.042E-004	5	8.083E-005			
Cor Total	1.57	19				
Additional ANOVA Data						
Std. Dev.	0.017					
R^2	0.9978					
Adj. R^2	0.9965					
Pred. R^2	0.9908					
Adequate Precision	100.998					

Appendix G: Modeling Data for RE4

Aluminum (Al)

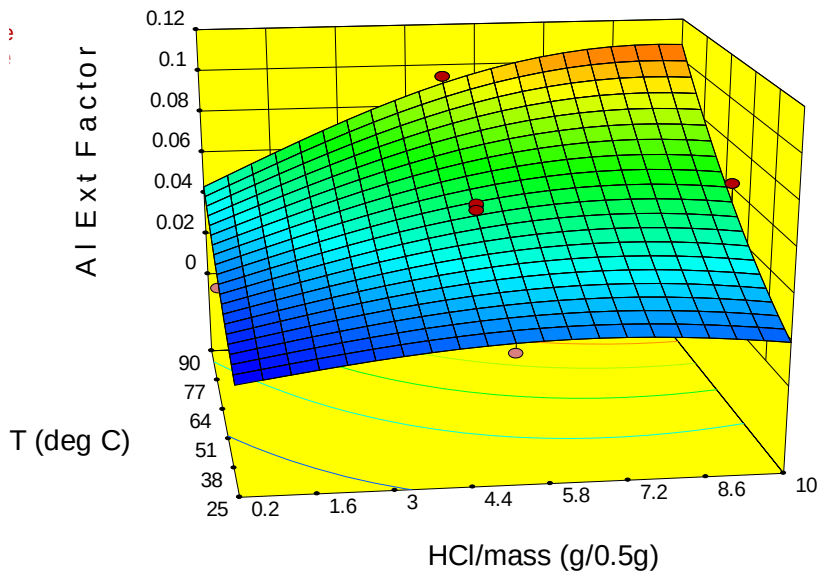

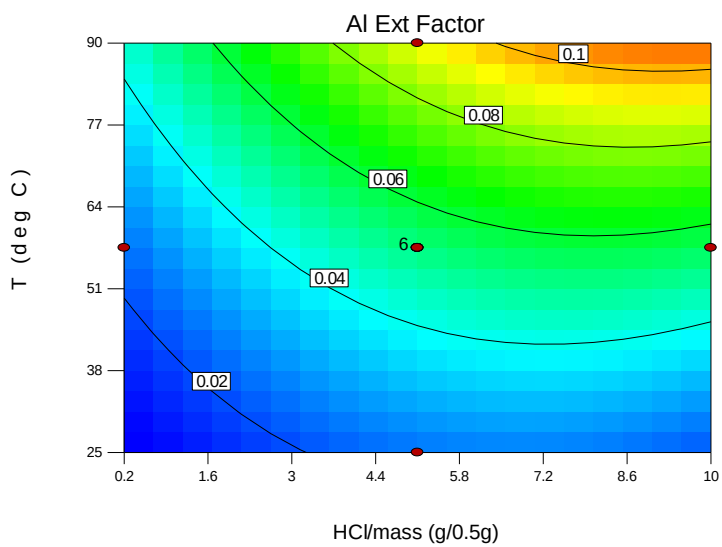

Equation: $\sqrt{Al} = 0.031548 + 0.015388C + 1.66306 \times 10^{-3}T + 3.03725 \times 10^{-4}t + 9811.23 \times 10^{-4}CT - 1.41417 \times 10^{-3}C^2$

Figure 96: Contour Plot, Model Equation, and Response Surface of Al Extraction from RE4 (Time: 75 min)

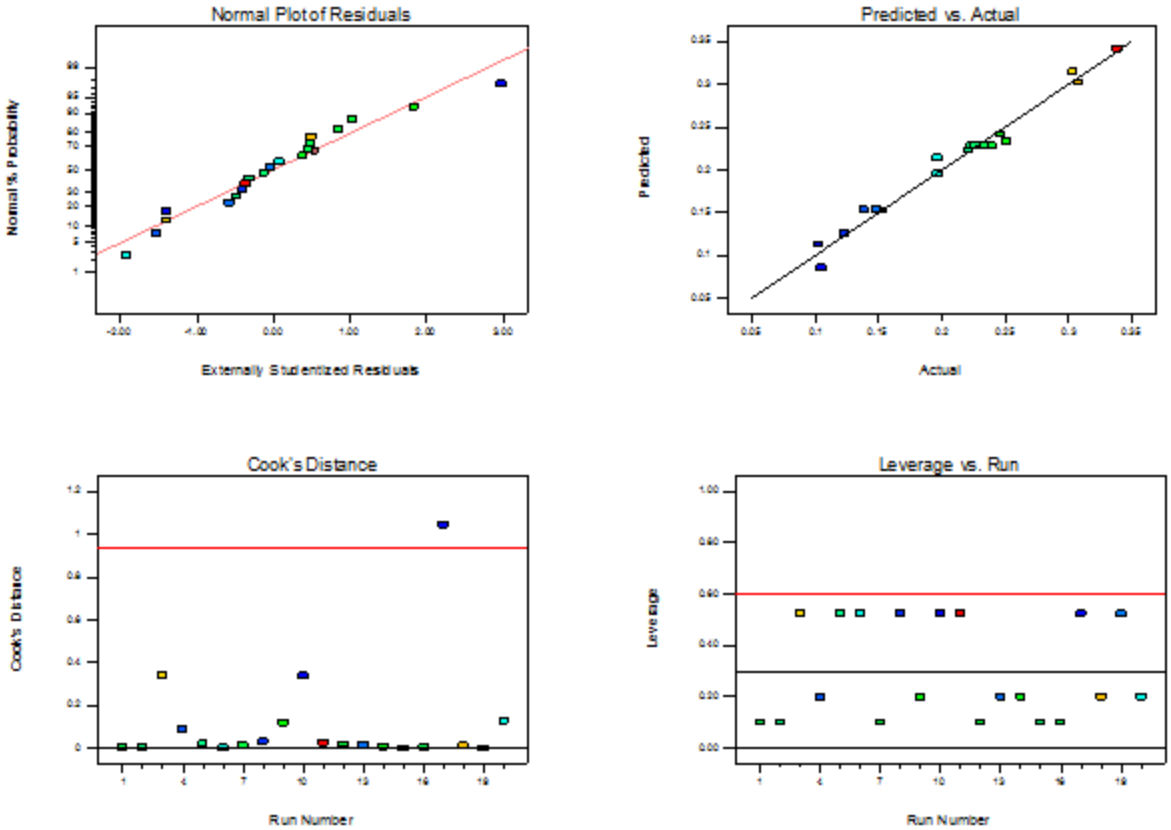

Figure 97: Diagnostics for Al Extraction Model (RE4)

Table LXII: ANOVA Data for Al Extraction from RE4

Source	Sum of Squares	df	Mean Square	F-Value	p-value	Notes
Model	0.082	5	0.016	123.40	< 0.0001	significant
C-HCl/mass	0.016	1	0.016	118.12	< 0.0001	
T-Temp	0.056	1	0.056	418.11	< 0.0001	
t-Time	1.868E-003	1	1.868E-003	14.03	0.0022	
CT	3.119E-003	1	3.119E-003	23.43	0.0003	
C^2	5.764E-003	1	5.764E-003	43.31	< 0.0001	
Residual	1.863E-003	14	1.331E-004			
Lack of Fit	1.661E-003	9	1.845E-004	4.55	0.0549	not significant
Pure Error	2.027E-004	5	4.053E-005			
Cor Total	0.084	19				
Additional ANOVA Data						
Std. Dev.	0.012					
R^2	0.9778					
Adj. R^2	0.9699					
Pred. R^2	0.9454					
Adequate Precision	40.487					

Cerium (Ce)

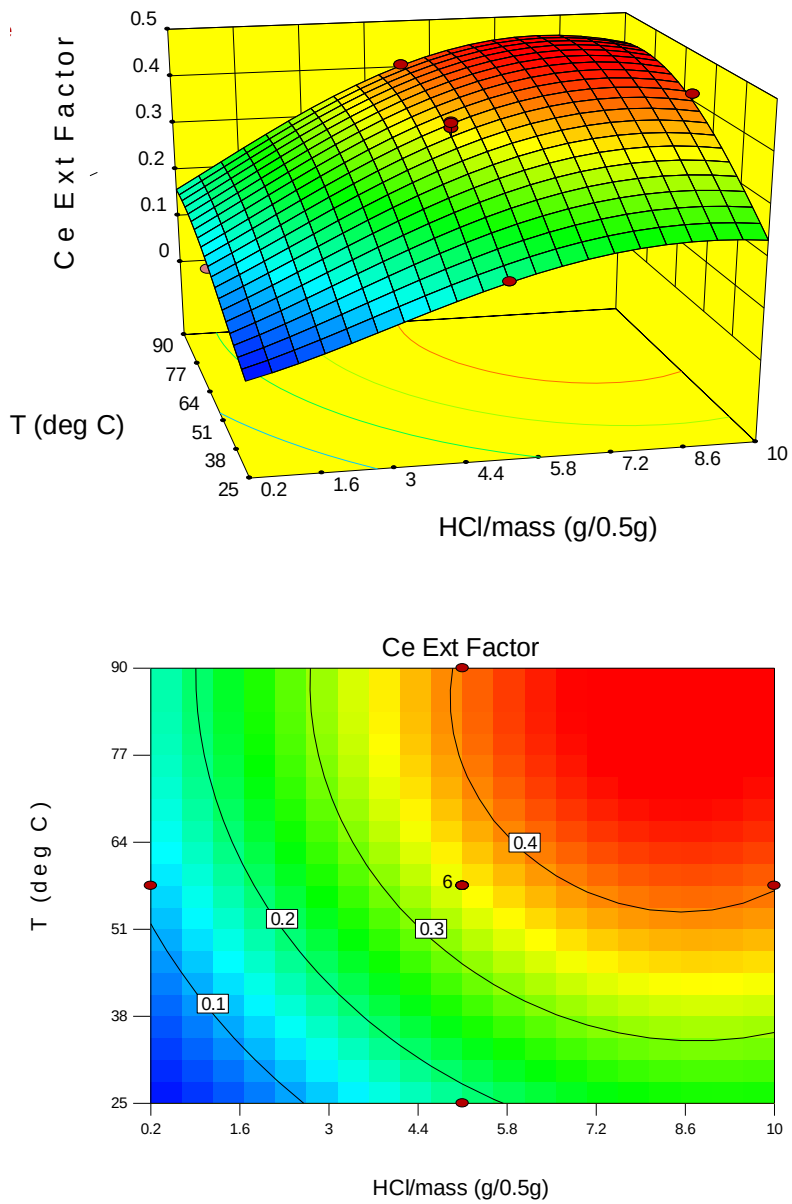

Equation: $\sqrt{Ce} = -0.19752 + 0.081622C + 0.011415T + 1.50822 \times 10^{-3}t - 1.07376 \times 10^{-4}CT - 1.31011 \times 10^{-5}Tt - 4.44071 \times 10^{-3}C^2 - 5.79444 \times 10^{-4}T^2$

Figure 98: Contour Plot, Model Equation, and Response Surface of Ce Extraction from RE4 (Time: 75 min)

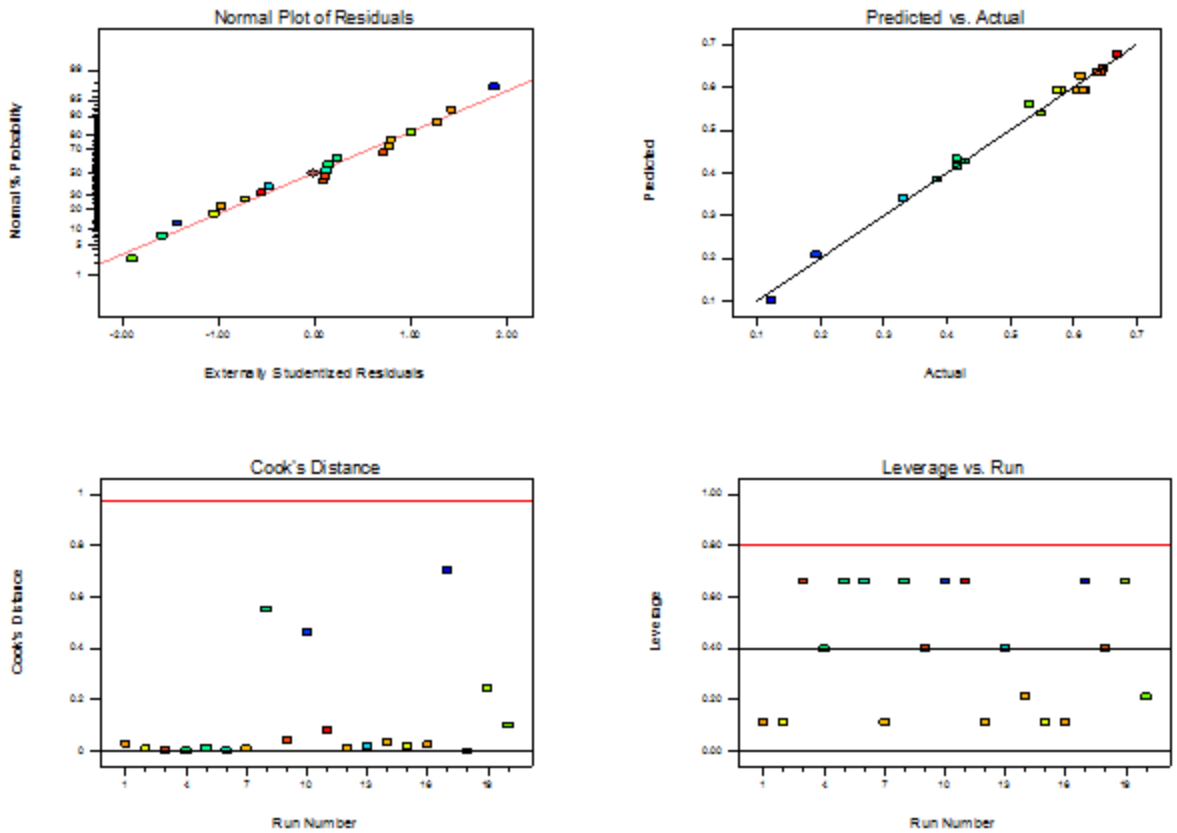

Figure 99: Diagnostics for Ce Extraction Model (RE4)

Table LXIII: ANOVA Data for Ce Extraction from RE4

Source	Sum of Squares	df	Mean Square	F-Value	p-value	Notes
Model	0.46	7	0.066	178.06	< 0.0001	significant
C-HCl/mass	0.22	1	0.22	592.26	< 0.0001	
T-Temp	0.11	1	0.11	297.27	< 0.0001	
t-Time	0.012	1	0.012	31.31	0.0001	
CT	2.339E-003	1	2.339E-003	6.35	0.0269	
Tt	2.937E-003	1	2.937E-003	7.97	0.0154	
C^2	0.036	1	0.036	98.70	< 0.0001	
T^2	0.012	1	0.012	32.52	< 0.0001	
Residual	4.423E-003	12	3.686E-004			
Lack of Fit	2.675E-003	7	3.822E-004	1.09	0.4776	not significant
Pure Error	1.748E-003	5	3.496E-004			
Cor Total	0.46	19				
Additional ANOVA Data						
Std. Dev.	0.019					
R^2	0.9905					
Adj. R^2	0.9849					
Pred. R^2	0.9695					
Adequate Precision	47.173					

Dysprosium (Dy)

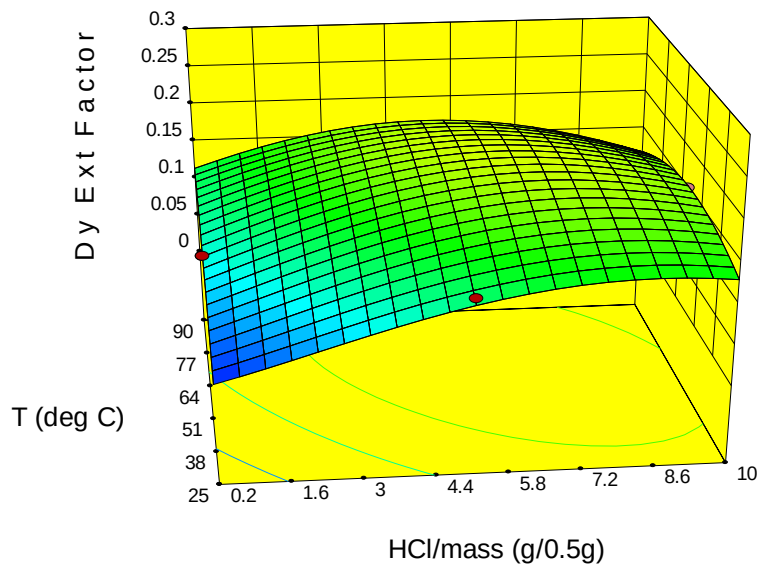

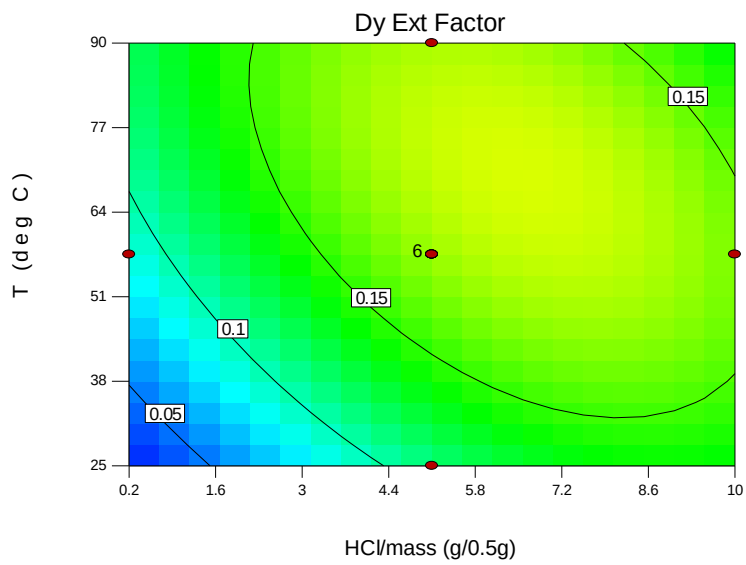

Equation: $\sqrt{Dy} = -6.80228 \times 10^{-3} + 0.058062C + 7.33867 \times 10^{-3}T - 3.02699 \times 10^{-4}CT - 2.95750 \times 10^{-3}C^2 - 3.96572 \times 10^{-5}T^2$

Figure 100: Contour Plot, Model Equation, and Response Surface of Dy Extraction from RE4 (Time: 75 min)

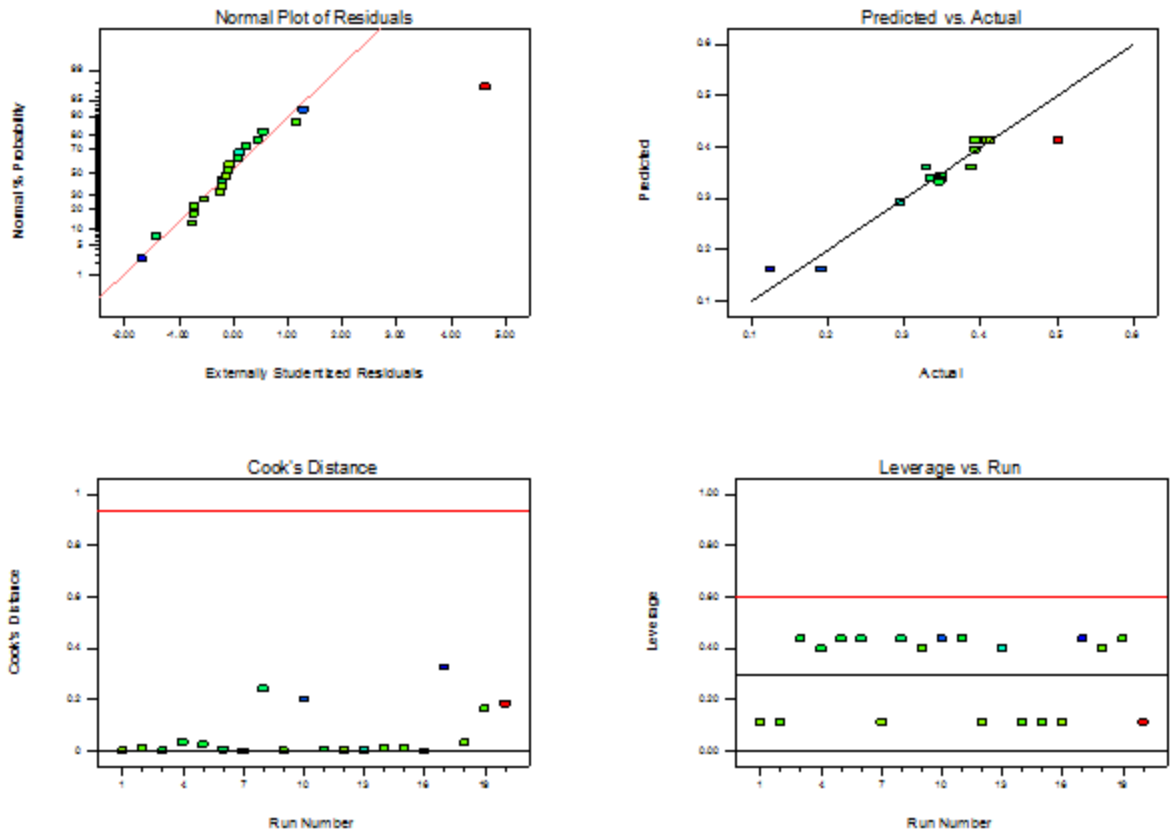

Figure 101: Diagnostics for Dy Extraction Model (RE4)

Table LXIV: ANOVA Data for Dy Extraction from RE4

Source	Sum of Squares	df	Mean Square	F-Value	p-value	Notes
Model	0.11	5	0.023	23.09	< 0.0001	significant
C-HCl/mass	0.026	1	0.026	27.01	0.0001	
T-Temp	0.016	1	0.016	16.45	0.0012	
CT	0.019	1	0.019	19.00	0.0007	
C^2	0.016	1	0.016	16.49	0.0012	
T^2	5.615E-003	1	5.615E-003	5.74	0.0311	
Residual	0.014	14	9.782E-004			
Lack of Fit	0.013	9	1.478E-003	18.89	0.0024	significant
Pure Error	3.912E-004	5	7.824E-005			
Cor Total	0.13	19				
Additional ANOVA Data						
Std. Dev.	0.031					
R^2	0.8919					
Adj. R^2	0.8532					
Pred. R^2	0.7961					
Adequate Precision	14.747					

Gadolinium (Gd)

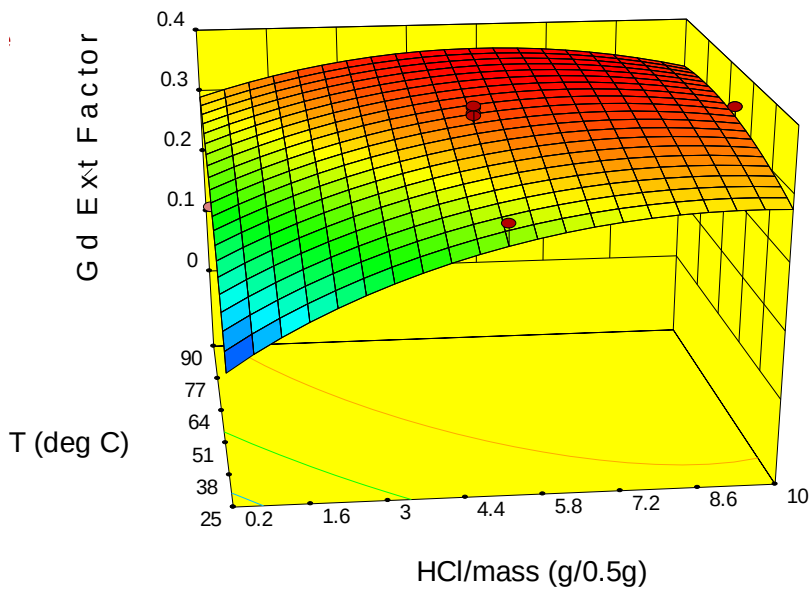

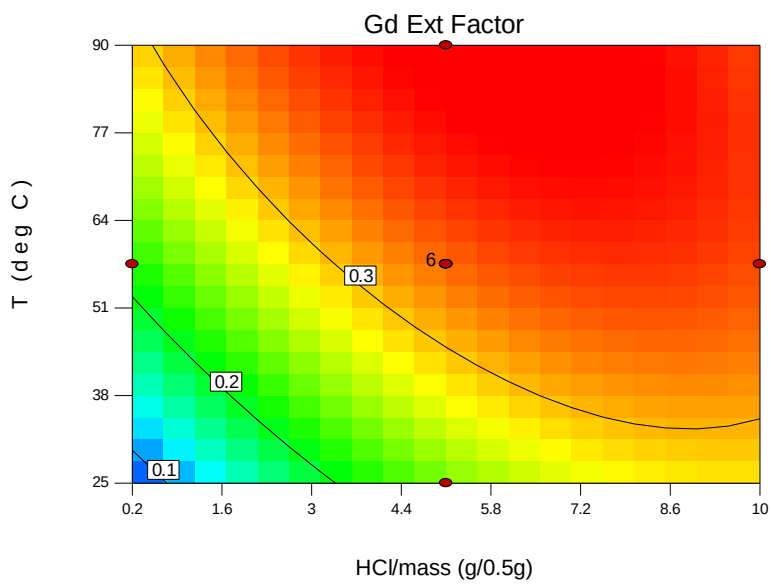

Equation: $Gd^{1.23} = -0.13237 + 0.043926C + 5.91480 \times 10^{-3}T + 6.34017 \times 10^{-4}t - 2.22483 \times 10^{-4}CT - 9.33029 \times 10^{-6}Tt - 2.05277 \times 10^{-3}C^2 - 2.08052 \times 10^{-5}T^2$

Figure 102: Contour Plot, Model Equation, and Response Surface of Gd Extraction from RE4 (Time: 75 min)

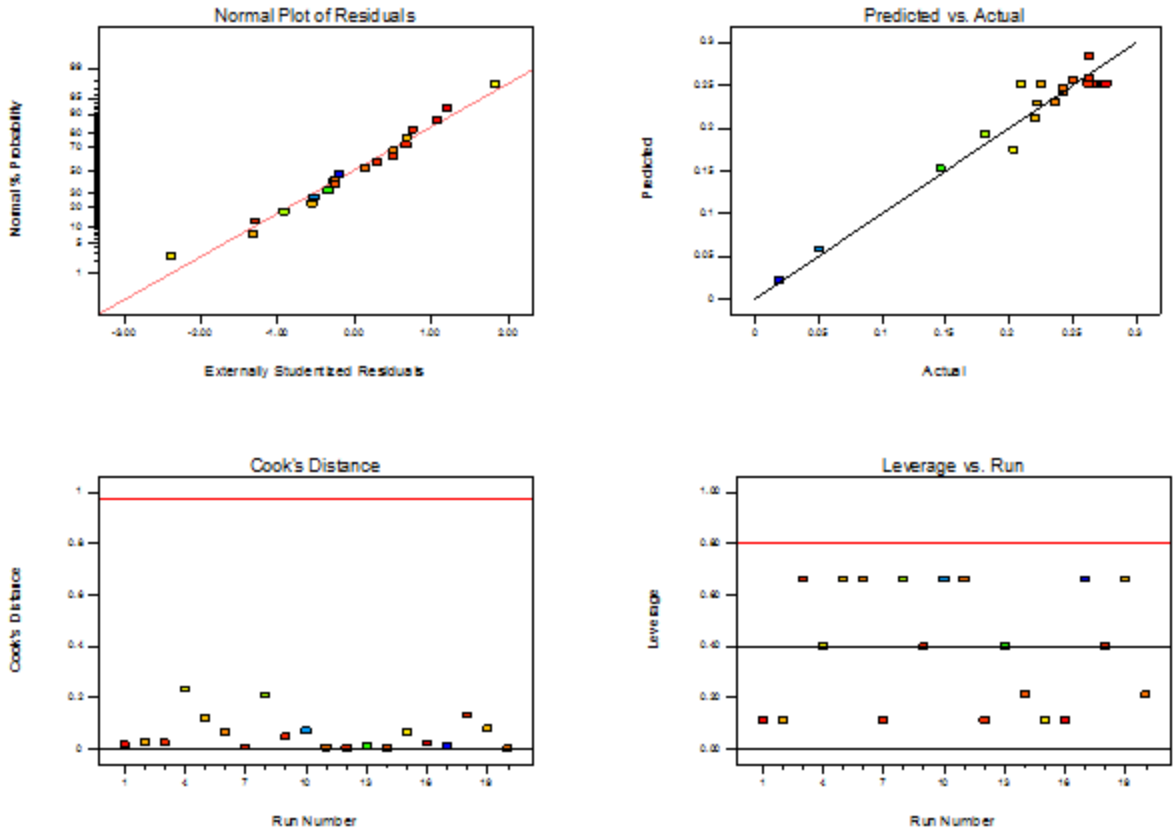

Figure 103: Diagnostics for Gd Extraction Model (RE4)

Table LXV: ANOVA Data for Gd Extraction from RE4

Source	Sum of Squares	df	Mean Square	F-Value	p-value	Notes
Model	0.088	7	0.013	25.57	< 0.0001	significant
C-HCl/mass	0.025	1	0.025	50.86	< 0.0001	
T-Temp	0.030	1	0.030	61.31	< 0.0001	
t-Time	1.926E-004	1	1.926E-004	0.39	0.5427	
CT	0.010	1	0.010	20.46	0.0007	
Tt	1.490E-003	1	1.490E-003	3.04	0.1070	
C^2	7.773E-003	1	7.773E-003	15.84	0.0018	
T^2	1.545E-003	1	1.545E-003	3.15	0.1013	
Residual	5.889E-003	12	4.907E-004			
Lack of Fit	1.959E-003	7	2.798E-004	0.36	0.8946	not significant
Pure Error	3.930E-003	5	7.860E-004			
Cor Total	0.094	19				
Additional ANOVA Data						
Std. Dev.	0.022					
R^2	0.9372					
Adj. R^2	0.9005					
Pred. R^2	0.8640					
Adequate Precision	18.730					

Lanthanum (La)

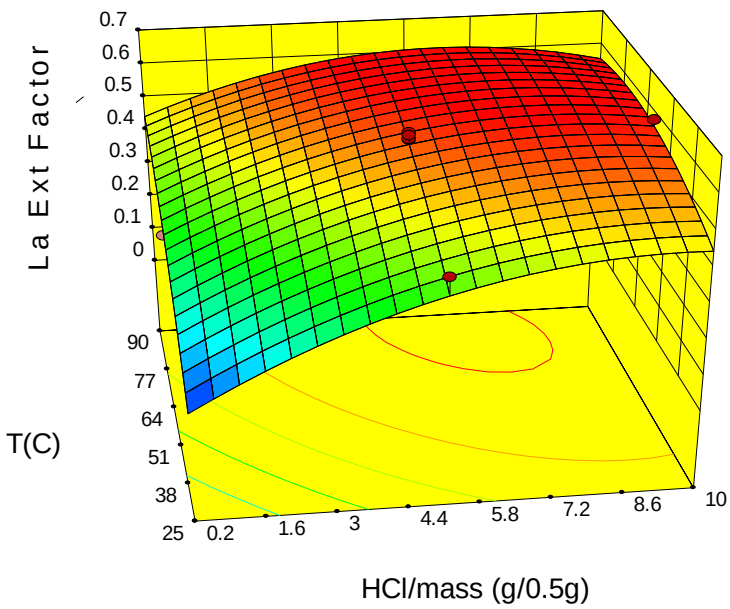

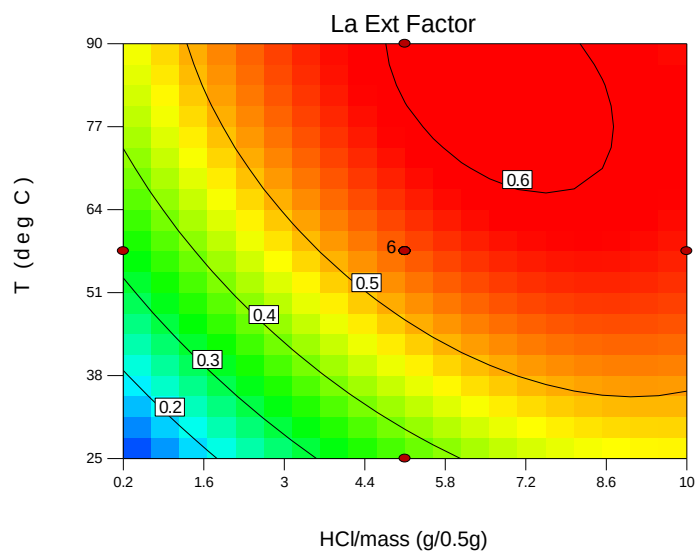

Equation: $La = -0.24510 + 0.090589C + 0.012198T + 5.65253 \times 10^{-4}t - 4.00014 \times 10^{-4}CT - 422978 \times 10^{-3}C^2 - 5.66677 \times 10^{-5}T^2$

Figure 104: Contour Plot, Model Equation, and Response Surface of La Extraction from RE4 (Time: 75 min)

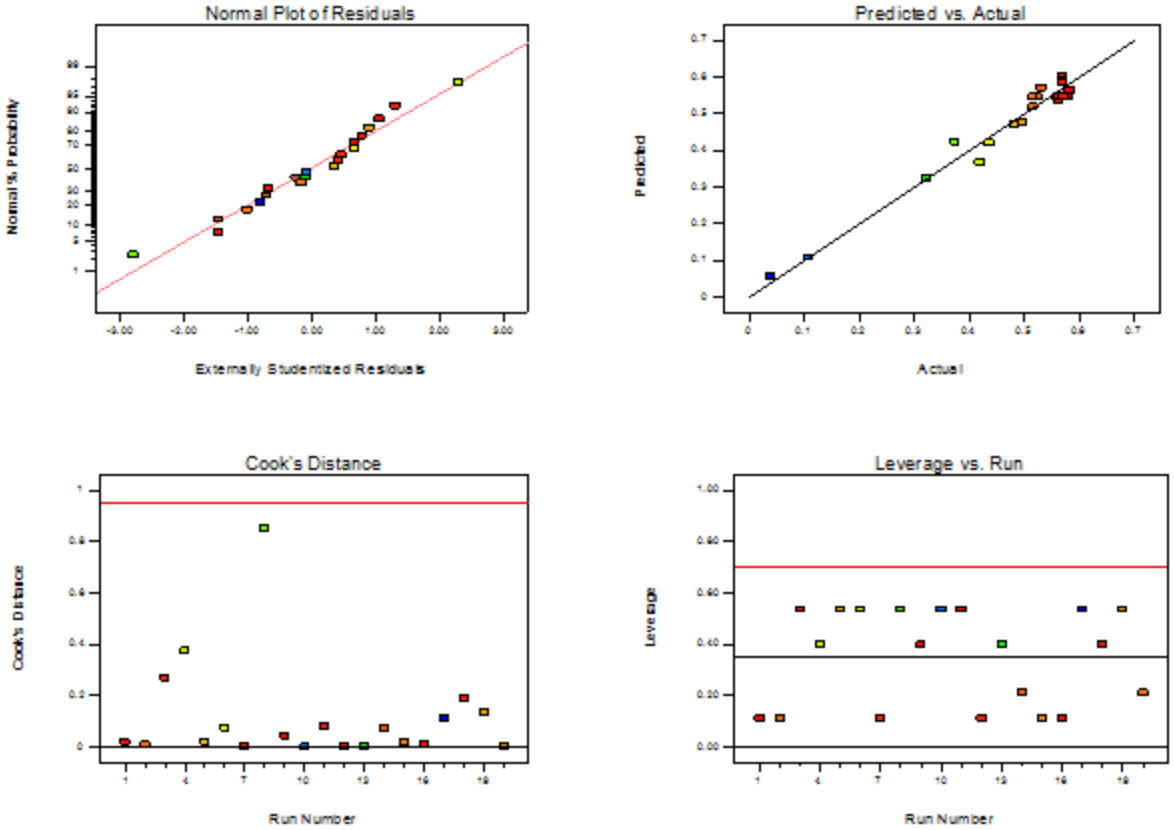

Figure 105: Diagnostics for La Extraction Model (RE4)

Table LXVI: ANOVA Data for La Extraction from RE4

Source	Sum of Squares	df	Mean Square	F-Value	p-value	Notes
Model	0.43	6	0.071	66.58	< 0.0001	significant
C-HCl/mass	0.14	1	0.14	133.78	< 0.0001	
T-Temp	0.14	1	0.14	130.61	< 0.0001	
t-Time	6.470E-003	1	6.470E-003	6.03	0.0289	
CT	0.032	1	0.032	30.27	0.0001	
C^2	0.033	1	0.033	30.78	< 0.0001	
T^2	0.011	1	0.011	10.69	0.0061	
Residual	0.014	13	1.072E-003			
Lack of Fit	0.011	8	1.325E-003	1.98	0.2341	not significant
Pure Error	3.343E-003	5	6.686E-004			
Cor Total	0.44	19				
Additional ANOVA Data						
Std. Dev.	0.033					
R^2	0.9685					
Adj. R^2	0.9539					
Pred. R^2	0.9090					
Adequate Precision	28.243					

Neodymium (Nd)

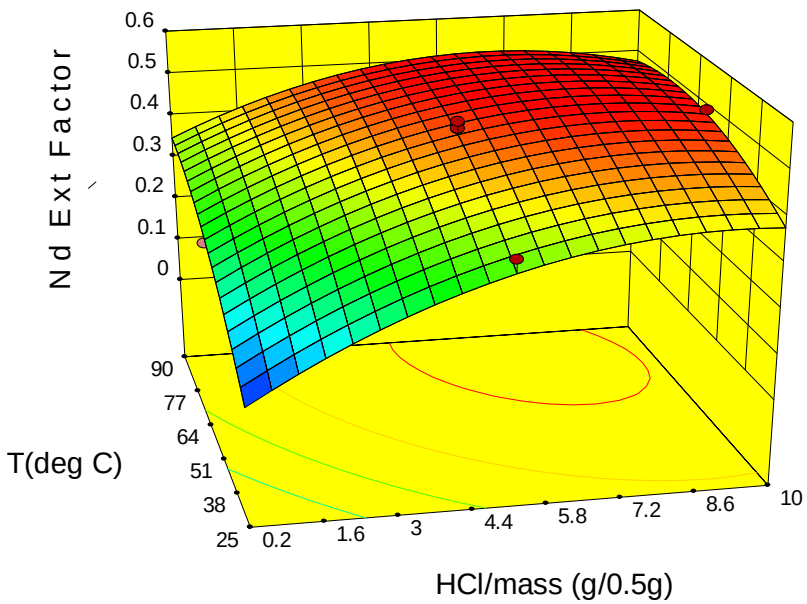

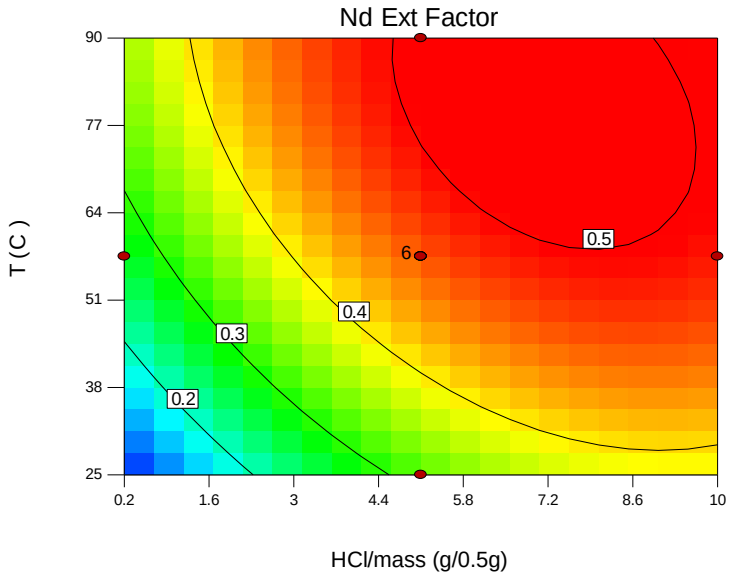

Equation: $Nd = -0.20464 + 0.078419C + 0.010170T + 4.96242 \times 10^{-4}t - 2.84884 \times 10^{-4}CT - 3.88546 \times 10^{-3}C^2 - 5.04989 \times 10^{-5}T^2$

Figure 106: Contour Plot, Model Equation, and Response Surface of Nd Extraction from RE4 (Time: 75 min)

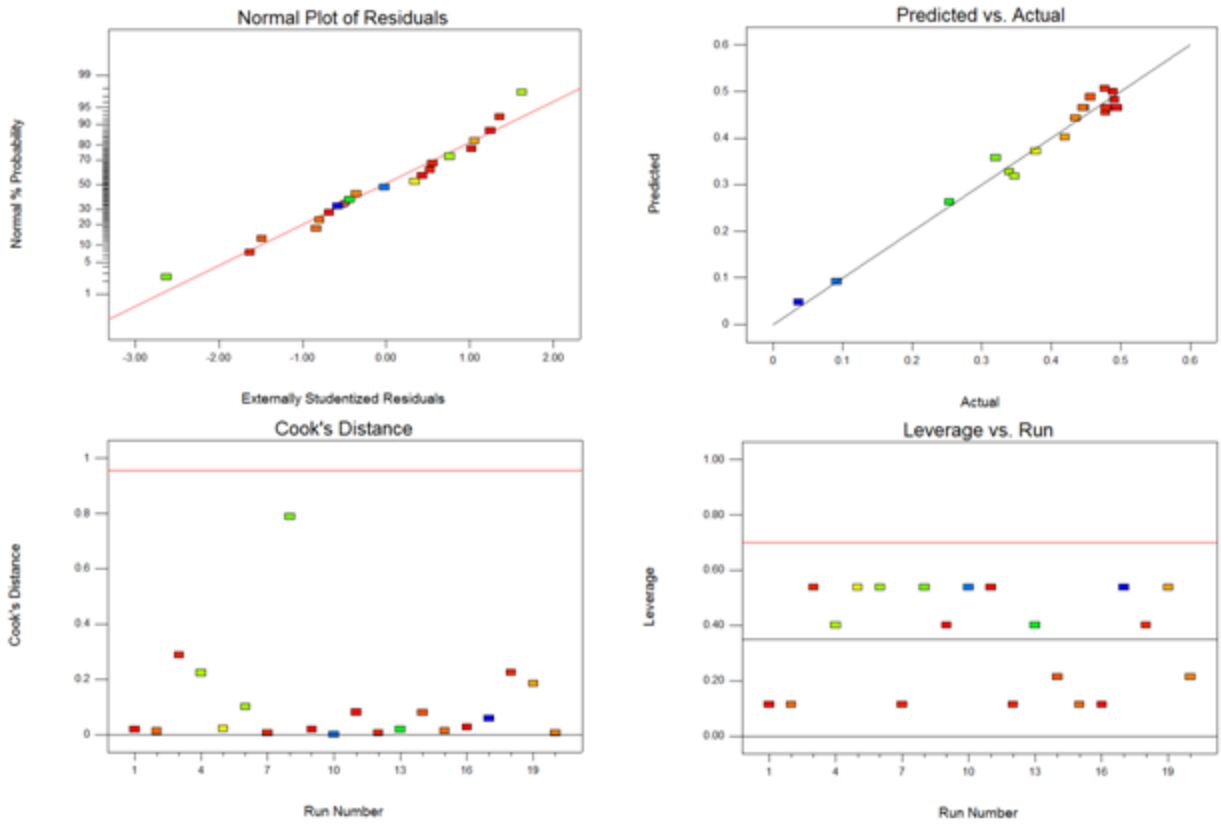

Figure 107: Diagnostics for Nd Extraction Model (RE4)

Table LXVII: ANOVA Data for Nd Extraction from RE4

Source	Sum of Squares	df	Mean Square	F-Value	p-value	Notes
Model	0.32	6	0.053	85.70	< 0.0001	significant
C-HCl/mass	0.12	1	0.12	194.31	< 0.0001	
T-Temp	0.089	1	0.089	144.12	< 0.0001	
t-Time	4.987E-003	1	4.987E-003	8.04	0.0140	
CT	0.016	1	0.016	26.54	0.0002	
C^2	0.028	1	0.028	44.89	< 0.0001	
T^2	9.104E-003	1	9.104E-003	14.68	0.0021	
Residual	8.064E-003	13	6.203E-004			
Lack of Fit	5.842E-003	8	7.303E-004	1.64	0.3030	not significant
Pure Error	2.222E-003	5	4.444E-004			
Cor Total	0.33	19				
Additional ANOVA Data						
Std. Dev.	0.025					
R^2	0.9753					
Adj. R^2	0.9640					
Pred. R^2	0.9315					
Adequate Precision	31.210					

Praseodymium (Pr)

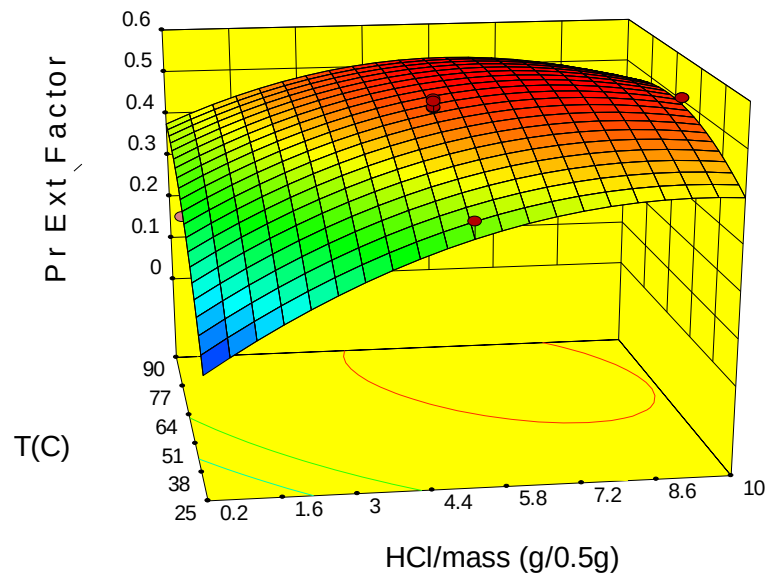

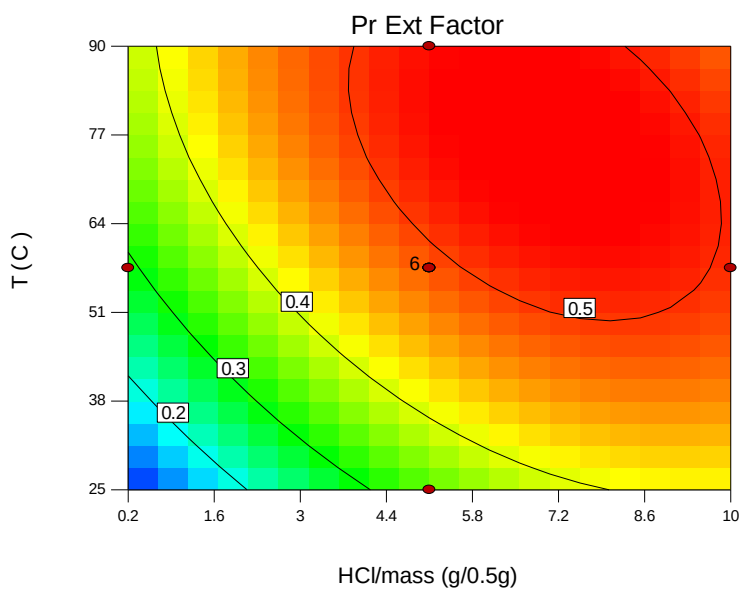

Equation: $Pr = -0.23172 + 0.085458C + 0.011752T + 4.43126 \times 10^{-4}t - 3.96984 \times 10^{-4}CT - 4.09287 \times 10^{-3}C^2 - 6.05072 \times 10^{-5}T^2$

Figure 108: Contour Plot, Model Equation, and Response Surface of Pr Extraction from RE4 (Time: 75 min)

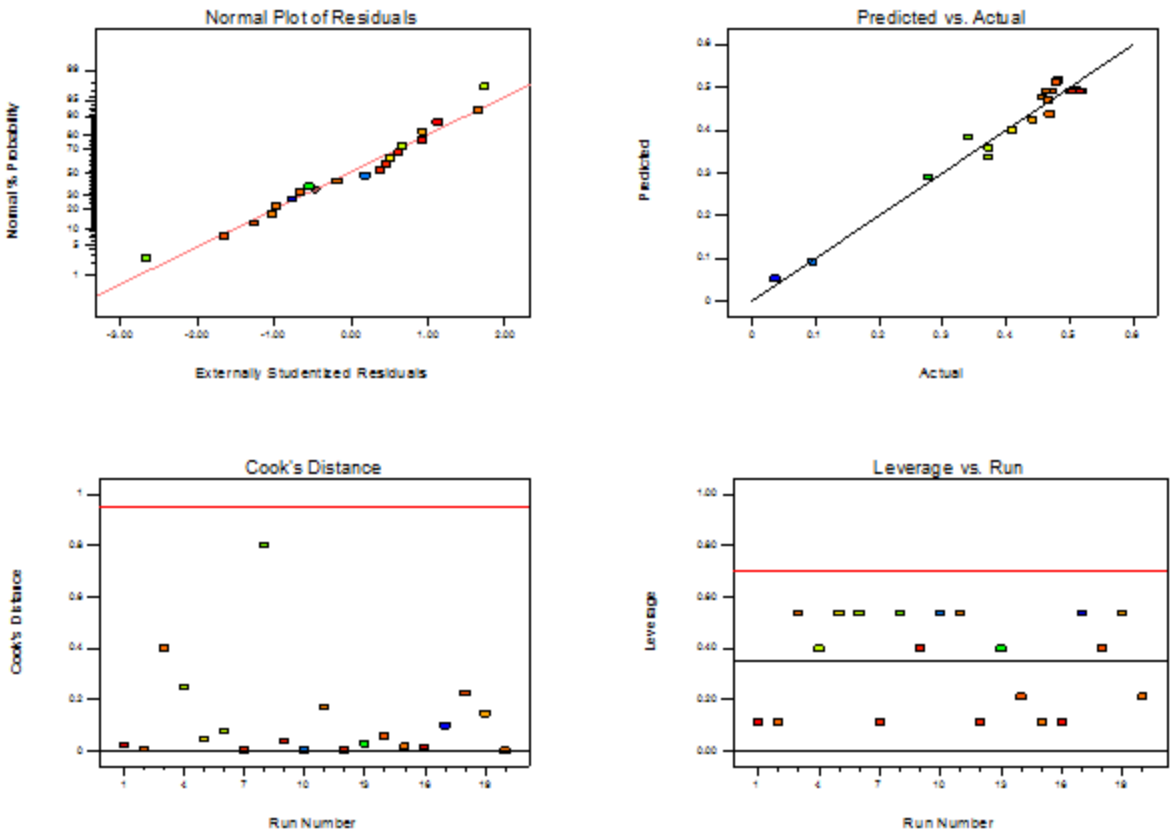

Figure 109: Diagnostics for Pr Extraction Model (RE4)

Table LXVIII: ANOVA Data for Pr Extraction from RE4

Source	Sum of Squares	df	Mean Square	F-Value	p-value	Notes
Model	0.33	6	0.055	64.70	< 0.0001	significant
C-HCl/mass	0.10	1	0.10	123.93	< 0.0001	
T-Temp	0.081	1	0.081	95.82	< 0.0001	
t-Time	3.976E-003	1	3.976E-003	4.71	0.0492	
CT	0.032	1	0.032	37.84	< 0.0001	
C^2	0.031	1	0.031	36.57	< 0.0001	
T^2	0.013	1	0.013	15.47	0.0017	
Residual	0.011	13	8.450E-004			
Lack of Fit	8.250E-003	8	1.031E-003	1.89	0.2513	not significant
Pure Error	2.735E-003	5	5.470E-004			
Cor Total	0.34	19				
Additional ANOVA Data						
Std. Dev.	0.029					
R^2	0.9676					
Adj. R^2	0.9526					
Pred. R^2	0.9035					
Adequate Precision	26.965					

Thorium (Th)

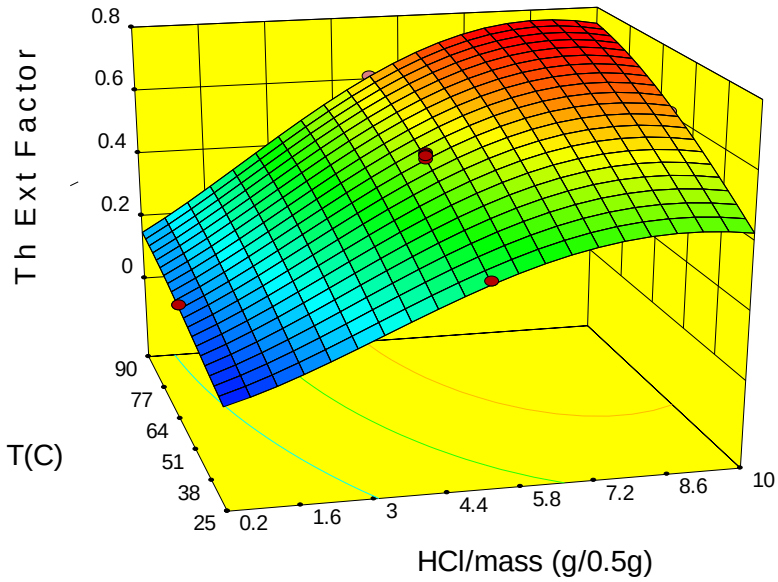

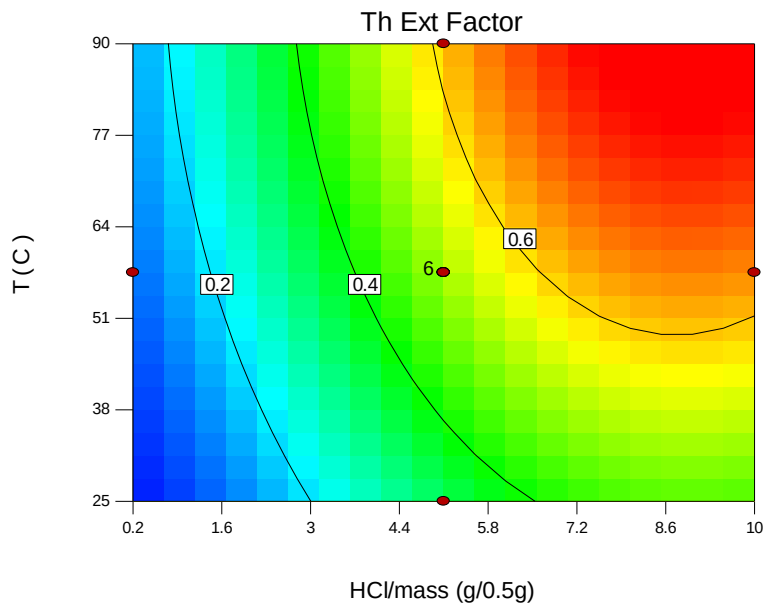

Equation: $Th^{0.45} = -0.13921 + 0.11019C + 7.56170 \times 10^{-3}T + 4.06532 \times 10^{-3}t - 1.28508 \times 10^{-5}Tt - 6.28162 \times 10^{-3}C^2 - 3.13741 \times 10^{-5}T^2 - 1.79576 \times 10^{-5}t^2$

Figure 110: Contour Plot, Model Equation, and Response Surface of Th Extraction from RE4 (Time: 75 min)

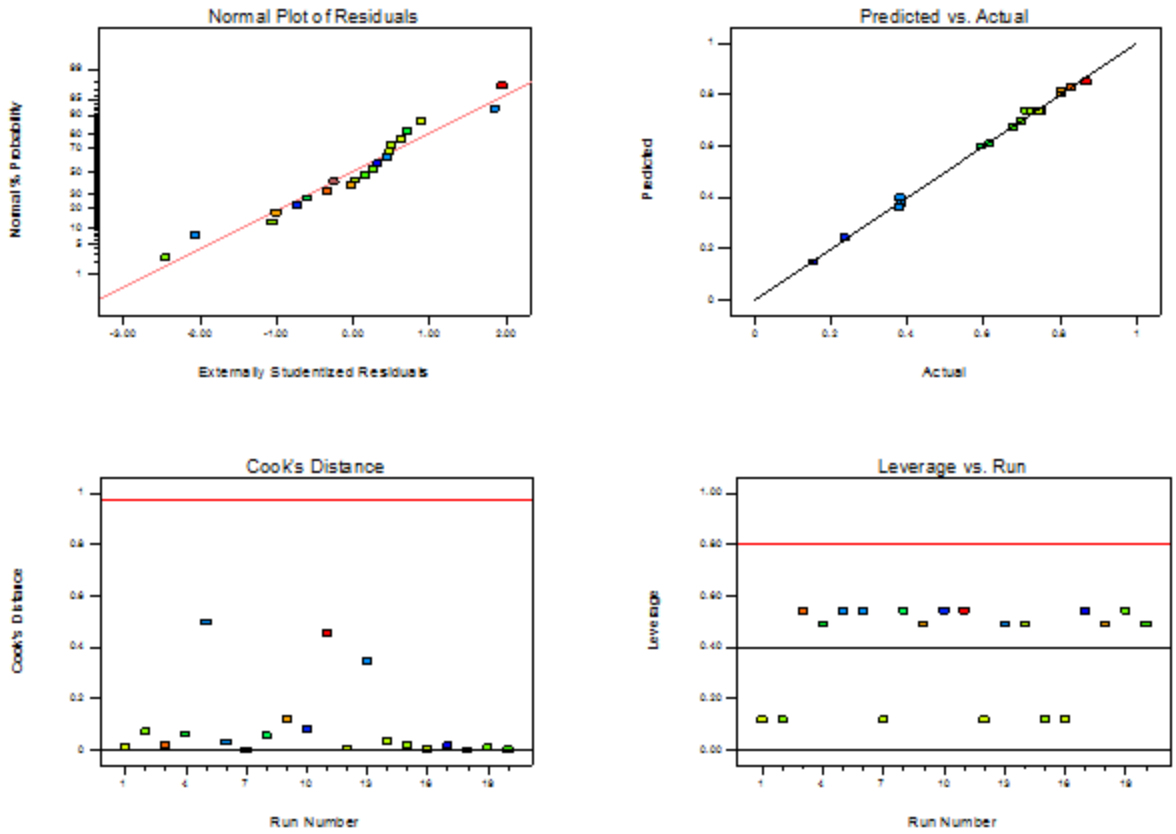

Figure 111: Diagnostics for Th Extraction Model (RE4)

Table LXIX: ANOVA Data for Th Extraction from RE4

Source	Sum of Squares	df	Mean Square	F-Value	p-value	Notes
Model	0.81	7	0.12	530.75	< 0.0001	significant
C-HCl/mass	0.51	1	0.51	2336.39	< 0.0001	
T-Temp	0.094	1	0.094	432.07	< 0.0001	
t-Time	8.108E-003	1	8.108E-003	37.10	< 0.0001	
Tt	2.826E-003	1	2.826E-003	12.93	0.0037	
C^2	0.063	1	0.063	286.25	< 0.0001	
T^2	3.020E-003	1	3.020E-003	13.82	0.0029	
t^2	3.636E-003	1	3.636E-003	16.64	0.0015	
Residual	2.622E-003	12	2.185E-004			
Lack of Fit	1.342E-003	7	1.917E-004	0.75	0.6495	not significant
Pure Error	1.280E-003	5	2.561E-004			
Cor Total	0.81	19				
Additional ANOVA Data						
Std. Dev.	0.015					
R^2	0.9968					
Adj. R^2	0.9949					
Pred. R^2	0.9908					
Adequate Precision	75.214					

Iron (Fe)

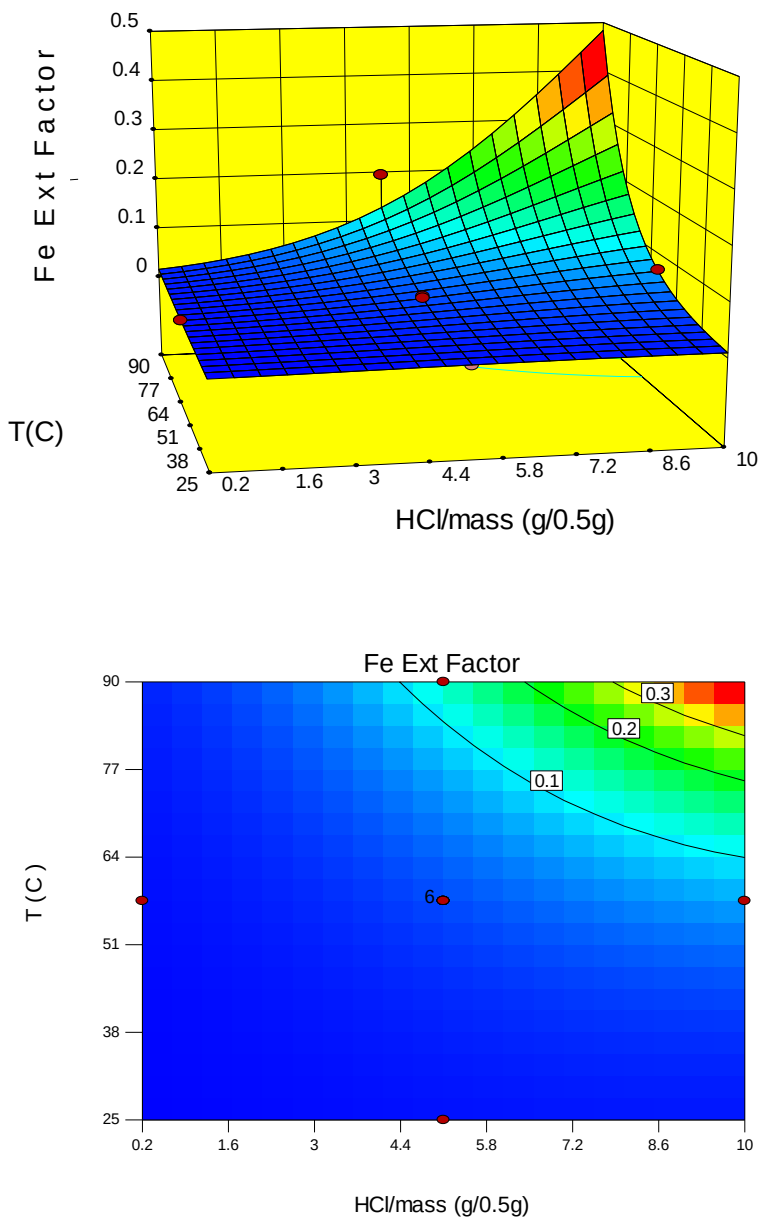

Equation: $Log_{10}(Fe) = -3.47711 + 0.090974C + 0.011157T + 0.013596t + 1.51304 \times 10^{-3}CT - 7.29265 \times 10^{-3}C^2 - 7.31855 \times 10^{-5}T^2$

Figure 112: Contour Plot, Model Equation, and Response Surface of Fe Extraction from RE4 (Time: 75 min)

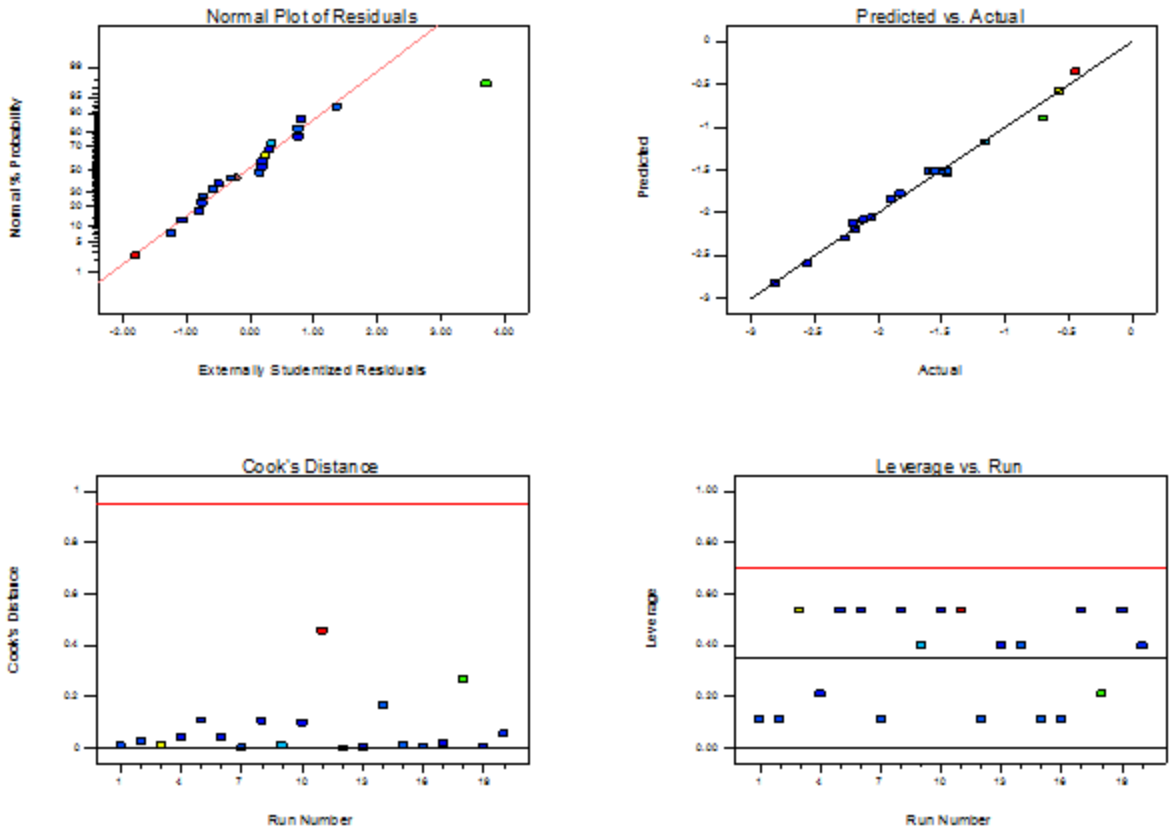

Figure 113: Diagnostics for Fe Extraction Model (RE4)

Table LXX: ANOVA Data for Fe Extraction from RE4

Source	Sum of Squares	df	Mean Square	F-Value	p-value	Notes
Model	7.36	6	1.23	183.09	< 0.0001	significant
C-HCl/mass	2.58	1	2.58	384.50	< 0.0001	
T-Temp	3.76	1	3.76	561.51	< 0.0001	
t-Time	0.14	1	0.14	20.72	0.0005	
CT	0.46	1	0.46	69.32	< 0.0001	
C^2	0.098	1	0.098	14.64	0.0021	
T^2	0.070	1	0.070	10.49	0.0065	
Residual	0.087	13	6.701E-003			
Lack of Fit	0.072	8	9.037E-003	3.05	0.1173	not significant
Pure Error	0.015	5	2.962E-003			
Cor Total	7.45	19				
Additional ANOVA Data						
Std. Dev.	0.082					
R^2	0.9883					
Adj. R^2	0.9829					
Pred. R^2	0.9739					
Adequate Precision	51.161					

Appendix H: Modeling Data for RE5

Aluminum (Al)

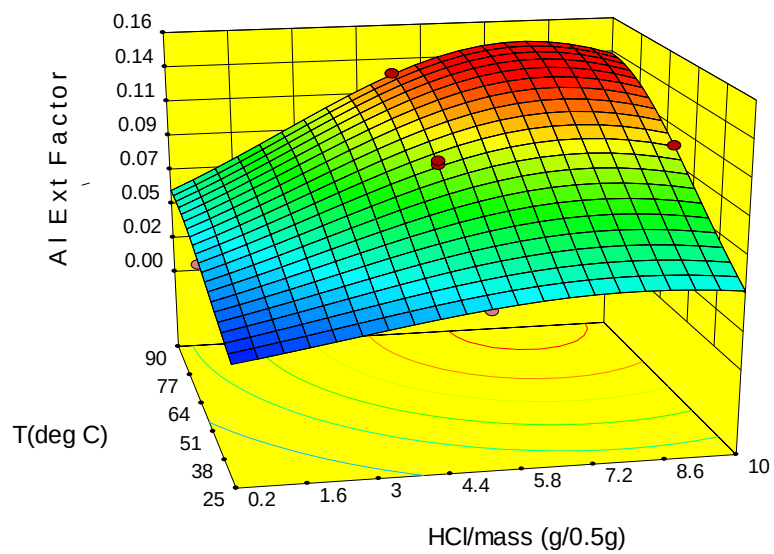

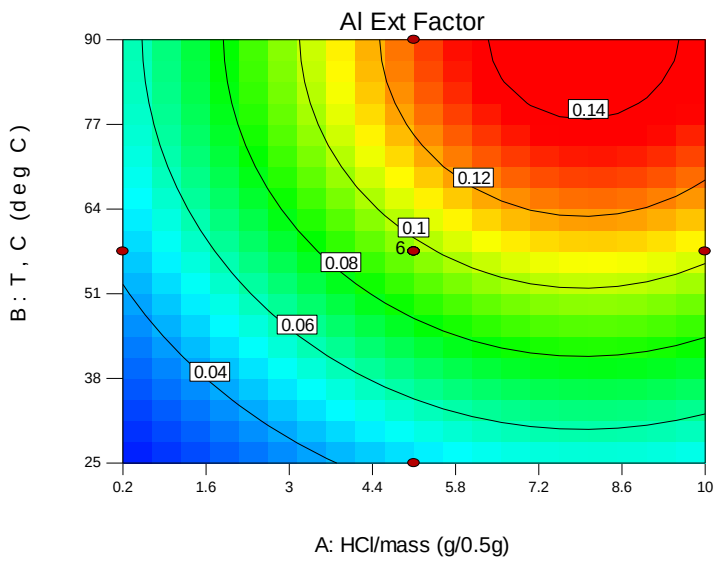

Equation: $Al^{-0.12} = 1.81887 - 0.043064C - 7.26164 \times 10^{-3}T - 1.29824 \times 10^{-3}t + 2.70645 \times 10^{-5}CT + 3.31174 \times 10^{-6}Tt + 2.58121 \times 10^{-3}C^2 + 3.85623 \times 10^{-5}T^2 + 3.52650 \times 10^{-6}t^2$

Figure 114: Contour Plot, Model Equation, and Response Surface of Al Extraction from RE5 (Time: 75 min)

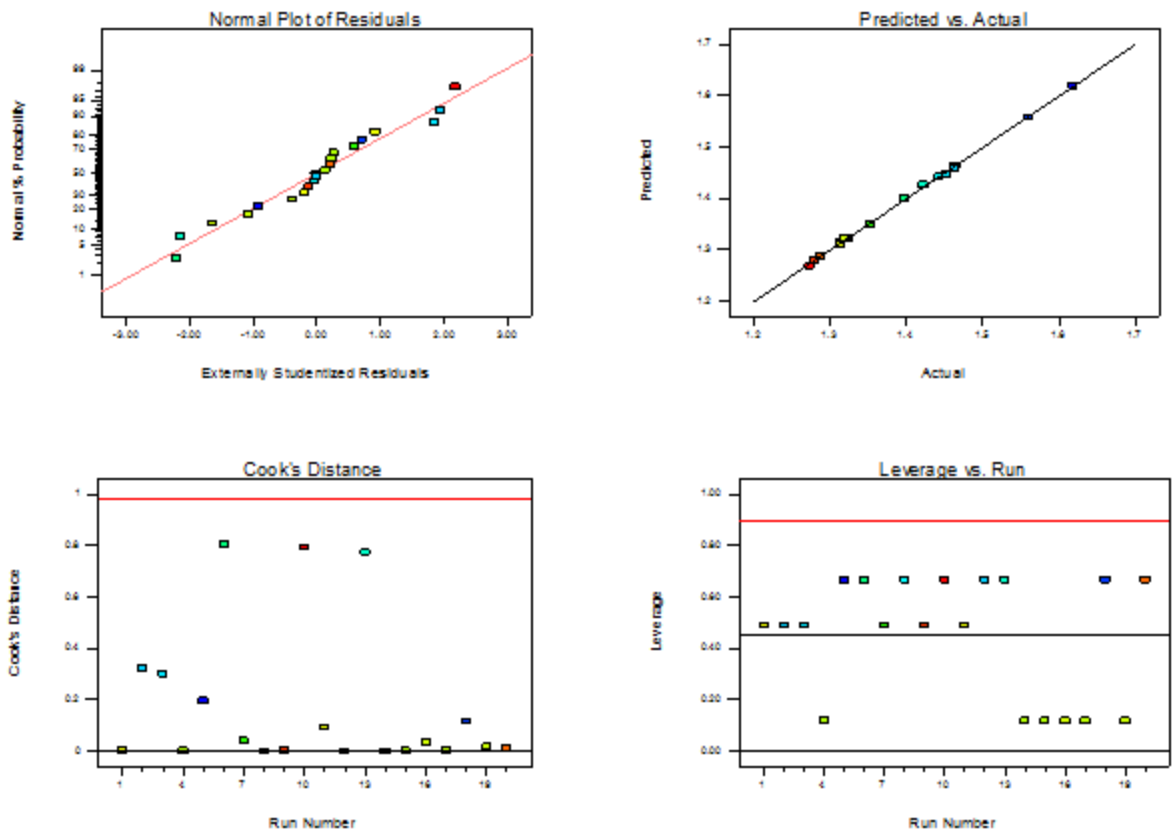

Figure 115: Diagnostics for Al Extraction Model (RE5)

Table LXXI: ANOVA Data for Al Extraction from RE5

Source	Sum of Squares	df	Mean Square	F-Value	p-value	Notes
Model	0.17	8	0.022	1351.32	< 0.0001	significant
C-HCl/mass	0.052	1	0.052	3228.49	< 0.0001	
T-Temp	0.070	1	0.070	4366.92	< 0.0001	
t-Time	3.935E-003	1	3.935E-003	244.67	< 0.0001	
CT	2.849E-004	1	2.849E-004	17.72	0.0015	
Tt	1.877E-004	1	1.877E-004	11.67	0.0058	
C^2	0.011	1	0.011	656.76	< 0.0001	
T^2	4.562E-003	1	4.562E-003	283.68	< 0.0001	
t^2	1.402E-004	1	1.402E-004	8.72	0.0131	
Residual	1.769E-004	11	1.608E-005			
Lack of Fit	1.358E-004	6	2.263E-005	2.75	0.1434	not significant
Pure Error	4.116E-005	5	8.232E-006			
Cor Total	0.17	19				
Additional ANOVA Data						
Std. Dev.	4.010E-003					
R^2	0.9990					
Adj. R^2	0.9982					
Pred. R^2	0.9949					
Adequate Precision	130.621					

Cerium (Ce)

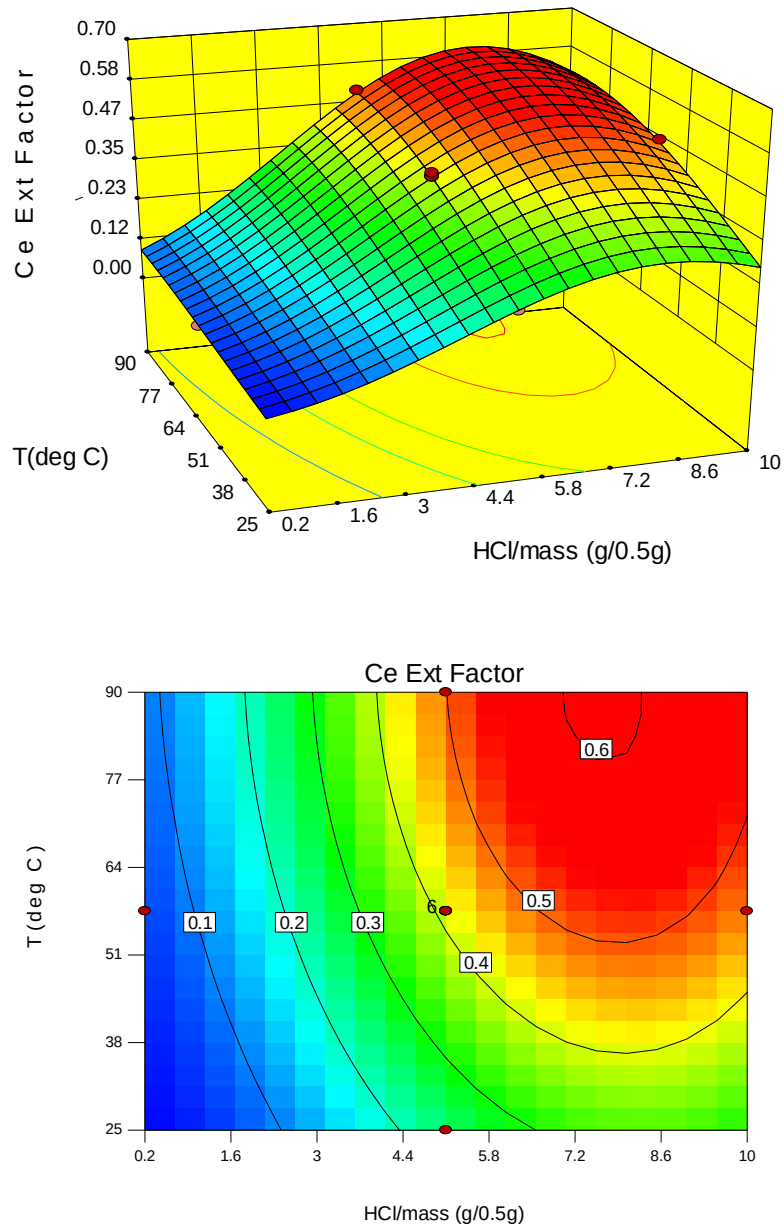

Equation: $Ce^{0.18} = 0.85 + 0.13C + 0.055T + 0.018t - 9.859 \times 10^{-3}CT - 0.12C^2 - 0.025T^2$

Figure 116: Contour Plot, Model Equation, and Response Surface of Ce Extraction from RE5 (Time: 75 min)

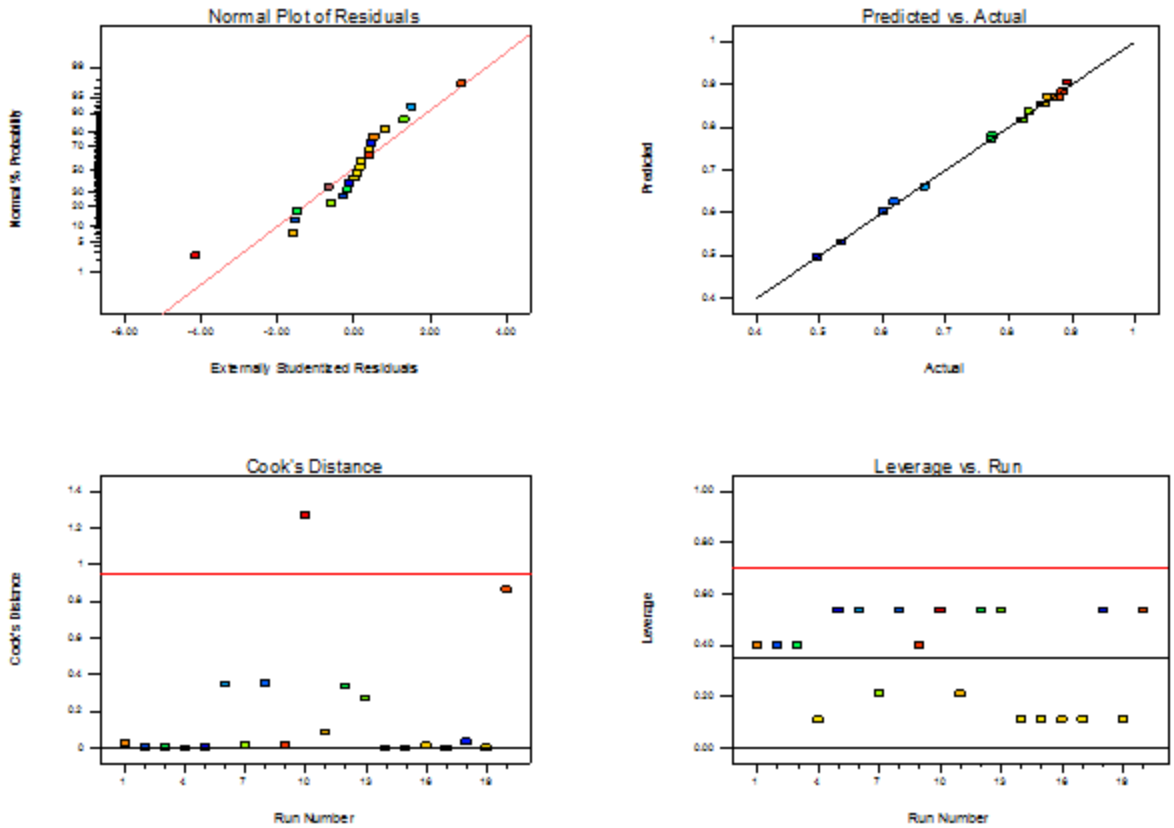

Figure 117: Diagnostics for Ce Extraction Model (RE5)

Table LXXII: ANOVA Data for Ce Extraction from RE5

Source	Sum of Squares	df	Mean Square	F-Value	p-value	Notes
Model	0.30	6	0.050	1180.62	< 0.0001	significant
C-HCl/mass	0.17	1	0.17	4151.33	< 0.0001	
T-Temp	0.030	1	0.030	707.05	< 0.0001	
t-Time	3.077E-003	1	3.077E-003	73.01	< 0.0001	
CT	7.776E-004	1	7.776E-004	18.45	0.0009	
C^2	0.044	1	0.044	1046.47	< 0.0001	
T^2	2.048E-003	1	2.048E-003	48.60	< 0.0001	
Residual	5.479E-004	13	4.215E-005			
Lack of Fit	5.317E-004	8	6.646E-005	20.50	0.0020	significant
Pure Error	1.621E-005	5	3.243E-006			
Cor Total	0.30	19				
Additional ANOVA Data						
Std. Dev.	6.492E-003					
R^2	0.9982					
Adj. R^2	0.9973					
Pred. R^2	0.9928					
Adequate Precision	106.440					

Dysprosium (Dy)

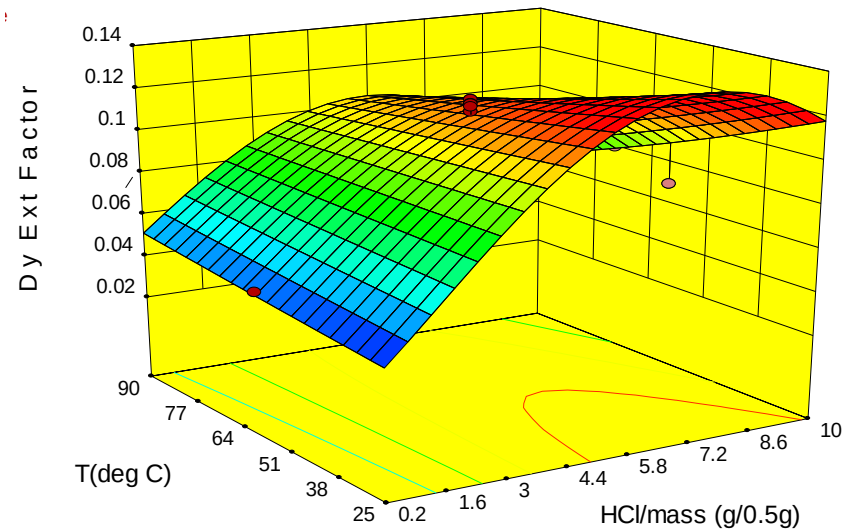

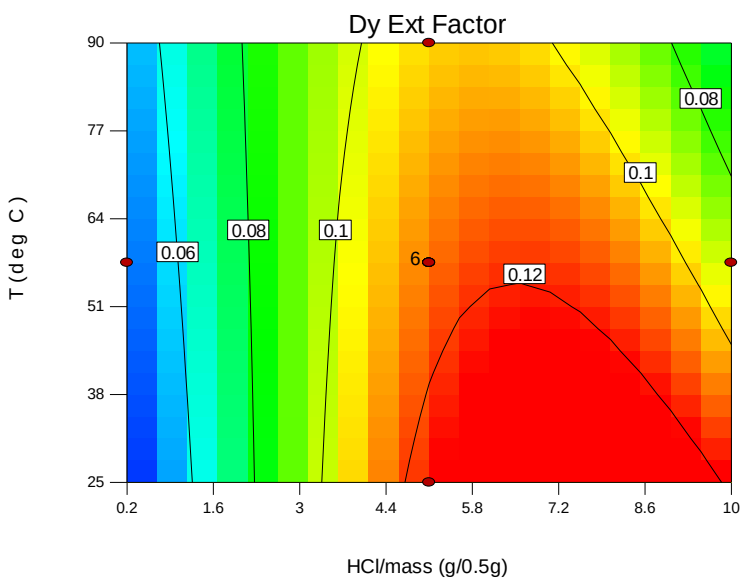

Equation: $Dy^{0.48} = 0.18819 + 0.055038C + 4.91602 \times 10^{-4}T - 1.84485 \times 10^{-4}CT - 3.46540 \times 10^{-3}C^2$

Figure 118: Contour Plot, Model Equation, and Response Surface of Dy Extraction from RE5 (Time: 75 min)

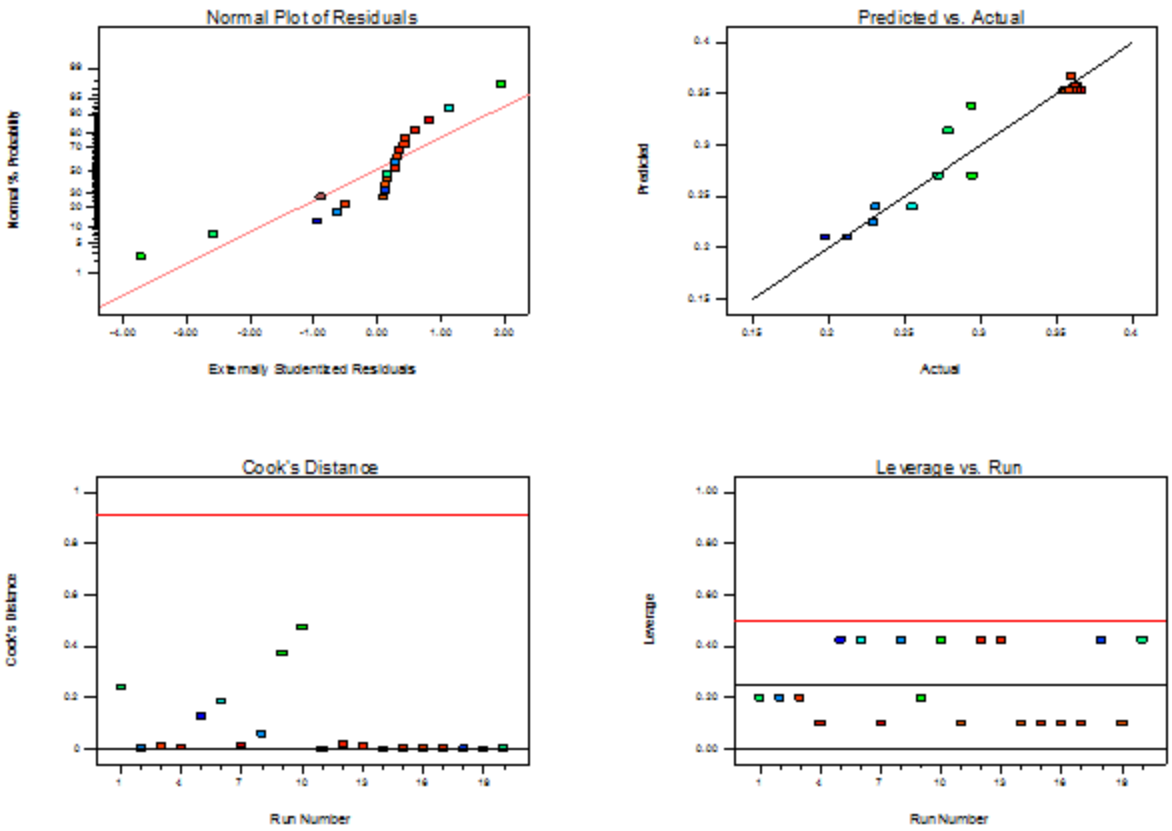

Figure 119: Diagnostics for Dy Extraction Model (RE5)

Table LXXIII: ANOVA Data for Dy Extraction from RE5

Source	Sum of Squares	df	Mean Square	F-Value	p-value	Notes
Model	0.063	4	0.016	49.22	< 0.0001	significant
C-HCl/mass	0.020	1	0.020	61.46	< 0.0001	
T-Temp	2.132E-003	1	2.132E-003	6.61	0.0213	
CT	6.905E-003	1	6.905E-003	21.42	0.0003	
C^2	0.035	1	0.035	107.39	< 0.0001	
Residual	4.835E-003	15	3.223E-004			
Lack of Fit	4.786E-003	10	4.786E-004	48.64	0.0002	significant
Pure Error	4.920E-005	5	9.839E-006			
Cor Total	0.068	19				
Additional ANOVA Data						
Std. Dev.	0.018					
R^2	0.9292					
Adj. R^2	0.9103					
Pred. R^2	0.8678					
Adequate Precision	17.500					

Gadolinium (Gd)

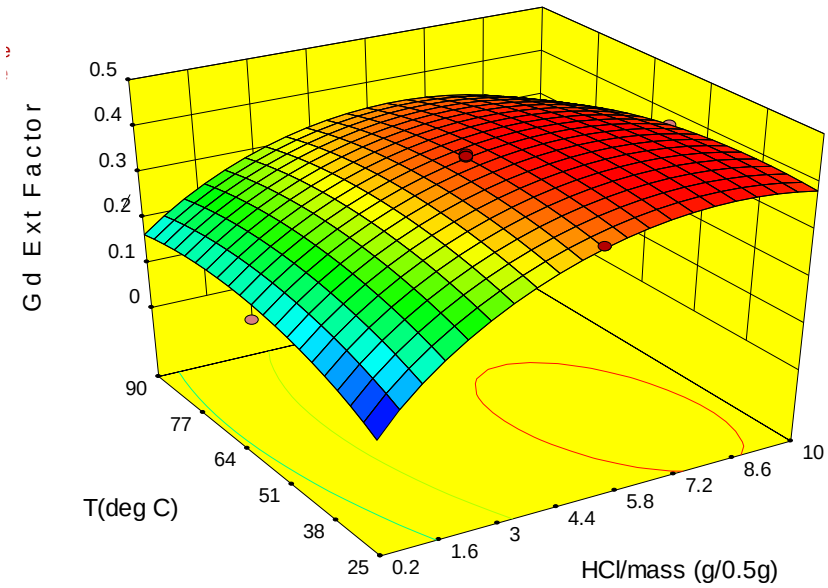

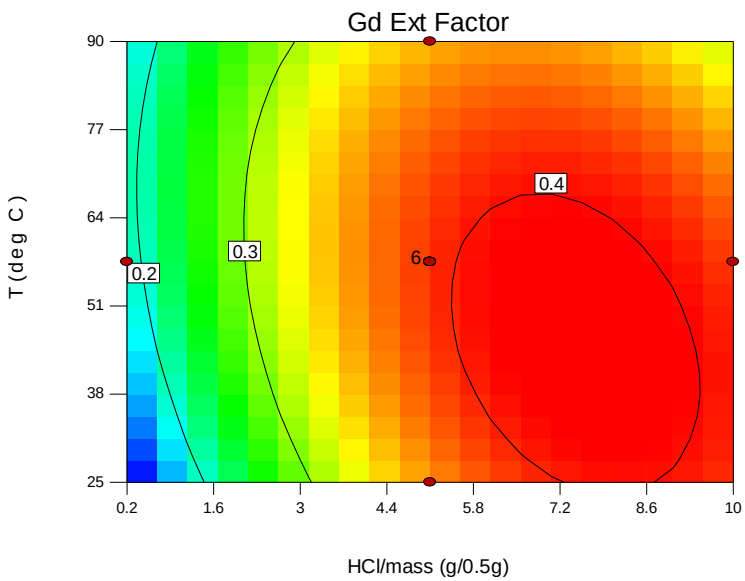

Equation: $Gd^{1.39} = -0.074176 + 0.070632C + 4.67821 \times 10^{-3}T - 2.17042 \times 10^{-4}CT - 4.07909 \times 10^{-3}C^2 - 3.37087 \times 10^{-5}T^2$

Figure 120: Contour Plot, Model Equation, and Response Surface of Gd Extraction from RE5 (Time: 75 min)

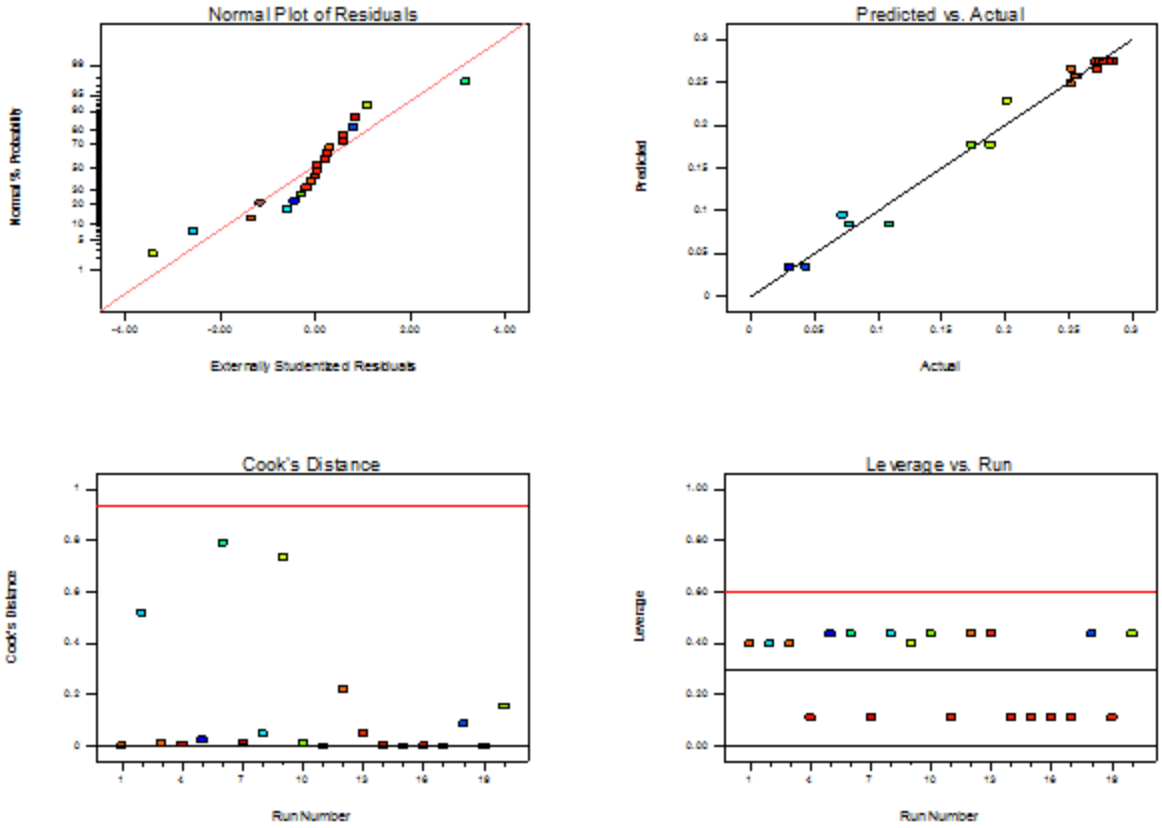

Figure 121: Diagnostics for Gd Extraction Model (RE5)

Table LXXIV: ANOVA Data for Gd Extraction from RE5

Source	Sum of Squares	df	Mean Square	F-Value	p-value	Notes
Model	0.15	5	0.030	160.48	< 0.0001	significant
C-HCl/mass	0.066	1	0.066	348.14	< 0.0001	
T-Temp	9.840E-004	1	9.840E-004	5.21	0.0386	
CT	9.557E-003	1	9.557E-003	50.62	< 0.0001	
C^2	0.031	1	0.031	162.57	< 0.0001	
T^2	4.057E-003	1	4.057E-003	21.49	0.0004	
Residual	2.643E-003	14	1.888E-004			
Lack of Fit	2.584E-003	9	2.871E-004	24.29	0.0013	significant
Pure Error	5.912E-005	5	1.182E-005			
Cor Total	0.15	19				
Additional ANOVA Data						
Std. Dev.	0.014					
R^2	0.9829					
Adj. R^2	0.9767					
Pred. R^2	0.9516					
Adequate Precision	31.791					

Lanthanum (La)

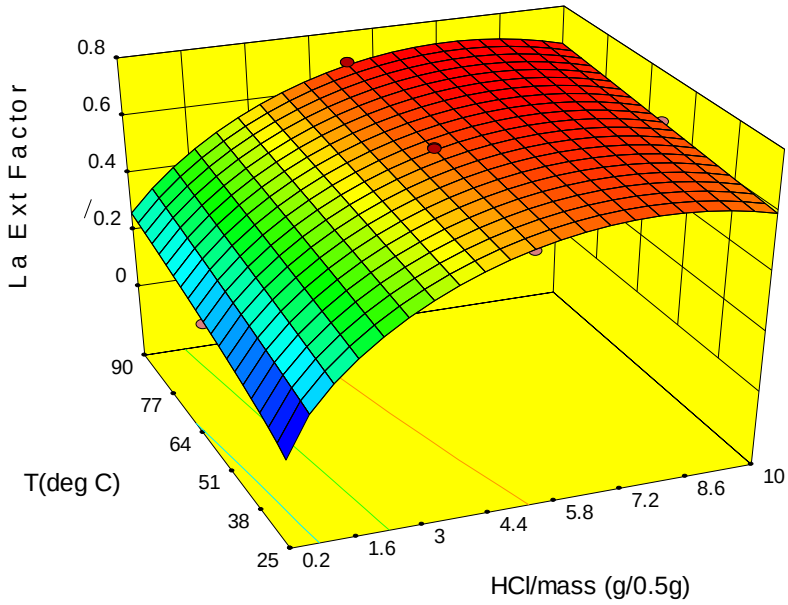

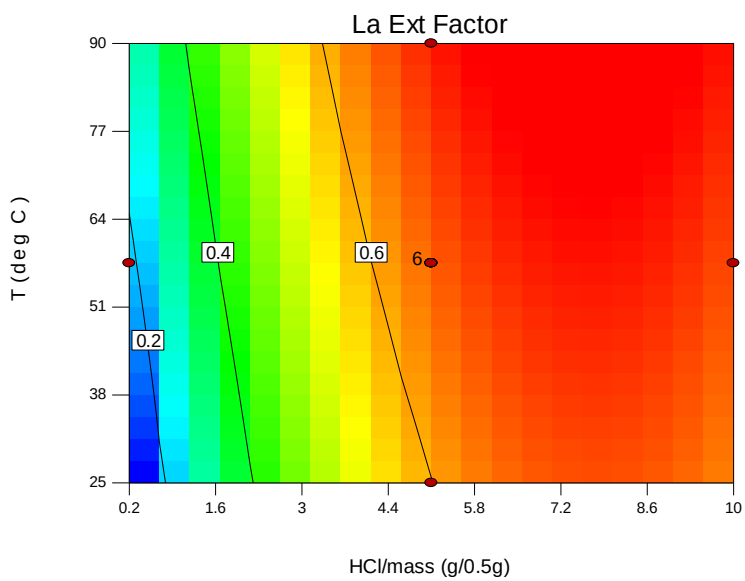

Equation: $La^{1.52} = -0.068049 + 0.14230C + 1.47222 \times 10^{-3}T + 4.33411 \times 10^{-5}t - 5.98147 \times 10^{-5}CT - 5.96658 \times 10^{-6}Tt - 9.31797 \times 10^{-3}C^2$

Figure 122: Contour Plot, Model Equation, and Response Surface of La Extraction from RE5 (Time: 75 min)

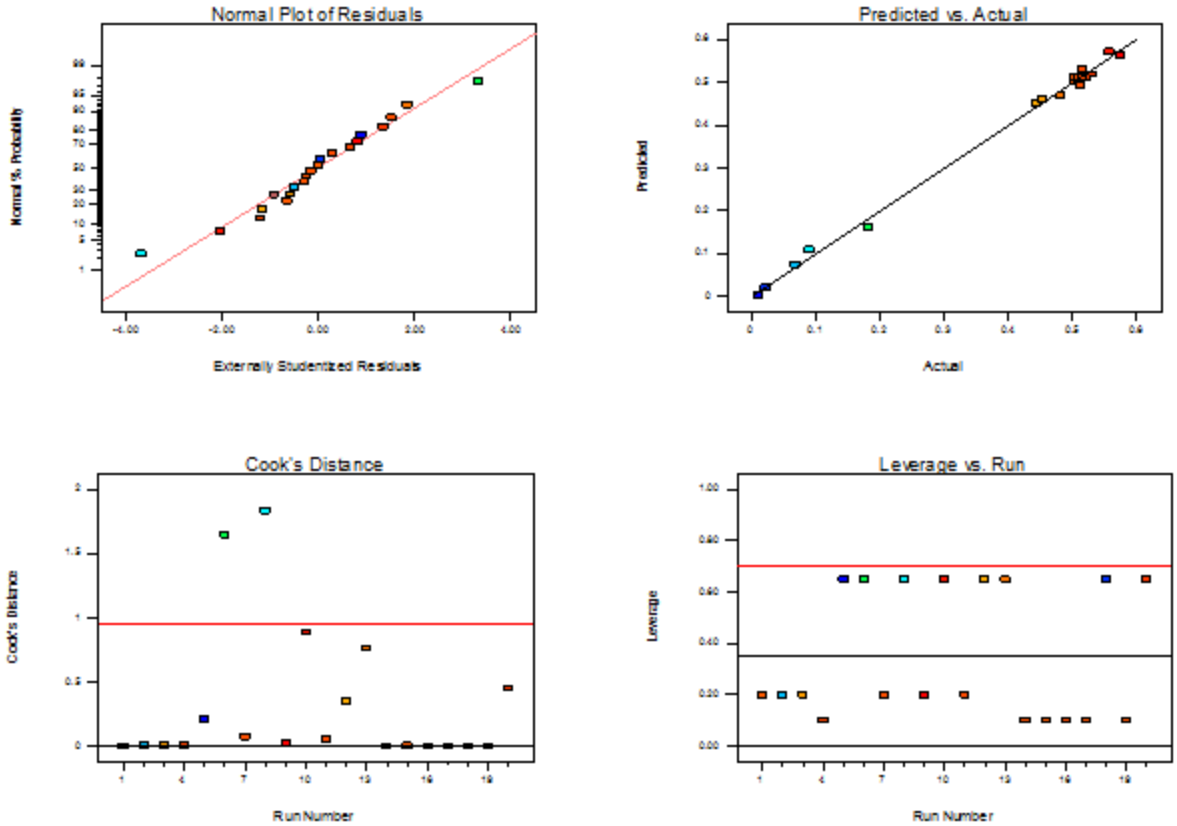

Figure 123: Diagnostics for La Extraction Model (RE5)

Table LXXV: ANOVA Data for La Extraction from RE5

Source	Sum of Squares	df	Mean Square	F-Value	p-value	Notes
Model	0.74	6	0.12	730.42	< 0.0001	significant
C-HCl/mass	0.46	1	0.46	2718.59	< 0.0001	
T-Temp	0.028	1	0.028	162.39	< 0.0001	
t-Time	3.024E-003	1	3.024E-003	17.83	0.0010	
CT	7.259E-004	1	7.259E-004	4.28	0.0590	
Tt	6.092E-004	1	6.092E-004	3.59	0.0805	
C^2	0.25	1	0.25	1475.82	< 0.0001	
Residual	2.204E-003	13	1.696E-004			
Lack of Fit	2.030E-003	8	2.538E-004	7.28	0.0213	significant
Pure Error	1.743E-004	5	3.486E-005			
Cor Total	0.75	19				
Additional ANOVA Data						
Std. Dev.	0.013					
R^2	0.9970					
Adj. R^2	0.9957					
Pred. R^2	0.9833					
Adequate Precision	73.878					

Neodymium (Nd)

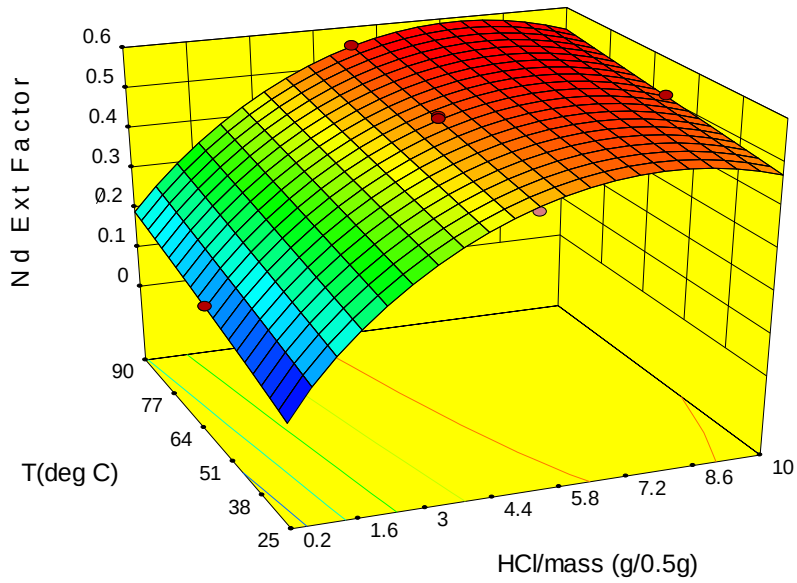

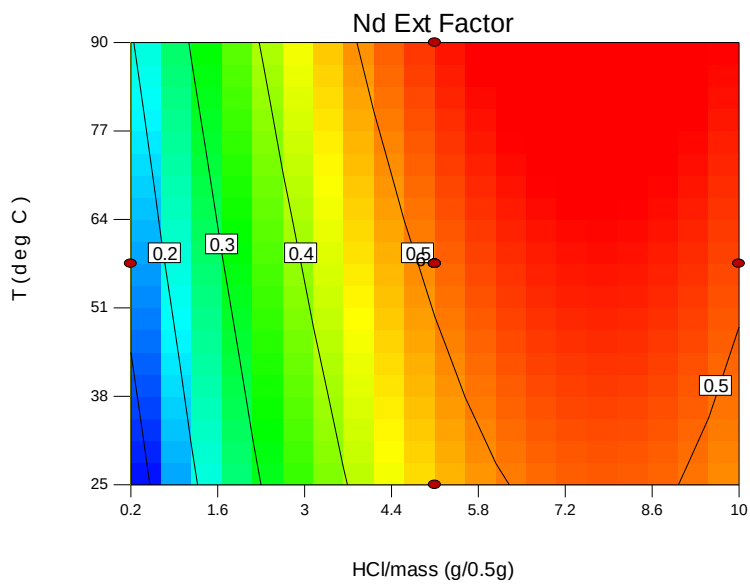

Equation: $Nd^{1.24} = -0.062063 + 0.11446C + 1.62067 \times 10^{-3}T + 3.40631 \times 10^{-4}t - 4.59976 \times 10^{-5}CT - 7.40577 \times 10^{-3}C^2$

Figure 124: Contour Plot, Model Equation, and Response Surface of Nd Extraction from RE5 (Time: 75 min)

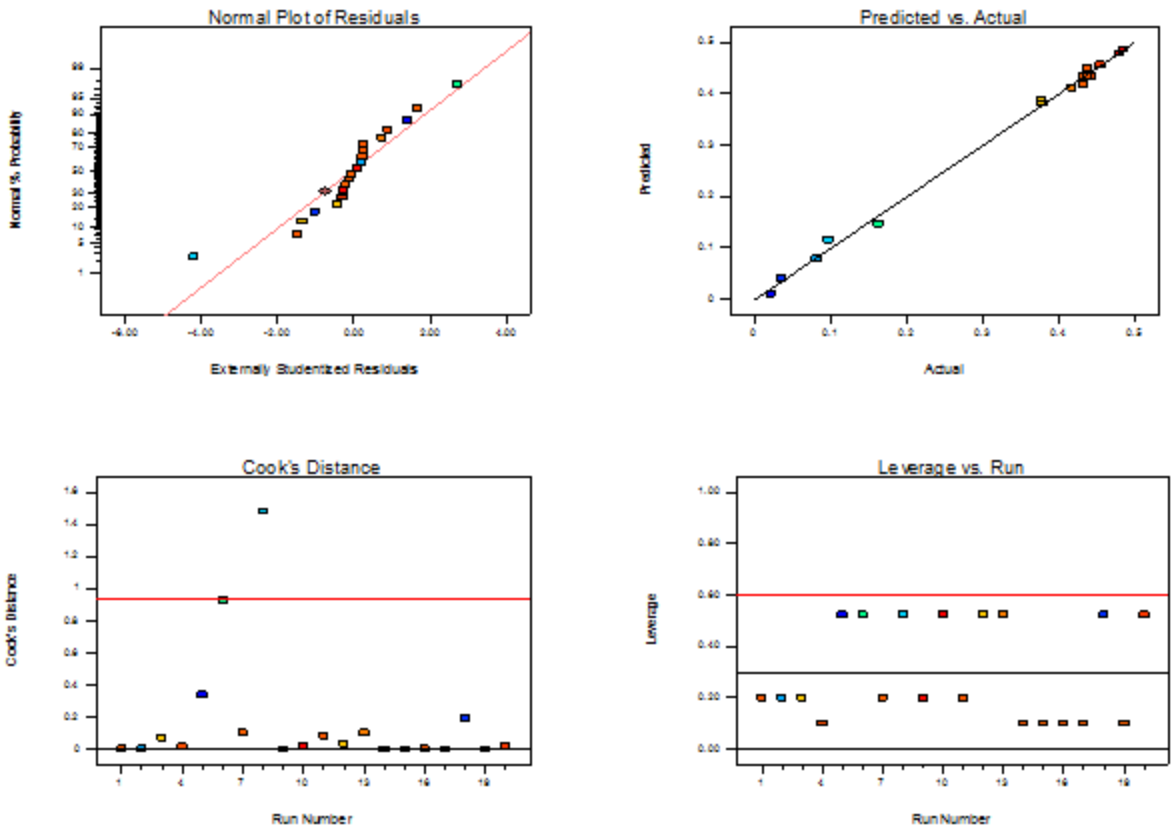

Figure 125: Diagnostics for Nd Extraction Model (RE5)

Table LXXVI: ANOVA Data for Nd Extraction from RE5

Source	Sum of Squares	df	Mean Square	F-Value	p-value	Notes
Model	0.50	5	0.099	982.00	< 0.0001	significant
C-HCl/mass	0.32	1	0.32	3120.46	< 0.0001	
T-Temp	0.020	1	0.020	200.46	< 0.0001	
t-Time	2.350E-003	1	2.350E-003	23.21	0.0003	
CT	4.293E-004	1	4.293E-004	4.24	0.0586	
C^2	0.16	1	0.16	1561.61	< 0.0001	
Residual	1.417E-003	14	1.012E-004			
Lack of Fit	1.342E-003	9	1.491E-004	9.94	0.0105	significant
Pure Error	7.502E-005	5	1.500E-005			
Cor Total	0.50	19				
Additional ANOVA Data						
Std. Dev.	0.010					
R^2	0.9972					
Adj. R^2	0.9961					
Pred. R^2	0.9909					
Adequate Precision	86.414					

Praseodymium (Pr)

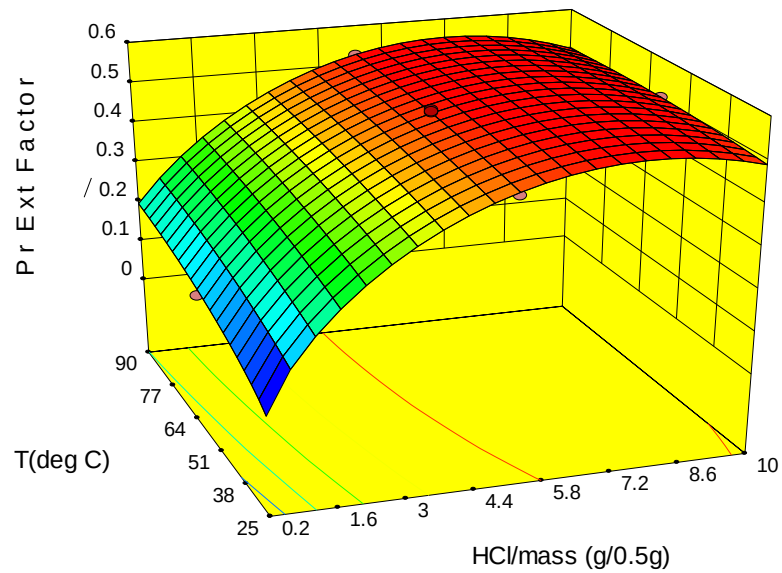

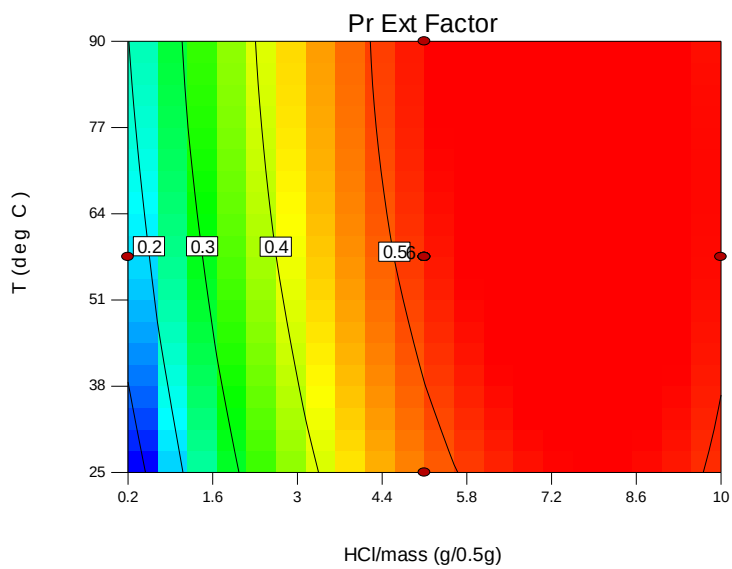

Equation: $Pr^{1.44} = -0.086910 + 0.10890C + 2.56533 \times 10^{-3}T + 2.64192 \times 10^{-4}t - 1.19510 \times 10^{-4}CT - 6.89322 \times 10^{-3}C^2 - 1.05806 \times 10^{-5}T^2$

Figure 126: Contour Plot, Model Equation, and Response Surface of Pr Extraction from RE5 (Time: 75 min)

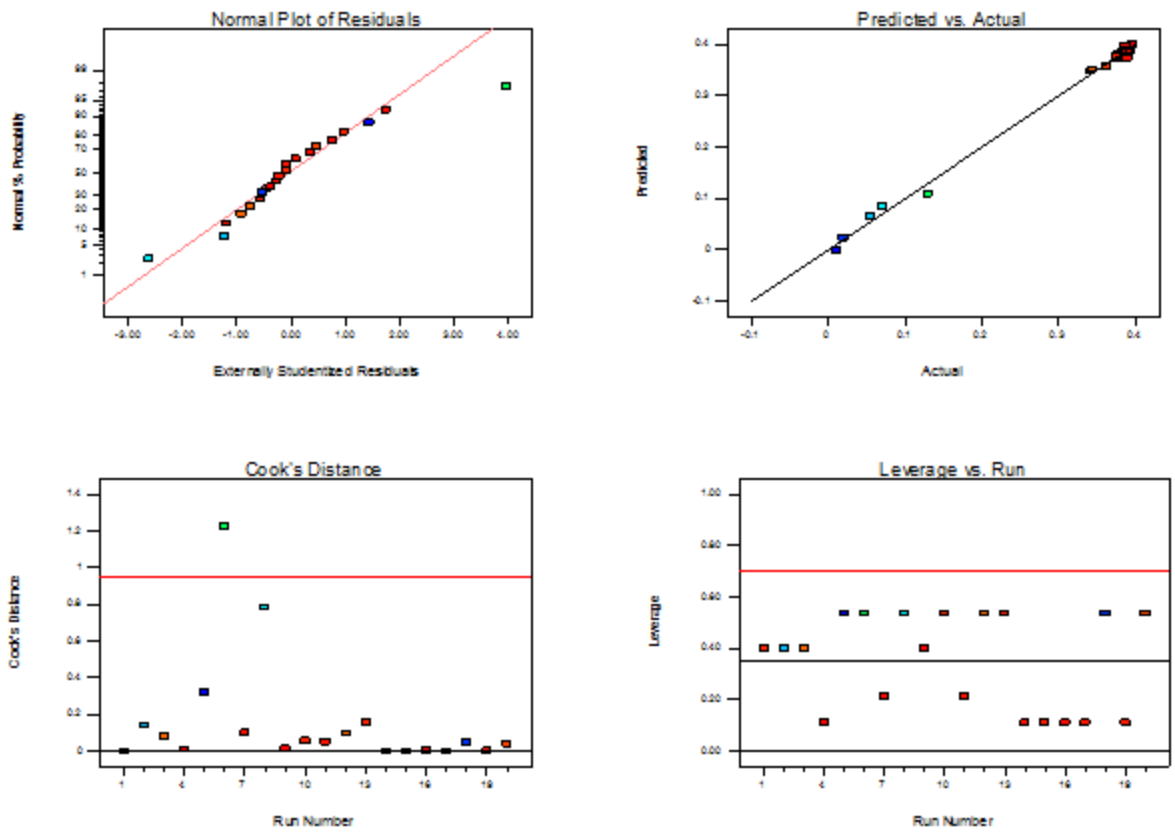

Figure 127: Diagnostics for Pr Extraction Model (RE5)

Table LXXVII: ANOVA Data for Pr Extraction from RE5

Source	Sum of Squares	df	Mean Square	F-Value	p-value	Notes
Model	0.40	6	0.067	563.34	< 0.0001	significant
C-HCl/mass	0.24	1	0.24	2039.68	< 0.0001	
T-Temp	5.769E-003	1	5.769E-003	48.71	< 0.0001	
t-Time	1.413E-003	1	1.413E-003	11.93	0.0043	
CT	2.898E-003	1	2.898E-003	24.46	0.0003	
C^2	0.088	1	0.088	740.03	< 0.0001	
T^2	3.997E-004	1	3.997E-004	3.37	0.0892	
Residual	1.540E-003	13	1.184E-004			
Lack of Fit	1.456E-003	8	1.819E-004	10.79	0.0090	significant
Pure Error	8.431E-005	5	1.686E-005			
Cor Total	0.40	19				
Additional ANOVA Data						
Std. Dev.	0.011					
R^2	0.9962					
Adj. R^2	0.9944					
Pred. R^2	0.9865					
Adequate Precision	62.109					

Thorium (Th)

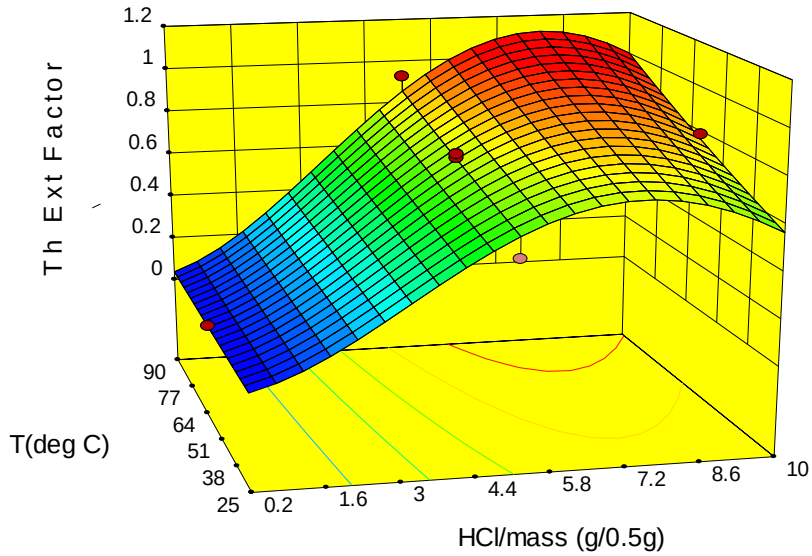

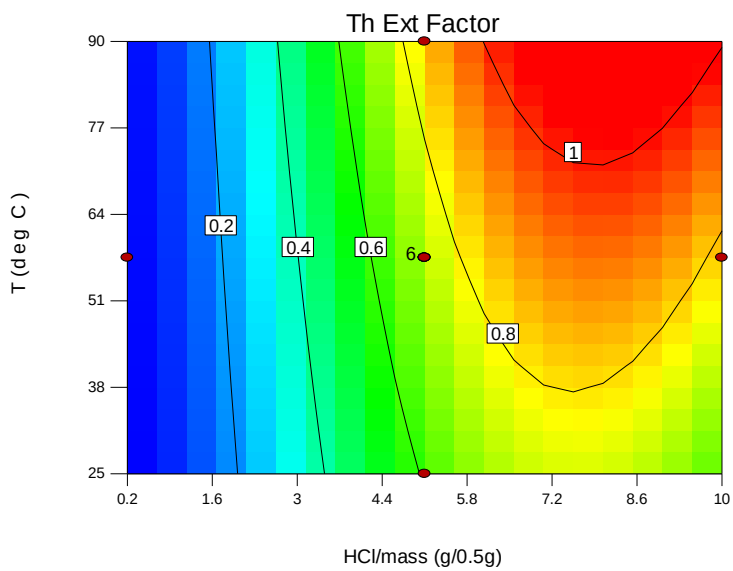

Equation: $Th^{0.44} = 0.10023 + 0.18900C + 6.21708 \times 10^{-4}T + 4.53249 \times 10^{-4}t + 2.77142 \times 10^{-4}CT - 0.013270C^2$

Figure 128: Contour Plot, Model Equation, and Response Surface of Th Extraction from RE5 (Time: 75 min)

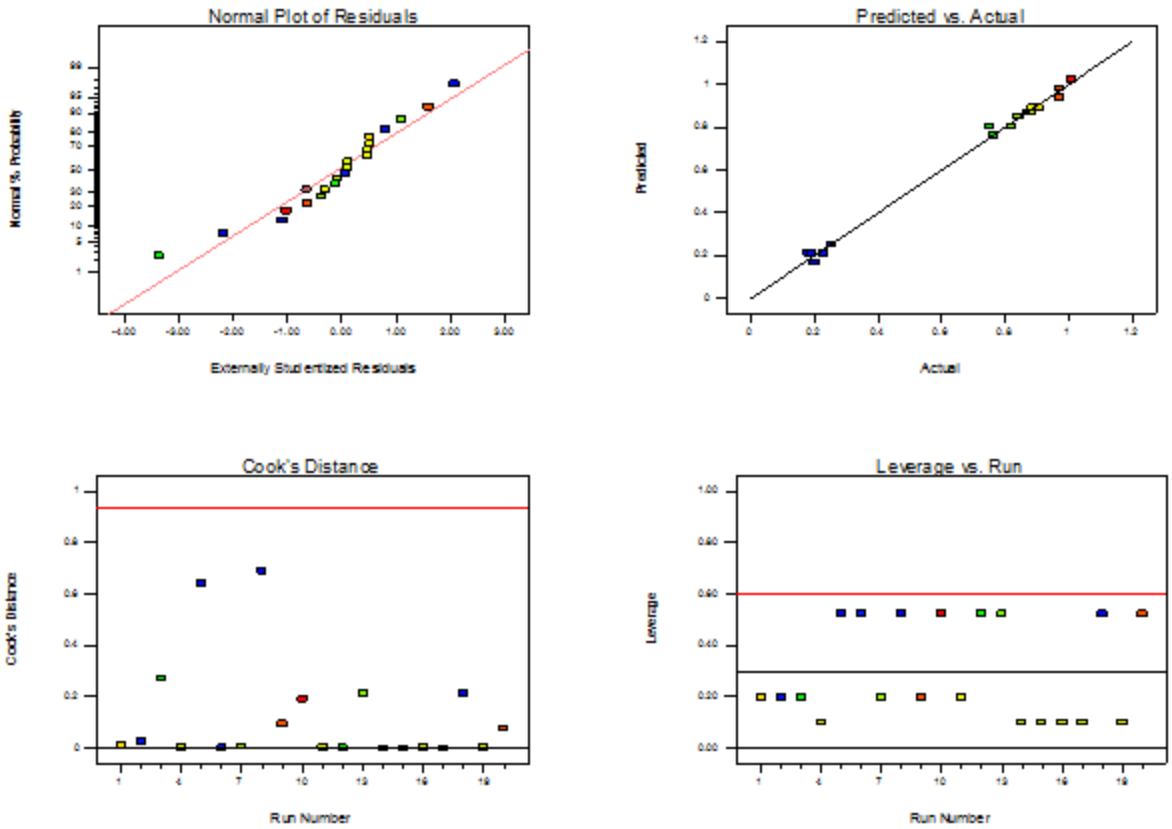

Figure 129: Diagnostics for Th Extraction Model (RE5)

Table LXXVIII: ANOVA Data for Th Extraction from RE5

Source	Sum of Squares	df	Mean Square	F-Value	p-value	Notes
Model	1.73	5	0.35	580.87	< 0.0001	significant
C-HCl/mass	1.16	1	1.16	1947.68	< 0.0001	
T-Temp	0.044	1	0.044	73.29	< 0.0001	
t-Time	4.160E-003	1	4.160E-003	6.97	0.0194	
CT	0.016	1	0.016	26.11	0.0002	
C^2	0.51	1	0.51	850.30	< 0.0001	
Residual	8.357E-003	14	5.969E-004			
Lack of Fit	8.177E-003	9	9.085E-004	25.18	0.0012	significant
Pure Error	1.804E-004	5	3.608E-005			
Cor Total	1.74	19				
Additional ANOVA Data						
Std. Dev.	0.024					
R^2	0.9952					
Adj. R^2	0.9935					
Pred. R^2	0.9874					
Adequate Precision	63.893					

Iron (Fe)

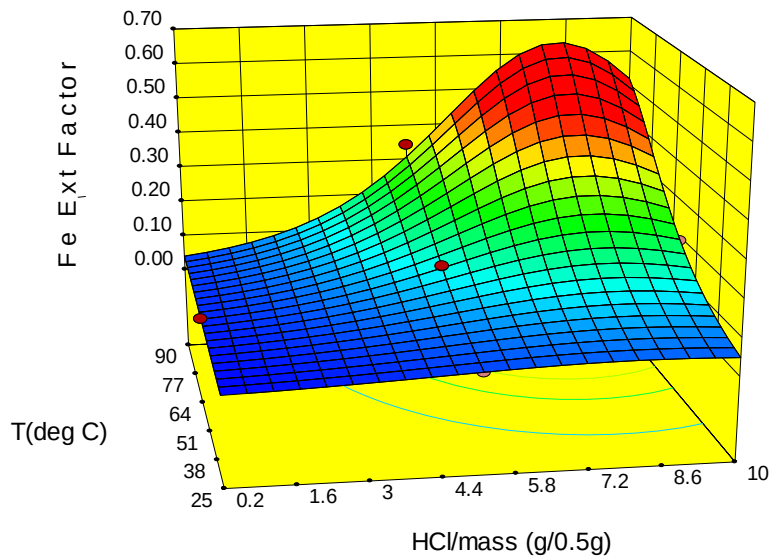

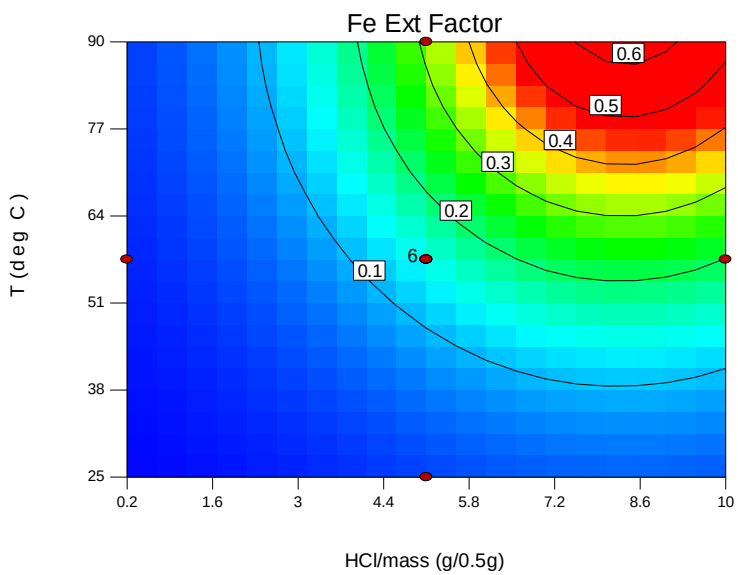

Equation: $Fe^{-0.4} = 8.27049 - 0.61757C - 0.075957T - 0.018863t - 2.32321 \times 10^{-4}CT + 4.07911 \times 10^{-4}Ct + 5.95752 \times 10^{-5}Tt + 0.036277C^2 + 3.72741 \times 10^{-4}T^2 + 5.50652 \times 10^{-5}t^2$

Figure 130: Contour Plot, Model Equation, and Response Surface of Fe Extraction from RE5 (Time: 75 min)

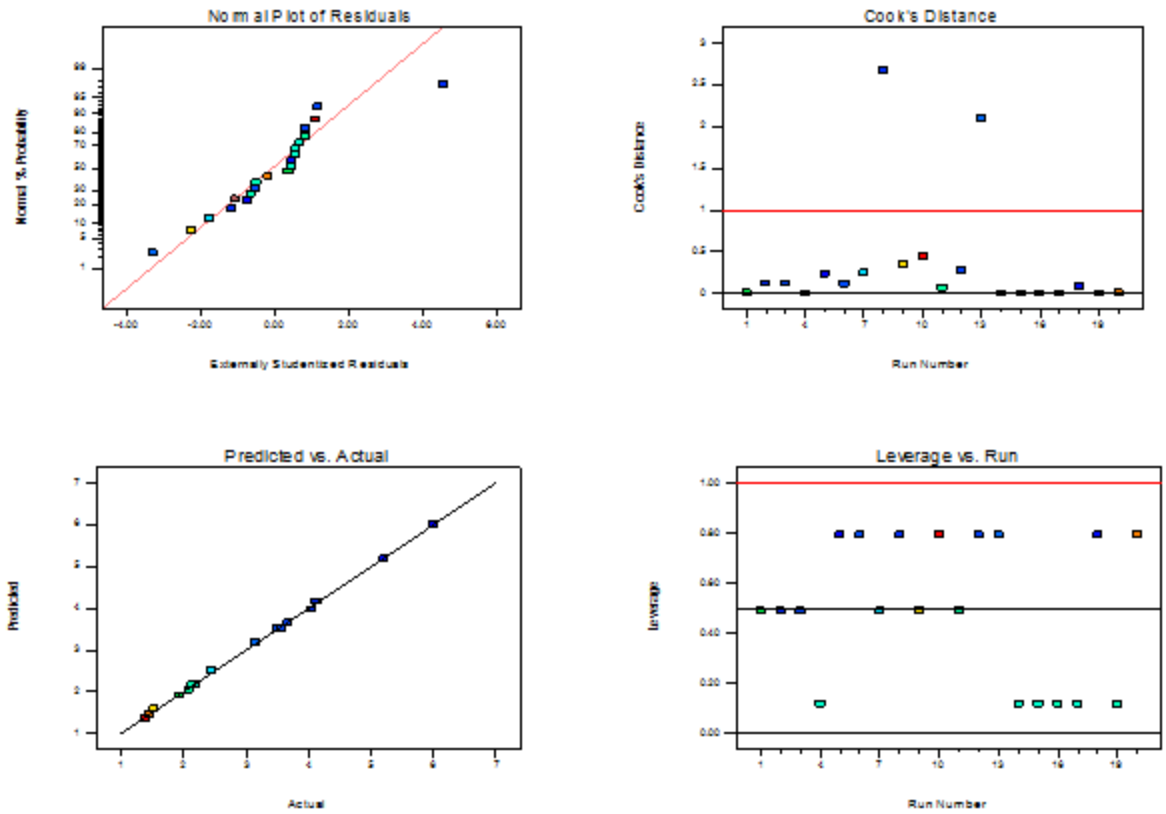

Figure 131: Diagnostics for Fe Extraction Model (RE5)

Table LXXIX: ANOVA Data for Fe Extraction from RE5

Source	Sum of Squares	df	Mean Square	F-Value	p-value	Notes
Model	30.32	9	3.37	1292.67	< 0.0001	significant
C-HCl/mass	12.73	1	12.73	4886.93	< 0.0001	
T-Temp	9.39	1	9.39	3601.56	< 0.0001	
t-Time	0.53	1	0.53	201.93	< 0.0001	
CT	0.011	1	0.011	4.20	0.0675	
Ct	0.065	1	0.065	24.84	0.0006	
Tt	0.061	1	0.061	23.31	0.0007	
C^2	2.09	1	2.09	800.62	< 0.0001	
T^2	0.43	1	0.43	163.58	< 0.0001	
t^2	0.034	1	0.034	13.12	0.0047	
Residual	0.026	10	2.606E-003			
Lack of Fit	0.022	5	4.333E-003	4.93	0.0523	not significant
Pure Error	4.393E-003	5	8.786E-004			
Cor Total	30.34	19				
Additional ANOVA Data						
Std. Dev.	0.051					
R^2	0.9991					
Adj. R^2	0.9984					
Pred. R^2	0.9917					
Adequate Precision	128.914					

Appendix I: Modeling Data for RE6

Aluminum (Al)

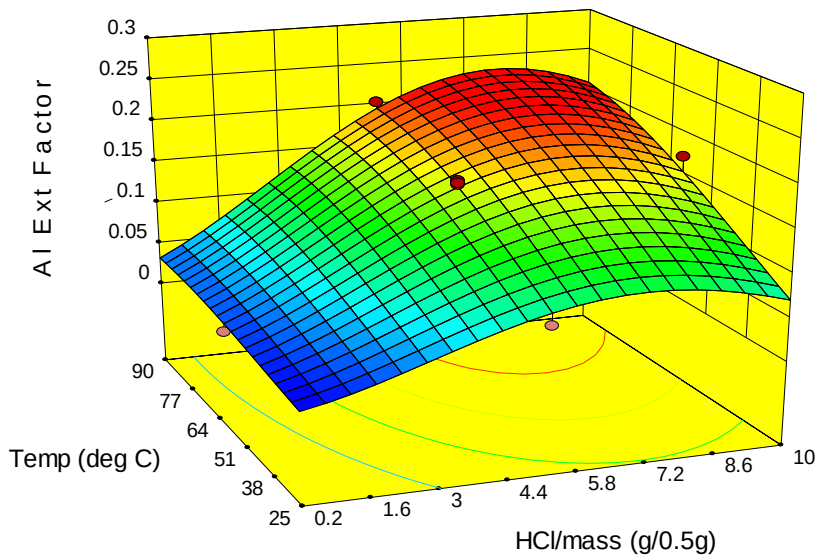

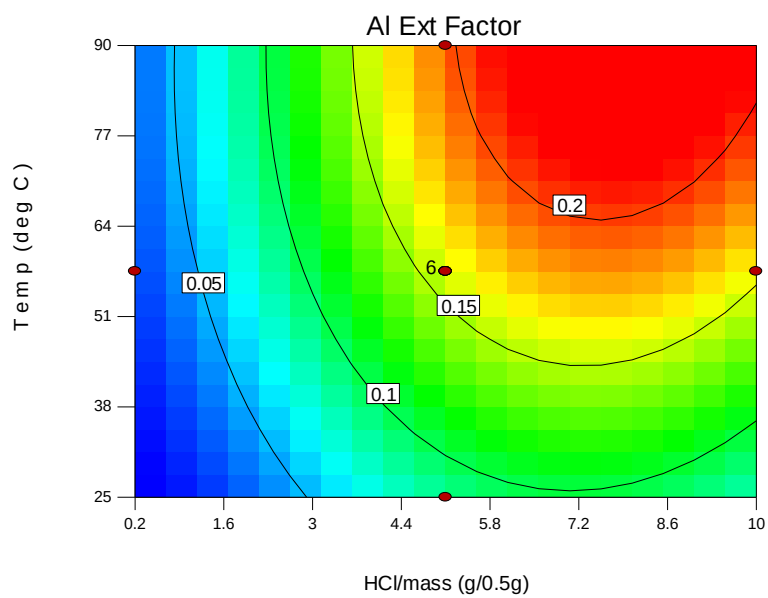

Equation: $Al^{0.43} = -0.054485 + 0.072146C + 5.20529 \times 10^{-3}T + 5.90225 \times 10^{-4}t + 1.24655 \times 10^{-4}CT - 5.33174 \times 10^{-3}C^2 - 3.07697 \times 10^{-5}T^2$

Figure 132: Contour Plot, Model Equation, and Response Surface of Al Extraction from RE6 (Time: 75 min)

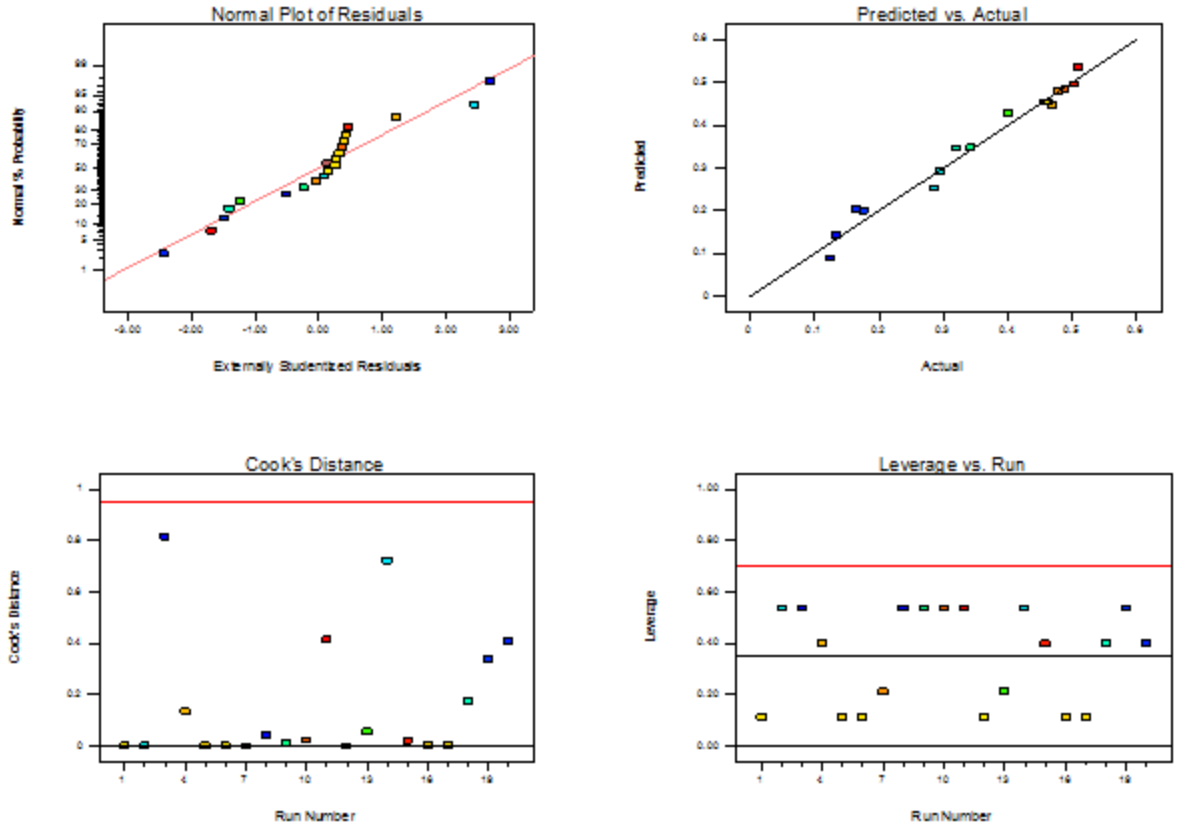

Figure 133: Diagnostics for Al Extraction Model (RE6)

Table LXXX: ANOVA Data for Al Extraction from RE6

Source	Sum of Squares	df	Mean Square	F-Value	p-value	Notes
Model	0.33	6	0.055	94.40	< 0.0001	significant
C-HCl/mass	0.15	1	0.15	257.99	< 0.0001	
T-Temp	0.056	1	0.056	96.81	< 0.0001	
t-Time	7.054E-003	1	7.054E-003	12.20	0.0040	
CT	3.153E-003	1	3.153E-003	5.45	0.0362	
C^2	0.052	1	0.052	90.67	< 0.0001	
T^2	3.380E-003	1	3.380E-003	5.84	0.0311	
Residual	7.519E-003	13	5.784E-004			
Lack of Fit	7.494E-003	8	9.367E-004	183.84	< 0.0001	significant
Pure Error	2.548E-005	5	5.095E-006			
Cor Total	0.34	19				
Additional ANOVA Data						
Std. Dev.	0.024					
R^2	0.9776					
Adj. R^2	0.9672					
Pred. R^2	0.9199					
Adequate Precision	31.423					

Cerium (Ce)

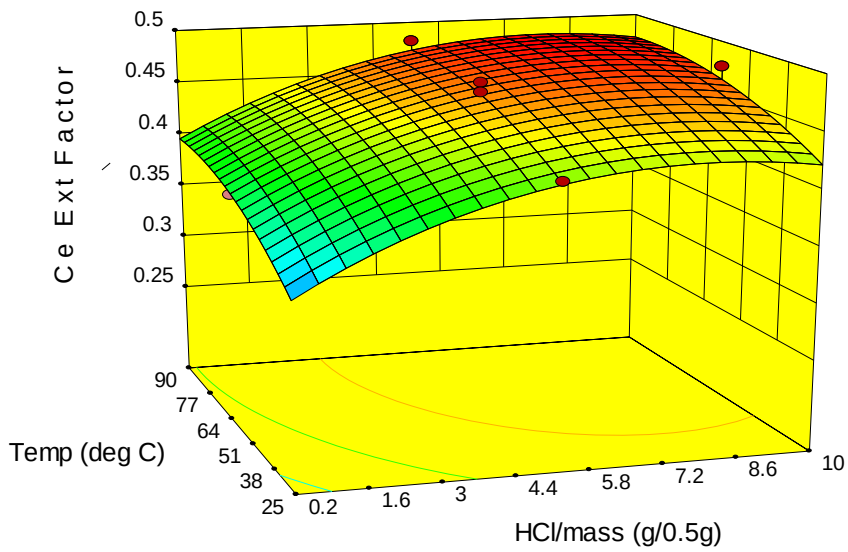

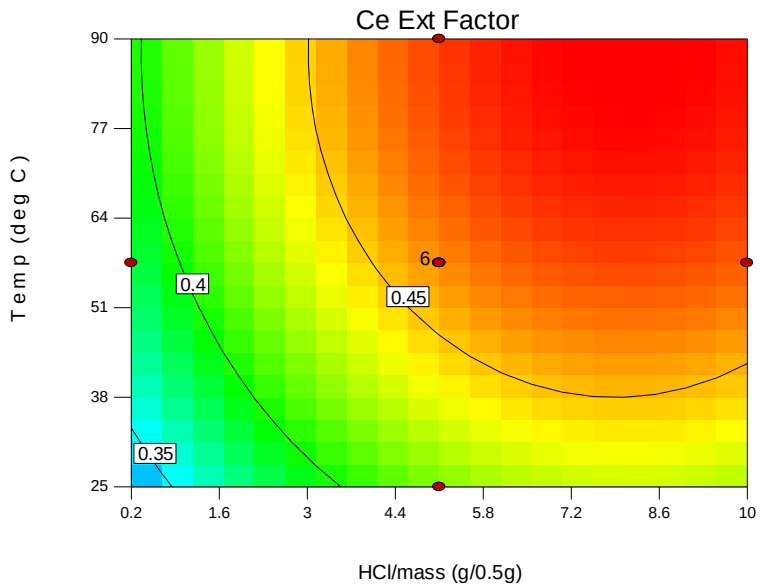

Equation: $Ce^{1.6} = 0.081529 + 0.024964C + 2.42758 \times 10^{-3}T + 4.61418 \times 10^{-4}t - 2.78782 \times 10^{-5}CT - 1.44849 \times 10^{-3}C^2 - 1.37853 \times 10^{-5}T^2$

Figure 134: Contour Plot, Model Equation, and Response Surface of Ce Extraction from RE6 (Time: 75 min)

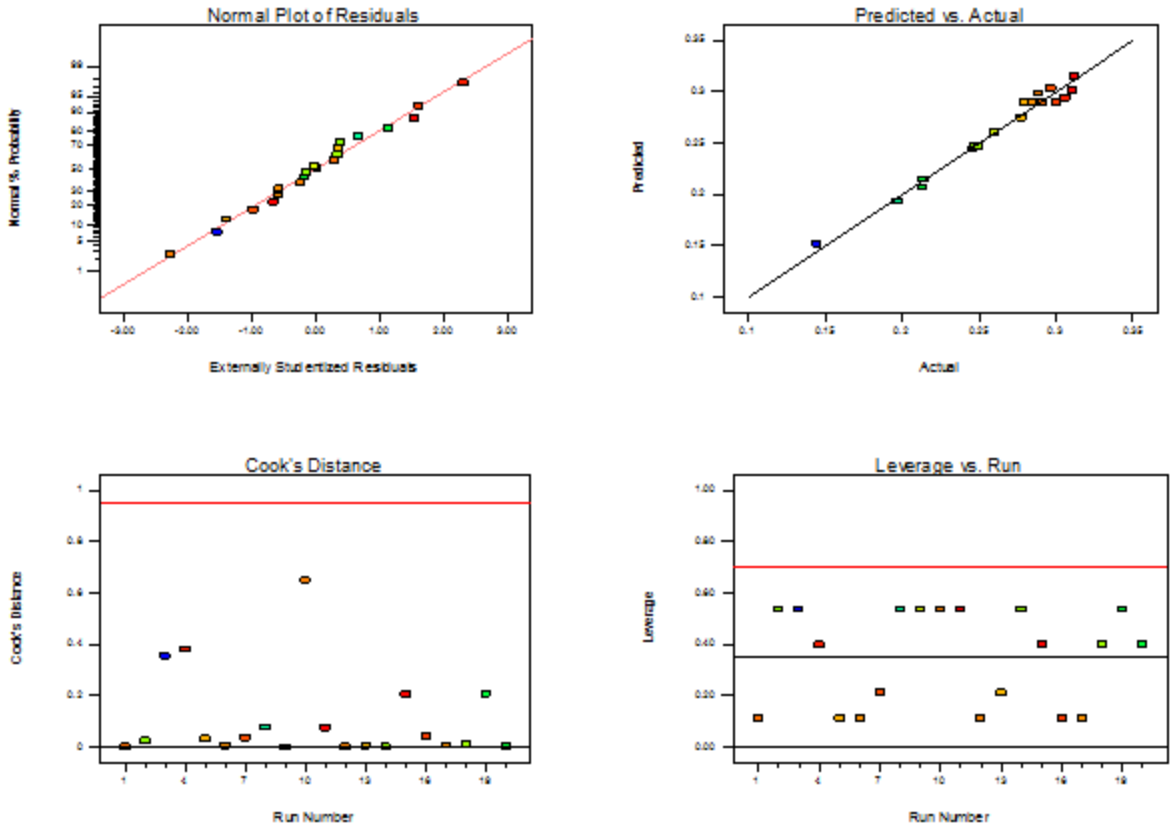

Figure 135: Diagnostics for Ce Extraction Model (RE6)

Table LXXXI: ANOVA Data for Ce Extraction from RE6

Source	Sum of Squares	df	Mean Square	F-Value	p-value	Notes
Model	0.036	6	5.959E-003	99.02	< 0.0001	significant
C-HCl/mass	0.016	1	0.016	261.68	< 0.0001	
T-Temp	7.493E-003	1	7.493E-003	124.53	< 0.0001	
t-Time	2.064E-003	1	2.064E-003	34.30	< 0.0001	
Tt	3.023E-004	1	3.023E-004	5.02	0.0431	
C^2	3.870E-003	1	3.870E-003	64.32	< 0.0001	
T^2	6.784E-004	1	6.784E-004	11.27	0.0051	
Residual	7.822E-004	13	6.017E-005			
Lack of Fit	5.225E-004	8	6.531E-005	1.26	0.4179	not significant
Pure Error	2.597E-004	5	5.195E-005			
Cor Total	0.037	19				
Additional ANOVA Data						
Std. Dev.	7.757E-003					
R^2	0.9786					
Adj. R^2	0.9687					
Pred. R^2	0.9411					
Adequate Precision	35.484					

Dysprosium (Dy)

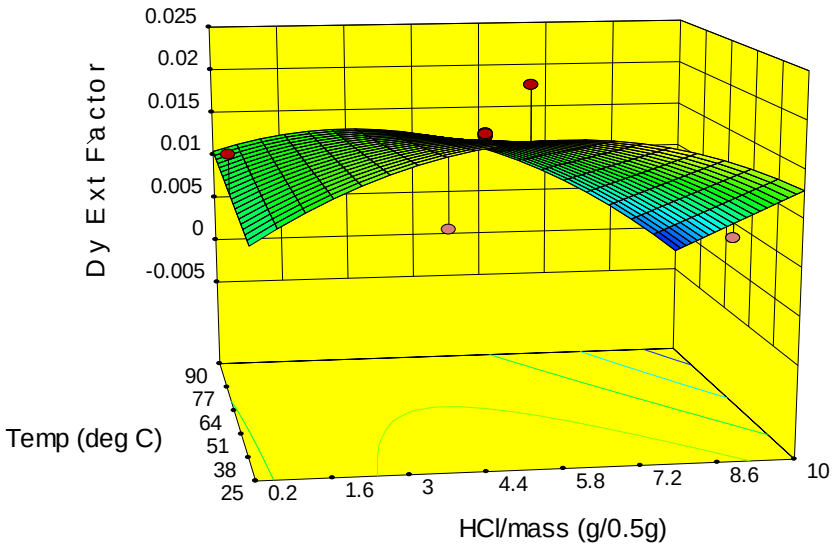

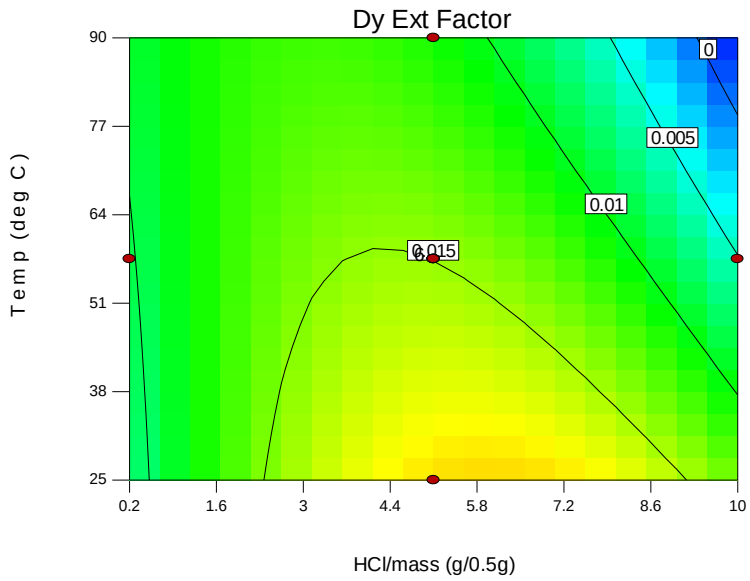

Equation: $Dy = 7.46291 \times 10^{-3} + 4.29338 \times 10^{-3}C + 3.08137 \times 10^{-5}T - 2.73899 \times 10^{-5}CT - 3.12741 \times 10^{-4}C^2$

Figure 136: Contour Plot, Model Equation, and Response Surface of Dy Extraction from RE6 (Time: 75 min)

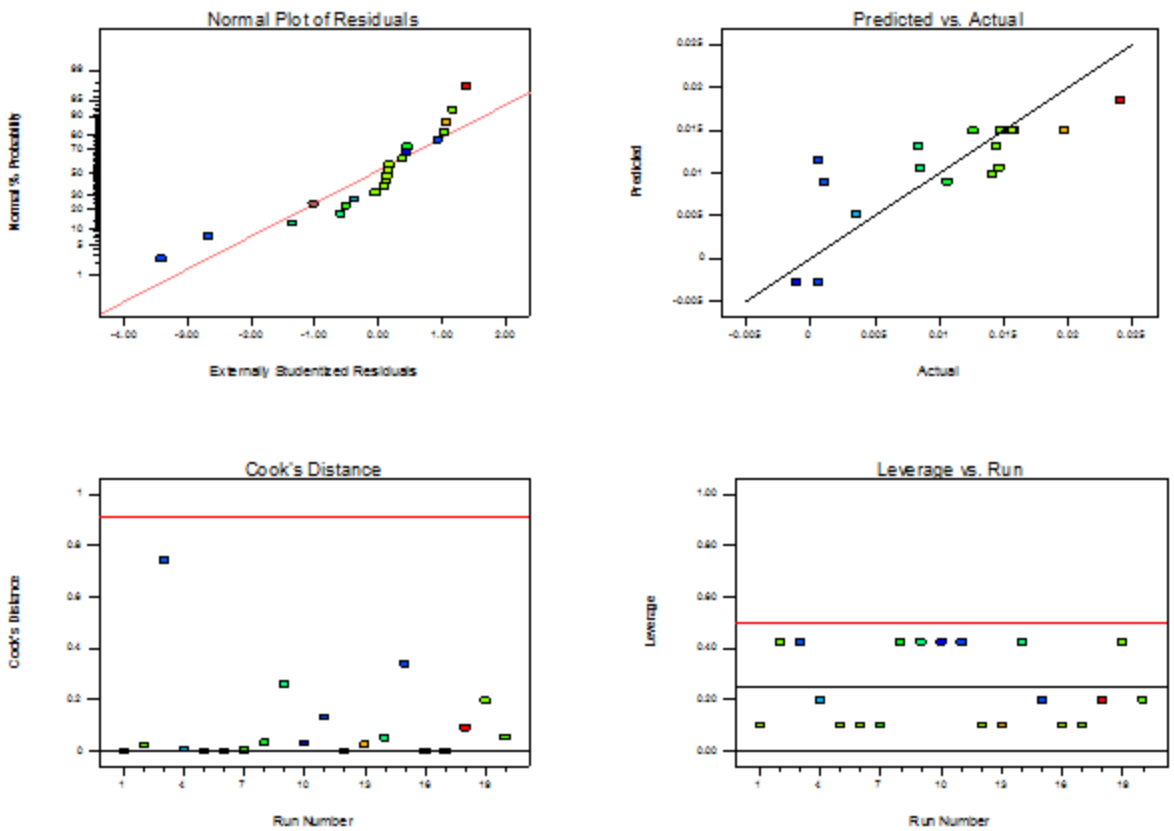

Figure 137: Diagnostics for Dy Extraction Model (RE6)

Table LXXXII: ANOVA Data for Dy Extraction from RE6

Source	Sum of Squares	df	Mean Square	F-Value	p-value	Notes
Model	6.127E-004	4	1.532E-004	7.08	0.0021	significant
C-HCl/mass	5.338E-005	1	5.338E-005	2.47	0.1370	
T-Temp	1.252E-004	1	1.252E-004	5.79	0.0295	
CT	1.522E-004	1	1.522E-004	7.04	0.0181	
C^2	2.819E-004	1	2.819E-004	13.04	0.0026	
Residual	3.243E-004	15	2.162E-005			
Lack of Fit	3.237E-004	10	3.237E-005	240.55	< 0.0001	significant
Pure Error	6.727E-007	5	1.345E-007			
Cor Total	9.370E-004	19				
Additional ANOVA Data						
Std. Dev.	4.650E-003					
R^2	0.6539					
Adj. R^2	0.5616					
Pred. R^2	0.2759					
Adequate Precision	9.143					

Gadolinium (Gd)

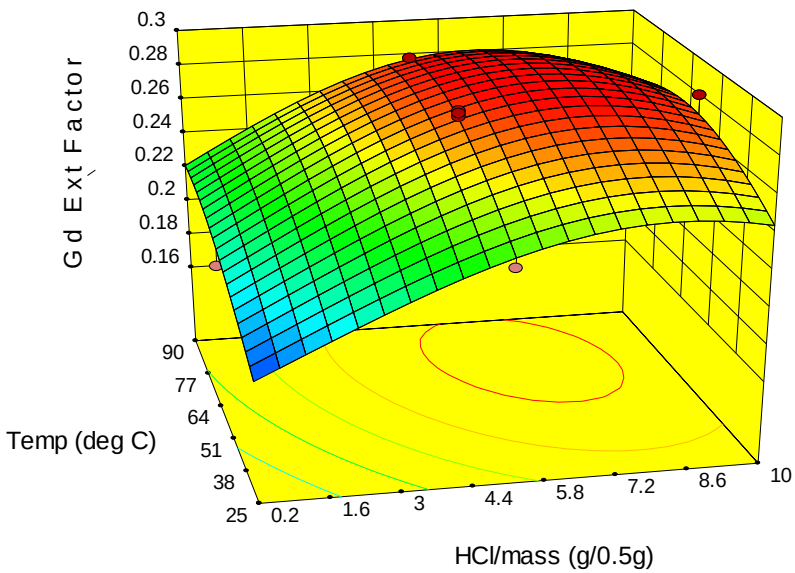

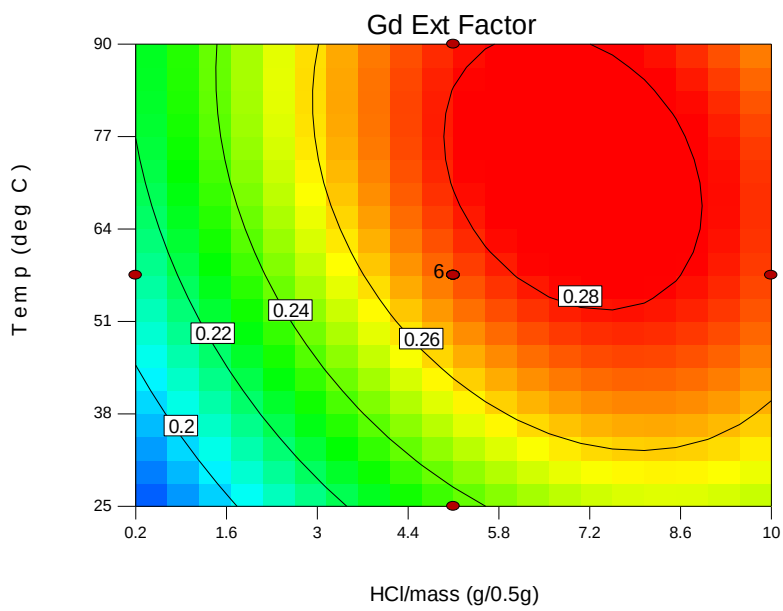

Equation: $Gd^{-1} = 7.56463 - 0.49914C - 0.053488T - 0.012886t + 1.26590 \times 10^{-3}CT + 9.66621 \times 10^{-4}Ct + 1.08803 \times 10^{-4}Tt + 0.024166C^2 + 2.53523 \times 10^{-4}T^2$

Figure 138: Contour Plot, Model Equation, and Response Surface of Gd Extraction from RE6 (Time: 75 min)

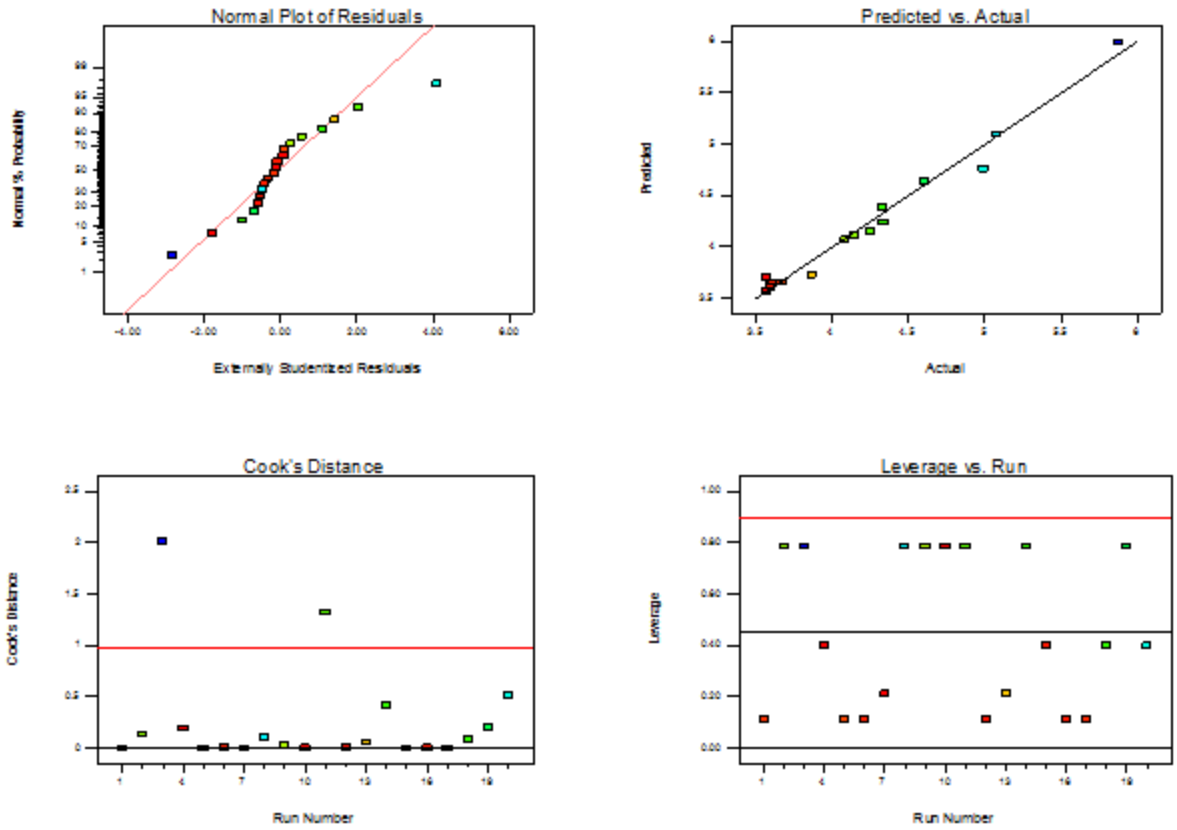

Figure 139: Diagnostics for Gd Extraction Model (RE6)

Table LXXXIII: ANOVA Data for Gd Extraction from RE6

Source	Sum of Squares	df	Mean Square	F-Value	p-value	Notes
Model	7.69	8	0.96	75.86	< 0.0001	significant
C-HCl/mass	2.77	1	2.77	218.47	< 0.0001	
T-Temp	1.00	1	1.00	78.71	< 0.0001	
t-Time	0.058	1	0.058	4.62	0.0548	
CT	0.33	1	0.33	25.67	0.0004	
Ct	0.36	1	0.36	28.69	0.0002	
Tt	0.20	1	0.20	15.99	0.0021	
C^2	1.08	1	1.08	85.04	< 0.0001	
T^2	0.23	1	0.23	18.11	0.0014	
Residual	0.14	11	0.013			
Lack of Fit	0.14	6	0.023	28.91	0.0010	significant
Pure Error	3.904E-003	5	7.808E-004			
Cor Total	7.83	19				
Additional ANOVA Data						
Std. Dev.	0.11					
R^2	0.9822					
Adj. R^2	0.9693					
Pred. R^2	0.8871					
Adequate Precision	32.161					

Lanthanum (La)

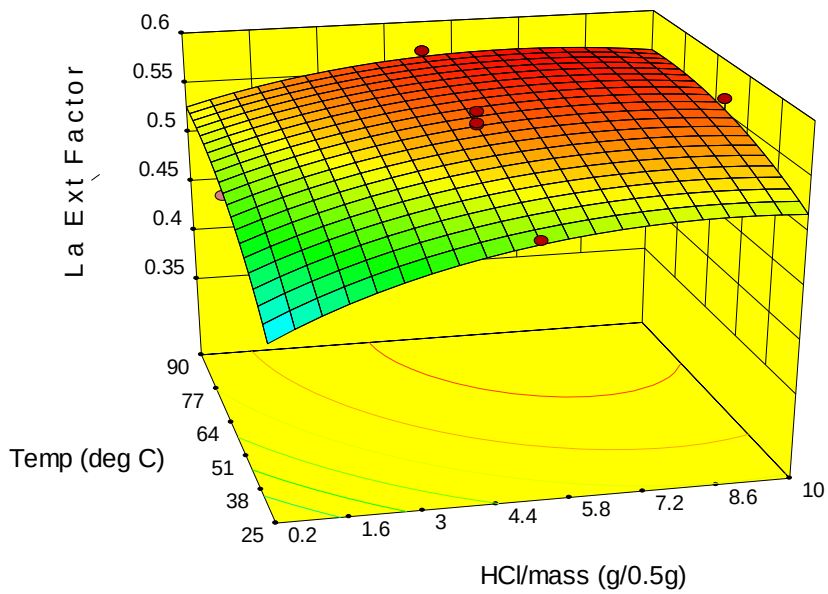

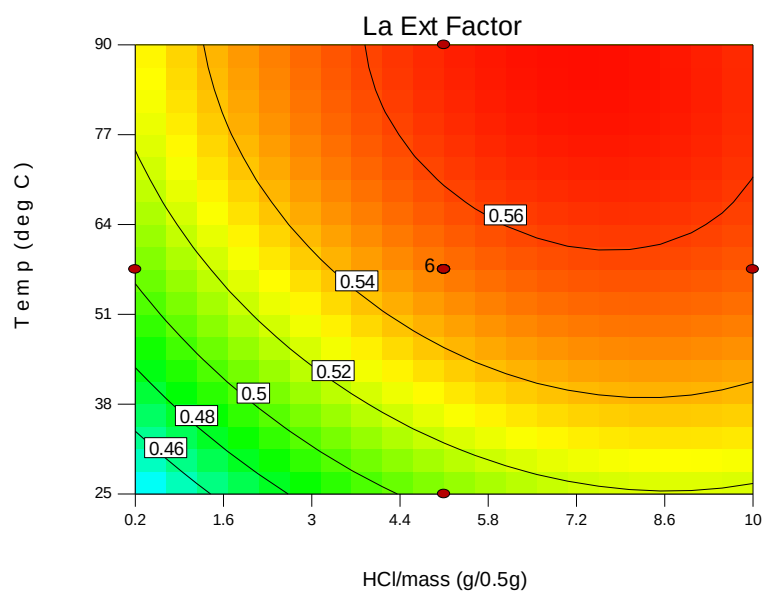

Equation: $La^3 = -6.16295 \times 10^{-3} + 0.017380C + 2.37553 \times 10^{-3}T + 4.52910 \times 10^{-4}t - 4.20383 \times 10^{-5}CT - 3.17940 \times 10^{-5}Ct - 8.04213 \times 10^{-4}C^2 - 1.19819 \times 10^{-5}T^2$

Figure 140: Contour Plot, Model Equation, and Response Surface of La Extraction from RE6 (Time: 75 min)

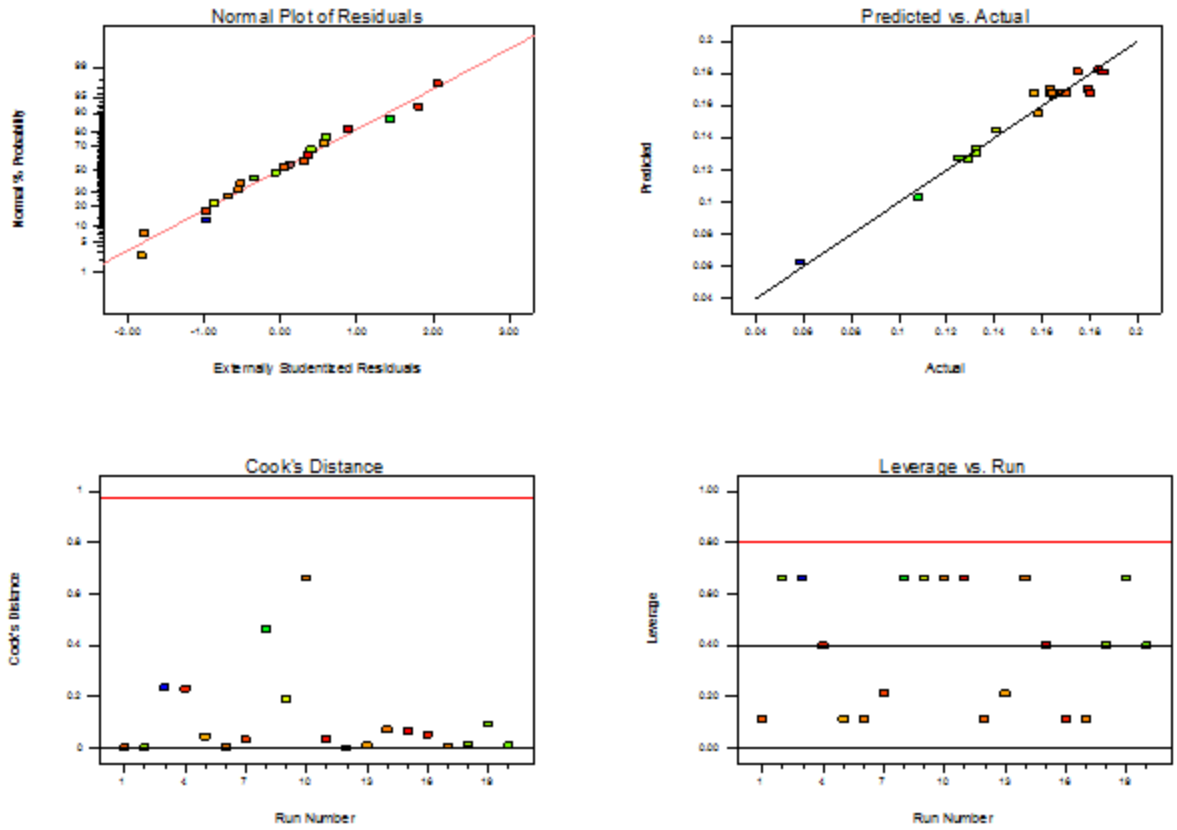

Figure 141: Diagnostics for La Extraction Model (RE6)

Table LXXXIV: ANOVA Data for La Extraction from RE6

Source	Sum of Squares	df	Mean Square	F-Value	p-value	Notes
Model	0.018	7	2.524E-003	49.07	< 0.0001	significant
C-HCl/mass	4.596E-003	1	4.596E-003	89.34	< 0.0001	
T-Temp	6.479E-003	1	6.479E-003	125.96	< 0.0001	
t-Time	1.712E-003	1	1.712E-003	33.28	< 0.0001	
CT	3.585E-004	1	3.585E-004	6.97	0.0216	
Ct	3.932E-004	1	3.932E-004	7.64	0.0171	
C^2	1.193E-003	1	1.193E-003	23.20	0.0004	
T^2	5.126E-004	1	5.126E-004	9.96	0.0083	
Residual	6.172E-004	12	5.144E-005			
Lack of Fit	3.001E-004	7	4.287E-005	0.68	0.6928	not significant
Pure Error	3.171E-004	5	6.343E-005			
Cor Total	0.018	19				
Additional ANOVA Data						
Std. Dev.	7.172E-003					
R^2	0.9662					
Adj. R^2	0.9466					
Pred. R^2	0.8954					
Adequate Precision	26.445					

Neodymium (Nd)

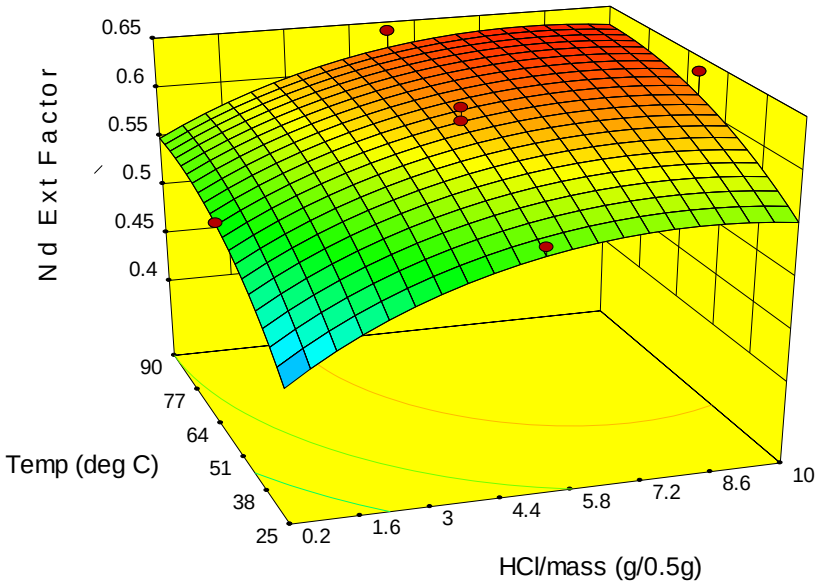

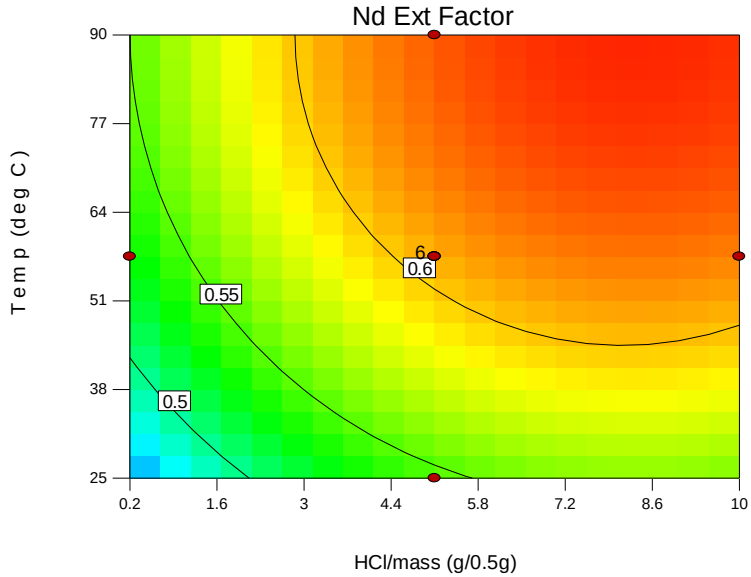

Equation: $Nd^{2.57} = 3.68439 \times 10^{-3} + 0.025083C + 3.74596 \times 10^{-3}T + 5.10885 \times 10^{-4}t - 1.54353 \times 10^{-3}C^2 - 2.08342 \times 10^{-5}T^2$

Figure 142: Contour Plot, Model Equation, and Response Surface of Nd Extraction from RE6 (Time: 75 min)

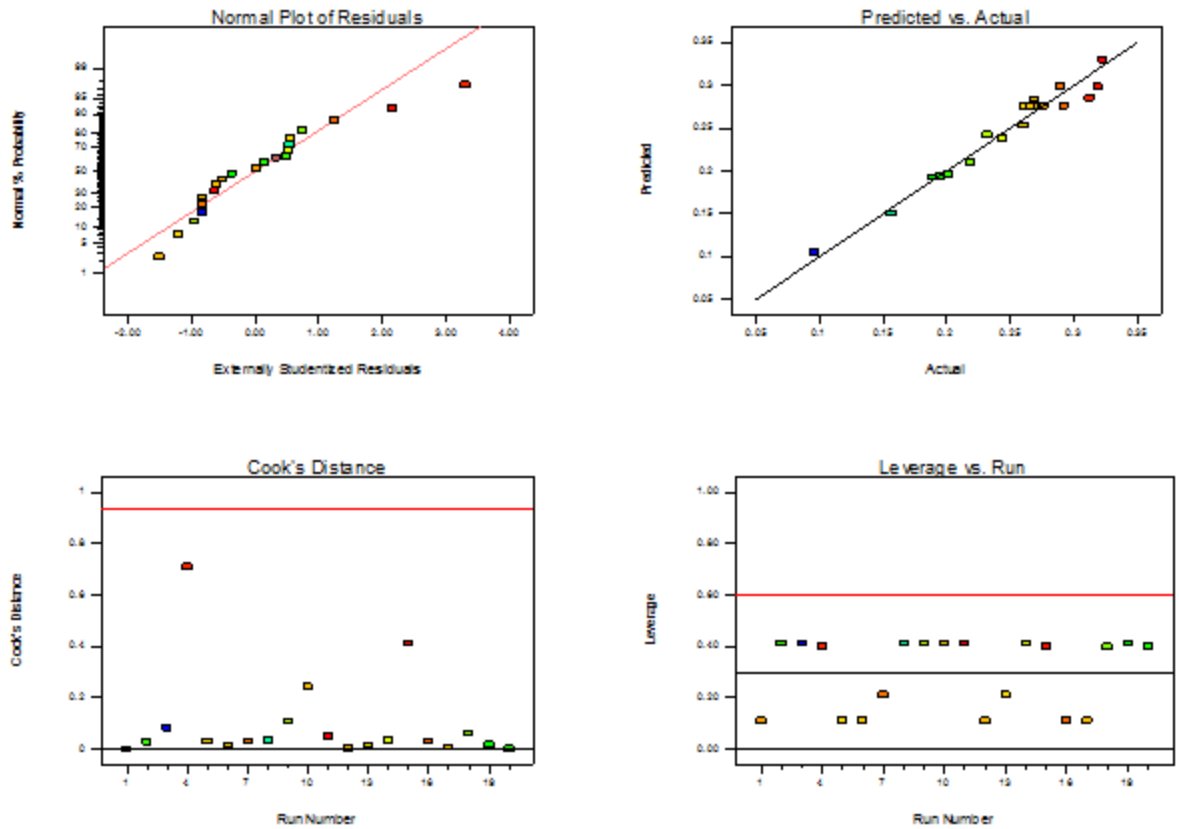

Figure 143: Diagnostics for Nd Extraction Model (RE6)

Table LXXXV: ANOVA Data for Nd Extraction from RE6

Source	Sum of Squares	df	Mean Square	F-Value	p-value	Notes
Model	0.060	5	0.012	61.74	< 0.0001	significant
C-HCl/mass	0.021	1	0.021	108.36	< 0.0001	
T-Temp	0.019	1	0.019	99.62	< 0.0001	
t-Time	5.285E-003	1	5.285E-003	27.35	0.0001	
C^2	4.395E-003	1	4.395E-003	22.74	0.0003	
T^2	1.550E-003	1	1.550E-003	8.02	0.0133	
Residual	2.705E-003	14	1.932E-004			
Lack of Fit	2.085E-003	9	2.317E-004	1.87	0.2546	not significant
Pure Error	6.203E-004	5	1.241E-004			
Cor Total	0.062	19				
Additional ANOVA Data						
Std. Dev.	0.014					
R^2	0.9566					
Adj. R^2	0.9411					
Pred. R^2	0.8990					
Adequate Precision	29.584					

Praseodymium (Pr)

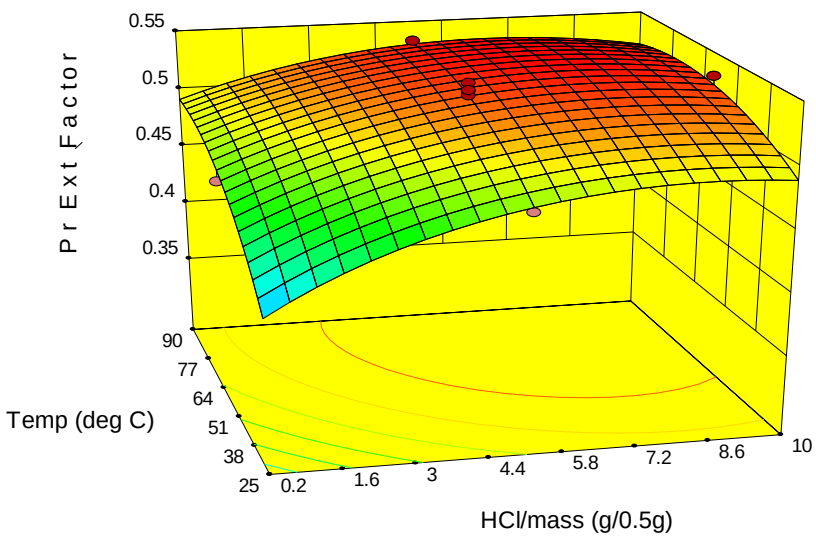

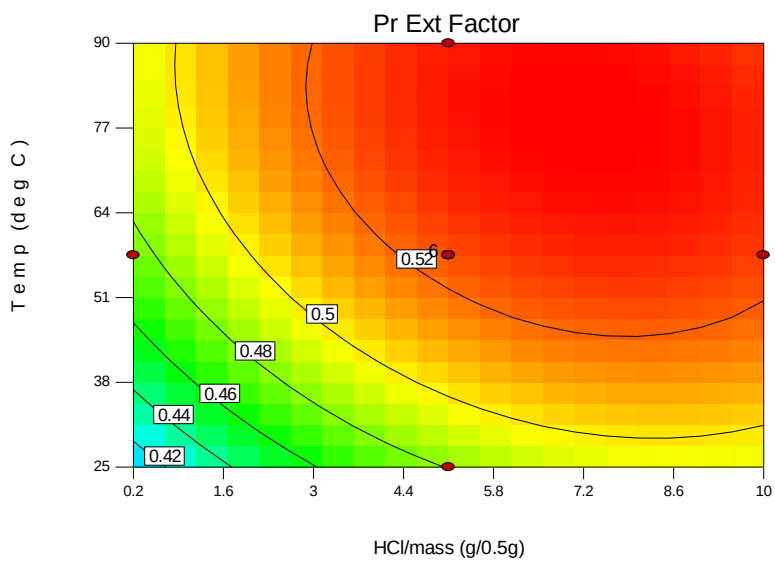

Equation: $Pr^{2.81} = -2.76313 \times 10^{-3} + 0.017540C + 2.47923 \times 10^{-3}T + 3.67898 \times 10^{-4}t - 4.55093 \times 10^{-5}CT - 3.25323 \times 10^{-5}Ct - 8.28424 \times 10^{-4}C^2 - 1.40835 \times 10^{-5}T^2$

Figure 144: Contour Plot, Model Equation, and Response Surface of Pr Extraction from RE6 (Time: 75 min)

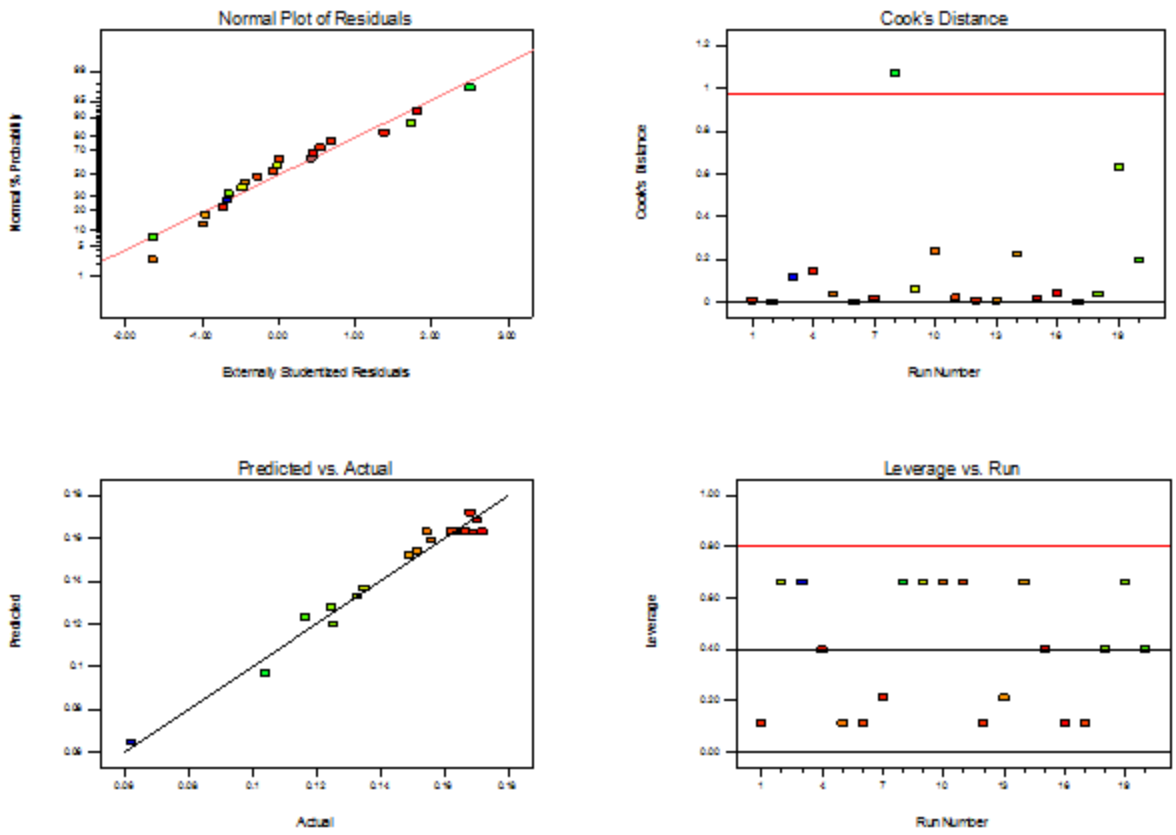

Figure 145: Diagnostics for Pr Extraction Model (RE6)

Table LXXXVI: ANOVA Data for Pr Extraction from RE6

Source	Sum of Squares	df	Mean Square	F-Value	p-value	Notes
Model	0.015	7	2.083E-003	62.91	< 0.0001	significant
C-HCl/mass	3.906E-003	1	3.906E-003	117.94	< 0.0001	
T-Temp	4.160E-003	1	4.160E-003	125.60	< 0.0001	
t-Time	8.261E-004	1	8.261E-004	24.95	0.0003	
CT	4.202E-004	1	4.202E-004	12.69	0.0039	
Ct	4.117E-004	1	4.117E-004	12.43	0.0042	
C^2	1.266E-003	1	1.266E-003	38.23	< 0.0001	
T^2	7.081E-004	1	7.081E-004	21.38	0.0006	
Residual	3.974E-004	12	3.312E-005			
Lack of Fit	2.309E-004	7	3.299E-005	0.99	0.5229	not significant
Pure Error	1.665E-004	5	3.329E-005			
Cor Total	0.015	19				
Additional ANOVA Data						
Std. Dev.	5.755E-003					
R^2	0.9735					
Adj. R^2	0.9580					
Pred. R^2	0.9025					
Adequate Precision	29.543					

Thorium (Th)

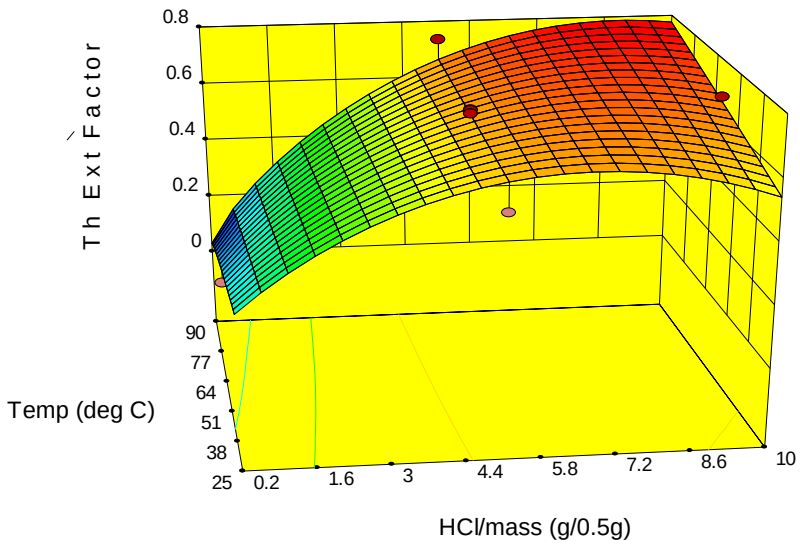

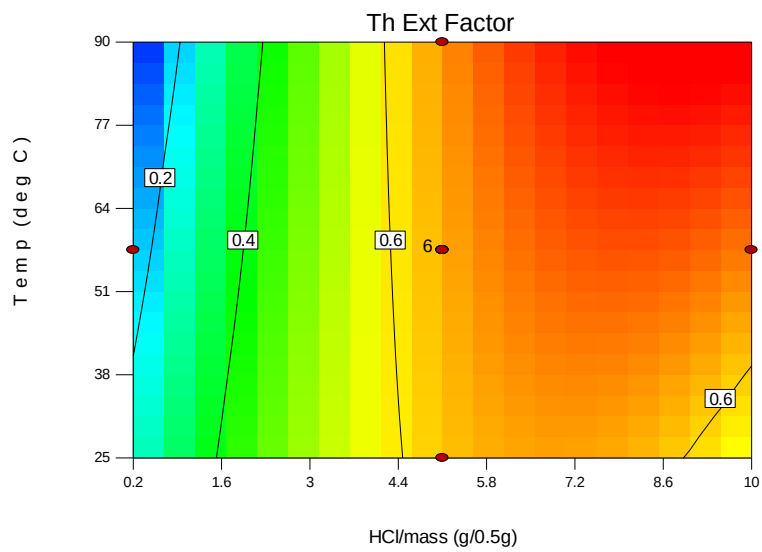

Equation: $Th^{1.24} = 0.21225 + 0.11211C - 2.50089 \times 10^{-3}T + 6.45828 \times 10^{-4}CT - 9.58139 \times 10^{-3}C^2$

Figure 146: Contour Plot, Model Equation, and Response Surface of Th Extraction from RE6 (Time:75 min)

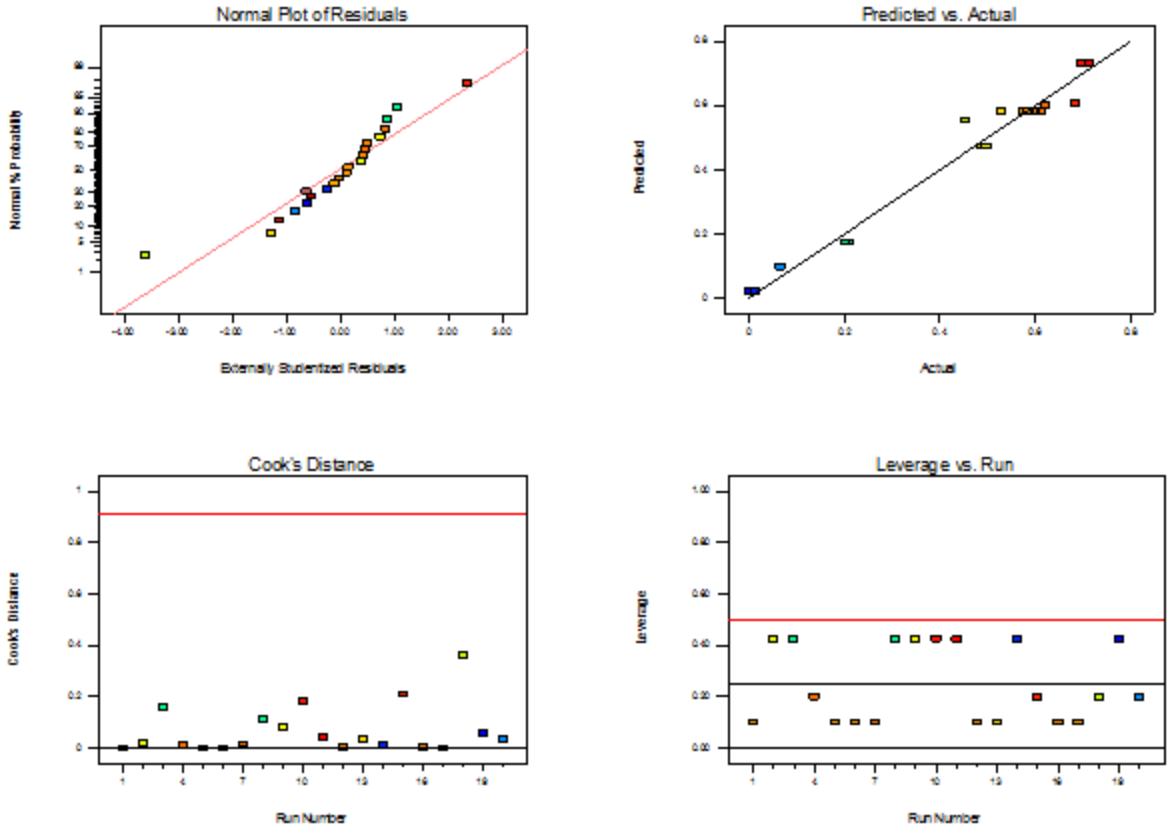

Figure 147: Diagnostics for Th Extraction Model (RE6)

Table LXXXVII: ANOVA Data for Th Extraction from RE6

Source	Sum of Squares	df	Mean Square	F-Value	p-value	Notes
Model	0.99	4	0.25	137.95	< 0.0001	significant
C-HCl/mass	0.64	1	0.64	354.05	< 0.0001	
T-Temp	6.639E-003	1	6.639E-003	3.69	0.0740	
CT	0.085	1	0.085	47.02	< 0.0001	
C^2	0.26	1	0.26	147.03	< 0.0001	
Residual	0.027	15	1.800E-003			
Lack of Fit	0.027	10	2.652E-003	28.04	0.0009	significant
Pure Error	4.730E-004	5	9.460E-005			
Cor Total	1.02	19				
Additional ANOVA Data						
Std. Dev.	0.042					
R^2	0.9735					
Adj. R^2	0.9665					
Pred. R^2	0.9534					
Adequate Precision	33.498					

Iron (Fe)

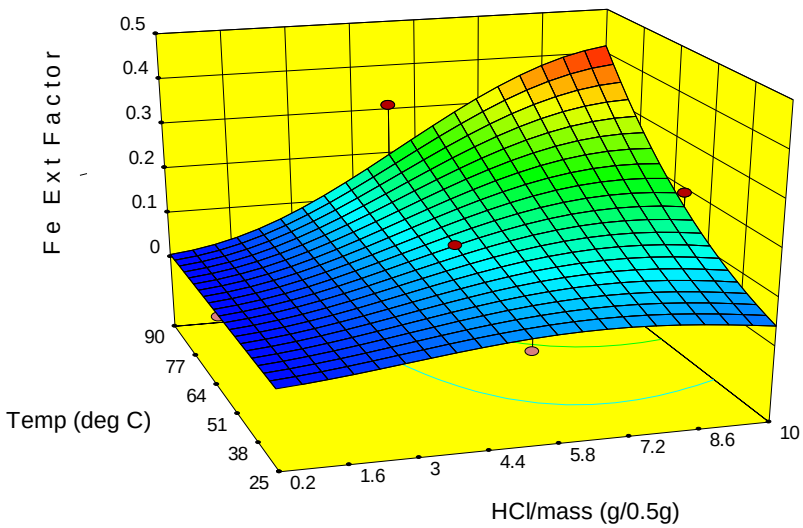

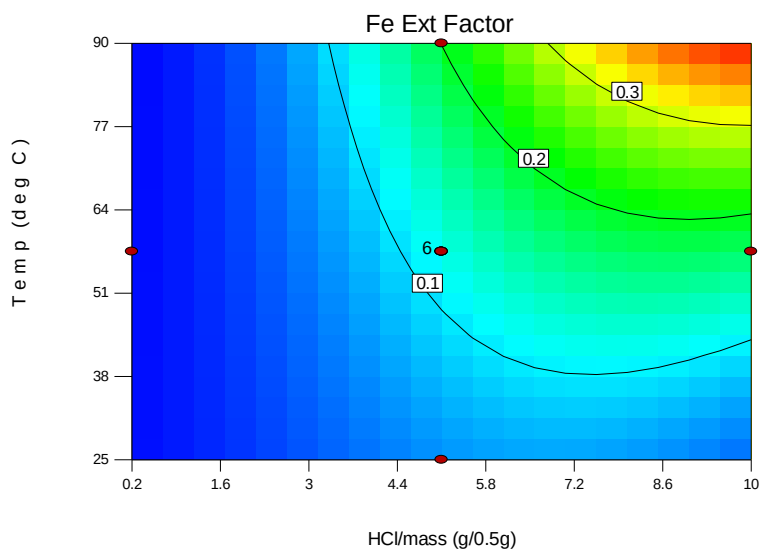

Equation: $Fe^{0.34} = 0.13067 + 0.053785C - 4.42115 \times 10^{-4}T + 5.82016 \times 10^{-4}t + 6.66506 \times 10^{-4}CT - 5.30919 \times 10^{-3}C^2$

Figure 148: Contour Plot, Model Equation, and Response Surface of Fe Extraction from RE6 (Time: 75 min)

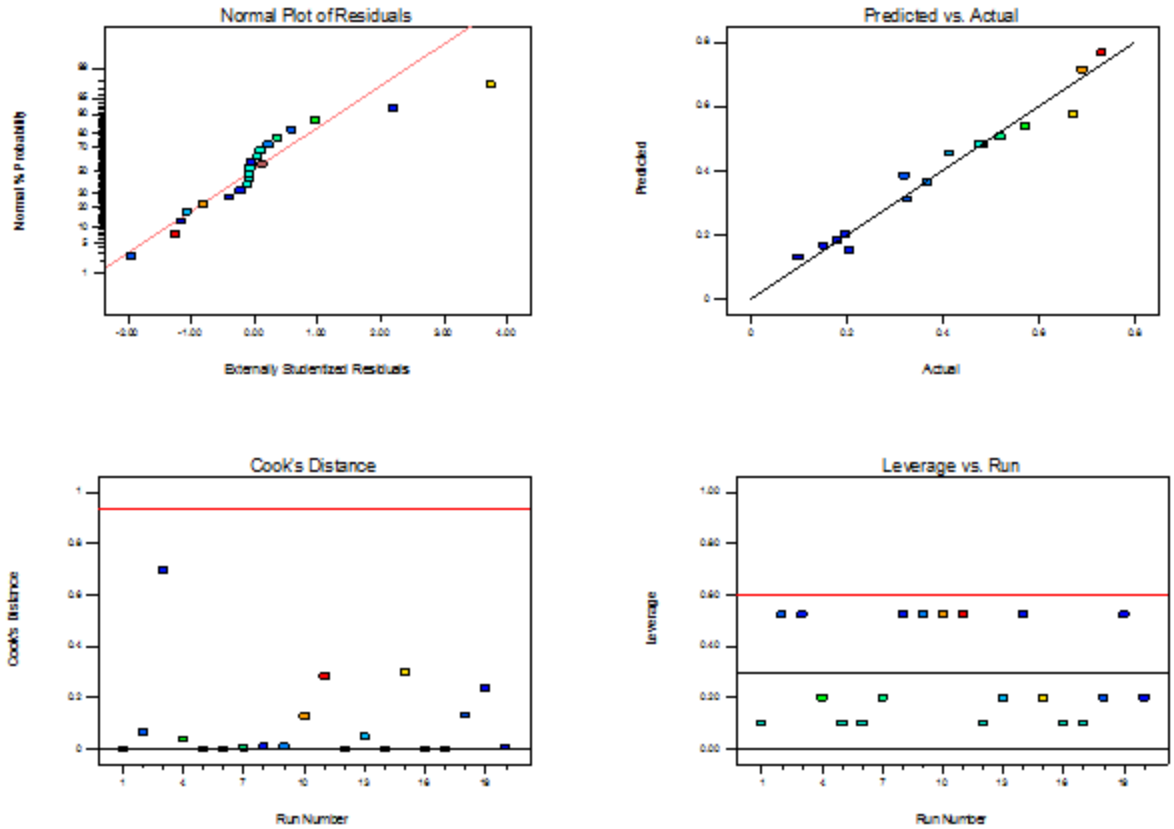

Figure 149: Diagnostics for Fe Extraction Model (RE6)

Table LXXXVIII: ANOVA Data for Fe Extraction from RE6

Source	Sum of Squares	df	Mean Square	F-Value	p-value	Notes
Model	0.62	5	0.12	75.77	< 0.0001	significant
C-HCl/mass	0.35	1	0.35	212.55	< 0.0001	
T-Temp	0.092	1	0.092	56.76	< 0.0001	
t-Time	6.860E-003	1	6.860E-003	4.22	0.0592	
CT	0.090	1	0.090	55.38	< 0.0001	
C^2	0.081	1	0.081	49.93	< 0.0001	
Residual	0.023	14	1.627E-003			
Lack of Fit	0.023	9	2.526E-003	245.44	< 0.0001	significant
Pure Error	5.145E-005	5	1.029E-005			
Cor Total	0.64	19				
Additional ANOVA Data						
Std. Dev.	0.040					
R^2	0.9644					
Adj. R^2	0.9516					
Pred. R^2	0.9173					
Adequate Precision	28.813					

Appendix J: ANOVA Data for Eu Extraction Models

The following tables of data contain the ANOVA analysis for Eu extraction from the RER samples presented in the main body of this thesis.

Table LXXXIX: ANOVA Data for Eu Extraction from RE1

Source	Sum of Squares	df	Mean Square	F-Value	p-value	Notes
Model	0.16	4	0.039	53.63	< 0.0001	significant
C-HCl/mass	0.056	1	0.056	77.13	< 0.0001	
T-Temp	0.047	1	0.047	65.51	< 0.0001	
t-Time	0.016	1	0.016	22.21	0.0003	
CT	0.036	1	0.036	49.65	< 0.0001	
C^2	0.010	14	7.229E-004			
Residual	0.010	10	1.011E-003	494.14	< 0.0001	significant
Lack of Fit	8.186E-006	4	2.046E-006			
Pure Error	0.17	18				
Cor Total	0.16	4	0.039	53.63	< 0.0001	significant
Additional ANOVA Data						
Std. Dev.	0.027					
R^2	0.9387					
Adj. R^2	0.9212					
Pred. R^2	0.8677					
Adequate Precision	24.952					

Table XC: ANOVA Data for Eu Extraction from RE2

Source	Sum of Squares	df	Mean Square	F-Value	p-value	Notes
Model	0.48	6	0.081	308.97	< 0.0001	significant
C-HCl/mass	0.22	1	0.22	862.79	< 0.0001	
T-Temp	0.095	1	0.095	363.90	< 0.0001	
t-Time	5.643E-003	1	5.643E-003	21.65	0.0005	
CT	0.013	1	0.013	50.69	< 0.0001	
C^2	0.063	1	0.063	240.08	< 0.0001	
T^2	6.246E-003	1	6.246E-003	23.97	0.0003	
Residual	3.388E-003	13	2.606E-004			
Lack of Fit	3.143E-003	8	3.929E-004	8.02	0.0173	significant
Pure Error	2.449E-004	5	4.898E-005			
Cor Total	0.49	19				
Additional ANOVA Data						
Std. Dev.	0.040					
R^2	0.9644					
Adj. R^2	0.9516					
Pred. R^2	0.9173					
Adequate Precision	28.813					

Table XCI: ANOVA Data for Eu Extraction from RE4

Source	Sum of Squares	df	Mean Square	F-Value	p-value	Notes
Model	0.36	6	0.060	101.14	< 0.0001	significant
C-HCl/mass	0.15	1	0.15	251.04	< 0.0001	
T-Temp	0.100	1	0.100	168.05	< 0.0001	
t-Time	6.370E-003	1	6.370E-003	10.76	0.0060	
CT	0.011	1	0.011	18.07	0.0009	
C^2	0.031	1	0.031	52.69	< 0.0001	
T^2	8.966E-003	1	8.966E-003	15.14	0.0019	
Residual	7.700E-003	13	5.923E-004			
Lack of Fit	5.066E-003	8	6.332E-004	1.20	0.4386	not significant
Pure Error	2.634E-003	5	5.268E-004			
Cor Total	0.37	19				
Additional ANOVA Data						
Std. Dev.	0.024					
R^2	0.9790					
Adj. R^2	0.9693					
Pred. R^2	0.9454					
Adequate Precision	34.302					

Table XCII: ANOVA Data for Eu Extraction from RE5

Source	Sum of Squares	df	Mean Square	F-Value	p-value	Notes
Model	0.62	5	0.12	1425.90	< 0.0001	significant
C-HCl/mass	0.39	1	0.39	4498.44	< 0.0001	
T-Temp	0.036	1	0.036	421.85	< 0.0001	
t-Time	4.019E-003	1	4.019E-003	46.54	< 0.0001	
C^2	0.11	1	0.11	1277.52	< 0.0001	
T^2	4.792E-004	1	4.792E-004	5.55	0.0336	
Residual	1.209E-003	14	8.635E-005			
Lack of Fit	1.107E-003	9	1.230E-004	6.05	0.0308	significant
Pure Error	1.017E-004	5	2.034E-005			
Cor Total	0.62	19				
Additional ANOVA Data						
Std. Dev.	9.293E-003					
R^2	0.9980					
Adj. R^2	0.9973					
Pred. R^2	0.9955					
Adequate Precision	109.040					

Table XCIII: ANOVA Data for Eu Extraction from RE6

Source	Sum of Squares	df	Mean Square	F-Value	p-value	Notes
Model	0.071	6	0.012	171.65	< 0.0001	significant
C-HCl/mass	0.030	1	0.030	435.69	< 0.0001	
T-Temp	0.019	1	0.019	271.61	< 0.0001	
t-Time	3.276E-003	1	3.276E-003	47.28	< 0.0001	
Ct	5.048E-004	1	5.048E-004	7.29	0.0182	
C^2	7.473E-003	1	7.473E-003	107.86	< 0.0001	
T^2	1.050E-003	1	1.050E-003	15.16	0.0018	
Residual	9.007E-004	13	6.928E-005			
Lack of Fit	6.912E-004	8	8.640E-005	2.06	0.2207	not significant
Pure Error	2.095E-004	5	4.189E-005			
Cor Total	0.072	19				
Additional ANOVA Data						
Std. Dev.	8.324E-003					
R^2	0.9875					
Adj. R^2	0.9818					
Pred. R^2	0.9635					
Adequate Precision	47.284					

SIGNATURE PAGE

This is to certify that the thesis prepared by Grant Wallace entitled "Optimization of Rare Earth Leaching From Ores and Concentrates" has been examined and approved for acceptance by the Metallurgical and Materials Engineering Department , Montana Tech of The University of Montana, on this 29th day of April, 2015.

William Gleason, Ph.D., Associate Professor
Metallurgical and Materials Engineering Dept.
Chair, Examination Committee

Courtney Young, Ph.D., Professor and Department Head
Metallurgical and Materials Engineering Dept.
Member, Examination Committee

Jerome Downey, Ph.D., Associate Professor
Metallurgical and Materials Engineering Dept.
Member, Examination Committee

Larry Twidwell, D.Sc., Professor Emeritus
Metallurgical and Materials Engineering Dept.
Member, Examination Committee

Mchael Webb, Ph.D., Assistant Professor
Chemistry and Geochemistry Dept.
Member, Examination Committee